Telma Godinho Barroso Maciel Fernandes

Mestre em Engenharia Química e Bioquímica

Functional monolithic platforms for antibody purification

Dissertação para obtenção do Grau de Doutor em
Química Sustentável

Orientadores: Prof. Doutora Ana Aguiar-Ricardo

Prof. Doutora Ana Cecília Roque

FACULDADE DE
CIÊNCIAS E TECNOLOGIA
UNIVERSIDADE NOVA DE LISBOA

January 2014

Functional monolithic platforms for antibody purification

ACKNOWLEDGMENTS

The PhD was more than four years of scientific research combined with my intellectual skills. In fact, it was a test to my personal resistance (Márcio Temtem you were completely right! Thanks very much for your advices, and for all friendship and teachings! You were a great professor). Fortunately, I believe that I passed it with a feeling of "job done". However, PhD was not possible without the support and reinforcement of several people that I would like to acknowledge.

First of all, I would like to acknowledge my supervisors Prof. Ana Aguiar-Ricardo and Prof. Cecilia Roque that gave me the opportunity to work on this project. I am very grateful for all their effort and dedication to me, and to the work that together we were able to develop. Prof. Ana Aguiar-Ricardo many thanks to be an exigent and outstanding supervisor, and an especial friend when I needed. I will always remember our brainstorming, the phone calls after hours, and the happy and frustrating moments together, but the true is: I got here because you never gave up of me. Prof. Cecilia Roque, I am very thankful to your patience with me as well as to your good vibes that you always transmitted to me (yûûûû oooouuu). Without you, the biochemical world would be utopic for me! If I have biochemistry in my education, I owe it to you.

I also would like to acknowledge to Polymer Synthesis and Processing Group and to Biomolecular Engineering Group. I could find numerous words to say to each one however, it will become another thesis. Thus, I reserved some special words for each one of you. Starting with Polymer Synthesis and Processing Group: Raquel Viveiros (Yesterday, today and tomorrow…you will be forever in my heart, thanks for everything), Vanessa Correia (I will miss you, and I will keep great memories of us including brainstorming ☺), Rita Restani (*"Gazeada Girl"*: sometimes the life is hard, but at same time is amazing…please hold it☺), Patrícia Morgado (Thanks for your sympathy and friendship), Ana Silva (For you, the sky is the limit…close your eyes, close your mouth and forget the others, you are "the important" because you have everything to be it☺), Anita Lourenço (Thank you for your participation in this chapter of my life), Márcia Tavares (*"Hard Rock Girl"*; It was a pleasure to work with you), Renato Cabral *("Great Engineer"*: it was a pleasure to meet you), Vasco Bonifácio (*"The Chemist Man"*: thanks for all your patience in try to explain me organic chemistry, it was not easy, but it was possible ☺) and Teresa Casimiro (*"Great scientist and friend"*: Thanks to clean my tears and support my euphoric moments. You had a fundamental role on this chapter of my life). Now the Biomolecular Engineering Group: Íris Batalha (*"Keep Calm Girl*": thank you very much for all funny and *zen* moments that only you could give me), Margarida Dias *("Special friend and great professional"*: I will miss you a lot), Susana Palma (It was a pleasure to meet you), Henrique Carvalho *("Alternative Guy"*: I always remember your good mode), Vijaykumar Dhadge ("*Patents Man*": Great Doctor! One day we will be rich!!!), Abid Hussain *("Great colleague, researcher and English professor"*: Thanks for everything that you taught me), Ricardo Branco (*"The Modeling Man"*: I am very grateful for all your effort and dedication for me and for my

work; I will miss our brainstorming about computational modelling), Cláudia Fernandes and Bianca Gonçalves (*"Recent acquisitions"*: I adored to meet you). And finally Ana Pina! For you all words are not enough. During the last four years you were one of the main pieces of this game and when the motivation disappeared, you were the reason that made me to continue. I will remember all nights that we spent in the lab, all the "balcony moments" where we laugh and where we cried, all conferences, all days, everything…You are simply the best.
Sincerely, thank you all for everything. This thesis has pieces of you thus, it is also yours.

To Professor Manuel Nunes da Ponte I would like to express my sincere acknowledgments for all teachings in green chemistry which formatted me to be a sustainable engineer☺. A special thanks also to professor Ana Maria Rego for all XPS discussions and friendship.
A special thanks to Maria José and Isabel Rodrigues for their assistance in bureaucratic work, and to Maria de Palma, Idalina and Conceição for providing me clean laboratory material to develop me research. For all, a distinctive thank also for your love and kindness. I want also to acknowledge the Analytical Services Laboratory of REQUIMTE for the characterization of materials, and to the Animal Cell Technology Unit of ITQB-UNL/IBET (Dr. Paula M Alves and Dr. Ana Teixeira) for providing the cell culture bulks of antibodies.

To all my family, I am very grateful for all your support and patience. Due to all of you (father, sister, nephew (Ti), cousins, uncles, aunts, brothers-in-law, Manuela e Armando) I am the person that was able to get here. I am sorry for the moments that I missed with you (especially with my nephew, Tiago) but this work was hard. However, believe in me, you were always in my heart. Specially, I would like to acknowledge two persons: Sónia Barroso that more than a sister, she was and is the mother that I never had. I love you! The second person is my husband Nuno Fernandes that was the light that appeared in my life, and make me believe that I was able to do everything that I wanted. Thank you for your love, friendship, patience and encouraging words. Without you my life will be uncoloured. Love you! To all my friends, that are a lot, but you know who I am referring, many thanks for always being there for me! *Beetocada* (all members and staff☺) thanks very much for all sportive and relax weekends and moments. "Nephews" (Joana, Porco, Li, Central, Pêlo, Caixinha, and all others) for you a special thanks for all happy moments that you gave me, and that I will always keep in my heart. I love you all in the same way☺. For the ones that life turned difficult their presence (Bru, Inês, Meguy and Tropa), a special kiss. You were also my driving force to continue. You are great friends.

Lastly, I would like to thank the financial support from Fundação para a Ciência e Tecnologia, Portugal, through contracts PEst-C/EQB/LA0006/2011, MIT-Pt/BS-CTRM/0051/2008, PTDC/EBB-BIO/102163/2008, PTDC/EBBBIO/ 098961/2008, PTDC/EBB-BIO/118317/2010 and doctoral grant SFRH/ BD/62475/2009, and Fundação Calouste Gulbenkian.

ABSTRACT

This work aimed at the development of monolithic chromatographic platforms for antibody purification. A sustainable strategy, comprising the use of natural polymers such as chitosan, agarose and dextran, was employed to create 3D porous structures. In order to improve the mechanical properties and biodegradability of monoliths, natural polymers were physically blended with synthetic ones. All supports were, in a first stage, produced by freeze-drying methods while in a second attempt were prepared by an integrated approach involving gelation process, water-acetone substitution and $scCO_2$ drying. A further optimization for opening the porous network was evaluated involving swelling and freeze-drying procedures. To optimize the efficacy of monoliths, magnetic nanoparticles were embedded in monoliths structure to confer them a magnetic responsive behaviour. This additional feature improved antibody recovery when performing a magnetically-assisted elution (93% recovery of bound IgG) complemented to less time processing. The selectivity of monoliths for antibody, IgG, was guaranteed by the immobilization of ligand 22/8 (artificial Protein A) and a new triazine-based ligand (TPN-BM) onto their surfaces. The functionalization strategy of TPN-BM, which synthesis followed the principles of green chemistry, was induced by plasma technology. This alternative strategy allowed the reduction of time and solvents consumption while maximizing the functionalization yield of supports (2-fold, comparing to the traditional procedures). Moreover, the binding/elution mechanism between TPN-BM and IgG at a molecular level was validated through molecular docking studies and dynamic simulations.

Overall, TPN-BM functionalized natural-based monoliths revealed values of pore size diameter, porosity, and flux between 1-96 µm, 28-88 % and 3-220 (L m^{-2} h^{-1}). Chitosan/poly(vinyl alcohol)-based monoliths revealed the best binding and elution capacities, 160 mg IgG g^{-1} support and 97%, respectively, at least over four consecutive cycles. Moreover, tested with crude samples, supports exhibited a good specificity for mAbs, recovering them with 96-98% of purity.

KEYWORDS: Biopolymers, monoliths, affinity ligand, plasma technology, supercritical carbon dioxide, green chemistry, antibody purification.

RESUMO

Este trabalho teve como objectivo o desenvolvimento de suportes monolíticos para a purificação de anticorpos por cromatografia de afinidade. Para tal, utilizou-se uma estratégia sustentável para produzir essas estruturas porosas 3D (monólitos), envolvendo polímeros naturais tais como quitosano, dextrano e agarose. Para melhorar as propriedades mecânicas e biodegradáveis dos monólitos, os polímeros naturais foram misturados fisicamente com polímeros sintéticos. Primeiramente, todos os suportes foram produzidos por liofilização, e numa segunda fase por processos de gelificação, substituição de água por acetona e secagem por $scCO_2$. A optimização da abertura da rede porosa foi efectuada recorrendo à capacidade de inchamento dos suportes e subsequente liofilização. Para melhorar a performance dos monólitos, incorporaram-se nanopartículas magnéticas nas redes monolíticas por forma a conferir-lhes a capacidade de resposta magnética e consequente deformação quando sob acção de um campo magnético. Realizaram-se assim eluições assistidas por campo magnétco o que permitiu o aumento do rendimento de recuperação de anticorpo (IgG) ligado (93%) e diminuir o tempo do passo de eluição. A selectividade dos monólitos para o anticorpo foi garantida através da imobilização de dois ligandos sintéticos mimetizando a Proteína A (ligando 22/8 e o novo ligando TPN-BM) na superfície dos suportes. A estratégia de funcionalização do TPN-BM, cuja síntese seguiu os princípios da química verde, foi feita utilizando a tecnologia de plasma. Esta estratégia permitiu reduzir tempo e uso de solventes bem como maximizar todo o processo (em 2 vezes) comparativamente aos procedimentos tradicionais. O mecanismo de ligação/eluição do TPN-BM e IgG foi validado através de estudos de acoplamento molecular e simulações dinâmicas.

Em geral, todos os monólitos TPN-BM-funcionalizados exibiram valores de diâmetro de poro, porosidade e fluxo entre 1-96 µm, 28-88 % e 3-220 (L $m^{-2}h^{-1}$), respectivamente. Os monólitos de quitosano/poli(vinil álcool) revelaram as melhores capacidades de ligação e de eluição, 160 mg IgG g^{-1} suporte e 97%, respectivamente, pelo menos durante quatro ciclos consecutivos. Adicionalmente, quando testados com extractos brutos, exibiram uma boa especificidade para mAbs, recuperando-os com 96-98% de pureza.

.

PALAVRAS-CHAVE - Biopolímeros, monólitos, ligandos de afinidade, tecnologia de plasma, dióxido de carbono supercrítico, química verde, purificação de anticorpos.

TABLE OF CONTENTS

INDEX OF FIGURES

PAGE

INDEX OF TABLES

ABBREVIATIONS

AAm - Acrylamide

Ab - Antibody

AC - Affinity chromatography

AE - Atom economy

AG - Agarose

AG_M - Magnetic agarose-based monolith

AG_M_TPN-BM - Magnetic agarose-based monolith functionalized with ligand TPN-BM

AG_M_Amine - Magnetic and aminated agarose-based monolith

AGE - Allyl glycidyl ether

Ala - Alanine

AN - Adsorption nitrogen

API - Active pharmaceutical ingredients

APS - Ammonium peroxodisulphate

Ar - Argon

Asn - Aspargine

BE - Binding energy

BCA - Bicinchoninic acid

BSA - Bovine serum albumin

CBS - Consensus binding site

CE - Carbon efficiency

CIP – Cleaning-in-place

CIM - Convective interaction media

CG - Chitosan-glycidyl methacrylate

CG_N - Native chitosan-glycidyl methacrylate monolith

CG_22/8 - Chitosan-glycidyl methacrylate monolith functionalized with ligand 22/8

CG_TPN-BM - Chitosan-glycidyl methacrylate monolith functionalized with ligand TPN-BM

CHT - Chitosan

CHT_M_TPN-BM - Magnetic chitosan monolith functionalized with ligand TPN-BM

CHT_M - Magnetic chitosan monolith

CHT_N - Native chitosan monolith

C-NMR - Carbon nuclear magnetic resonance

CO_2 - Carbon dioxide

CP - Chitosan-poly(vinyl alcohol) monolith

CP_M - Chitosan-poly(vinyl alcohol) magnetic monolith

CP_M_TPN-BM - Magnetic chitosan-poly(vinyl alcohol) monolith functionalized with ligand TPN-BM

CP_M_Amine - Magnetic and aminated chitosan-poly(vinyl alcohol) monolith

CP_N - Native chitosan-poly(vinyl alcohol) monolith

CP_TPN-BM - Chitosan-poly(vinyl alcohol) monolith functionalized with ligand TPN-BM

CP_22/8 - Chitosan-poly(vinyl alcohol) monolith functionalized with ligand 22/8

CP 25:75 - Chitosan-poly(vinyl alcohol) monolith prepared by gelation, water-acetone replacement and $scCO_2$ drying

CP 25:75_TPN-BM - Chitosan-poly(vinyl alcohol) monolith prepared by gelation, water-acetone replacement and $scCO_2$ drying, and functionalized with ligand TPN-BM

CP 25:75_M - Magnetic chitosan-poly(vinyl alcohol) monolith prepared by gelation, water-acetone replacement and $scCO_2$ drying

CP 25:75_M^{FD} - Magnetic chitosan-poly(vinyl alcohol) monolith prepared by gelation, water-acetone replacement and $scCO_2$ drying, and submitted to an additional treatment for opening porous network involving swelling and freeze-drying procedures

CP 25:75_M_TPN-BM^{FD} - Magnetic chitosan-poly(vinyl alcohol) monolith prepared by gelation, water-acetone replacement and $scCO_2$ drying, and submitted to an additional treatment for opening porous network involving swelling and freeze-drying procedures, and functionalized with ligand TPN-BM

DMAEMA - *N',N'*-dimethylaminoethyl methacrylate

DMF - *N,N*-dimethylformamide

DMSO - Dimethylsulfoxide

DN – Desorption of nitrogen

DXT - Dextran

DXT_M - Dextran-based monolith

DXT_M_TPN-BM - Magnetic dextran-based monolith functionalized with ligand TPN-BM

EDMA - Ethylene glycol dimethacrylate

FAT - Fixed analyzer transmission

FT-IR - Fourier transform infrared spectroscopy

Gln - Glutamine

Glu - Glutamic acid

GMA - Glycidyl methacrylate

HCl - Hydrochloric acid

HEMA - Hydroxyethyl methacrylate

HIC - Hydrophobic interaction chromatography

hIgG - Human Immunoglobulin G

His - Histidine

^{1}H-NMR – Proton nuclear magnetic resonance

IgG - Immunoglobulin G

IgM - Immunoglobulin M

IDA - Iminodiacetate

IEC - Ion exchange chromatography

ISEC - Inverse size inclusion chromatography

K_a - Affinity constant

LCA - Life cycle assessment

Leu - Leucine

Ligand 22/8 - (2-(3-aminophenol)-6-(4-amino-1-naphthol)-4-chloro-s-triazine

mAbs - Monoclonal antibodies

MAH - N-methacryloyl-(L)-histidine methyl ester

MBA - *N',N'*-methylenebisacrylamide

MD - Molecular dynamics simulations

MI - Mass intensity

MIP - Mercury intrusion porosimetry

MNPs - Magnetic nanoparticles

MP - Mass productivity

NaOH - Sodium hydroxide

n - Langmuir–Freundlich coefficient

PDB - Protein data bank

PGPGE - Poly(glycerol polyglycidyl ether)

PVA - Poly(vinyl alcohol)

QA - Quaternary amine

Q_{max} - Theoretical maximum capacity

REACH - Registration evaluation and authorization of chemicals

RME - Reaction mass efficiency

SCF - Supercritical fluids

$scCO_2$ - Supercritical carbon dioxide

SDS-PAGE - Sodium dodecyl sulfate-polyacrylamide gel electrophoresis

SEM - Scanning transmission electron microscopy

SGE - Sun grid engine

SIP - Sterilization in place

SpA - Staphylococcus aureus Protein A

TEMED - *N,N,N',N'*-tetramethylene diamine

TEM - Transmission electron microscopy

THF - Tetrahydrofuran

TP-BM - 3-((4,6-dichloro-1,3,5-triazin-2-yl)oxy)phenol

TPN-BM - (4-((4-chloro-6-(3-hydroxyphenoxy)-1,3,5-triazin-2-yl)oxy)naphthalen-1-ol)

Tyr - Tyrsine

Trp - Tryptophan

XPS - X-ray photoelectron spectroscopy

BACKGROUND

The European market for therapeutic monoclonal antibodies (mAbs) is one of the fastest growing in the pharmaceutical sector.[1,2] Currently, about 25% of commercial pharmaceuticals are biopharmaceuticals and about half of the worldwide sales are referred to mAbs, representing the majority. Therefore, these values translate greatly the importance of these proteins.[2]

Nowadays, the high value of mAbs as therapeutic drugs is possible due to established synergy between the development of hybridoma technology and subsequent advancements in molecular biology and genetic engineering.[3] Presently, mAbs are employed on the treatment of several diseases being cancer and autoimmune disorders the most common targets. Thus, mAbs with high purity level are required and thus, considerable efforts have been made to restructure the purification process in terms of specificity, selectivity, reproducibility, economy, product recovery, storage and maintenance.[3,4,5] Although different downstream processes have been established for mAbs, affinity chromatography is still the most widely used technique.[4,6,7] This process relies on a chromatographic matrix which has covalently immobilized an affinity ligand able to establish highly specific and selective interactions to the target.

Up to now, different chromatographic supports and affinity ligands have been explored in order to improve antibody purification processes.[8] The most common affinity ligand used is the biological ligand Protein A. Although the biological ligands present highly biding and selectivity, their use presents several drawbacks such as: high associated costs, low stability and re-usability.[9] In order to overcome this, biomimetic ligands have emerged based on triazine and boronic molecules, and Ugi reactions based products.[9,10,11,12] An artificial protein A has been developed based on the triazine scaffold which showed great affinity and stability towards mAbs.[10] On the other side, also chromatographic matrices have been target of exhaustive optimization studies in order to reduce or eliminate mass diffusion and pressure drop problems associated to traditional chromatographic fillings (agarose beads or other polymeric particles).[13,14] Thus, membranes and more recently monoliths have been developed as the most attractive generation of chromatographic platforms able to overcome chromatography drawbacks.[15] Monoliths are 3D porous structures known by presenting an outstanding porous networks with well-defined and interconnected pores that enable to process faster, by convection transport, different viscous fluids, than typical chromatographic platforms that operate mainly by diffusion.[16]

Currently, monoliths have been produced from polymerization of different acrylate monomers and by chemical modifications of natural or synthetic polymers combining sol-gel, gelation, and freeze-drying methods.[17,18,19,20] Although powerful, these strategies are time consuming and involve the use of organic solvents. Therefore, in order to reverse the negative publicity associated to chemistry based processes, regarding ecological and social points of view,

chemists and engineers have made a strong effort to start to find out greener alternatives to processes and products design and development, respectively.[21] As an example of this is the use of supercritical fluids (SCF) in the preparation of 3D porous platforms. SCF-based processes offer significant environmental benefits, the drying steps are energy intensive and pores structure collapse is avoided.[22]

Once established, is essential that the support should be uniform, macroporous, hydrophilic, chemically and mechanically stable, selective and insoluble in the solvent used in purification.[14] Additionally, it must exhibit minimum non-specific absorption and ideal flow characteristics, and provide a large surface area for ligand attachment. Different methods for ligand coupling have been frequently used based on chemical approaches (e.g. epoxyactivation followed by amination procedures or aldehyde functionalization processes), to facilitate further ligand attachment.[23] Since these sequential methods also involve large time and solvent consumptions, it is required novel, sustainable and robust methods for ligand coupling, able to avoid ligand leaching, and reduce costs.

To date, there is no purification alternative that combines a sustainable approach with the most attractive features of a chromatographic support and affinity ligand. More important than creating something totally new, it is the redesign of processes already established using natural resources and minimizing the waste, the energy and solvents feedings. The regulatory laws call for a business strategy regarding environment, health, safety and social issues. This has been working as the most important driving force to change mentality in academy and industry to reinvent greener and sustainable processes and products. Based on this, herein it is intended to prepare, through greener methods, monoliths based on natural polymers, with well-defined pores architecture, tuneable mechanical properties and able to operate over a wide range of chemical conditions (e.g. pH and solution compositions) for antibody purification. Also the redesign, following green metrics, of a biomimetic synthetic ligand is envisioned as well as its study at atom level to predict the promising binding sites with the antibody. Moreover, the strategy of ligand attachment to the chromatographic matrices pretends to be optimized regarding time saving and the reduction of organic species involved. **Thus, this greener and integrated strategy aims to offer a sustainable solution for antibody purification processes, that can also be extended to other applications such as drug or cells delivery and tissue engineering**.

CHAPTER 1

FUNCTIONAL MONOLITHIC PLATFORMS: CHROMATOGRAPHIC TOOLS FOR ANTIBODY PURIFICATION

SUMMARY

Polymer monoliths are an efficient platform for antibody purification. The use of monoclonal antibodies (mAbs) and engineered antibody structures as therapeutics has increased exponentially over the past few decades. Several approaches use polymer monoliths to purify large quantities of antibody with defined clinical and performance requirements. Functional monolithic supports have attracted a great deal of attention as they offer practical advantages for antibody purification, such as faster analysis, smaller sample volume requirements and the opportunity for a greater target molecule enrichment. This chapter focuses on the development of synthetic and natural polymer-based monoliths for antibody purification. The materials and methods employed in monolith production are discussed, highlighting the properties of each system. It is also presented the structural characterization techniques available using monolithic systems and their performance under different chromatographic approaches to antibody capture and release. Finally, a summary of monolithic platforms developed for antibody separation is offered, as well as expected trends in research to solve current and future challenges in this field.

Article published: *Telma Barroso, Abid Hussain, Ana C. A. Roque and Ana Aguiar-Ricardo, Functional monolithic platforms: Chromatographic tools for antibody purification. Biotechnol. J. 2013, 8, 1-11.*

1.1 INTRODUCTION

In recent decades, the use of antibodies, monoclonal antibodies (mAbs) and engineered antibody structures for cancer, autoimmune, inflammation and infectious disease therapy has increased exponentially, with an overall annual market worth tens of billions of US dollars.[7,23,24] Therefore, innovative platforms for large scale antibody production and purification are required.[25] Current research is aimed at developing more selective isolation methods for antibody purification, rather than relying on traditional chromatographic techniques.[7,23,24] A chromatographic process can be defined as a separation process which allows the isolation of a target molecule from a complex mixture. This is enabled through the different chemical interactions between a specific ligand immobilized onto a chromatographic support and the target molecule. Presently, chromatographic methods such as hydrophobic interaction chromatography (HIC), ion exchange chromatography (IEC) and affinity chromatography (AC) dominate the manufacturing of biopharmaceuticals.[16,26] Numerous biological (antibodies, peptides, proteins, lectins) and non-biological (synthetic dyes, ion exchangers, metal chelates) ligands, materials and geometries (agarose beads, polymeric membranes, monoliths) may be incorporated into chromatographic separation matrices. The plethora of options available make chromatography the most commonly used technique for antibody purification.[9,26]

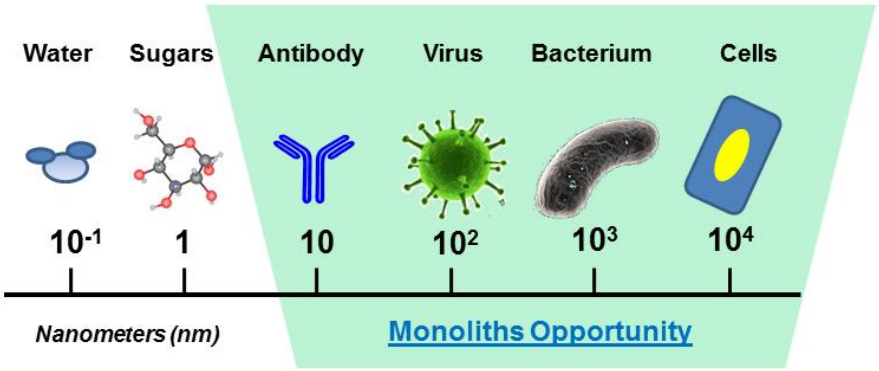

Figure 1.1 - Schematic representation of opportunity window for polymer monolith incorporation into chromatographic bioseparation processing technology on the basis of target molecule size.

Thus, the ideal bioseparation matrix must fulfill the following criteria: (i) high selectivity and high binding capacity for the target molecule; (ii) good mechanical, morphological and chemical stability; (iii) inhibition of non-specific molecular adsorption; (iv) high stability under cleaning in place (CIP) and sterilization in place (SIP) conditions; and (v) facilitation of short processing times for high volumes.[26] To date, materials typically employed in chromatographic processes are beads or gels manufactured from such raw materials as agarose and polymeric membranes.[7] These materials, while readily available, present certain shortcomings such as limitations with the mass transfer, gel compressibility and poor pore diffusion leading to high pressure drops and low flow rates – all of which incur process time and cost. These weaknesses have led to an investment on alternative chromatographic supports which maintain

the efficiency of the established processes while improving their associated limitations. One of these new generation of alternatives are monolithic supports, herein referred to as monoliths,[27] which were introduced in the early 1990's.[26]

1.2 MONOLITHIC PLATFORMS

We define monolith here as a porous, single-unit material introduced into a chromatographic device.[28] Individual monoliths are characterized by a network of large interconnected pores (or channels) which allow high operational fluxes and consequently lead to rapid processing times.[7] Due to their excellent morphological and mechanical properties, monoliths have attracted attention for use in antibody purification[14] (Fig. 1.1) both at research and industrial scale (table 1). Incorporation of monoliths into chromatography stationary phase also avoids a high-shear fractionation atmosphere, which is crucial for optimal recovery of shear-sensitive molecules such as viruses, sensitive proteins, DNA and cells.[27] A vital requirement for implementation within the pharmaceutical industry is translation to large-scale operation. High-throughput processing must be enabled at moderate pressure drops without sacrificing the product purity. In this respect, the main advantages associated with monoliths (convention dominated mass transport, high porosity, low cost preparation and simple column filling) has encouraged several manufacturers to examine monoliths as potential supports.[29] Nowadays there are several commercially available polymeric monolith based supports, for both small scale and analytical purposes, offering a wide range of pore diameters. These allow the purification of a large number of biomolecules ranging in size and features in a simple and effective way (Fig. 1.1 and Table 1.1).

Monoliths employed in antibody purification have been prepared using inorganic materials as well as natural and synthetic polymers. Recently, Arrua *et al.*[30] reviewed current developments and future possibilities for polymeric monolithic structures. Depending on the material, different manufacturing routes can be followed, including polymerization initiated by different stimuli,[31] sol-gel[32] and cryogelation,[19] creating porous networks with distinguishing structural properties. Since these polymers and materials adopt the format of the mould used, monolithic materials can be prepared in different formats, such as large rod polymers (used in standard HPLC/capillary columns), monolithic disks, cylinders and flat sheet polymers.[30] A classification according to the morphological features of different monolithic supports is indicated in Table 1.2 agreeing to the commonly defined literature criteria.[33]

Since the optimal performance of monoliths depends on the balance between morphological, mechanical and physicochemical properties, it is difficult to single out any specific parameter range to be set as the "gold standard". It is crucial to establish first whether the monolith will be for analytical or large scale applications. For analytical purposes, pore size diameter can be designed according to the target antibody. In contrast, at large scale pore size must be considered in light of the contaminants which also residing in the load solution, so that all components are able to permeate freely through the support. Hence, in general, a monolith for antibody purification must have a range of pore size diameter between 1 and 50 μm, a porosity

of around 60±10%, a surface area within 10–400 m^2 cm^{-3} with a permeability and a binding capacity of up to 100 L $m^{-2}h^{-1}atm^{-1}$ and 50 mg mL^{-1}, respectively.[34,35] This range of values can be tuned according to the components of the load solution by the methods selected to prepare the monoliths. Thus, different types of monoliths can be generated and customized to ensure maximum efficiency in the capture of the target antibody.

Table 1.1 - Overview of commercially available monoliths for applications in bioseparation.[29]

Trade name	Manufacturer	Material	Separation modes	Macro pore size (µm)
CIM	BIA Separations	Polymethacrylate	Ion exchange Hydrophobic interaction Reverse phase Bioaffinity	0.03-1.5
UNO	Bio-Rad	Polyacrylamide	Ion exchange	1
SWIFT	Isco	Polymethacrylate	Ion exchange Reversed phase	1.5
SepraSorb	Sepragen	Modified cellulose	Ion exchange	50-300
Chromolith	Merck	Silica	Reversed phase	≥ 2

Table 1.2 - Morphological features of different types of porous structure.[33]

	Micropore	Mesopore	Macropore
Pore Diameter (nm)	< 2	2-50	> 50
Porosity (%)	≤ 25	25-65	≥ 65
Surface Area (m^2cm^{-3})	≥ 1000	1000-350	≤ 350

1.2.1. SYNTHETIC POLYMER MONOLITHS

Polymer monoliths produced by organic synthesis were first used in chromatography columns in the late 1980's and the early 1990s, and so far, its production continues to grow.[14,19,29,30,31,32,33,34,35,36,37,38] Monolithic columns were prepared by radical polymerization of

monovinyl monomer in the presence of a crosslinker, radical initiator and porogen (responsible for pore formation) (Fig. 1.2 A). Inspired by this straightforward strategy of monolith production, different monomers such as acrylamide (AAm), methacrylate and styrene were then employed to create rigid monoliths with desired morphological properties and dimensions.[14,39,40,41,42,43,44]

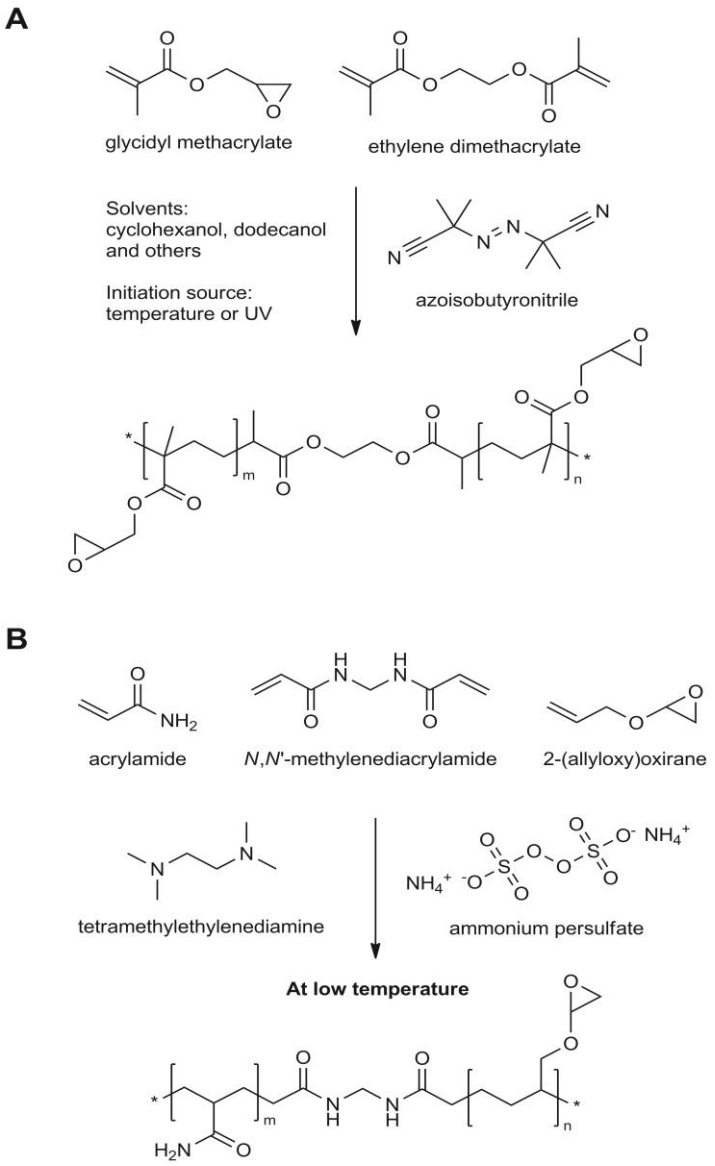

Figure 1.2 - Preparation of GMA-EDMA monoliths (A) and of AA-AGE cryogels (B) and their chemical structures.

In particular, glycidyl methacrylate (GMA) and ethylene glycol dimethacrylate (EDMA) have become the most commonly employed monomers for the preparation of synthesized monoliths.[31,45] The great advantages of using these monomers is that GMA, which carries the very reactive epoxy group, facilitates further functionalization for target molecule capture; while EDMA, as an excellent crosslinker, confers mechanical stability to the final monolith. As an example, Hahn *et al.*[46] developed an affinity poly(GMA-co-EDMA) monolith using a simple strategy for ligand immobilization. The model peptide (or ligand) was directly immobilized by

reaction with the epoxy groups on the GMA chains incorporated into the matrix of monolith. Spacer arms can be introduced between the ligand and the support to promote the accessibility of the ligand functional groups to interact with the target biomolecule. As an example, reactive macroporous monoliths of poly(GMA-co-EDMA) were prepared by *in situ* copolymerization of GMA and EDMA in the presence of porogenic agents, followed by Protein A and L-histidine linkage to the monoliths either directly or through the use of a spacer arm. The IgG adsorption capacity of the monolith functionalized with Protein A was greatly increased with the introduction of the spacer.[47] Poly(GMA-co-EDMA) monoliths have also been functionalized with Protein L and Protein G with promising results,[48,49,50] sufficient to justify their commercialization.[51,52]

To evaluate the application of synthetic monoliths for antibody purification, several studies have been performed. Lokman *et al.*[53] developed a novel porous monolithic system for effective IgG purification from human plasma based on the preparation of porous monoliths through the bulk polymerization of (hydroxyethyl) methacrylate HEMA and N-methacryloyl-(L)-histidine - methylester (MAH). An upper adsorption value (>96.5 mg g^{-1}) was achieved from human plasma with an associated purity value of 95.3%. Moreover, the authors verified that IgG could be reversibly adsorbed using poly(HEMA-MAH) monolith. Another strategy from the same group[54] involved the preparation of imprinted poly(hydroxyethyl methacrylate-N-methacryloyl-l-tyrosine methyl ester) particles using hepatitis B antibody as the surface template. These particles demonstrated spectacular binding specificity, adsorbing an amount of hepatitis B antibody 18.3 times greater than anti-hepatitis A antibody, and 2-fold greater than immunoglobulin E. The self-polymerization of poly(glycerol poly(glycidyl ether) (PGPGE) using methyl tert-butyl ether as a porogenic agent resulted in the formation of a particularly rigid monolith where the epoxy groups of the poly(glycerol polyglycidyl ether) served a dual purpose: firstly, to provide functional groups for the polymerization reaction, and secondly to allow direct binding of Protein A to the monolith surface. Capillary columns loaded with this monolith allowed the isolation of IgG (5.3±0.9 µg) and presented a capacity of 0.44±0.08 mg mL^{-1} within a capillary volume of 12 µL.[50] In addition to affinity-based monoliths, anion-exchange methacrylate monolithic systems constituted by a monolithic macroporous convective interaction media (CIM) were tested and proved to be effective in the isolation of anti-glycophorin-A IgG1 mouse mAbs from cell culture supernatant. Also, CIM-iminodiacetate (IDA) disks with four different metal ions (Zn^{2+}, Cu^{2+}, Co^{2+} and Ni^{2+}) immobilized were employed for mAb isolation from cell culture supernatant, achieving a maximum recovery of 85.4% of purified antibody.[55]

Synthetic polymer monoliths have also been employed in complex IgM purification systems. Recently, an epoxy-activated monolith CIM disc functionalized with an affinity peptide[56] was developed for IgM, IgG and mAb isolation from embryonic stem cells. With this approach, it was possible to recover 67%, 83% and 95% of IgG, IgM and mAbs, respectively. In addition, the binding capacity was reproducible over two thousand cycles. Recently, ammonium quaternized monolith CIM disks (CIM –QA (quaternary amine) and –EDA from Bia Separations) have also been used to purify IgM from mammalian cell cultures, with recovery yields up to 85%.[57,58] CIM-QA and CIM-EDA discs can separate IgM from human plasma and can fractionate low

abundance plasma proteins.[59] Other approaches regarding IgM isolation have also been developed[31,60,61] using synthetic polymer monoliths.

1.2.1.1. Hydrogels and cryogels

Cryogels and hydrogels are synthetic polymer monoliths which can be defined as supermacroporous gels.[19] In cryogels, networks are formed by the cryogelation of monomers (e.g. GMA, allyl glycidyl ether (AGE)) at sub-zero temperatures using ammonium persulfate (APS) as an initiator and *N,N,N',N'*-tetramethylene diamine (TEMED) as the catalyst (Fig. 1.2 B). Hydrogels are formed by the polymerization of acrylamide (AAm), *N',N'*-methylenebisacrylamide (MBA) and AGE in an aqueous buffer which works as a porogen, just as in the formation of acrylamide gels for gel electrophoresis assays.[26] The use of GMA and AGE allows a direct introduction of epoxy groups enabling further functionalization with ligands or other synthetic and natural species.

The macroporous network of hydrogels and cryogels makes them very attractive for cell and antibody separation,[61] due to their higher porosity (up to 90%) and larger pore size (0.1–200 μm).[26,62,63,64] Unlike methacrylate or silica monoliths, cryogels and hydrogels have poor mechanical behaviour. Low material rigidity can be minimized through crosslinking procedures, physical blends or the addition of stiff polymers to the initial casting solution.[30]

Over the past decade, different polymeric cryogel systems such as AAm and MBA grafted with N,N-dimethylaminoethyl methacrylate (DMAEMA) and poly(methacrylic acid (MAA)-co-polyethylene glycoldiacrylate) embedded with polystyrene or poly(EDMA) nanoparticles have been prepared at sub-zero temperatures. Due to the large porous network, efficient separation of highly purification antibody from fermentation broth was achieved using affinity supermacroporous monolithic cryogels functionalized with Protein A.[64,65,66]

Poly(AAm-AGE) cryogels functionalized with concanavalin A (Con A) were able to capture IgG from pure aqueous solutions and human plasma, with high capacity (up to 25.6 mg g^{-1}) and eluent purity (85%).[67] Similar approaches were developed to purify IgM using polyHEMA cryogels activated with cyanogen bromide for further functionalization with Protein A. Due to their hemocompatibility, these systems enabled IgM and IgG isolation from human plasma with high reproducibility over repeated cycles.[68,69] In related work, Cibacron Blue F3GA and (IDA)-Cu^{2+} covering PGMA particles incorporated into the polyHEMA cryogel allowed IgG and albumin isolation from human serum with efficiency of 93.6 and 89.4%, respectively.[70] N-methacryloyl-(L)-histidine methyl ester (MAH) was selected to function as a pseudospecific ligand and as co-monomer simultaneously to prepare polyhydroxyethyl methacrylate-N-methacryloyl-(L)-histidinemethylester cryogel.[71] The MAH incorporation into the support elevated the specific surface area up to one hundred times and allowed the highest registered quantity of IgG adsorbed from human plasma (97.3 mg g^{-1} of cryogel) with an associated purity of 94.6%.

1.2.2. MONOLITHS BASED ON NATURALLY OCCURRING POLYMERS

Societal, environmental, and regulatory drivers are pressing industry to design engineered products from "cradle to grave".[71] This has been a driving force for the use of natural and biodegradable polymers at an industrial level. The most widespread natural polymers are polysaccharides, such as cellulose, chitosan and agarose.[71] The popularity of agarose beads as first-choice supports for traditional affinity chromatography stems from bead hydrophilicity and good chemical stability, even under extremes of pH.[9] Thus, it is not surprising that agarose has been used for monolith preparation.[72] Unfortunately, agarose based monolith supports exhibit poor mechanical properties, and at the time of writing they are only known as porous particles confined in a mold or as a macroporous gel.[72,73]

Chitosan (CHT) is also a natural polymer obtained by deacetylation of chitin originated from the xoskeleteon of crustaceans.[74] Chitosan has been extensively investigated in diverse fields of work[73,75] due to its nontoxic, antimicrobial, biocompatible, and biodegradable properties and sensitivity towards changes in pH.[76] Due to its high molecular weight, chitosan yields viscous solutions can be utilized to produce porous gels and structures through methodologies such as freeze drying and supercritical fluid technology.[20,75,77,78,79,80] Sun *et al.*[81] prepared chitosan-agarose cryogels *in situ* through cryopolymerization and linked 2-mercaptopyridine onto divinylsulfone-activated matrix, producing cryogels used to purify IgG. Cryogels presented interconnected pores of 10-100 μm size, a specific surface area of 350 m^2 g^{-1} and a high adsorption and elution capacity for IgG of 71.4 mg g^{-1} and 90%, respectively. These supports proved to be stable and reusable for more 10 cycles without substantial loss in their performance. More recently, Barroso *et al.*[82] prepared chitosan-based monoliths for IgG purification by combining freezing and lyophilization methods. The authors were able to improve the mechanical properties of chitosan through blending with poly(vinyl alcohol)(PVA) and by cryopolymerizing with GMA at sub-zero temperatures (Fig. 1.3). The supports were functionalized with a Protein A biomimetic ligand, through plasma technology, a free solvent technique. This sustainable and faster approach allowed high binding capacities (150±10 mg IgG g^{-1} support), and 90±5% recovery of the bound protein with 98% purity directly from cell-culture extracts.

Cellulose has also been employed in chromatographic procedures using cellulose derivatives in the form of discs/membranes retaining the possibility for further functionalization with different type of molecules for protein separation, and evaluation of affinity interactions.[83,84,85,86,87] Recently, Barroso *et al.*[88] prepared cellulose membranes/discs using an alternative approach to generate cellulose porous structures for different applications, namely that of human IgG purification.

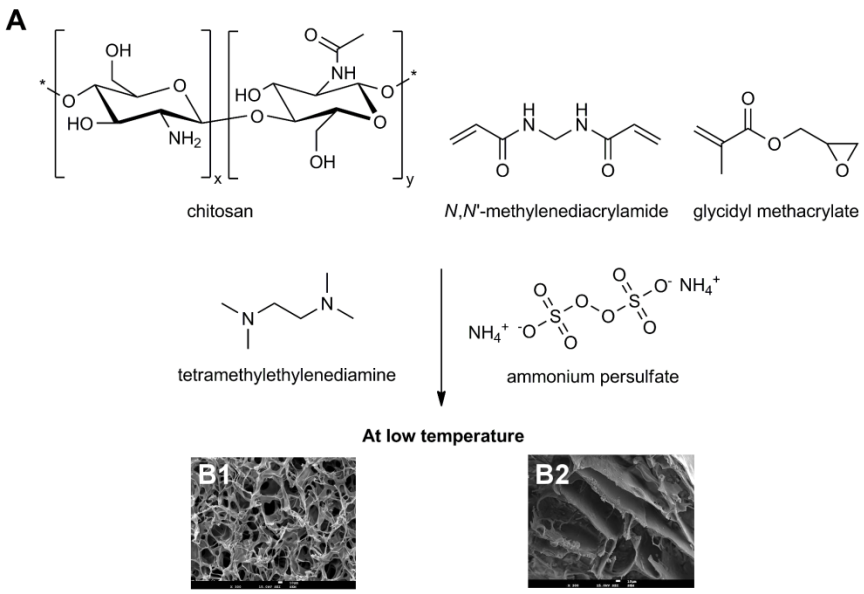

Figure 1.3 - (A) Schematic preparation of chitosan-based monoliths. (B1, B2) SEM micrographs of chitosan monoliths and chitosan cryopolymerized with glycidyl methacrylate (GMA) respectively,[82] adapted with the permission of The Royal Society of Chemistry.

Presently, the use of natural polymers for the preparation of chromatographic supports is still low, but this trend needs to be reversed in view of stricter chemical legislation regarding health and safety, thus pushing the industry towards greener and more sustainable processes. Table 1.3 provides a summary of the key supports, targets and separation criteria for the processes discussed above.

Table 1.3 - Monolithic materials for antibody purification.

Material	Mode	Ligand	Target	Surface area (m^2 g^{-1})	Flow rate (mL min^{-1})	Capacity	Recovery (%)	Purity	Ref's
GMA-EDMA	Affinity	Protein A	IgG, IgM, IgA	89.1	0.05; 1.0	20 (IgG) mg g^{-1}	99	High	[47] [49]
		Protein L	IgG	n.a.	1×10^{-5}	n.a.	n.a.	High	[45]
		Protein G	IgG	n.a.	0.05; 2.5	20 mg g^{-1}	n.a.	High	[49] [50]
		L-histidine	IgG	89.1	1.0	22.0 mg g^{-1}	n.a.	n.a.	[47]
	Anion Exchange	DEAE	MAbs	n.a.	1.0	n.a.	95.0	High	[51]
		EDA		n.a.	1.0	n.a.	91.4	High	[51]
	Ion Exchange	MAA	IgG	57.1	1.0-2.0	n.a.	98.8	Good	[48]
PG-PGE	Affinity	Protein A	IgG from rabbit serum	n.a.	n.a.	0.44 mg mL^{-1}	n.a.	n.a.	[49]
HEMA-MAH	Pseudo-affinity	(MAH)	IgG	145.8	1.0	96.5 mg g^{-1}	n.a.	95.3%	[53]
CIM-IDA	IMAC	Cu^{2+}/Ni^{2+}/Zn^{2+}/Co^{2+}	IgG/ Mab's	n.a.	2.0	n.a.	63/41/85/40	n.a.	[55]
	IMAC	Cu^{2+}/Ni^{2+}/Zn^{2}	IgG and Mab's	n.a.	3.0	0.5 mg mL^{-1}	82.4	n.a.	[89]
CIM	Pseudo-affinity	Peptide	IgM/IgG/ Mab's	n.a.	1.0-10	n.a.	83/67/95	n.a.	[56]
	Ion Exchange	QA/DEAE/EDA	IgM/IgG	n.a.	1.0-2.0	≈ 20 mg g^{-1}	n.a.	n.a.	[90]
			IgM	n.a.	n.a.	16-36 mg g^{-1}	n.a.	n.a.	[57]
DMAA-AGE cryogel	IMAC	IDA-Cu^{2+}	Fv antibody fragments from *E. Coli* cell culture	n.a.	n.a.	n.a.	84-96	High	[91]
	Affinity	Protein A	Cells bearing IgG antibodies	20.2	0.5	1.6×10^{6} cells mL^{-1} adsorbent	60-70	High	[68]
AAm-AGE cryogel	Affinity	Conc A	IgG	n.a.	1.0	25.6 mg g^{-1}	94	85%	[67]
	Afinity	Protein A	IgG labeled inclusion bodies	n.a.	0.5	n.a	n.a.	n.a.	[92]
HEMA-cryogel	Affinity	Protein A	IgM	20.2	0.5	42.7 mg g^{-1}	≥ 90	-	[68]
	IMAC	PGMA-IDA-Cu^{2+}		n.a.	0.5-2.0	257 mg g^{-1}	89.4	-	[93]
	Affinity	PGMA-Cibracron Blue F3GA	IgG	n.a.	0.5-2.0	342 mg g^{-1}	93.6	-	[93]
	Affinity	Protein A		n.a.	0.5-3.0	83.2 mg g^{-1}	85	85%	[69]
HEMA-MAH cryogel	Pseudo-affinity	(MAH)	IgG	n.a.	0.5-3.0	97.3 mg g^{-1}	80.7	94,6%	[93]
Chitosan-agarose	Affinity	2-mercaptopyridine	IgG	350	1.0	71.4 mg g^{-1}	90	High	[81]
Chitosan-PVA	Affinity	Artificial Protein A (Ligand 22/8)	IgG and MAbs	2.3	1.0	150 mg g^{-1}	90	98%	[82]

n.a.: not available

1.3 STRUCTURAL CHARACTERIZATION OF MONOLITHS

Ensuring optimal performance of a monolith based chromatographic medium requires accurate characterization to determine whether the monolith's morphological properties fall within the range of desired values. Thus, depending on the application, the best balance between porosity, pore size and surface area must be attained.[27] Larger pores decrease the available surface area and reduce the mechanical strength of the support. Conversely, smaller pores allow larger surface area and impart better mechanical integrity, albeit at the expense of lower fluxes and slower processes. One of the most critical issues is the pore size distribution. Various authors allude to the difficulty in producing monoliths with an acceptable degree of homogeneity.[94,95] Therefore, a number of methods have been described for evaluating the porosity within monolithic networks. These include scanning and transmission electron microscopy (SEM/TEM), mercury intrusion porosimetry (MIP), adsorption or desorption of nitrogen (AN/DN), and inverse size inclusion chromatography (ISEC).[30,96,97] However, all these techniques require a significant quantity (of the order of milligrams) of monolith sample to obtain representative results. Additionally, these analyses are often destructive. Electron microscopy samples require heavy metal sputter coating for analysis, while MIP requires samples to be impregnated with mercury. In case of studies evaluating adsorption or desorption of nitrogen, the samples may be destroyed through the degasification procedures and pressures employed during the analysis.

Developing non-invasive methods for characterizing monolith morphology has become a great challenge for some researchers. Petter *et al.*[98] utilized near-infrared spectroscopy to determine pore size, pore volume, total porosity and surface area in a single analysis. Although this technique is not destructive, it still does not provide comprehensive morphological detail such as potential wall defects and the degree of radial heterogeneity, both particularly important in evaluating monoliths as chromatographic devices.

The introduction of other recent techniques, such as scanning coupled contactless conductivity (sC4D) methods, confocal laser scanning microscopy, magnetic resonance imaging and small angle neutron scattering, offers innovative options to complement the aforementioned techniques in order to attain a thorough understanding of monolith structural features.[99,100,101]

1.4 PERFORMANCE EVALUATION OF MONOLITHIC PLATFORMS

Important key parameters that must be studied when developing new monoliths include static and dynamic binding capacity, scale up potential and resistance to cleaning and sterilization procedures.

An adsorption isotherm is a useful tool for estimating the maximum binding capacity to the target molecule as well as evaluating the level of non-specific adsorption.[102] By taking into account parameters describing the porous network, material and monolith surface area, different adsorption isotherms can be applied to achieve the best fit to the experimental data obtained through static studies.

To assess the monolith dynamic binding features and mass transfer, breakthrough curves obtained by frontal analysis are usually estimated. If breakthrough curves do not alter with feed concentration, or molecular dimension and velocity, it indicates that the adsorption is not restricted by mass transfer phenomena.[16] To obtain an effective mass transfer, the pores have to be sufficiently wide. For this reason, monoliths are ideal for the separation of antibodies and other biomolecules with diameters above ~5 nm, since it is technically difficult to produce particles with a pore size wide enough to allow permeation of these larger molecules.[25,27,103]

Regarding the cleaning and regeneration issues of monoliths, different protocols can be adopted according to the stability of the immobilized ligand and of the polymeric composition. Thus, cleaning and regeneration regimes need to be optimized for individual situations. However, the most common procedures employed involve the use of alkaline (0.1–1 M NaOH) and salt solutions (1–2 M NaCl) which contain competitor agents that force the removal of antibody and proteins from the monolithic supports. Alcohol solutions such as ethanol (up to 20%) and isopropyl alcohol (up to 30%) can also be used.[34,104] Moreover, the use of detergents (e.g. Tween 80) or organic solvents (acetone, ethanol, and isopropanol) may be required for sanitization of chromatographic media after use with particular feedstocks.

The pressure drop across monolith based media is typically lower than traditional beads or membranes. Monoliths used in biomolecules separation field should have a porosity higher than 50% allowing a pressure drop reduction of 50% compared with beads or membranes.[27]

An additional and also fundamental concern associated with monolith-based media is its scale up capability. This issue still needs to be addressed; however the preparation of monolithic devices capable of operating over multiple cycles without capacity loss is within the grasp of existing manufacturing processes.[105] Attachment of monolith to the column wall can also be challenging. Monoliths can be attached to a column with a flexible wall, though this set-up would prove cumbersome when working with high pressure gradients and high flow rates.[16,105] Concerns over column attachment may explain why silica monoliths are not yet available as industrial scale chromatography media. In marked contrast, the scale-up of CIM disks and tubes made from polymethacrylate has been widespread, since the preparation of these supports results in superior mechanical behaviour and resilience to aggressive regeneration conditions (e.g. 1 M NaOH). Thus, scale up is straightforward and amenable to biopharmaceutical process development strategies.[106]

At present, intermediate scale purification has been performed by linking monolith columns in parallel,[107] creating an array system with a volume capacity up to 1000 L. Effective scale-up from a 0.34 mL disk to 8 L radial columns and tubes is well established.[16] However, the incorporation of monoliths in industrial processes is still a challenge that deserves attention. In the near future it is expected that monoliths could increase processing capacity to directly compete with traditional chromatographic resins that are able to process hundreds of liters with high resolution. At the time of writing, 8 mL of a CIM monolith functionalized with Protein A is able to purify 10 mg IgG g^{-1} wet support, while 2 mL of Protein A agarose resin purifies 20 mg

IgG g^{-1} wet support. Thus, an improvement in monolith purification capacity is still required before large scale comparisons are attempted.

1.5 SUMMARY, CONCLUDING REMARKS AND FUTURE TRENDS

Interest in high-value biomolecules in medicine, pharmacology, biochemistry and diagnostics has resulted in the development of alternative systems for antibody isolation and purification. Monolithic support technology, though nascent, requires further maturation before its full potential can be exploited. The advantages and disadvantages of synthetic, cryogel and natural polymer monoliths are summarized in Table 1.4.

Up to now, silica-based monoliths have not been extended to antibody purification and therefore were not here included and discussed. However, silica-based monoliths have been applied to drug and chiral separations and for immunochromatography.[108,109]

The technologic transition in purification processes has already begun. There is a substantial amount of literature highlighting the virtues of monolithic supports. Commercially available monolith based chromatography media have demonstrated efficient biomolecule separation across a number of applications. Particularly, the successful technology may find a niche in the purification of antibodies of various formats. Additional work is needed to expand the range of ligands available, fine tune their immobilization and optimize the scale up of monolithic platforms.

Table 1.4 - Summary of monolithic platforms in antibody separation: pros and cons.

Monolith Base	Pros	Cons
Organic	High mechanical stability Easy preparation Numerous monomers available Easy scale up Easy ligands attachment	Some difficulties in processing biomolecules with high molecular weight (≥ 100 kDa)
Cryogels	High performance to process viscous fluids (e.g. blood and cells) Easy preparation	Low purification efficiencies for biomolecules with low molecular weight (< 100 kDa) Low mechanical properties Low surface area
Natural polymers	Easy preparation Tunable mechanical properties Biocompatible Biodegradable	Lack of processing methods

Protein A was known to biochemists long before its true potential as an antibody purification ligand was fully realized. This recognition resulted in a paradigm shift in biomolecular separations technologies. The recent advances in proteomics have led to the identification and classification of multitudes of new proteins with vital roles in living organisms. The call for technology to assist the efficient purification of large proteins from complex mixtures has never been greater. To meet this burgeoning demand, the time is ripe for the next leap in affinity supports. Monoliths may well prove to be the ideal bespoke chromatographic medium that takes

complex bioseparations from the research bench to sustainable large-scale industrial processes.

CHAPTER 2

BIOINSPIRED AND SUSTAINABLE CHITOSAN-BASED MONOLITHS FOR ANTIBODY PURIFICATION

SUMMARY

Chitosan-based monoliths activated by plasma technology induced the coupling of a robust biomimetic ligand, previously reported as an artificial Protein A, with high yields while minimizing the environmental impact of the procedure. Due to the high porosity, good mechanical and tuneable physicochemical properties of the affinity chitosan-based monoliths, it was possible to achieve high binding capacities (150 ±10 mg antibody per gram support), and to recover 90 ± 5% of the bound protein with 98% purity directly from cell-culture extracts. Therefore, the chitosan-based monoliths prepared by clean processes exhibited a remarkable performance for the one-step capture and recovery of pure antibodies.

Article published: *Telma Barroso, Ana C. A. Roque and Ana Aguiar-Ricardo, Bioinspired and sustainable chitosan-based monoliths for antibody capture and release. RSC Advances, 2012, 2, 11285–11294.*

Attended conference (poster apresentation): Telma Barroso, Ana C. A. Roque and Ana Aguiar-Ricardo, "Affinity porous structures for antibody purification" in Affinity, 2011, Tavira-Portugal.

Attended conference (oral apresentation, key note): Telma Barroso, Ana C. A. Roque and Ana Aguiar-Ricardo, "Bioinspired affinity monoliths: a fast and efficient alternative system for antibody purification" in European Society of Biochemical Engineering Sciences (ESBES), 2012, Istanbul-Turkey.

2.1. INTRODUCTION

Antibody-based biopharmaceuticals will be a major source of new therapies for at least the next 10 years.[4,110] The large number of antibody products in development certainly supports the case for optimized antibody manufacturing approaches. However, the large quantities in which some antibody products are required put considerable pressure on current manufacturing facilities.[69,111,112]

In particular, current purification processes are struggling to equal the high productivities already obtained in upstream antibody production. Affinity chromatography using Protein A from *Staphylococcus aureus* is the method of choice for antibody capture during the purification process.[4,110] However, protein A resins utilized in chromatography are expensive adsorbents with low stability, often causing the leaching of the affinity ligand together with the antibody product.[4,16,69] Thus, synthetic affinity ligands mimicking biological receptors have been developed in an attempt to overcome Protein A drawbacks.[113] Ligands based on a triazine scaffold, in particular ligand 22/8 or artificial protein A, are known to be low cost and highly resistant to the harsh conditions employed during CIP and SIP. [10,113] Ligand 22/8 has been immobilized on agarose,[113] cellulose membranes,[88] and magnetic particles,[114] and shown to selectively bind to hIgG when employed in chromatographic processes.

With the need to treat large volumes of concentrated antibody solutions, fast processes with high selectivity are desired.[18,40,115] Monoliths are porous materials cast in a single block and inserted into a chromatography housing. These porous supports have been successfully employed in the purification of biological species.[16,116,117,118,119] As convective transport is prevalent when using monoliths, faster volumetric throughput rates are achieved thus increasing the process speed and productivity.[40]

The aim of this work was to combine the robustness of synthetic affinity ligands, namely ligand 22/8, with monolith blocks prepared from biopolymeric materials, in particular chitosan (CHT). In addition, sustainable chemistry options have been adopted for the preparation and functionalization of the materials based on freeze-drying method[120,121] and plasma technology,[122,123,124] respectively. In particular, freeze drying processes work by freezing the casting solution and then reducing the surrounding pressure to allow the frozen water in the material to sublimate directly from the solid phase to the gas phase, resulting in attractive porous structures.[125] On the other hand, plasma technology is a fast and solvent free technique which allows surface modification through the introduction of chemical species.[122,123,124,125,126] Recently, plasma surface activation was combined for the first time with supercritical fluid technology to surface-graft stimuli-responsive hydrogels on differently shaped devices.[127] Herein, plasma surface activation was extended to introduce radicals on monolith surfaces for further coupling with the affinity ligand. The materials produced have been characterized in terms of morphological, mechanical and physicochemical properties, and have shown to recover antibodies directly from crude cell samples. CHT has been selected due to its nontoxic, antimicrobial, biocompatible, and biodegradable properties, as well as its pH sensitive behavior.[128] Owing to a high molecular weight, CHT forms viscous solutions in dilute aqueous

acetic acid that can be used to produce porous structures. The tensile strength of these structures can be improved through crosslinking with epichlorohydrin[129] or glutaraldehyde,[77,78] copolymerization with other monomers, or via blending.[130,131] In this work CHT was copolymerized (cryo-polymerization) with GMA at low temperatures in order to produce well defined porous monoliths with good tensile strength. PVA was also blended with CHT as an alternative strategy to improve the mechanical performance of CHT monoliths. The processing of these renewable materials into 3D structures with tuneable and controlled morphological and mechanical properties, and their subsequent functionalization with a low cost affinity ligand through green methodologies will offer a great contribution in materials design for bioseparation processes. This integrated process aims to replace traditional practices of monolith preparation and functionalization by new ones where the integrity of the support is maintained from its conception to its application even at industrial scale.

2.2. EXPERIMENTAL AND METHODS

2.2.1. MATERIALS

Ammonium peroxodisulphate (APS, purity≥98%), citric acid (purity≥99%), disodium hydrogen phosphate monodibasic (pro analysis), disodium hydrogen phosphate dibasic (pro analysis), disodium tetraborate, ethanol absolute and sodium citrate dihydrate were purchased from Merck. Isopropanol and sodium bicarbonate were purchased from Riedel-de-Haen. Acetone (purity≥99%), and ethyl acetate were supplied by Roth. Acetic acid (purity≥99%), Aminocaproic acid, 3-aminophenol, 4-amino-1-naphthol hydrochloride, cyanuric chloride (purity≥98%), 1,6-hexanediamine (purity≥98%), *N,N*-dimethylformamide (DMF), dimethylsulfoxide (DMSO), glycine, ninhydrin, potassium cyanide, pyridine, sodium hydroxide (purity≥99%) were purchased from Sigma Aldrich. Chitosan (75≈85% deacetylated, medium molecular weight), poly(vinyl alcohol) (purity≥99%), *N,N*-methylenebisacrylamide (MBAm, purity≥85%), *N,N,N',N'*-tetramethylethylenediamine (TEMED, purity≥99%), bicinchoninic acid (BCA) kit, bovine serum albumin (BSA) (purity≥98%) were supplied by Sigma Aldrich. Human IgG was purchased by Octapharma (Gammanorm, purity≥99%).

2.2.2. MONOLITHS PREPARATION

Chitosan-based monoliths were prepared blending different ratios of chitosan (0–100% (wt per wt)) with PVA (0–50%) and GMA (10%) in acetic acid aqueous solution (1% v per v). The crosslinker agent, MBA, was also added (2% (wt per wt)) and different casting solutions were placed in glass tubes and stirred until homogeneous casting solutions were obtained. After the initiator and catalyst, TEMED (23 µL) and APS (40 µL) respectively, were added to promote the crosslinking process that occurred at 0 ºC during 30 min under stirring.

The casting solutions were frozen at -80 ºC during 12 h and were lyophilized (Telstar cryodos-50) until dry.[132,133,134,135]

2.2.3. MONOLITHS CHARACTERIZATION

Chitosan-based monoliths morphology was investigated using scanning electron microscopy (SEM) in Hitachi S 2400 equipment with an accelerating voltage set to 15 kV. The samples were frozen and fractured in liquid nitrogen for cross-sectional analysis and gold coated before analysis. Chitosan-based monoliths porosity, average pore size diameter and surface area were determined by MIP (Micromeritics, autopore IV). Water fluxes were determined at 25 ºC and by varying the applied hydrostatic pressure (within 0–0.4 MPa) using a stainless steel high-pressure cell (with an effective volume of 1.2 cm^3). At least three measurements of distilled water flux were performed for each monolith. The permeability (L_p) of chitosan-based monoliths was obtained by the slope of linear relation between flux (F) and pressure (p), and is given by Darcy Law,[88] represented by:

$$F = L_p \times \Delta p$$

(Equation 2.1)

The wet and dry densities were determined through the ratio of wet weight as well as dry weight of the chitosan-based monoliths with respect to their volume. The apparent density in g cm^{-3} was calculated by the equation below as described by Tripathi *et al.*[118,119]

$$\rho = \frac{W}{\pi} \times \frac{D^2}{4} \times H$$

(Equation 2.2.)

where W is the weight of monolith sample in grams, D is the diameter of the sample in cm and H is the thickness of the sample in cm.

Uniaxial compression was used to determine the mechanical properties of the monoliths using tensile testing equipment (MINIMAT firmware v.3.1) at room temperature. Samples were prepared in a cylindrical shape (10 mm in diameter thickness). The length between clamps was set at 5 mm, the speed set to 1 mm min^{-1}, a full scale load of 20 N and maximum extension of 90 mm was used. The compression modulus was calculated from the slope of the linear portion of the stress-strain curve:[88]

$$Stress = \sigma = \frac{F}{A}$$

(Equation 2.3)

$$Strain = \varepsilon = \frac{\Delta l}{L}$$

(Equation 2.4)

where F is the applied force, A the cross sectional area, Δl is the change in length and L is the length between clamps. All samples were tested in dry state at room temperature.

2.2.4. MONOLITHS FUNCTIONALIZATION

The chitosan-based monoliths followed two different activation strategies for ligand 22/8 immobilization. The first one involved the introduction of reactive epoxy groups on monoliths by epoxy activation. CP (chitosan-poly(vinyl alcohol) monolith) and CG (chitosan-glycidyl methacrylate monolith) monoliths were covered with distilled water (10 mL), NaOH (72 µL, 0.1 M) and epichlorohydrin (0.83 mL) and then incubated for 3 h at 35 ºC on a rotary shaker (140 rpm). After incubation, the epoxy-activated chitosan-based monoliths were washed with distilled water (200 mL). The epoxy activation content was determined by adding sodium thiosulfate (3 mL, 1.3 M) to 1 gram of epoxy-activated chitosan-based monoliths and incubating them at room temperature for 20 min. This mixture was neutralized with HCl (0.1 M) and the amount of HCl was registered. The volume of HCl added corresponded to the amount of hydroxyl ions released. The second strategy (Fig. 2.1) involved the use of plasma treatment which was carried out in a radio frequency plasma reactor (Plasma system FEMTO, version 5). Native chitosan-based monoliths were introduced in a plasma chamber which was thoroughly purged with a continuous flow of argon to reduce trace amounts of air and moisture. During the treatment, the argon flow was adjusted in order to keep a constant pressure of 0.3 Torr inside the chamber.[122] A power of 60 W was applied over 5 min. At the end of the experiment the plasma chamber was ventilated and the activated samples were immediately introduced in an aqueous solution of 1 6-hexanediamine to be aminated. Activated chitosan-based monoliths reacted with an excess of 1 6-hexanediamine in water for 24 h at 45 ºC, and then thoroughly washed with water in order to remove residues of 1 6-hexanediamine which did not react. The extent of amination was determined using the Kaiser test.[88] This test is a colorimetric assay to quantify free amine groups and is based on the reaction of ninhydrin with primary amines, which gives a characteristic dark blue color. To perform the Kaiser test, each following reagents i) 80% crystalline phenol in ethanol (w/v), ii) 2% aqueous solution of potassium cyanide (0.001 M) in pyridine (v/v) and iii) 5% ninhydrin in ethanol (w/v) were added (50 µl of each one) to the aminated chitosan-based monolith samples (1 mL). The samples were then placed in a water-bath at 100 ºC during 5 min. The calibration curve was represented by standard solutions of glycine (0–5 µmol mL^{-1}) and the absorbance measurements of the samples (diluted 1:18) were performed at 560 nm. For ligand 22/8 immobilization, an excess of ligand 22/8 (3 equiv. to the amination content, 530 µmol, 200 mg), was added to the aminated chitosan-based monolith samples (approximately 60 mg) in water–DMF (1:2). The volume of solvent used was sufficient to cover the chitosan-based monoliths, and the solution was incubated on a rotary shaker (140 rpm) for 72 h at 85 ºC. The synthesis of ligand 22/8 followed the procedure described by Teng *et al.*[113] and Barroso *et.al.*[88] The synthesis of ligand 22/8 was confirmed by ^{1}H and C-NMR and FT-IR. Functionalized chitosan-based monolith samples were then washed with water–DMF (1:2) until the absorbance at 270 nm was zero.

In order to assure a complete exclusion of non-absorbed ligands into and onto chitosan-based monoliths, functionalized samples were introduced in a Varian column (a reservoir with 3 mL of capacity) and were submitted to several washes with water–DMF (1:2) and to CIP. The CIP

consisted of washing functionalized chitosan-based monoliths with NaOH (1 M) until the absorbance at 270 nm be zero, with water (10 mL), then with regeneration buffer (NaOH 0.1M in 30% of isopropanol) until the absorbance at 270 nm be zero, and finally, again with distilled water (10 mL). The functionalized chitosan-based monoliths were equilibrated with sodium phosphate buffer (50 mM, pH 8.0) and sodium citrate buffer (50 mM, pH 3.0) until the absorbance at 270 nm be zero. The extinction coefficient of ligand 22/8 was determined at its maximum absorbance wavelength (ε270 = 10.72 L g^{-1} cm^{-1}), respectively. The ligand 22/8 density was determined by subtracting the amount of ligand contained in all the washing liquors from the initial ligand used in the immobilization step. The chitosan-based monoliths containing ligand 22/8 were characterized in terms of morphological and mechanical properties as referred previously.

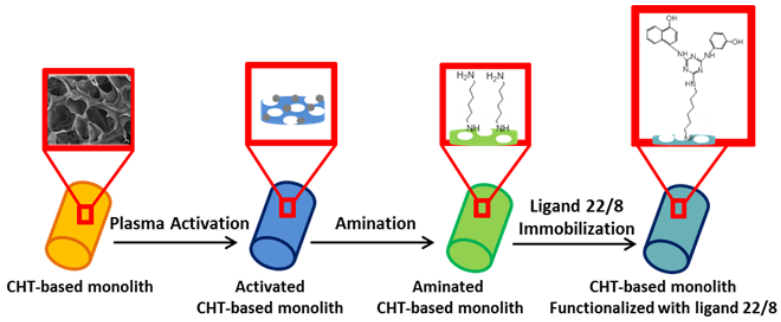

Figure 2.1- Schematic representation showing the functionalization strategy of chitosan-based monoliths with ligand 22/8 using non-thermal plasma surface activation.

2.2.5. STATIC PARTITION EQUILIBRIUM EXPERIMENTS

Partition equilibrium experiments were performed in a batch system as described by Barroso *et al.*[88] The adsorption of hIgG and BSA on the chitosan-based monoliths was investigated using a sample of native and functionalized chitosan-based (10 mg) monoliths varying the concentration of hIgG and BSA (0.0–45 mg mL^{-1}, 400 µL) in phosphate buffer (50 mM, pH 8.0) solutions. All experiments were conducted in duplicates at 25 ºC, at a stirring rate of 200 rpm during 12 h. At the end of this period, the native and functionalized chitosan-based monoliths were removed from the medium. The amount of adsorbed hIgG and BSA was determined by measuring the initial and final concentrations of hIgG within the adsorption medium. A calibration curve was prepared using hIgG and BSA in phosphate buffer solutions (50 mM, pH 8.0) (0.0–45 mg mL^{-1}). The concentration of protein was measured at 280 nm on a microplate reader (Tecan Infinite F200, filter, l = 280 nm). The adsorption phenomenon followed the Langmuir–Freundlich model[102,136] and it was represented by:

$$q = \frac{Q_m \times (C)^n}{K_d + (C)^n}$$

(Equation 2.5)

where K_d is the apparent dissociation constant (M) that includes contributions from ligand binding to support, Q_m is the maximum binding capacity (mg protein g^{-1} support), C is the concentration of protein in the liquid at the equilibrium (M) and n represents the Langmuir–Freundlich coefficient.

2.2.6. FRONTAL ANALYSIS-BREAKTHROUGH CURVES AND BINDING CAPACITY

The dynamic loading capacity of the packed columns with native and functionalized chitosan-based monoliths was determined using frontal analysis according with the equation below.[6]

$$Q = \frac{V_e}{[Protein]_{plateau}}$$

(Equation 2.6)

where Q corresponds to the estimated adsorbent capacity and V_e corresponds to the elution volume.

This technique consisted in loading hIgG and BSA solutions (8 mL, 0.5 mg mL^{-1}) in sodium phosphate buffer (50 mM, pH 8.0) through the equilibrated monolithic packed columns at different flow rates, 1 and 2 mL min^{-1} until the protein concentration of the output and input streams were identical. Then, packed monolithic columns were washed with phosphate buffer (50 mM, pH 8.0) and the bound protein was eluted with sodium citrate buffer (50 mM, pH 3.0). Each collected millilitre during loading, washing and elution steps were analysed by absorbance at 280 nm, using a microplate reader, in order to estimate the amount of protein bounded and eluted.

2.2.7. CHROMATOGRAPHIC EXPERIMENTS

In order to estimate the capacity of functionalized chitosan-based monoliths, Varian columns (with a capacity of 3 mL and an effective volume of 1.2 cm^3) were packed with these polymeric affinity structures. The columns were connected to a peristaltic pump using rubber tubing in order to allow flow control. The affinity capturing experiments were performed in a step-wise adsorption–desorption process by switching eluents at room temperature and at atmospheric pressure. Packed columns with functionalized chitosan-based monoliths were loaded with 1 mL of hIgG and BSA solution (5 mg mL^{-1}) in order to estimate the capacity of the columns for each protein. Then, columns were washed with sodium phosphate buffer (50 mM, pH 8.0) until the absorbance measured at 280 nm reached ≤0.005, in order to remove all the protein physically adsorbed. The bound protein was eluted and recovered with sodium citrate buffer (50 mM, pH 3.0). Packed columns with functionalized chitosan-based monoliths were then regenerated as described above in order to be reused. These chromatographic experiments were repeated during 3 cycles and one more after auto-claving in order to evaluate the column capacity over time. The total amount of IgG bound, eluted and regenerated from the chitosan-based monoliths

was initially determined by absorbance measured at 280 nm and by the BCA (microplate reader assay). As the results were consistent only absorbance measured at 280 nm was further used for protein quantification.

2.2.8. PURIFICATION OF MONOCLONAL ANTIBODIES FROM MAMMALIAN CRUDE EXTRACTS

In order to evaluate the possibility to capture directly antibodies from non-clarified crude extracts, packed columns with native and functionalized CP monoliths were loaded with a mammalian crude extract solution (1 mL, 1.3 mg of total protein per millilitre). After crude extract loading, packed columns were washed with the sodium phosphate buffer (15 mL, 50 mM, pH 8.0) until the absorbance measured at 280 nm reached ≤0.005, and the bound protein was after eluted and recovered with sodium citrate buffer (50 mM, pH 3.0). All collected samples were analysed by the BCA assay in order to quantify the amount of total protein bound and eluted from the solid support. The BCA assay consists in adding the BCA working reagent (200 µL) to the samples (25 µL). The microplates were incubated in the dark for 30 min at 37ºC. A standard curve was determined for each assay (200–1000 µg mL^{-1}). SDS-PAGE was performed on acrylamide gel (12.5%) in Tris-Glycine buffer system pH 8.3. Electrophoresis apparatus (from BIO-RAD) was connected with power supply at 120 V, 190 mA for 1 h. The gel was revealed using a silver staining kit from BIO-RAD.

2.3. RESULTS AND DISCUSSION

2.3.1. PREPARATION AND CHARACTERIZATION OF NATIVE CHITOSAN-BASED MONOLITHS

Supports for protein separation must ideally possess high hydrophilicity, chemical and mechanical resistance, a narrow pore size distribution, as well as enough reactive functional groups for ligand attachment.[4,40] In this work, chitosan-based monoliths were prepared by a combination of freezing and lyophilization methods and further evaluated according to their morphological and mechanical properties. It is known that the macromolecular morphology of monoliths is influenced by the conditions employed during their preparation - in general, the freezing and lyophilization processes generate open pore microstructures with a high degree of interconnecting pores in the composite materials. Large pores and high interconnectivities contribute to high fluxes across the materials and faster bioseparation processes.[120]

Native monoliths prepared only with chitosan (CHT_N) present regular and spherical pores (data not shown); the addition of PVA facilitates the formation of monoliths (CP_N) with large and semi-spherical pores (Fig. 2.2 A), while the copolymerization of GMA (CG_N) generates even larger and more elongated pores (Fig. 2.2 B).

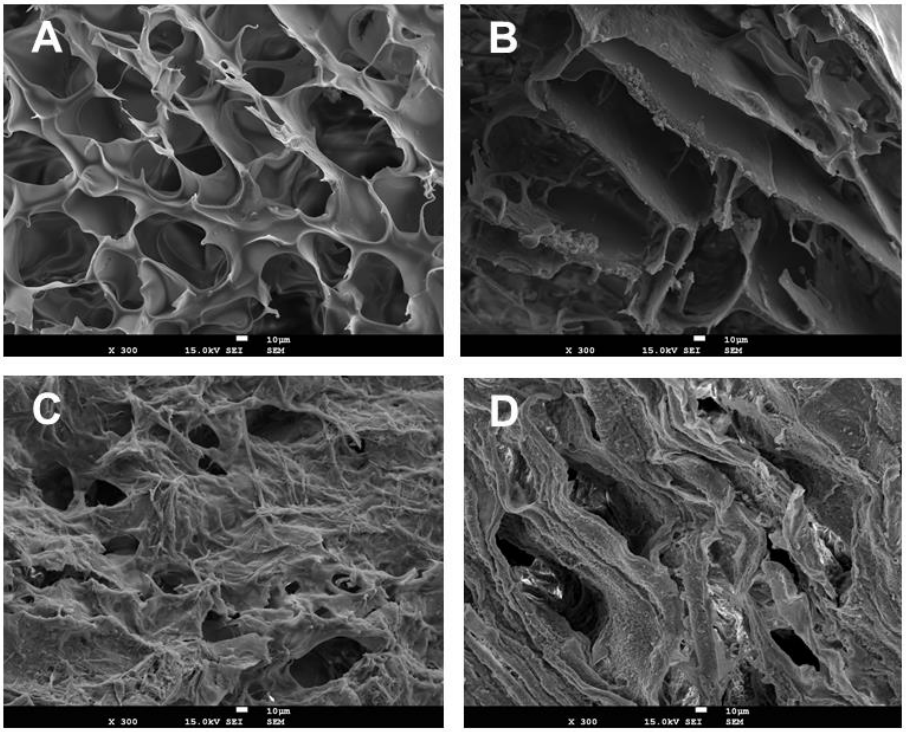

Figure 2.2 - SEM images of chitosan (CHT) based-monoliths before and after functionalization with the ligand 22/8: (A) CP_N, native monolith prepared from chitosan and poly(vinyl alcohol)(CP); (B) CG_N, native monolith prepared from chitosan and glycidyl methacrylate (CG); (C) CP_22/8, CP monolith functionalized with ligand 22/8 and (D) CG_22/8, CG monolith functionalized with ligand 22/8. All the images have a magnification of 300 and the scale bar in white indicates 10 µm.

In order to look deeper into the porous network prepared, analysis by MIP was performed. The average pore size diameter for CHT_N monoliths is 17 µm, while those of CP_N and CG_N monoliths are 53±5 and 123±5 µm, respectively (Table 1), which corroborate the conclusions taken from SEM image analysis. The porosity values are similar for all chitosan-based monoliths, varying between (70–75)±5%, which was expected due to the constant temperature conditions employed during monolith preparation. Typically, the pore size decreases with the decrease of freezing temperature.[120,121] During the freezing process, water ice crystals are formed and separate from the solutes which will be confined to the interstitial regions between ice crystals. Large ice crystal formation is expected in less viscous casting solutions and higher freezing temperatures, and the opposite is also true.[121] In this work, chitosan-based casting solutions were frozen at -80 ºC, a temperature at which a low average pore size diameter-between 20 and 100 µm is obtained.[40,121] This average pore size diameter is within the range of interest for the purpose of the work. Concerning bioseparation applications, monoliths with large pores and high porosities are required to enable the fast permeation of cellular components and proteins present in crude samples.[132] Therefore a delicate balance between pore size diameter, porosity and surface area is needed during monolith design. If monoliths have larger pores (≥150 µm) the surface area available for further functionalization decreases, leading to a low density of the affinity ligand.[40,121,135] Also, a decrease of specific surface area with increasing average pore size diameter is expected.

Table 2.1 - Morphological and mechanical characterization of chitosan-based monoliths before and after functionalization with ligand 22/8. All data was obtained from triplicated measurements.

Monolith	Average pore size diameter (μm) [a]	Porosity (%)[a]	Surface Area ($m^2 g^{-1}$) [a]	Permeability (L m^{-2} h^{-1} atm^{-1})	Density ×10^{-3} (g cm^{-3})		Compressive Modulus (kPa)	
					Dry	Wet	Dry	Wet
CP_N	53±5	70±5	1.3±0.1	294±15	4±2	165±10	0.41±0.5	0.2±5
CG_N	123±5	75±5	0.9±0.1	390±5	3±2	177±5	0.26±0.5	n.a[b]
CP_22/8	45±5	68±5	2.3±0.2	123±15	3±2	146±5	14±5	9±4
CG_22/8	85±10	60±10	1.5±0.2	323±10	5±2	131±10	8±2	4±2

[a]: Determined for dried monoliths by mercury porosimetry analysis.
[b]: The mechanical assay was impossible to perform due to high swelling of CG_N

The monoliths inner surface area (total pore area) is within the range of values of similar 3D porous structures reported in the literature.[132,133,134] The permeability and the compressive modulus of native chitosan-based monoliths are included in Table 2.1. The highest permeability value is registered to CG_N monolith, 390 L m^{-2} h^{-1} atm^{-1}, followed by CP_N and CHT_N monoliths with permeability values of 294 and 142 L m^{-2} h^{-1} atm^{-1}, respectively. These results indicate a clear concordance between the permeability of the materials and their morphological properties, and also a good interconnectivity between the pores. The density of the dried and wet chitosan-based monoliths (Table 2.1) was calculated by measuring the weight and dimensions of the prepared materials. Dried native chitosan-based monoliths present similar values of density. Wet native monoliths also showed similar densities although 50 times greater than the dried ones, due to their huge water uptake ability. The compressive mechanical properties were studied by uniaxial compression measurements also under dry and hydrated conditions. The compression modulus (kPa), given by the slope of stress–strain curves, translates the material stiffness (Table 2.1). In general, a high compression modulus indicates a stiffer material.[136] Native CHT-based monoliths present lower compression modulus values when compared to the functionalized materials. In more detail, CP_N monoliths at different stages, wet or dry, always present higher values of compression modulus than CG ones. The hydrated CG_N monolith exhibits a huge swelling and consequently becomes fragile, losing the initial integrity. These results are consistent with the morphological and mechanical properties previously discussed - supports with lower average pore size diameter and porosity are more rigid and present higher compression modulus. It is also known that the compression modulus of porous structures prepared at higher freezing temperatures (e.g. -30 and -20 ºC) are lower than those prepared at -80 ºC, due to the smaller pore size attained at this temperature.[132,133,134] Another factor that can influence the support stiffness is the water absorption ability, and the proof of it is the dramatic decrease of mechanical properties observed for monoliths in the hydrated sate.

2.3.2 PREPARATION AND CHARACTERIZATION OF AFFINITY CHITOSAN-BASED MONOLITHS

Several methodologies for affinity monoliths activation and ligand coupling have been described by diverse authors.[4,40] Herein the functionalization of chitosan monoliths with a triazine-based ligand (ligand 22/8) followed two different strategies. The first one was based on the optimized procedure for agarose[113] and also applied to cellulose membranes[88] due to the similarity in the chemical composition of these supports, namely the high content of free hydroxyl groups.

Native chitosan-based monoliths were activated with epichlorohydrin in order to add epoxide functionality for subsequent amination. As this epoxyactivation procedure occurs through the reaction of epichlorohydrin with free OH groups, the density and availability of OH groups determine the extension of the epoxide functionality achieved. The epoxy activation yielded densities for CHT, CP and CG were 187±51, 226±72 and 364±100 μmol g^{-1} of moist monolith, respectively. These epoxy densities are significantly higher than those reported in the literature for agarose (50 μmol of epoxy per gram of moist weight gel)[113] and for cellulose membranes (130±10 μmol of epoxy per gram of moist membrane)[88]. The second strategy consisted of the activation of native chitosan-based monoliths by argon (Ar)-plasma treatment. Plasma treatment is a solvent free technique which allows the surface modification according to the gas and power applied.[122] In this work, Ar-plasma treatment introduced radicals onto the chitosan materials for subsequent reaction with 1,6-diaminohexane in batch system out of plasma. The latter acts as a spacer arm[112,113] between the surface of the epoxy or plasma activated chitosan-based monoliths and the small biomimetic ligand 22/8, contributing to an optimal interaction between the ligand and the target protein (Fig. 2.1). The amination values achieved were significantly higher for all chitosan-based scaffolds activated by plasma treatment (Table 2.2).

Table 2.2 - Functionalization of monoliths with amine groups using either the traditional or the plasma activation routes and surface density of affinity ligand achieved by non-thermal plasma activation of the supports.

Monolith	**Epoxy activation**	**Plasma activation**	**Plasma activation**
	[NH_2] (μmol g^{-1} support)	[NH_2] (μmol g^{-1} support)	Ligand 22/8 immobilization (μmol g^{-1} support)
CP	226 ± 72	1747 ± 47	910 ± 17
CG	364 ± 100	906 ± 246	667 ± 24

The maximum amount of amines introduced using epoxy activated chitosan-based monoliths was 364±50 μmol g^{-1} support. In marked contrast, using the new approach based on plasma surface activation this value increased almost 5-fold (1747±47 μmol g^{-1} support). Due to these remarkable yields of amination, chitosan-based monoliths activated by plasma treatment were subsequently coupled with ligand 22/8. This ligand was prepared following the procedure

described by Lowe and colleagues[113] and was immobilized onto the aminated chitosan-based monoliths still containing a labile chloride on the triazine ring for nucleophilic substitution. Different yields of ligand immobilization were obtained (Table 2.2), according to the monolith materials. Although the highest value of ligand immobilization was obtained for the CP monolith, 910±17 μmol g^{-1} support, CG monolith also presented a very high functionalization ratio, 677±24 μmol g^{-1} support. The different ligand densities on CP and CG monoliths can be related with the surface area available in each support. CP monoliths have a smaller pore size diameter and porosity than CG monoliths suggesting that CP supports have higher surface area available for further functionalization. These facts contributed to a decrease of possible active sites in CG monoliths, and consequently to lower ligand density compared to the CP ones. Herein, the density of ligand 22/8 immobilized in chitosan-based monoliths was 10-fold the value reported for ligand 22/8 immobilized in agarose beads,[10,113] 70-fold on cellulose membranes,[88] and less than 2-fold on magnetic nanoparticles.[114] It can also be noted that, in general, the density of immobilized ligand 22/8 is quite high when compared to the values obtained for immobilized natural ligands.[47,129] To the best of our knowledge, this is the first report on the preparation of affinity monoliths with such a high ligand density. After ligand 22/8 immobilization, the morphological and mechanical properties of chitosan-based monoliths were evaluated. SEM images represented in Fig. 2.2 C and D show that the porous network and architecture did not change significantly after the functionalization procedure proving the potential of the new strategy developed in this work. The average pore size diameter, porosity and surface area values obtained for affinity CP_22/8 and CG_22/8 monoliths registered in Table 2.1 were kept approximately within the combined experimental errors. Permeability values obtained for CP and CG monoliths decreased from 294 to 123 L m^{-2} h^{-1} atm^{-1} for CP_22/8, and from 390 to 323 L m^{-2} h^{-1} atm^{-1} for CG_22/8 monoliths. The flow reduction can be explained by the presence of the affinity ligand which confers a hydrophobic character to the supports. However, it should be noted that the permeability still shows the target values for separation processes whilst allowing enough residence time for the contact between the protein and the support.[112] The apparent density of dried affinity monolithic supports did not change compared to the native ones at the same conditions, while wet monoliths showed a slight increase.

After functionalization, CP_22/8 and CG_22/8 registered a decrease in density values which can be also explained by the hydrophobic nature of ligand 22/8 leading to a reduction in water uptake capability. The compressive modulus increased (~10-fold) for all monoliths after ligand coupling (refer to Table 2.1). The improvement of the monolith mechanical properties whether in dry or wet conditions was expected as the incorporation of a synthetic ligand confers rigidity and robustness to the monoliths. Therefore, the sustainable functionalization strategy of the monoliths based on plasma activation, and further ligand 22/8 coupling is able to keep most morphological properties of the native supports while improving their mechanical properties.

In order to evaluate the stability of the affinity monoliths at typical operating conditions used during purification processes, monoliths were incubated at several pH solutions (from pH 1 to 12), corresponding to those employed in equilibration, elution, regeneration and cleaning-in-

place of chromatographic matrices. The amount of ligand released from the support was monitored (Fig. 2.3). The maximum amount of ligand 22/8 released from CP_22/8 and CG_22/8 was 12% and 7%, after 4 and 2 h of incubation, respectively (Fig. 2.3 A and C). In particular, at the pH conditions used in the binding and elution of antibodies from ligand 22/8 supports, pH 3 and 8 respectively, the greatest amount of ligand leaching was observed after 2 and 4 h, for CP_22/8 and CG_22/8, respectively. In general, the maximum time of monolith exposure to these conditions during a typical purification run is 30 min, far below the threshold time for ligand leaching, which was only observed after 2 h of exposure. On the other hand, the highest loss of ligand from CP_22/8 and CG_22/8 occurs with sodium hydroxide solutions after 2 h (Fig. 2.3 B and D). Nevertheless the maximum contact time of each functionalized monolith at these harsh conditions (CIP conditions) is about 10–20 min, the time at which no ligand release was registered.

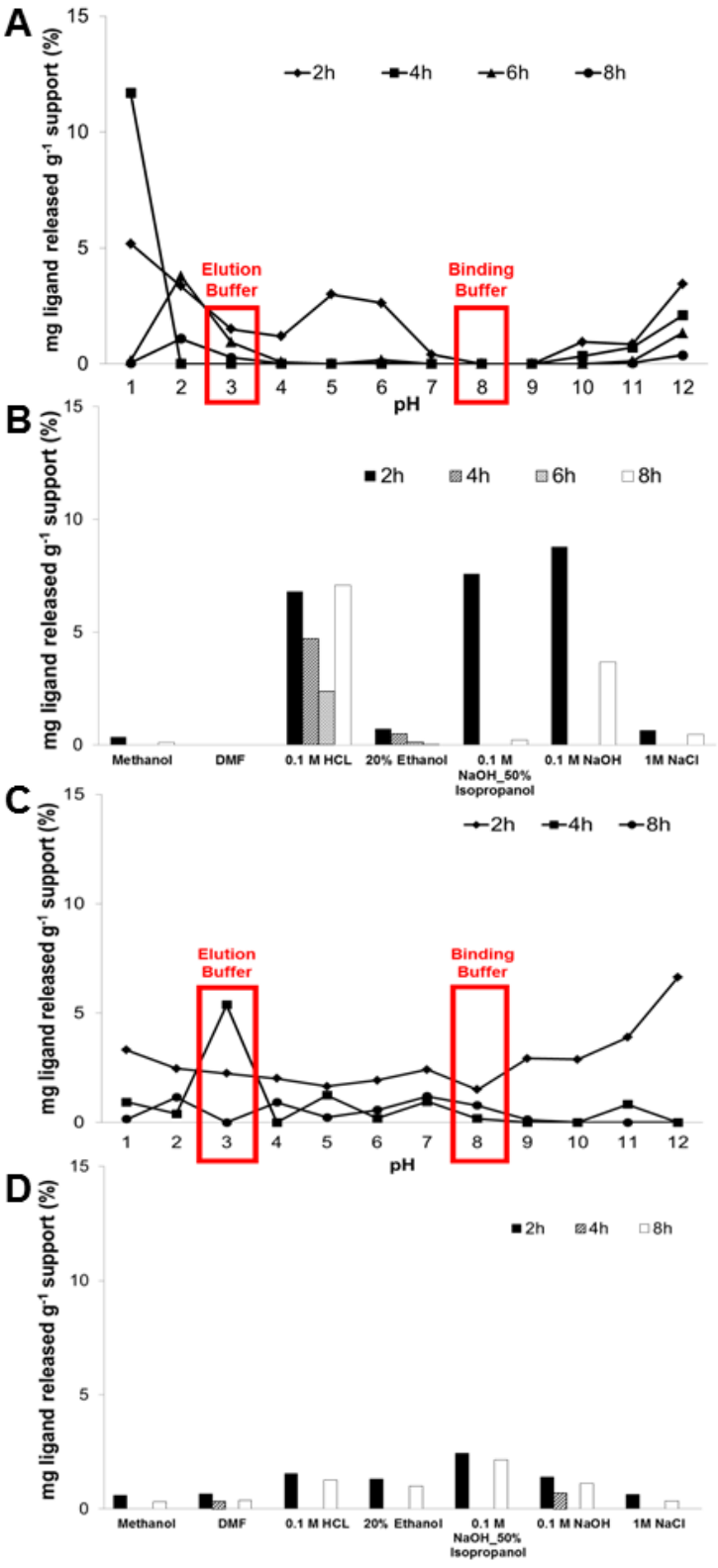

Figure 2.3 - Stability evaluation of CP_22/8 (A and B) and CG_22/8 (C and D) monoliths immersed over 12 h in solutions typically used during cleaning-in-place (CIP) procedures, including solutions with pH values between 1 and 12. All data was obtained from duplicated measurements with errors of ±5.

2.3.3. EVALUATION OF AFFINITY MONOLITHS FOR ANTIBODY PURIFICATION

To evaluate the affinity constants for hIgG and BSA on native and functionalized chitosan-based monoliths, static partition equilibrium measurements were performed in duplicate. To attain the equilibrium between proteins and affinity supports,[115] partition equilibrium studies were performed in a batch system over 12 h, varying the protein concentration.

The experimental data was fitted using a Langmuir–Freundlich isotherm that is the indicated model for porous structures with heterogeneous morphology.[102] Different affinity constants (K_a), theoretical maximum capacity (Q_{max}) and Langmuir–Freundlich coefficients (n) were obtained (Fig. 2.4) with errors of ±0.5, ±40.0 and ±0.1, respectively. The affinity monoliths always presented higher values of K_a and Q_{max} (14 and 3-fold, respectively) when compared to the native ones. The CG_22/8 monolith registered the highest value of K_a and Q_{max}, 4.0×10^4 M^{-1} and 590 mg hIgG g^{-1} support, respectively. Calculated K_a values exhibit the same order of magnitude usually obtained for similar affinity devices fitted with Langmuir–Freundlich isotherm.[136,137,138] In addition, K_a values obtained for CP_22/8 and CG_22/8 are an order of magnitude lower than the K_a values reported for agarose,[113] magnetic nanoparticles[114] and cellulose membranes[88] functionalized with ligand 22/8 and fitted with a Langmuir isotherm model. However, it should be remarked that values of K_a in a range between 10^4 and 10^6 M^{-1} indicate a medium affinity interaction, considered optimal for bioseparation processes while facilitating protein recovery.[6] The values of Q_{max} for CP_22/8 and CG_22/8, 475 and 590 mg hIgG g^{-1} support respectively, are 2-fold those for agarose[113] and magnetic particles[114] functionalized with ligand 22/8, and very close to the one obtained for cellulose membrane.[88]

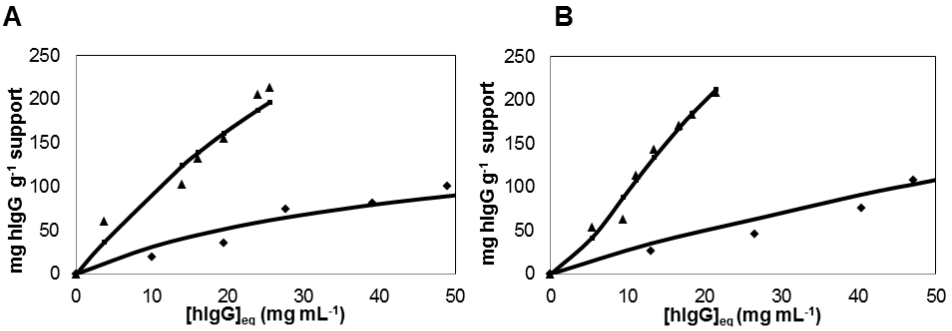

C

Monolith	K_a / (10^4 M^{-1})		$Q_{máx}$ (mg hIgG g^{-1} support)		n		R^2	
	CP	CG	CP	CG	CP	CG	CP	CG
Native	0.08	0.3	270	185	1.2	0.96	0.95	0.97
22/8	1.1	4.0	475	590	1.5	1.05	0.97	0.96

Figure 2.4 - Langmuir–Freundlich adsorption isotherms for (A) CP and (B) CG monoliths: (♦) native and (▲) functionalized. (C) Summarizes the estimated parameters of the Langmuir–Freundlich isotherms and standard errors for CP and CG monoliths before and after functionalization with ligand 22/8.

Values of Langmuir–Freundlich coefficients higher than 1 (n>1) were registered for all functionalized monoliths suggesting a positive cooperativity in binding (attractive forces due to lateral interactions) and a heterogeneous nature of protein adsorption. The cooperativity depends on the macromolecular nature and multiple functional groups, which usually results in multiple interactions.[102,136,139] It should be noted that the same adsorption assays were performed with bovine serum albumin (BSA), a model contaminant protein of antibodies in serum and cell culture supernatants and none of the tested isotherms could fit the experimental data. This result indicates a nonspecific adsorption of BSA.

The dynamic binding capacity of a stationary phase is one of the most critical factors to evaluate its chromatographic performance. To assess the mass transfer and dynamic binding properties of the affinity monoliths, breakthrough curves of purified hIgG were measured in duplicates for two flow rates (Fig. 2.5), as the binding capacity and elution efficiency of supports are affected by the residence time on the monolithic chromatographic column.

Both supports, CP_22/8 and CG_22/8, duplicated the binding and elution capacities when the flow rate decreased from 2 to 1 mL min^{-1} (Fig. 2.5). The estimated binding capacities for CP_22/8 and CG_22/8 were 57±10 and 15±5 mg hIgG g^{-1} support respectively, when using a flow rate of 2 mL min^{-1} and 110±15 and 26±8 mg hIgG g^{-1} support for a flow rate of 1 mL min^{-1}, respectively. The elution capacity for CP_22/8 and CG_22/8 increased from 40 to 90±5% and from 30 to 60±5% when the flow rate decreased from 2 to 1 mL min^{-1}.

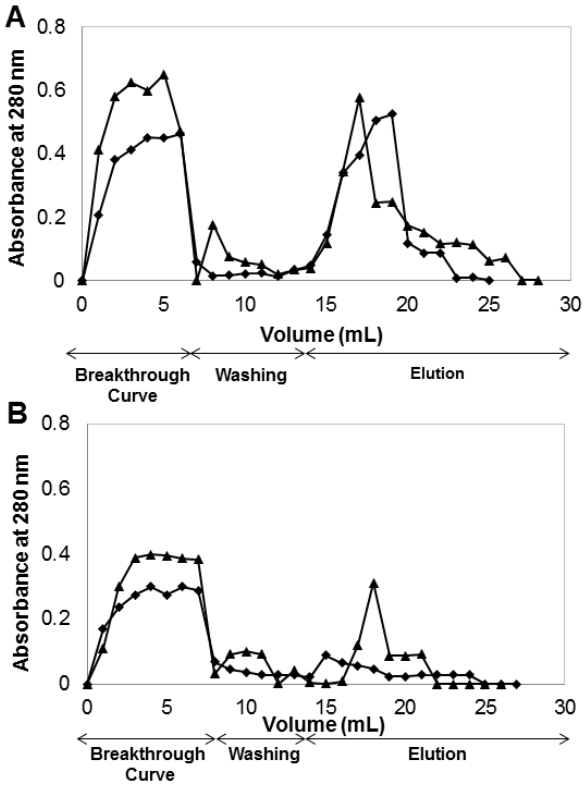

Figure 2.5 - Breakthrough profiles for human IgG upon (A) CP_22/8 and (B) CG_22/8 monoliths at different flow rates: (♦) 1 mL min^{-1} and (▲) 2 mL min^{-1}. All data was obtained from duplicated measurements with errors of ±0.05.

2.3.4. OPTIMIZATION OF AN AFFINITY MONOLITH FOR ANTIBODY RECOVERY

Due to the promising morphological, mechanical and physicochemical properties, high stability at different pH conditions and high static and dynamic binding capacities towards hIgG, CP monoliths were selected for the optimization of IgG purification process. In order to evaluate and enhance the efficiency of affinity CP monoliths for antibody capture and recovery, three consecutive chromatographic cycles and a fourth one after monolith autoclaving (After_AC) were performed in duplicates at two different flow rates, 2 and 1 mL min^{-1}. BSA, the model contaminant, was used as a control in the same experiments in order to evaluate the selectivity and affinity of CP_N and CP_22/8 towards hIgG. CP monoliths exhibited different performances on capturing and eluting hIgG and BSA (Fig. 2.6 and Fig. 2.7). In detail, Fig. 2.6 A and B show that CP_N has approximately the same low capacity to capture and elute hIgG and BSA over the four cycles, suggesting residual non-specific interactions between the support and the proteins. In marked contrast, the functionalized CP_22/8 monoliths showed a substantial increase in binding and elution capacity towards hIgG (Fig. 2.6 C) while only a negligible amount of BSA was retained (Fig. 2.6 D). Although presenting affinity and selectivity to hIgG molecule, the affinity monoliths lost their capacity for re-utilization, especially after autoclaving which is translated by a slight decrease in the bind and elution values. At these operational conditions, CP_22/8 loses around 20% of capacity after 3 chromatographic cycles, and 50% after autoclaving (Fig. 2.6 C).

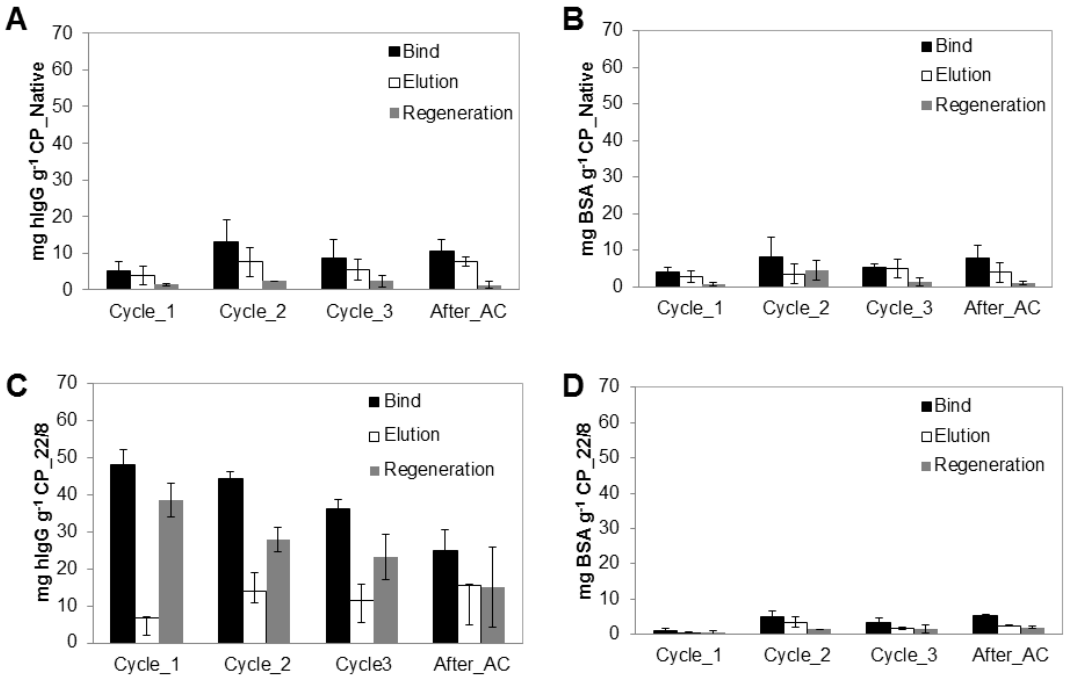

Figure 2.6 - Evaluation of chromatographic performance for (A, B) native and (C, D) functionalized CP monoliths using pure IgG and BSA solutions, respectively. The chromatographic procedures (bind, elution and regeneration steps) were performed consecutively along four cycles at a flow rate of 2 mL min^{-1}. The last cycle was performed after autoclaving (After_AC).

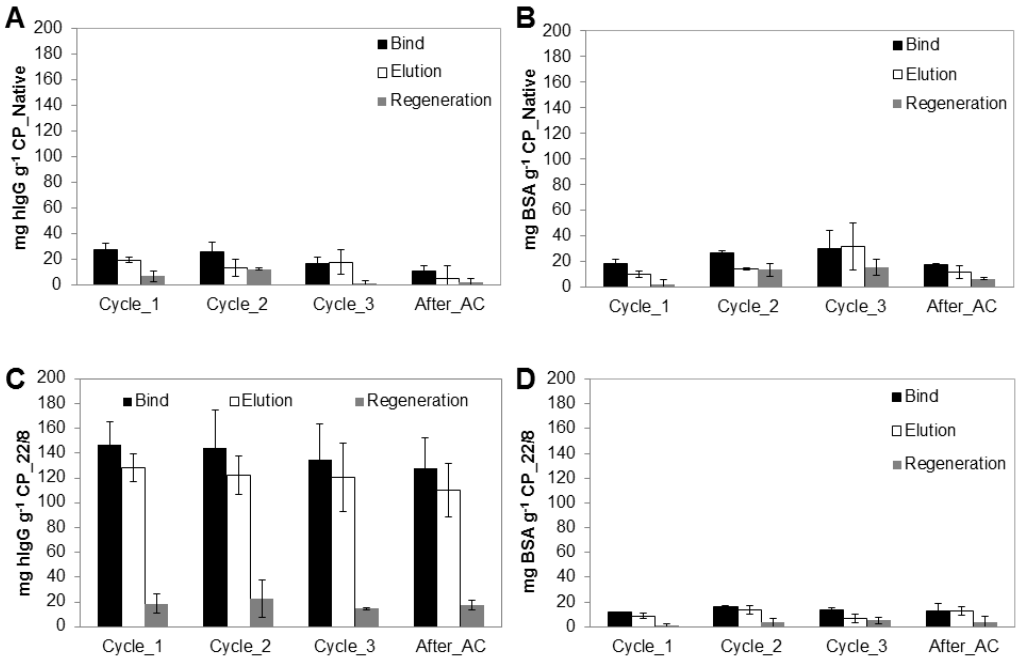

Figure 2.7 - Evaluation of chromatographic performance for (A, B) native and (C, D) functionalized CP monoliths using pure IgG and BSA solutions, respectively. The chromatographic procedures (bind, elution and regeneration steps) were performed consecutively along four cycles at a flow rate of 1 mL min^{-1}. The last cycle was performed after autoclaving (After_AC).

On the other hand, only 25% of the captured hIgG was recovered in the elution step, whereas 75% was washed during the regeneration step under extremely harsh conditions deleterious for the protein. Subsequent assays, performed at a lower flow rate (1 mL min^{-1}), allowed an increase of the residence time and the achievement of affinity equilibrium between the attached ligand and the receptor in the solution (Fig. 2.7). Comparing the chromatographic runs showed in Fig. 2.6 C and 2.7 C, it is clear that CP_22/8 exhibited a great improvement in the binding and elution of hIgG as only reducing the flow rate to a half led to an over 3-fold increase of captured and eluted hIgG, 150±10 and 135±5 mg g^{-1} support, respectively. Consequently, the amount of hIgG recovered during the regeneration step was significantly reduced, 10±5 mg g^{-1} support. The bind and elution capacity of the monoliths was maintained with a slight decrease after autoclaving (a decrease of 15%). This remarkable performance of monoliths for recovering IgG using the flow rate of 1 mL min^{-1} led to results that depart considerably from the reported outcomes obtained with affinity membranes, particles and other monoliths used in antibody purification.[88,113,114,135,140,141]

The most critical part of the study was to evaluate the direct capture of monoclonal antibodies (mAbs) from a non-clarified homogenate.

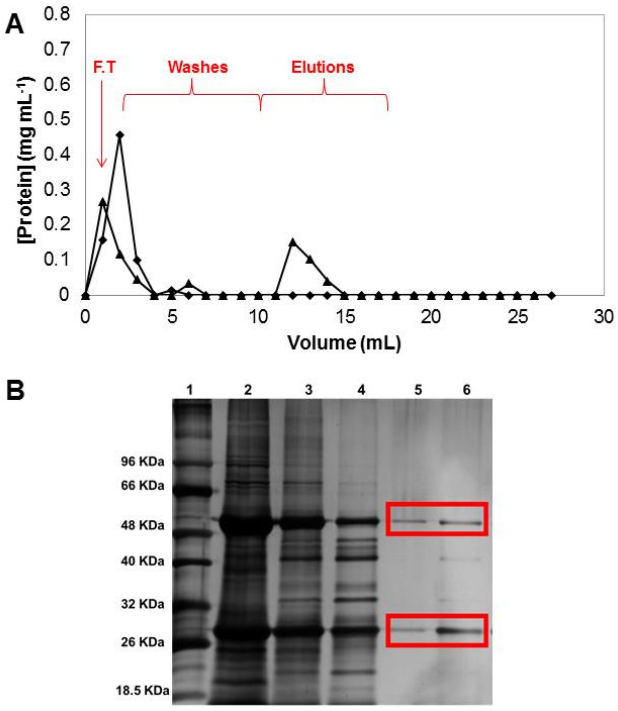

Figure 2.8 - Chromatogram of mAbs purification from crude extract using (A) CP monoliths: (♦) native and (▲) functionalized, at a flow rate of 1 mL min^{-1}. The fractions collected included the flowthrough (F.T.) followed by the washing and elution steps. The acrylamide gel from SDS-PAGE performed with the fractions collected during the mAbs purification (B): lane 1 corresponds to the molecular weight marker, lane 2 represents the loading, lane 3 is the flowthrough, lane 4 corresponds to the first wash (phosphate buffer (50 mM, pH 8.0)), and lane 5 and lane 6 are the first and second elution fractions (sodium citrate buffer (50 mM, pH 3.0)).

Fig. 2.8 presents the chromatogram of non-clarified crude extract of mAbs using CP_N and CP_22/8 monoliths (A) as well as the SDS-PAGE gel,[142,143] revealed using a silver staining kit from BIO-RAD, obtained from the recovered samples during the chromatographic experiment (B). The chromatogram obtained from crude extract sample shows that CP_N did not capture any protein (Fig. 2.8 A) while the affinity monolith CP_22/8 captured 61±10% of mAbs from a mammalian crude extract with initially 1.3 mg of total protein per millilitre, and eluted 80±8% of bounded protein. When considering the purity of the samples, the flow-through (3) and the wash (4) contained contaminant proteins and antibody, while the elution fractions (5, 6) showed a high purity of the antibody (estimated as 98% by ImageJ analysis). These results confirm the efficacy of CP_22/8 in capturing and eluting mAbs with great purity from a real crude extract.

2.4. CONCLUDING REMARKS

Herein, it was developed a strategy to prepare affinity chitosan-based monoliths by combining a freeze drying process with surface activation by plasma treatment to modify them with a robust biomimetic affinity ligand, previously reported as an artificial Protein A, for antibody purification. It was demonstrated that the morphological and mechanical properties of monoliths can be tuned according to the polymer blend composition, while the new strategy to couple the affinity ligand was able to improve the chemical and physical stability towards the final application. The functionalization strategy based on plasma activation proved to be safer and more efficient than traditional activation procedures which involve multiple steps and numerous organic solvents. The main practical advantages of the strategy described are that by fast and solventless plasma activation of different substrates, a direct procedure of functionalization could be applied leading to robust affinity monoliths able to selectively capture and elute antibodies even from homogenate crude extracts. Preliminary results of mAbs capture from a non-clarified homogenate suggested that CP_22/8 is able to recover mAbs with 98% of purity.

A straightforward extension of the materials and functionalization approach based on plasma technology herein described can be envisaged for the production of polymeric devices with different geometries and properties, and for the conjugation of a wide range of biological and artificial receptors. The properties of affinity polymeric devices can be tuned towards different applications in addition to the example here presented. For instance, they can find applications on the pre-concentration and solid-phase extraction of compounds, on organo- and bio-catalysis processes, on analytical and biosensing systems, on tissue engineering and as supports for cellular growth and expansion.

CHAPTER 3

A SUSTAINABLE BIOMIMETIC LIGAND FOR DIRECT IMMOBILIZATION ON (BIO)POLYMERIC SUPPORTS

SUMMARY

This work presents a sustainable strategy for improving the capture of antibodies by affinity chromatography. A novel biomimetic ligand (4-((4-chloro-6-(3-hydroxyphenoxy)-1,3,5-triazin-2-yl)oxy)naphthalen-1-ol) (TPN-BM) was synthesized using a greener and simple protocol to overcome solubility limitations associated to ligand (2-(3-aminophenol)-6-(4-amino-1-naphthol)-4-chloro-s-triazine (22/8), known as artificial Protein A. Furthermore, its subsequent immobilization on chitosan-based monoliths induced by plasma surface activation allowed the design of a fast and efficient chromatographic platform for IgG purification. The TPN-BM functionalized monoliths exhibited high binding capacity (160±10 mg IgG per gram of support), and a selective capture of monoclonal antibodies directly from mammalian crude extracts in 85±5% yield and 98% of purity. The synthesis of ligand TPN-BM and the routes followed for monoliths preparation and functionalization were inspired in the green chemistry principles allowing the reduction of processing time, solvents and purification steps involved, turning the integrated system attractive from an economical and chemical point of view.

Article published: *Telma Barroso, Anita Lourenço, Marco Araújo, Vasco D. B. Bonifácio, Ana C. A. Roque and Ana Aguiar-Ricardo, Green approach toward antibody purification: a sustainable biomimetic ligand for direct immobilization on (bio)polymeric supports. J. Mol. Recognit., 2013, DOI: 10.1002/jmr.2309.*

Attended conference (poster apresentation): Telma Barroso, Anita Lourenço, Marco Araújo, Vasco Bonifácio, Ana Cecília Roque and Ana Aguiar-Ricardo, "Polymeric macroporous monoliths for antibody rescue" in 11th National Meeting of Physico-Chemistry, 2013, Porto-Portugal.

3.1. INTRODUCTION

The ability to produce substantial quantities of pure, safe and efficacious therapeutic proteins from isolated genes is an on-going challenge for the biotechnology industry.[144] The impact of cost-containment in healthcare management, environmental and safety legislation together with the imminent appearance of generic biopharmaceuticals, is likely to drive the industry towards the introduction of high throughput, cost-effective and flexible manufacturing processes.[11,144] Highly selective techniques, such as affinity chromatography, play a crucial role in downstream processing.[11,145] However, there is still scope for improvement of the affinity ligands and the chromatographic supports employed in this process.

The majority of the affinity adsorbents currently adopted is based on natural biological ligands such as proteins A, G and L which present high affinity to IgG-Fc and IgG-Fab.[4] However, these biological ligands tend to be fragile and extremely expensive to produce and optimize. Thus, a strong effort has been made by manufacturers and researchers to find alternative ligands with improved capacity and chemical stability that could offer similar selectivity at a lower cost.[4,146,147]

In recent years, special attention has focused on different biomimetic approaches using synthetic affinity ligands based on the triazine scaffold,[144] ´one-pot´ multi-component reaction,[12] boronic acids[24] and small peptides.[148] Triazine-based ligands are the older generation of the affinity biomimetic ligands however, they are still ideally suited for the purification of high value biopharmaceutical proteins since they are inexpensive, chemically defined, nontoxic, and contain no fissile bonds.[11,144] Also, these ligands are resistant to both chemical and biological degradation, are sterilizable, can be cleaned *in situ* and readily immobilized to yield selective affinity adsorbents with workable capacities for their complementary proteins.[4,145] Some of these are already commercially available and offer excellent selectivity, high binding capacities and chemical stability.[146,147] The design and development of such ligands has been greatly boosted by an increasing access to structural data, the advances in computer-assisted molecular design, and by combinatorial chemistry coupled to high throughput screening methodologies.[4,11] These approaches have been used to obtain ligands that mimic protein A,[138,149] being ligand 22/8 the most popular for the purification of hIgG[150] and monoclonal antibodies from either simple and complex media. This ligand has been immobilized on different supports such as, agarose,[11] magnetic particles,[114] cellulose[88] and chitosan-based monoliths.[82] However, despite of its high performance for antibody purification, this ligand presents low solubility in most common polar and non-polar solvents, becoming hard to manipulate.[150] In an attempt to overcome these drawbacks, this work presents the synthesis and characterization of a new triazine-based biomimetic ligand (TPN-BM) and the evaluation of its performance for antibody purification.

Ligand TPN-BM is structurally similar to ligand 22/8, where the amino groups attached to the triazine core were replaced by ether groups. The core substituents from ligand 22/8 were maintained to ensure IgG recognition. (Fig. 3.1) The synthesis of this novel ligand was inspired in the principles of green chemistry,[151] which seeks reinvention of production routes capable of minimize the inherent cost and wastes as well as the elimination of hazardous

compounds/solvents during their conception. Therefore, TPN-BM was designed in order to save time and energy consumption and to reduce solvents and purification steps.

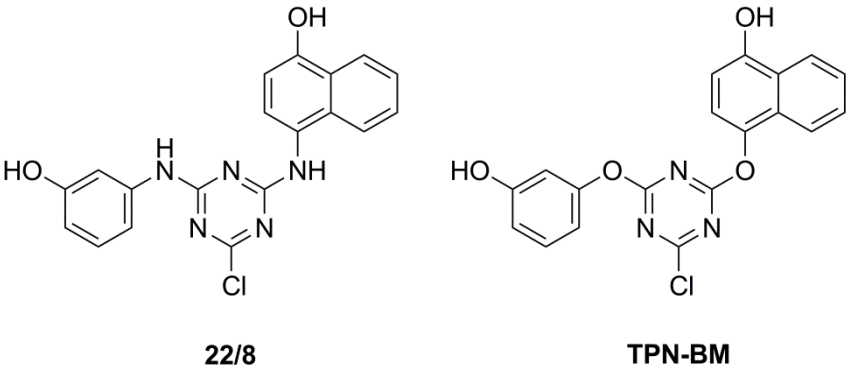

Figure 3.1 - Chemical structures of ligand 22/8 and TPN-BM.

Monolithic supports based on chitosan and activated by solvent-free plasma treatment,[82,122] as described in Chapter 2, were selected as the best stationary phases for ligand attachment by representing the greener option among the diversity of matrices tested.[11,82,88,114,150] Taking advantage of the best available chromatographic tools, this work envisages the development of an integrated green "bottom-up" strategy to produce affinity chromatographic devices through the introduction of a new optimized synthetic affinity ligand, and its immobilization on a chitosan-based monolith by solvent-free plasma treatment. Having considered the main issues of an affinity separation process as well as the need to design it according to restricted chemical regulations, a new low cost and sustainable approach to purify antibodies is proposed.

3.2. EXPERIMENTAL AND METHODS

3.2.1. MATERIALS

Ammonium persulphate (purity≥98%), citric acid (purity≥99%), sodium hydrogen phosphate monobasic (pro analysis), disodium hydrogen phosphate dibasic (pro analysis), disodium tetraborate, ethanol absolute and sodium citrate dihydrate were purchased from Merck. Isopropanol and sodium bicarbonate were purchased from Riedel-de-Haën. Acetone (purity≥99%), and ethyl acetate were supplied by Roth. Acetic acid (purity≥99%), caproic acid, 1,4-dihydroxynaphthalen (purity≥99%), cyanuric chloride (purity≥98%), 1,6-hexanediamine (purity≥98%), diisopropylethylamine, *N,N*-dimethylformamide (DMF), dimethylsulfoxide (DMSO), tetrahydrofuran (THF), ninhydrin, potassium cyanide, pyridine, sodium hydroxide (purity≥99%) and resorcinol (purity≥99%) were purchased from Sigma Aldrich. Chitosan (75~85% deacetylated, medium molecular weight), poly(vinyl alcohol) (purity≈99%), N,Nmethylenebisacrylamide (MBAm, purity≥85%), tetramethylethylenediamine (TEMED) (purity≈99%), bicinchoninic acid (BCA) kit, bovine serum albumin (BSA) (purity≥98%) were

supplied by Sigma Aldrich. Human IgG was purchased by Octapharma (Gammanorm, purity≥99%).

3.2.2. LIGAND SYNTHESIS AND CHARACTERIZATION

The synthesis of ligands 3-((4,6-dichloro-1,3,5-triazin-2-yl)oxy)phenol (TP-BM) and 4-((4-chloro-6-(3-hydroxyphenoxy)-1,3,5-triazin-2-yl)oxy)naphthalen-1-ol (TPN-BM) (Fig. 3.1) was performed following a modified procedure.[152]

Following a typical procedure for an aromatic nucleophilic substitution,[152] cyanuric chloride (5.55 g, 0.03 moles), resorcinol (1.65 g, 0.015 moles) and diisopropylethylamine (3.02 mL) were reacted in dry THF at 0 ºC for 2h under stirring (120 rpm). The volume of THF used was just sufficient to dissolve the reactants: approximately 10 mL to dissolve 5.55 g of cyanuric chloride and 4 mL to dissolve 1.65 g of resorcinol. After warming to room temperature, the reaction mixture was filtered to remove amine salts and the solvent was evaporated under vacuum. The resultant solid was recrystallized from acetone to yield TP-BM as a white powder (7.13 g, 90% yield). FT-IR (KBr) λ_{max} (cm^{-1}): 3396, 1506, 1404, 1295, 1257, 1224, 1179, 1018, 922, 852, 803, 788, 691. 185 ^{1}H NMR (400 MHz, $CDCl_3$) δ (ppm): 11.28 (1H, OH), 7.56 (1H, t, J= 8.4 Hz, H_b), 7.20 (2H, dd, J= 2.0, 8.4 Hz, H_c+H_d), 7.10 (1H, s, He). ^{13}C NMR (100 MHz, $CDCl_3$) δ (ppm): 173.39 (Triazine-O), 172.62 (Triazine-Cl), 170.85 (Phenol-OH), 151.55 (Phenol-O), 131.01 (Phenol-H), 119.91 (Phenol-H), 115.10 90 (Phenol-H). The isolated TP-BM ligand revealed a persistent chemical instability which precluded complete microanalytic characterization. For the synthesis of TPN-BM, TP-BM (6.00 g, 0.023 moles), 1,4-dihydroxynaphthalen (3.74 g, 0.023 moles), dissolved in dry THF (approximately 10 and 5 mL, respectively), and diisopropylethylamine (33 mL) were reacted at 0 ºC for 2h (Fig. 3.1). The crude reaction mixture was then filtered to remove amine salts and the solvent evaporated, giving brownish oil, which was dried under vacuum. The crude mixture was then recrystallized from acetone at -78ºC to yield TPN-BM as a pasty brownish solid (8.11 g, 88% yield). FT-IR (KBr) λ_{max} (cm^{-1}): 3225, 1594, 1535, 1479, 1392, 1357, 1270, 1147, 1064, 850, 818, 769. ^{1}H NMR (400 MHz, $CDCl_3$ + DMSO-d_6 drops) δ (ppm): 10.69 (2H, OH), 8.00 (1H, d, J= 8.4 Hz, H_b), 7.71-7.62 (3H, m, H_c+H_d+H_e), 7.12-6.91 (4H, m, H_f+H_g+H_h+H_i), 6.49 (2H, m, H_j+H^l). ^{13}C NMR (100 MHz, $CDCl_3$) δ (ppm): 173.26 (Triazine-O-Phenol), 171.21 (Triazine-O-Naphtol), 170.72 (Triazine-Cl), 152.33 (Phenol-OH), 150.42 (Phenol-O), 146.62 (Naphtol-OH), 138.66 (Naphtol-O), 135.23 (Phenol-H), 133.93 (Naphtol-C), 131.89 (Naphtol-C), 130.29 (Naphtol-H), 127.38 (Phenol-H), 126.41 (Phenol-H), 110 122.67 (Naphtol-H), 121.31 (Naphtol-H), 119.77 (Phenol-H), 117.36 (Phenol-H). MS (EI) calculated for $C_{19}H_{12}ClN_3O_4$, 381.1; found 381.1$[M]^+$.

^{1}H NMR spectra were recorded on a Bruker ARX 400MHz spectrometer. Approximately 10 mg of sample were dissolved in 500 µL of deuterated chloroform with a few drops of dimethylsulfoxide, for TP-BM and TPN-BM, respectively. FT-IR measurements were performed using Winfirst 5 Lite equipment (16 scans and 1 cm^{-1} resolution). Thin pellets containing a small amount of each product mixed with dried KBr (1:5 mass ratio) were made before recording. All

mass spectral analyses were carried out by the Laboratory for Mass Spectrometry at Santiago de Compostela (Spain).

3.2.3. MONOLITHS PREPARATION AND FUNCTIONALIZATION WITH TPN-BM

Chitosan-based monoliths were prepared according to Barroso *et al.*[82] by blending chitosan with Poly(vinyl alcohol)(monolith designated by CP) and by cryopolymerizing of glycidyl methacrylate, GMA, (monolith designated by CG). The functionalization of chitosan-based monoliths with TPN-BM followed the strategy based on plasma activation, as in previously chapter for the immobilization of ligand 22/8 in same supports.[82] Thus, plasma surface activation was used to introduce radicals on monolith surfaces for further amination (outside plasma) and it was carried out in a radio frequency plasma reactor (Plasma system FEMTO, version 5). Native (N) chitosan-based monoliths (30 mg of CP and CG) were introduced in plasma chamber which was thoroughly purged with a continuous flow of argon to reduce trace amounts of air and moisture. During the treatment, the argon flow was adjusted to maintain a constant pressure of 0.3 Torr inside the chamber. A power of 60 W was applied during 5 minutes. At the end of the experiment the plasma chamber was ventilated and the activated samples were immediately immersed in 7 mL of 1,6-hexanediamine to be aminated for 12 h at 45 ºC. At the end aminated samples were washed with water (10 mL) in order to remove unreacted 1,6-hexanediamine. The extent of amination was determined by the Kaiser test.[82] The immobilization of ligand TPN-BM followed a similar protocol adapted for the immobilization of ligand 22/8 in the same supports using just DMF as solvent and not a DMF-water mixture as in the case of ligand 22/8. An excess of TPN-BM (3 equiv. to the amination content, 530 µmol, 200 mg), was added to the aminated chitosan-based monolith samples (approximately 60 mg) in DMF (5 mL). The volume of solvent used was sufficient to cover the chitosan-based monoliths, and the solution was incubated on a rotary shaker (140 rpm) for 72 h at 85 ºC. Then, functionalized chitosan-based monoliths were washed with DMF (6 mL) until no detection of absorbance at 267 nm. Moreover, in order to assure a complete exclusion of non-absorbed ligands into and onto monoliths, the functionalized samples were introduced in a Varian column (a reservoir with a capacity of 3 mL and an internal diameter of 10 mm) and were loaded with 5 mL of DMF and submitted to a clean-in-place (CIP) procedure. The CIP procedure consisted in a sequential washing of the functionalized chitosan-based monoliths: first with NaOH (1 M, 5 mL), (until no absorbance was observed at 267nm), then with water (10 mL) and regeneration buffer (NaOH 0.1 M in 30 % of isopropanol, 5 mL) until no absorbance at 267 nm, and finally with distilled water (10 mL). The functionalized chitosan based monoliths were equilibrated with sodium phosphate buffer (50 mM, pH 8.0) and sodium citrate buffer (50 mM, pH 3.0) until no absorbance at 267 nm. The extinction coefficient of TPN-BM was determined at its maximum absorbance wavelength ($\varepsilon 267 = 3.72$ L g^{-1} cm^{-1}), and extend of coupling was determined by subtracting the amount of ligand contained in all the washing liquors from the initial quantity used in the immobilization step. In order to reuse the unreacted TPN-BM and the DMF collected

from the washes for further immobilizations procedures, the ligand was precipitated by adding diethyl ether as an anti-solvent and the DMF recovered.

3.2.4. BIOMIMETIC MONOLITHS CHARACTERIZATION

Morphological and mechanical properties of native (used as control) and functionalized monoliths (modified with the affinity ligand) were evaluated. The morphology was investigated using scanning electron microscopy (SEM) in Hitachi S 2400 equipment with accelerating voltage set to 15 kV. The samples were frozen and fractured in liquid nitrogen for cross-sectional analysis and gold coated before analysis. The porosity, average pore size diameter and surface area were determined in duplicate by MIP (Micromeritics, autopore IV). Water fluxes were determined at 25 ºC and varying the applied hydrostatic pressure (within 0-0.4 MPa) using a stainless steel high-pressure cell (with an effective volume of 1.2 cm^3). At least, three measurements of distilled water flux were performed for each monolith. The permeability (L_p) was calculated from the slope of the linear relation between flux and pressure, using the Darcy law (see Chapter 2). Uniaxial compression was used to determine the mechanical properties of the monoliths using tensile testing equipment (MINIMAT firm-ware v.3.1) at room temperature in dry and wet state. Samples were prepared in a cylindrical shape (10 mm in diameter thickness). The length between clamps was set to 5 mm, the speed set to 1 mm min^{-1}, a full scale load of 20 N and maximum extension of 90 mm was used. The compression modulus was calculated from the slope of the linear portion of the stress-strain curve (see Chapter 2).[82]

3.2.5. STATIC PARTITION EQUILIBRIUM STUDIES

Partition equilibrium experiments were performed in a batch system as described in a previously work.[82] The adsorption of hIgG and BSA on the chitosan based monoliths was investigated using a sample of native and functionalized ones (15 mg) varying the concentration of hIgG and BSA (0.0-45.0 mg mL^{-1}, 400 µL) in phosphate buffer solutions (50 mM, pH 8.0). All experiments were conducted in duplicates at 25 ºC, under orbital agitation at 200 rpm during 12 h. After incubation, monoliths were removed from the medium. The amount of adsorbed hIgG and BSA was determined by measuring the initial and the final concentrations of protein in the supernatant. A calibration curve was constructed using hIgG and BSA (0.0–45.0 mg mL^{-1}) in phosphate buffer solutions (50 mM, pH 8.0). The concentration of protein was measured at 280 nm on a microplate reader (Tecan Infinite F200). The adsorption phenomenon followed the Langmuir-Freundlich model,[139,141] represented by the equation below:

$$q = \frac{Q_m \times (C)^n}{K_d + (C)^n}$$

Equation 3.1

where K_d is the apparent dissociation constant (M), K_d is the inverse of the affinity constant K_a, that includes contributions from ligand binding to support, Q_m is the maximum binding capacity

(mg protein g^{-1} support), *C* is the concentration of protein in the liquid at the equilibrium (M) and *n* represents the Langmuir-Freundlich coefficient.

3.2.6. FRONTAL ANALYSIS – BREAKTHROUGH CURVES AND BINDING CAPACITY

The dynamic loading capacity of the packed columns (for both native and functionalized chitosan-based monoliths) was determined using frontal analysis according with the equation below:[6]

$$Q = \frac{V_e}{[Protein]_{plateau}}$$

Equation 3.2

where *Q* is the estimated adsorbent capacity and V_e is the elution volume.

This technique consisted in the loading of hgG and BSA solutions (8 mL, 0.5 mg mL^{-1}) in sodium phosphate buffer (50 mM, pH 8.0) through equilibrated monoliths inserted in Varian columns (with a capacity of 3 mL and an internal diameter of 10 mm) at a flow rate of 1 mL min^{-1} until the protein concentration of the output and input streams were identical. Then, packed columns were washed with phosphate buffer (50 mM, pH 8.0) and the bound protein was eluted with sodium citrate buffer (50 mM, pH 3.0). Each millilitre collected during loading, washing and elution steps were analysed by absorbance at 280 nm, using a microplate reader, in order to estimate the amounts of bounded and eluted protein.

3.2.7. CHROMATOGRAPHIC EXPERIMENTS WITH PURIFIED PROTEIN SOLUTIONS

Functionalized CP and CG monoliths were packed in Varian columns (with a capacity of 3 mL and an internal diameter of 10 mm). The columns were connected to a peristaltic pump using rubber tubing. The affinity capturing experiments were performed in a step-wise adsorption-desorption process by switching eluents at room temperature and at atmospheric pressure. The packed columns with functionalized chitosan-based monoliths were loaded with 1 mL of hIgG or BSA solution (5 mg mL^{-1}) and then washed with sodium phosphate buffer (50 mM, pH 8.0) until the absorbance measured at 280 nm reached ≤0.005. The bound protein was then eluted and recovered with sodium citrate buffer (50 mM, pH 3.0). The packed columns with functionalized chitosan-based monoliths were then regenerated using a buffer solution (NaOH 0.1M in 30% of isopropanol). These chromatographic experiments were repeated twice along 3 cycles and one more cycle was performed after monoliths autoclaving for 20 min at 120 ºC.

3.2.8. PURIFICATION OF MONOCLONAL ANTIBODIES FROM MAMMALIAN CRUDE EXTRACTS

To evaluate the possibility of capturing antibodies directly from non-clarified crude extracts, columns packed with native and functionalized CP monoliths were loaded with a mammalian crude extract solution (1 mL, 1.3 mg of total protein per millilitre). After loading, packed columns were washed with sodium phosphate buffer (15 mL, 50 mM, pH 8.0) until the absorbance

measured at 280 nm reached a value ≤0.005 and the bound protein was further eluted with sodium citrate buffer (50 mM, pH 3.0). All collected samples were analysed by the BCA assay (microplate reader assay) to quantify the amount of total protein bound and eluted from the solid support. All collected samples (Loading (LD), Flowthrough (FT) and Elutions (E)) were analysed by SDS-PAGE 12.5 % acrylamide/bisacrylamide in denaturing conditions and stained with Silver Staining kit (BioRad). The electrophoresis apparatus (from BIO-RAD) was connected with a power supply at 120 V, 190 mA for 1 h.[143]

3.3. RESULTS AND DISCUSSION

3.3.1. TPN-BM SYNTHESIS

The structure of ligand 22/8 was refined to improve the synthesis procedure and ligand solubility. The improved ligand designated as TPN-BM maintained the functionalities necessary for protein recognition. The first reaction led to the formation of TP-BM using cyanuric chloride as a starting material. Cyanuric chloride is a valuable scaffold for ligand design, combinatorial chemistry and self-assembly since triazine-based molecules can act both as hydrogen donors and acceptors.[152] Acting as an electrophilic core, it reacted with resorcinol which was added dropwise to avoid di-substitution at 0 °C for 2h under stirring. The intermediate formed (TP-BM) was isolated in very good yield (90%) and characterized by NMR, FT-IR (Fig. 3.2 A and B, respectively) and mass spectrometry.

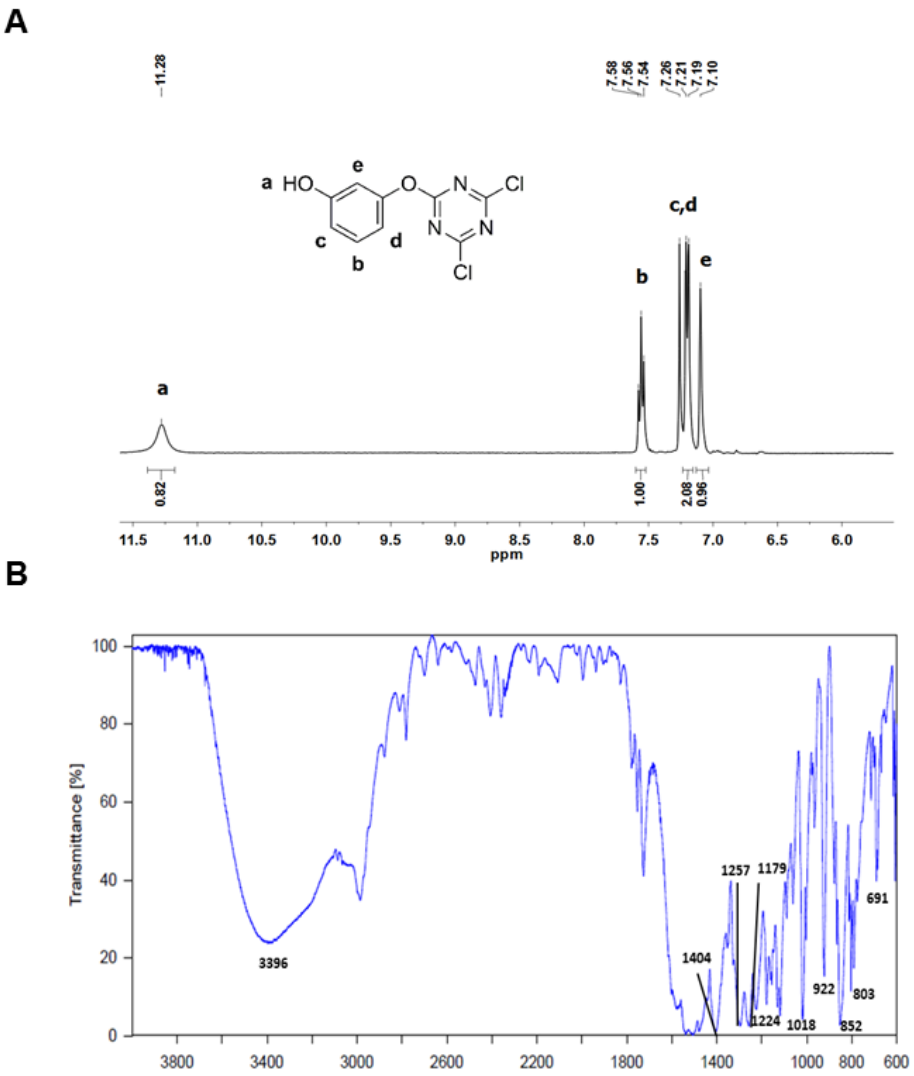

Figure 3.2 – (A) ^{1}H-NMR spectrum of TP-BM in $CDCl_3$ and (B) FT-IR spectrum of TP-BM.

In the ^{1}H NMR spectra a downfield shift in the aromatic protons of resorcinol was observed, caused by the deshielding effect arising from the presence of the triazine ring. In the FT-IR spectrum the appearance of an intense band near 1257 cm^{-1}, characteristic of CO stretching vibration in aryl ethers, confirm the formation of the desired compound and thus, the success of the reaction. The purification of TP-BM was found to be much easier than the one in which the first product of ligand 22/8 synthesis is obtained, as it only involved the evaporation of THF under vacuum and washings of the product with distilled water (20 mL) in order to remove unreacted diisopropylethylamine. In a similar procedure 1,4-dihydroxynaphthalen, which was also added dropwise to avoid disubstitution, reacted smoothly with TP-BM to afford ligand TPN-BM in very good yield (88%). The ^{1}H NMR spectrum of TPN-BM (Fig. 3.3 A) is very similar to ligand 22/8,[88] only showing a downfield shift corresponding to the protons of the naphthol ring. The presence of a peak with m/z=381.1 in the mass spectra also confirmed the presence of the desired product.

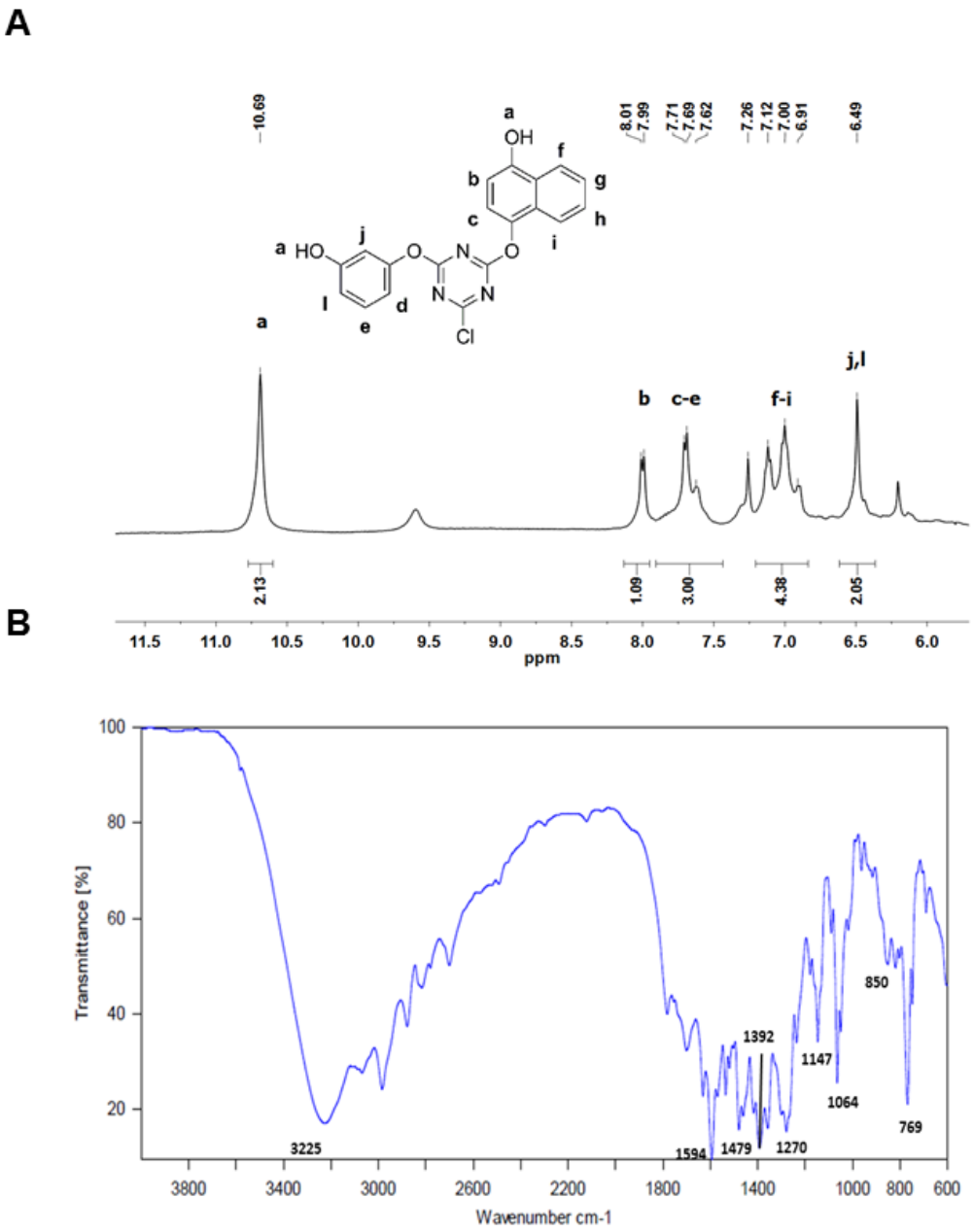

Figure 3.3 – (A) ^{1}H-NMR spectrum of TPN-BM in $CDCl_3$ and (B) FT-IR spectrum of TPN-BM.

Comparing the two syntheses (ligand 22/8[88] versus TPN-BM) it was found that in the case of TPN-BM a more sustainable protocol was achieved, with a clear reduction of purification steps, solvents, energy and time (Table 3.1).

Table 3.1 - Comparison between synthetic routes of ligand 22/8 and TPNBM from a green chemistry point of view.

Process Parameters	Ligand 22/8	TPN-BM	Green Chemistry
Solvents involved	6	4	Safer solvents
Temperatures involved (ºC)	0-45	0	Energy maximization
Purification steps	6	4	Design for separation
Time consuption (h)	7	4	Time efficiency
Mass productivity (%)	2.4	26	Atom economy

3.3.2. IMMOBILIZATION OF LIGAND TPN-BM ONTO NATIVE CHITOSAN-BASED MONOLITHS

Numerous methodologies for the activation of monoliths and ligand coupling have been described.[18,40] Herein, the immobilization of ligand TPN-BM onto native chitosan-based monoliths followed a procedure based on plasma activation surface as described in our previous work.[82] This strategy demonstrated to be more efficient to induce ligand 22/8 attachment onto chitosan-based monoliths with a 5-fold higher amination yield achieved, (1.75± 0.05)×10^3 µmol g^{-1} support, comparing with traditional strategies. Thus, argon (Ar)-plasma treatment produces highly reactive radicals in the monoliths surface, that allow its coupling with the spacer 1,6-diaminehexane.[11] Since the TPN-BM triazine core still has a reactive chloride that can participate again in an aromatic nucleophilic substitution, the ligand is easily immobilized onto aminated surfaces. The immobilization yields are registered in Table 3.2, and are compared with the results previously obtained for ligand 22/8.

Table 3.2 - Amination and ligand densities of chitosan-based monoliths.

Monolith	[NH_2] ×10^{-3} (µmol g^{-1} support)	TPN-BM immobilization ×10^{-3} (µmol g^{-1} support)	22/8 immobilization ×10^{-3} (µmol g^{-1} support)[82]
CP	1.75 ± 0.05	0.89 ± 0.02	0.91 ± 0.02
CG	0.9 ± 0.2	0.74 ± 0.02	0.67 ± 0.02

[a] All the values were obtained in duplicates.

The highest value for TPN-BM immobilization was obtained using the CP monolith, (0.89±0.02)×10^3 µmol g^{-1} support, which was similar to the one obtained for the same support using ligand 22/8. The CG monolith also presented a high functionalization capacity, (0.74±0.02)×10^3 µmol g^{-1} support, a value that is slightly higher than the one obtained using the same support but with ligand 22/8. The difference between amination yields and consequently ligand immobilization values of CP and CG monoliths might be due to their distinguished

morphological features such as average pore size diameter and specific surface area. These results suggest that the strategy involving the plasma treatment is much more efficient than traditional activation procedures based on epoxy chemistry, and it can be extended to other ligands, independently of the type of support used.[82,88,114] Additionally, the novel strategy applied for the immobilization step also simplified the overall ligand functionalization procedure. Considering that ligand TPN-BM is completely soluble in DMF, it was possible to avoid the use of the DMF-water system enabling an easier DMF recovery. More importantly, the high solubility of the ligand enables its accurate quantification on the monolithic supports.

After ligand TPN-BM immobilization, the morphological, mechanical and physico-chemical properties of chitosan-based monoliths were studied in order to evaluate the integrity of the modified structures. The SEM images (Fig. 3.4) show that a different surface topology was obtained after ligand coupling. A surface roughness appeared due to the ligand covering the porous network, suggesting that the coupling procedure was successfully achieved. The average pore size diameter and the porosity values obtained for native and functionalized CP_TPN-BM and CG_TPN-BM monoliths are registered in Table 3.3 and suggest that the porous network was not strongly affected by the functionalization procedure or by the ligand nature. Permeability values obtained for CP and CG monoliths decreased from 294 to 163 L m^{-2} h^{-1} atm^{-1} for CP_TPN-BM and from 390 to 290 L m^{-2} h^{-1} atm^{-1} for CG_TPN-BM monoliths. The flow reduction, as previously observed for ligand 22/8 functionalized chitosan-based monoliths,[82] can be explained by the hydrophobic character of the material after ligand coupling. However, it should be noted that this property can be much favourable to the separation process, since the permeability values are still acceptable allowing enough residence time for the contact between the protein and the affinity support during chromatographic experiments. Also, a decrease of the specific surface area was expected with the increase of average pore size diameter. The inner surface area (total pore area) is within the range determined for chitosan-based monoliths functionalized with ligand 22/8 and are also similar to other 3D porous structures designed for the same.[82,133,134] The compressive modulus increased (~10-fold) for all monoliths after ligand coupling in dry or wet state (refer to Table 3.3), as observed in our previous work using ligand 22/8,[82] probably because the triazine-based ligands confer rigidity to all porous network. Thus it should be underlined that the ligand TPN-BM that was synthesized by a greener chemical route presented the same structural rigidity than ligand 22/8.

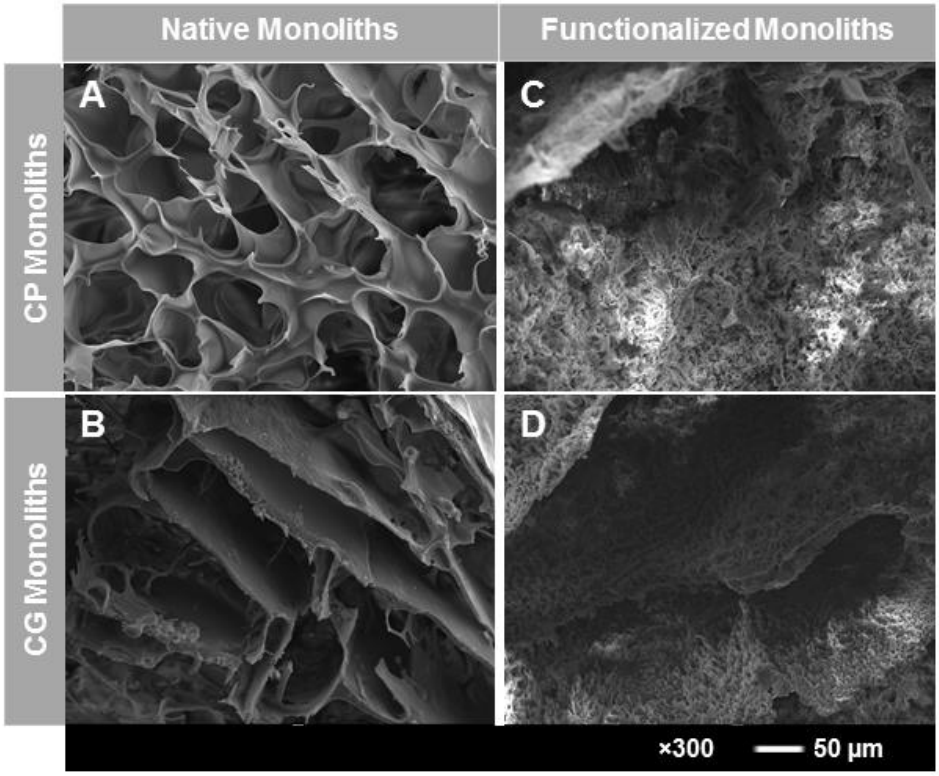

Figure 3.4 - SEM images of chitosan based-monoliths before and after functionalization of ligand TPN-BM: (A) CP_N, native monolith prepared from chitosan and polyvinyl alcohol; (B) CG_N, native monolith prepared from chitosan and glycidyl methacrylate; (C) CP_TPN-BM, CP monolith functionalized with TPN-BM and (D) CG_TPN-BM, CG monolith functionalized with TPN-BM. All the images have a magnification of 300 and the scale bar in white corresponds to 50 µm.

Table 3.3 - Morphological and mechanical characterization of chitosan-based monoliths before and after functionalization of ligand TPN-BM.

Monolith	Average pore size diameter[a] (µm)	Porosity[a] (%)	Surface Area[a] (m^2g^{-1} monolith)	Permeability[b] (L m^{-2} h^{-1} atm^{-1})	Compressive Modulus (kPa)[b]	
					Dry	Wet
CP_N	53±5	70±5	1.3±0.1	294±15	0.41±0.2	0.2±0.2
CG_N	123±5	75±5	0.9±0.1	390±5	0.26±0.2	n.a[c]
CP_TPN-BM	57±7	72±10	2.9±0.2	163±10	10±4	6±4
CG_TPN-BM	101±10	83±10	1.3±0.1	290±15	7±5	2.5±2

[a] Determined for dried monoliths by mercury porosimetry analysis in duplicates; [b] The experiments were performed in triplicates; [c] The mechanical assay was impossible to perform due to the high swelling of CG_N.

The stability at typical operating conditions used during the purification processes was further evaluated, and the monoliths were incubated at several pH conditions (from pH 1 to 12), corresponding to those employed in equilibration, elution, regeneration and CIP of chromatographic matrices. The amount of ligand released from the support at each condition was examined (Fig. 3.5), and the maximum amount of ligand TPN-BM released from CP_TPN-BM and CG_TPN-BM was 18% and 15%, after 2 and 4 hours of incubation, and at pH 2 and 12,

respectively (Fig. 3.5 A and C). Specifically, at the pH used in the binding (pH 8) and elution (pH 3) of antibodies from TPN-BM ligand supports, the highest amount of ligand leaching was observed after 2 and 4 hours, for CP_TPN-BM and CG_TPN-BM, respectively. In general, during a typical purification run of 30-60 minutes, the maximum contact time of the monolith with these conditions is far below the onset for ligand leaching, as it was observed for monoliths functionalized with ligand 22/8.[82] In contact with the typical aggressive solutions used in downstream processes (Fig. 3.5 B and D), especially in chromatographic steps, the highest loss (approximately 20%) of ligand from CP_TPN-BM and CG_TPN-BM occurs when using hydrochloridric acid (0.1 M) after 2 and 4 hours (Fig. 3.5 B and D), respectively. However, the maximum contact time of each functionalized monolith under CIP conditions is around 30 minutes; time at which no ligand was released. Comparing the stability profile obtained for the monoliths TPN-BM at different pH and conditions with those obtained for chitosan-based monoliths functionalized with ligand 22/8 under similar conditions (see Chapter 2), it is possible to verify that a higher quantity of ligand TPN-BM is leached from the support. A primary conclusion could be that ligand TPN-BM is less robust at drastic conditions than ligand 22/8. However, it should be noted that ligand TPN-BM was designed to overcome the poor solubility of 22/8 and, consequently, its quantification became much more rigorous and valid. Thus, we can postulate that in previous experiments the amount of ligand 22/8 released to the medium[82] probably was not accurately determined due to solubility issues, and lower amounts of released ligand were detected.

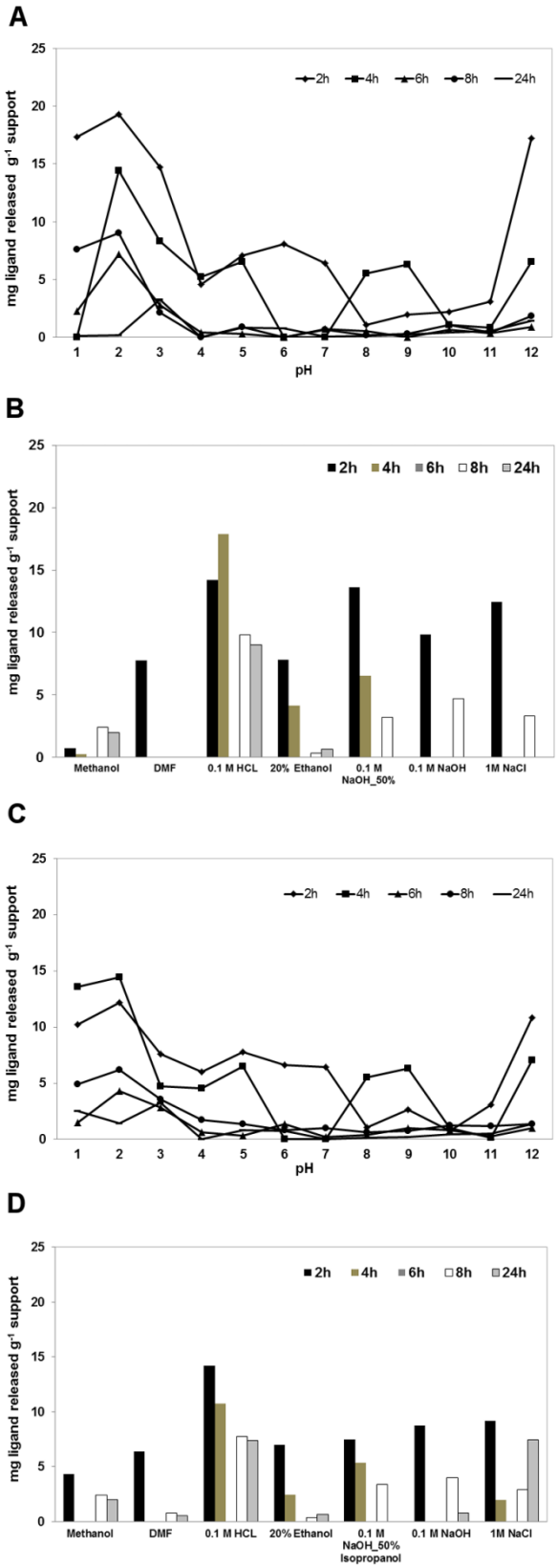

Figure 3.5 - Stability evaluation of CP_TPN-BM (A and B) and CG_TPN-BM (C and D) monoliths immersed, over 12 hours, in solutions typically used during cleaning-in-place (CIP) procedures, including solutions with pH values between 1 and 12. All data was obtained from duplicated measurements with errors of ± 6.

3.3.3. EVALUATION OF TPN-BM MONOLITHS AS AFFINITY DEVICES FOR hIgG PURIFICATION

To evaluate the affinity constants for hIgG and BSA on native and functionalized chitosan-based monoliths, static partition equilibrium experiments were performed in duplicates. To attain the equilibrium between proteins and affinity supports, partition equilibrium studies were performed in a batch system for 12 hours varying the proteins concentration.

The experimental data was fitted using a Langmuir-Freundlich isotherm since it has been indicated to predict the adsorption equilibrium for affinity heterogeneous systems.[137,153] According to the monolith's material, different affinity constants (K_a), theoretical maximum capacity (Q_{max}) and Langmuir-Freundlich coefficients (n) were estimated (Fig. 3.6) with an error of ±0.5, ±40.0 and ±0.1, respectively. The TPN-BM monoliths always presented higher values of K_a and Q_{max} when compared with the native ones. CG_TPN-BM monolith that registered a small decrease in the K_a and Q_{max} values (3.5 M^{-1} and 410 mg IgG g^{-1} support) comparing with the ones registered for CG_22/8 (4.0 M^{-1} and 590 mg hIgG g^{-1} support).[82] These results show the less regular behaviour exhibited by CG monoliths.

As it was observed for supports functionalized with ligand 22/8, the obtained K_a values for TPN-BM monoliths have the same order of magnitude (10^{-4} M). This order of magnitude is lower than the one verified for K_a reported for agarose[11], magnetic nanoparticles[114] and cellulose membranes[88] functionalized with ligand 22/8, fitted with a Langmuir isotherm model. Nevertheless, values of K_a in a range between 10^4 and 10^6 M^{-1} indicate a medium affinity interaction, ideal in purification processes for target protein capture and release.[154] The values of Q_{max} for CP_TPN-BM and CG_TPN-BM, 810 and 410 mg hIgG g^{-1} support, respectively, are at least 2-fold higher than those obtained for other affinity supports functionalized with ligand 22/8.[82,114,138] In addition, the results registered for Langmuir-Freundlich coefficients of TPN-BM monoliths were higher than those obtained for native monoliths, and higher than 1, clearly suggesting a positive cooperativity in binding and an heterogeneous nature in protein adsorption.[141] It should be noted that the same adsorption assays were performed BSA, a model contaminant protein of antibodies in serum and cell culture supernatants and none of the tested isotherms could fit the experimental data, which indicates a nonspecific adsorption profile of BSA.

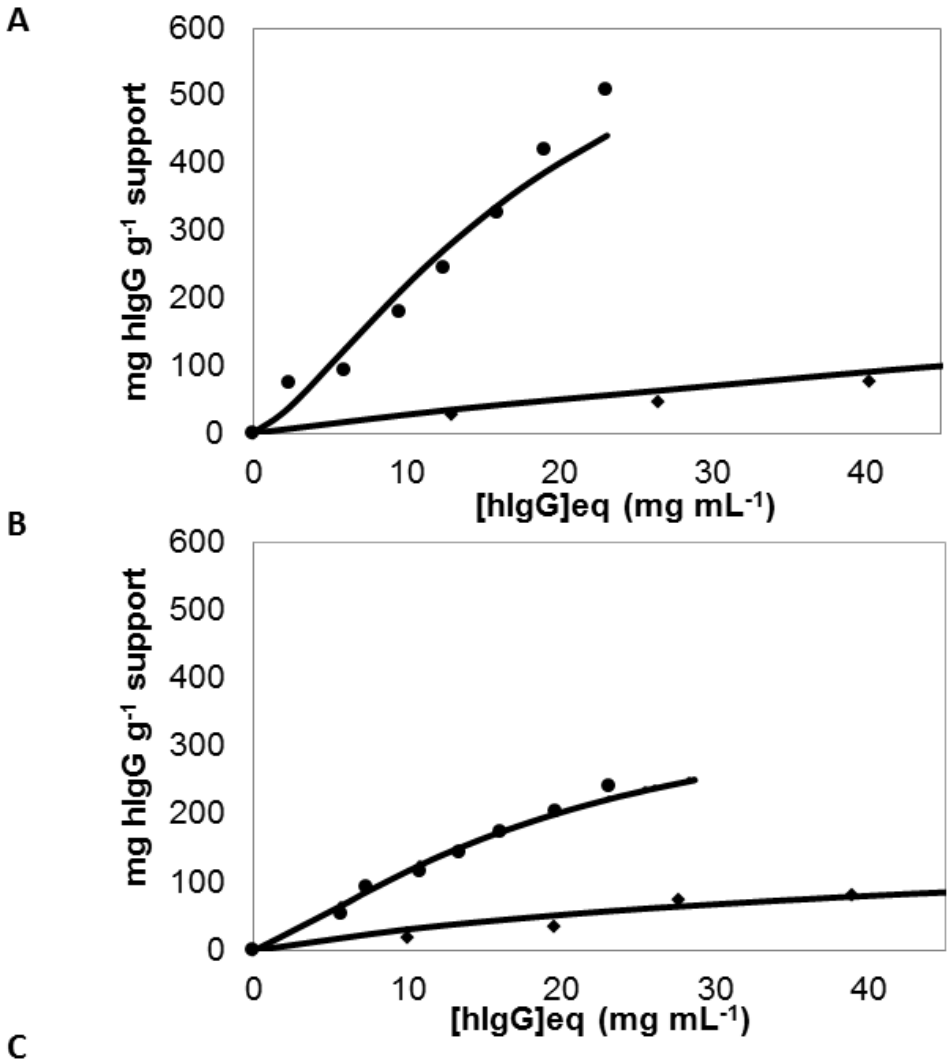

C

Monolith	K_a / (10^4 M^{-1})		$Q_{máx}$ (mg hIgG g^{-1} support)		n		R^2	
	CP	CG	CP	CG	CP	CG	CP	CG
Native	0.08	0.3	270	185	1.2	0.96	0.95	0.97
22/8[a]	1.1	4.0	475	590	1.5	1.05	0.97	0.96
TPN-BM	4.5	3.5	810	410	1.4	1.3	0.97	0.96

Figure 3.6 - Langmuir-Freundlich adsorption isotherms for (A) CP and (B) CG monoliths: (♦) native and (●) functionalized with TPN-BM. In (C) are summarized the estimated parameters of Langmuir-Freundlich isotherms and standard errors, for CP and CG monoliths before and after functionalization with ligand TPN-BM and ligand 22/8 ([a]).[82]

In order to evaluate the mass transfer and dynamic binding properties of TPN-BM affinity monoliths, breakthrough curves of purified hIgG were performed in duplicates at a flow rate of 1 mL min^{-1} (Fig. 3.7). The residence time of a protein in a column is intrinsically related with the supports nature and morphological properties. Since the availability to interact with the protein of an immobilized ligand depends on the stereo-chemical hindrance, and on the morphological

and physicochemical properties of the monolith porous network, the flow rate has a key role in the establishment of ligand-protein interaction. Thus, based on the knowledge acquired in our previous work (Chapter 2),[82] where the optimal operating conditions for functionalized chitosan-based monoliths were evaluated, an optimal flow rate of 1 mL min^{-1} was chosen. Moreover, since the chemical groups of TPN-BM available after its coupling on chitosan-based monoliths are the same than ligand 22/8, the hydrophilicity of the affinity system will be similar justifying the use of the best flow-rate previously estimated. The estimated binding capacities for CP_TPN-BM and CG_TPN-BM were 125±7 and 60±5 mg hIgG g^{-1} support, with associated elution capacities of 78 and 40±5%, respectively.

Comparatively the analogue supports functionalized with ligand 22/8, show similar binding capacities: CP_22/8 (110±15 hIgG g^{-1} support, 90±5%) and CG_22/8 (90±5 mg hIgG g^{-1} support, 60±5%).

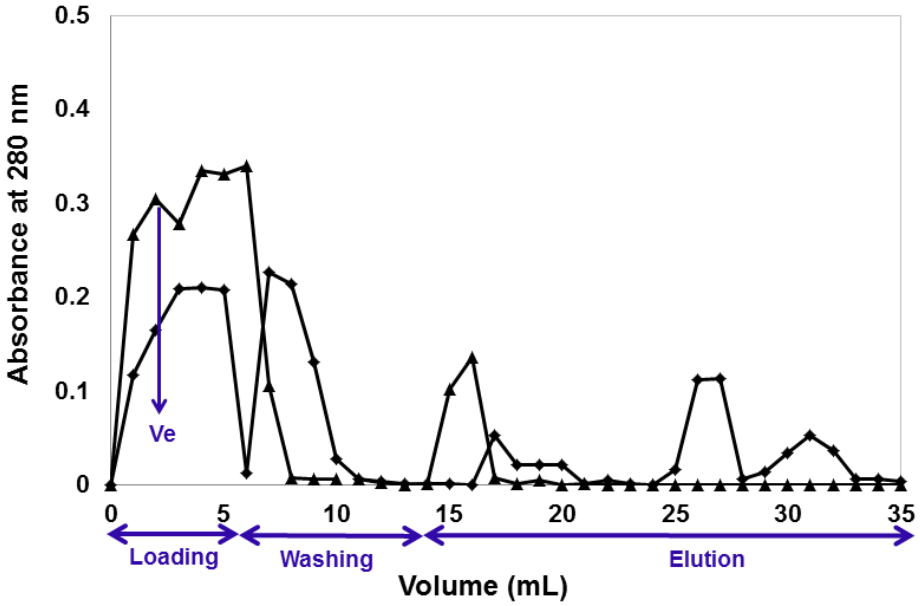

Figure 3.7 - Breakthrough profiles for human IgG upon CP_TPN-BM (♦) and CG_TPN-BM (▲) monoliths at a flow rate of 1 mL min^{-1}. All data was obtained from duplicated measurements with errors of ± 0.05.

3.3.4. OPTIMIZATION OF TPN-BM AFFINITY MONOLITH FOR ANTIBODY PURIFICATION

The optimization of the purification process was developed for CP_TPN-BM, since this monolith revealed the most promising morphological and mechanical properties, and presented also more attractive dynamic binding and elution capacities towards hIgG. The reuse capacity of the TPN-BM affinity monoliths for binding hIgG and BSA was assessed during three consecutive cycles, and a last cycle after autoclaving. BSA, a model protein, was used as a model contaminant. Based on our knowledge, native CP monoliths (before functionalization) exhibited similar performances on capturing and eluting hIgG and BSA, which are expressed by the low capacity to bind (20±5 mg protein per gram of monolith) and to elute (10±5 mg protein per gram of monolith) both proteins over the four cycles. On the opposite, CP_TPN-BM monoliths showed an extensive increase in binding and elution capacities towards hIgG (Fig. 3.8 A) while only a

minor amount of BSA was retained in the column (Fig. 3.8 B). Also, the most interesting feature was that the affinity and selectivity towards hIgG molecule is maintained over re-utilization, even after autoclaving. CP_TPN-BM monoliths are able to recover around 160±10 mg hIgG g^{-1} monolith and to elute 140±10 mg hIgG g^{-1} monolith. On the other hand, the amount of hIgG recovered during the regeneration step was negligible, around 20±5 mg g^{-1} support. This outstanding performance of CP monoliths functionalized with the TPN-BM ligand is very similar to those obtained for the same support functionalized with ligand 22/8. Furthermore, the binding and elution capacities of these sustainable CP_TPN-BM monoliths towards IgG are highly competitive with the ones obtained using affinity membranes, particles and other monoliths applied for antibodies purification, with the advantages resulting from their greener preparation.[11,13,82,114,135,139,141] To utterly validate the performance of the CP_TPN-BM monoliths, the purification of monoclonal antibodies (mAbs) from a non-clarified homogenate was evaluated.

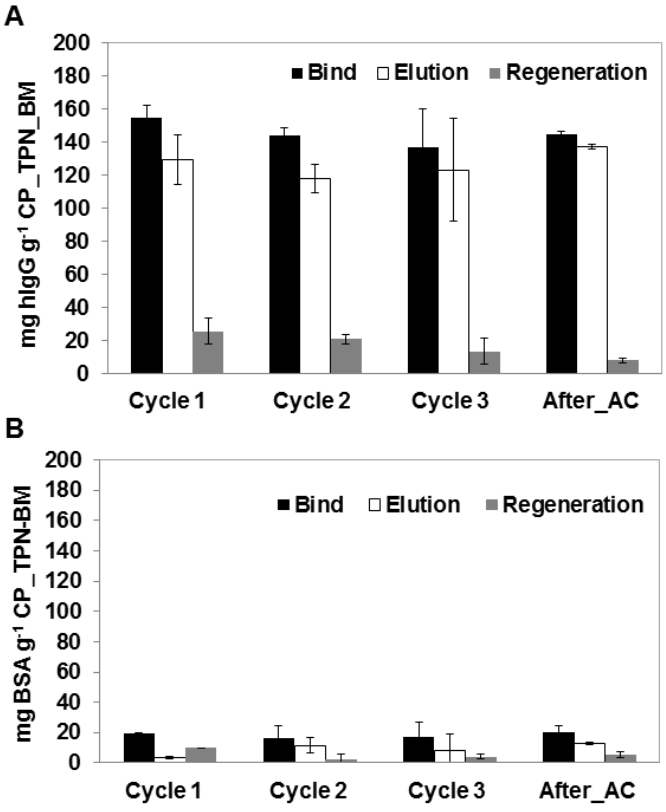

Figure 3.8 - Evaluation of chromatographic performance for CP_TPN-BM monoliths using pure human IgG (A) and BSA (B) solutions, respectively. The chromatographic procedures (binding, elution and regeneration steps) were performed consecutively along four cycles at a flow rate of 1 mL min^{-1}. The last cycle was performed after autoclaving (After_AC).

The data of CP_22/8 related with mAbs purification was added to enable a direct comparison between the performance of CP monoliths functionalized with ligands TPN-BM and 22/8. The chromatogram obtained from crude extract sample confirms that the non-functionalized monolith CP_N did not capture any protein (Fig. 3.9 A) while the affinity monoliths CP_22/8 and CP_TPN-BM captured respectively 61±10 and 75±5% of mAbs from a mammalian crude extract

with initial 1.3 mg of total protein per millilitre, eluting both around 80±10% of bounded protein. Additionally, concerning the purity of the samples (SDS-PAGE), the flow-through (3, 7) and washes (4, 8) bands showed the presence of contaminated proteins and antibody, while the elution (5, 6, 9, 10) fractions exposed only the corresponding bands of the mAbs fragments with high purity (estimated as 98% by densitometry analysis with Image J software).

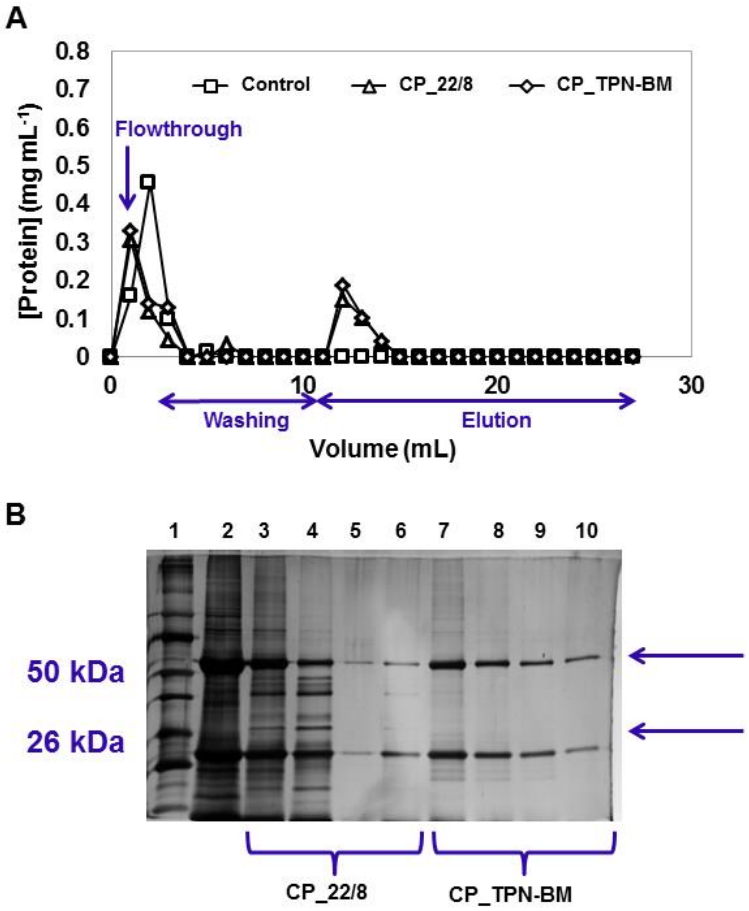

Figure 3.9 - Chromatogram of mAbs purification from crude extracts using (A) CP monoliths: (□) native, (◊) functionalized with ligand 22/8 and (Δ) functionalized with TPN-BM at a flow rate of 1 mL min^{-1}. The fractions collected included the flowthrough followed by the washing and elution steps. Acrylamide gel from SDS-PAGE performed with the fractions collected during the mAbs purification (B): lane 1 corresponds to the calibration proteins, lane 2 represents the loading for CP_22/8 and CP_TPN-BM, lane 3 and 7 are the flowthrough for CP_22/8 and CP_TPN-BM, lane 4 and 8 corresponds to CP_22/8 and CP_TPN-BM first wash using phosphate buffer (50 mM, pH 8.0), and lane 5, 6, 9 and 10 are the first and second elution fractions of CP_22/8 and CP_TPN-BM using sodium citrate buffer (50 mM, pH 3.0).

3.4. CONCLUDING REMARKS

This work proposes a sustainable strategy to produce new affinity platforms for antibody purification with particular regard to the material support (chitosan), functionalization procedure of the supports (based on plasma activation) and the affinity ligand synthesis. Specifically, this novel approach is focused on the replacement of ligand 22/8 (artificial protein A) by an analogous biomimetic ligand (TPN-BM) synthesized using a green protocol (with high chemical yield, fast reaction time, and less solvents and purification steps involved). If at small scale the synthesis herein proposed presented benefits, at larger scales the advantages are expected to be considerably higher, specially the reduction in time which allows for advances and/or refinements to be made in other stages of the process. TPN-BM was also characterized and further immobilized onto plasma-activated chitosan monoliths, creating a greener purification device which exhibited high performance towards antibody capture and elution (160±10 and 145±5 mg hIgG per gram support, respectively), and mAbs purification from a non-clarified homogenate with 98% of purity.

The strategy presented for the production of affinity purification devices can be a strong competitor to traditional affinity beads and membranes currently employed in chromatographic processes. It is expected that this new affinity platform will give an efficient answer to the current demand of antibodies in the diagnostic medicine and pharmaceutical fields with potential for industrial scale implementation.

CHAPTER 4

STRUCTURAL EVALUATION OF AN ALTERNATIVE PROTEIN A BIOMIMETIC LIGAND TOWARDS ANTIBODY PURIFICATION

SUMMARY

In this chapter it is intended to evaluate the potential of TPN-BM as an alternative affinity ligand towards antibody recognition and binding, namely IgG, at an atomic level, since it has already been tested, after immobilization onto chitosan-based monoliths, and demonstrated interesting affinity behaviour for this purpose. Herein, combining automated molecular docking and molecular dynamics simulations (MD) it was predicted that TPN-BM has high propensity to bind IgG through the same binding site found in the crystallographic structure of SpA_IgG complex as well as theoretically predicted for ligand 22/8_IgG complex. Furthermore, it was found that TPN-BM established preferential interactions with aromatic residues at the Fab domain (Trp 50, Tyr 53, Tyr 98 and Trp 100), while in the Fc domain the main interactions are based on hydrogen bonds with pH sensitive residues at operational regime for binding and elution like histidines (His 460, His 464, His 466). Moreover, the pH dependence of TPN-BM_IgG complex formation was more evident for the Fc domain, where at pH 3 the protonation state and consequently the charge alteration of histidine residues sited at the IgG binding site induced ligand detachment, which explains the optimal elution condition at this pH observed experimentally.

Article: *Telma Barroso, Ricardo Branco, Ana Aguiar-Ricardo and Ana C. A. Roque, Structural evaluation of an alternative Protein A biomimetic ligand towards antibody purification, Submitted.*

4.1. INTRODUCTION

Over the last decade, the evaluation of biological and chemical interactions at atomic level has become central to understand numerous phenomena, like molecular recognition and specific binding found in Nature.[155]

Currently, there is a plethora of computational methods and bioinformatic tools[155,156,157] available which comprise different protein-ligand docking algorithms, or molecular mechanics force fields that together enable to create strategies to address complex biochemical systems with a direct impact and potential applications in different areas of knowledge, like protein purification through affinity chromatography.[150,158,159,160]

As aforementioned, an extensive computational and experimental effort has been made to optimize affinity chromatographic methods in order to reduce associated costs to antibody purification.[23,112] Consequently, the development of synthetic affinity ligands has been pursued in order to design mimetic ligands of Protein A with better chemical stability, and an analogous specificity profile to the natural counterparts, at lower cost.[9] Particularly, ligands 22/8 and TPN-BM are biomimetic ligands based on substituted triazine ring that up to now, have shown great proficiency in antibody purification, from simple and complex mediums, when immobilized onto different supports such as: agarose,[11] magnetic nanoparticles,[114] cellulose membranes[88] and chitosan-poly(vinyl alcohol) (CP) monoliths.[82,161] However, in contrast to ligand 22/8 that after a theoretical evaluation through extensive molecular dynamic studies revealed to be an excellent Protein A biomimetic ligand, regarding the similar molecular interactions found in this affinity pair,[150,159,158] the molecular recognition and binding mechanism between TPN-BM and IgG affinity pair remains unveiled. Furthermore, the pH dependence that is required for the affinity chromatography elution and that was also rationalized for ligand 22/8 and Protein A in complex with IgG, is also unknown for ligand TPN-BM. Therefore, it is important to characterize the potential binding sites between the ligand TPN-BM and IgG, as well as to understand, at atomic level, the main intermolecular interactions responsible for the binding/unbinding molecular mechanism both at physiological (pH 7) and elution conditions (pH 3).[159]

In the following chapter, automated molecular docking followed by MD simulations,[160] were performed with TPN-BM and human IgG fragments, Fab and Fc, at pH 7 and 3, based on previous computational and experimental knowledge, in order to better understand the potential of this affinity pair for chromatographic purposes, in comparison with the performance of ligand 22/8 and natural Protein A.

4.2 METHODS

4.2.1. MOLECULAR MODELLING

The Fab fragment (Chains L and H with 214 and 230 amino acids, respectively) and Fc fragment (Chains H and K with 239 and 236 amino acids, respectively), were retrieved from the crystallographic structure of human IgG, with the Protein Data Bank (PDB) code 1HZH,[162] and used as the target protein in this study. Ligand TPN-BM was used as the synthetic affinity ligand. The 4-chloro position of the triazine ring was substituted by a HN-CH_3 moiety, to model the chemical effect of the spacer arm used experimentally for the immobilization of the ligand on a solid support afterwards (Fig. 4.1).

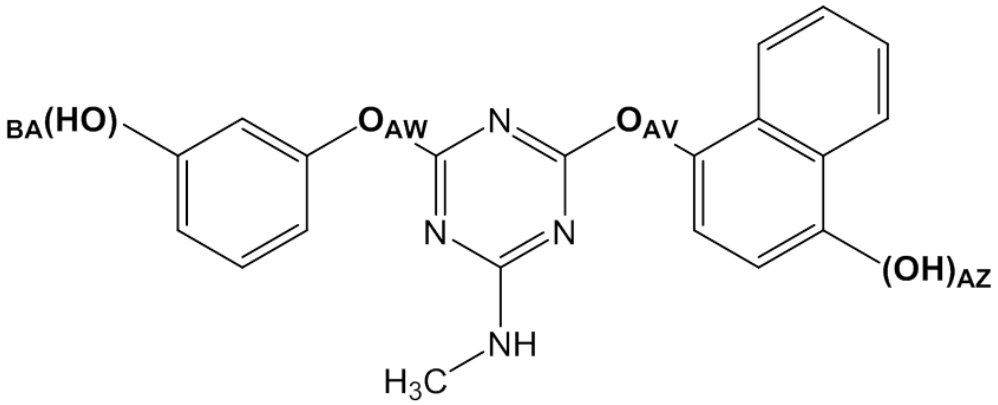

Figure 4.1 - Schematic representation of the ligand 4-((4-chloro-6-(3-hydroxyphenoxy)-1,3,5-triazin-2-yl)oxy)naphthalen-1-ol (TPN-BM) labeled with the atom identification for convenience. (Software used: ChemBioDraw Ultra 13.0).

4.2.2. MOLECULAR DOCKING

The Gasteiger partial charges and AutoDock atom types were automatically assigned to the receptor and ligand coordinate files through the AutoDock 4.2 python scripts. A blind docking using a grid map with 78 Å side (comprising 100 grid points in each orthogonal x, y and z axis, with a grid spacing of 0.78 Å), covering entirely the special volume occupied by each IgG fragment, was setup around the receptor's centre of mass using the AutoDock 4.2 tool package.[163] A sigmoidal distance-dependent dielectric function was used for the dielectric continuum solvent with a constant value of −0.1465 by default.[164] A total of 256 independent solutions were evaluated during conformational search using a Lamarckian Genetic Algorithm (LGA) with the following parameters set: an initial population of 150 conformations, a maximum number of 2,500.000 energy evaluations, a maximum number of 27,000 generations, a mutation rate of 0.02, and a crossover rate of 0.8. Non-specified settings were assumed by default. A RMSD cut-off value of 2.0 Å was used in the automated cluster analysis. The total number of torsional degrees of freedom on the TPN-BM (TORSDOF) was 4. Docking results were interpreted taking into account two criteria: (i) energy criteria – the top-scoring docking solutions with the best estimated binding free energy were selected; (ii) geometry criteria – as the affinity

ligands are used for purification purposes, docking solutions leading to ligand interactions in the target receptor inner cavities were discarded. Additionally, only solutions where the anchoring point of TPN-BM affinity ligand to the solid support was exposed to the solvent were selected, taking into account the constraints imposed by the solid support on the conformational space available for ligand to explore.[165]

4.2.3. MD SIMULATIONS

Molecular dynamics were performed using the GROMACS 4.5 simulation package[166] running in parallel on the in-house Sun Grid Engine (SGE) high performance computing cluster. The top-ranked docking solutions of ligand TPN-BM with Fab and Fc fragments of IgG were taken as starting structures for the MD simulation runs. Amino acids protonated state was adjusted according to their pKa values, at specific pH condition. The topology and force field parameterization of the ligand TPN-BM were derived from the Dundee PRODRG web server.[167] The TPN-BM_IgG complex was solvated in a truncated octahedral box with explicit SPC water model, keeping a buffer distance between the protein and the box edges of 12 Å due to the periodic boundary simulation conditions. The electro neutrality of the box was ensured by the addition of a correspondent number of Na^+ or Cl^- counter ions, depending on the global charge of the protein system. The complex was simulated using the GROMOS 53A6 force field.[168] The simulation protocol comprised three phases: (1) potential atomic clashes were removed through a steepest descent minimization algorithm in 2,000 steps followed by 1,000 steps using the conjugate gradient algorithm, (2) TPN-BM_IgG complex system was equilibrated in three subsecutive steps of 100 ps each, reducing gradually the force constant for positional restraint of heavy atoms from 1,000, 100 to 10 KJ mol^{-1} and (3) total relaxation of the system during production phase. All simulations ran under periodic boundary conditions in an isothermal-isobaric (NPT) ensemble, coupled to the Berendsen barostat with a reference pressure of 1.0 bar and a coupling time constant of 0.6 ps,[169] as well as to the V-rescale thermostat with a reference temperature 300 K and a coupling time constant of 0.1 ps.[170] A simulation time step of 2 fs was used. The LINKS algorithm was applied to constrain all H-bonds,[171] and the electrostatic term was described by using the particle mesh Ewald algorithm for long-range electrostatics, as implemented in GROMACS software. Finally, in the production phase all atomic force constraints were removed and each system was simulated during 20 ns. The particle composition of MD simulation boxes are summarized in Table 4.1.

Table 4.1 - Properties of molecular system used on MD simulation.

		Simulation conditions		System composition			
MD trajectory ID	**IgG fragment**	**pH**	**Box dimensions**	**Counter ions**	**Number of water molecules**	**Total number of atoms in the system**	**MD trajectory lenght (ns)**
103	**Fab**	7.0	11.31; 10.66; 9.23	9 Cl	34507	108031	20
		3.0	11.31; 10.66; 9.23	37 Cl	34485	108021	20
049		7.0	10.72; 10.11; 8.75	9 Cl	29394	92692	20
		3.0	10.72; 10.11; 8.75	37 Cl	29367	92667	20
024		7.0	10.72; 10.11; 8.75	9 Cl	29390	92680	20
		3.0	10.70; 10.10; 8.74	37 Cl	29381	92681	20
145		7.0	10.72; 10.11; 8.75	9 Na	29387	92671	20
		3.0	10.72; 10.11; 8.75	37 Cl	29356	92643	20
204	**Fc**	7.0	10.62; 10.01; 8.67	3 Na	28209	89136	20
		3.0	10.57; 9.97; 8.64	41 Cl	28179	89128	20
255		7.0	10.62; 10.01; 8.67	3 Na	28202	89115	20
		3.0	10.62;10.01; 8.67	41 Cl	28162	89077	20

The sequence numbering further referred to in this chapter was based on the numbering of the crystallographic structure PDB code 1HZH. The visualization software PyMol 1.2[172] and VMD 1.9[173] were used to generate the graphical artwork.

4.3. RESULTS AND DISCUSSION

The main interactions of SpA and ligand 22/8 with Fab and Fc fragments from immunoglobulin G (IgG) are very well studied in the literature.[150,159,158] It was found that SpA binds to hIgG at a consensus binding site (CBS) located in the hinge between the C_H2 and C_H3 regions of Fc domain and composed by the residues: Met 252, Ile 253, Gln 330, His 464, Asn 465, His 466 and Tyr 467, according to the 1HZH protein sequence numbering.[158] The binding site predicted for the interaction of ligand 22/8 with the Fc domain comprised the following amino acids: Leu 333, Asn 334, Gln 330, His 329, Glu 461, Ala 462, Leu 463, His 464, Asn 465 and His 466 which correspond to the CBS predicted for the biological interaction with SpA.[150] Moreover, also Zamolo *et al.* found out a similar set of molecular interactions for the small biomimetic ligand - A2P.[165] In this work, docking studies were firstly performed to evaluate preferential binding sites between ligand TPN-BM and IgG fragments separately. The top-ranked docking solutions, e.g. the ones with the higher estimated binding free energy in module, were evaluated in terms of

the population size of each cluster of solutions and eventual geometrical constraints at the protein binding site. According to the selection criteria, the chosen docking solutions were further investigated through MD simulations. Since the affinity purification of antibody fragments by adsorption/desorption mechanisms is known to be pH dependent,[159] the evaluation of ligand-protein interactions at the commonly used experimental conditions for chromatographic loading and elution of antibody (pH 7 and 3, respectively) was also performed.

4.3.1. INTERACTIONS OF LIGAND TPN-BM WITH IgG FRAGMENTS

The top-ranked docking solution of ligand TPN-BM at the Fab domain of IgG presented an estimated binding free energy of −7.32 kcal mol^{-1} and a cluster population of 4 docking solutions. Additionally, the second and third top-ranked clusters with an estimated binding free energies ranging between -6.78 and −7.32 kcal mol^{-1} and with a significant population of 8 and 13 solutions each, were also filtered and further analysed, according to energetic and geometrical criteria described in the Methods Section. The remaining clusters were discarded because they exhibited either lower estimated binding energies or represented unreachable inner binding cavity solutions, which from a practical point of view could never take place in a real situation for an immobilized ligand onto a support. Remarkably, 3 out of 5 docking solutions showed a clear preference to interact with the Fab domain in a specific aromatic region located in the heavy chain H and establishing main interactions with residues: Trp 50, Tyr 53 and Tyr 98. The 3 similar cluster solutions reinforce the preference of ligand binding to Fab fragment, with an estimated associated affinity constant (K_a) of 2.11×10^5 M^{-1} (-7.08 kcal mol^{-1}, average of estimated binding free energies) (Table 4.2). This value is in accordance with previous theoretical predictions, since it is within the range of the affinity constants obtained for SpA_IgG (4.64×10^7 M^{-1}) and ligand 22/8_IgG systems (7.00×10^3 M^{-1}) (Table 4.2).[150]

Regarding the docking of ligand TPN-BM at the Fc fragment, the maximum estimated binding free energy was -7.77 kcal mol^{-1}. After applying the same filtering criteria as for Fab domain, only 4 out of 31 clusters were considered with estimated binding free energies of -6.79, -6.73, -6.70 and -6.67 kcal mol^{-1} with 7, 2, 3 and 1 elements, respectively. The first 2 top-ranked cluster solutions were selected, considering the highest affinity constant of $K_a=8.60\times10^4$ M^{-1} (Table 4.2). The K_a obtained is one order of magnitude inferior when compared with the one estimated for Protein A and ligand 22/8, 8.09×10^5 and 1.47×10^5 M^{-1}, respectively.[150] However, a range 10^3-10^9 M^{-1} for K_a corresponds to a median affinity value[6] thus, the estimated K_a value obtained for the complex between Fc fragment and ligand TPN-BM is significant. Moreover, comparing theoretical and experimental K_a*'s* obtained for CP monolith functionalized with ligand TPN-BM ($K_a=4.50\times10^4$ M^{-1}) it is possible to observe that the values are comparable, and are in agreement.

Table 4.2 - Experimental and theoretical values of affinity constants for Immunoglobulin G and protein A, or ligand 22/8 or ligand TPN-BM.

	Experimental, K_a (M^{-1})			Theoretical, K_a (M^{-1}) (ΔG in kcal mol^{-1})	
	IgG	**Fab**	**Fc**	**Fab**	**Fc**
Protein A[150]	1.40×10^7 3.65×10^5	1.20×10^7	10^3 (10.46)	4.64×10^7	8.09×10^5
Ligand 22/8[150]	1.40×10^5	n.a.	n.a	7.00×10^3 (-5.24)	1.47×10^5 (-7.05)
Control 0/0[150]	~0.0	~0.0	~0.0	No significant docking solutions below 3.00×10^3 (ca. −4.74)	No significant docking solutions below 4.00×10^3 (ca. −4.94)
Ligand TPN-BM	n.a.	n.a.	n.a.	2.11×10^5 (-7.08)	8.60×10^4 (-6.73)
CP_22/8[82]	4.00×10^4	n.a.	n.a.	n.a.	n.a.
CP_TPN-BM[161]	4.50×10^4	n.a.	n.a.	n.a.	n.a.

Therefore, the characterization of the predicted TPN-BM_IgG complexes was fully investigated by MD, over 20 ns in total. The main amino acids contributions for the affinity ligand binding were then evaluated and quantified in order to understand better the recognition and binding mechanism behind.

From the MD simulations of TPN-BM_Fab complexes, it was noticeable a high preference of ligand TPN-BM to bind to a narrow aromatic pocket defined by the side chains of **Trp 50**, **Tyr 53**, **Tyr 98** and **Trp 100** residues at the surface of heavy chain H. In fact, TPN-BM is stabilized by the π-π* stacking interaction established between the phenolic group of the ligand, and the side chains of Tyr 53 and Tyr 50, representing ca. 34% of total simulation time. Furthermore, an H-bond interaction between O_{AW} and O_{AV} oxygen atoms from the ligand and Tyr 53 hydroxyl group respectively, act as driving forces by positioning the ligand toward additional H-bond interactions. These interactions induce the repositioning of the ligand, which become entrapped by the naphtol ring between Trp100 and Tyr 98 through a typical π-π* stacking interaction, both with the two ligand substituents at the opposite side of the binding pocket, has depicted in Fig. 4.2. These interactions prevail during 24% of the simulation time (Table 4.3). Moreover, Tyr 96, Tyr 91 and Trp 50 side chains also exhibit a considerable influence on the capture of TPN-BM by this hydrophobic binding site, considering a threshold distance of 5 Å between TPN-BM atoms and IgG residues as well as bellow 3 Å between heavy atoms for a strong interaction. The aromatic interactions that drive the complex formation between the ligand TPN-BM and Fab fragment are well supported by previous theoretical studies.[150,158,159]

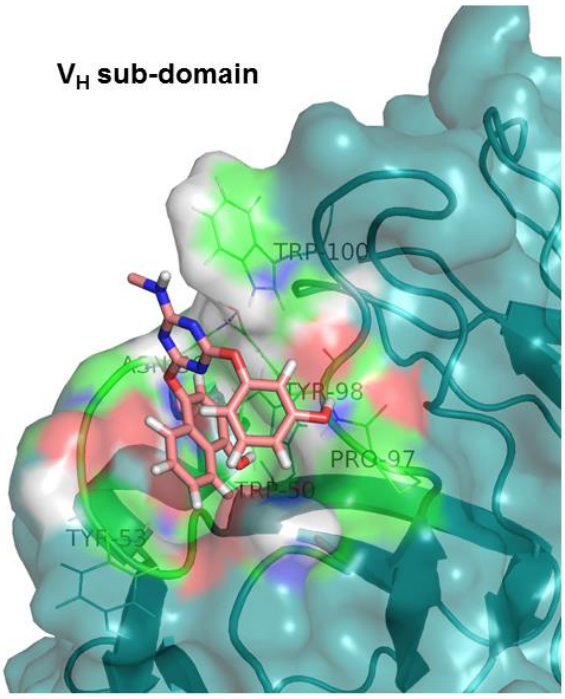

Figure 4.2 - Image showing the preferential binding site of ligand TPN-BM in the Fab fragment of IgG (PDB code 1HZH). Highlighted regions in the Fab represent residues that are within 5 Å from the ligand, colored by hydrophobicity. (Software used: Pymol 1.3. and VMD 1.9.1).

Considering the dynamical behavior of TPN-BM when complexed with the Fc fragment of IgG, two binding poses from docking were further evaluated. The first one, in the CBS, was also reported by Branco *et al.*[150] and Huang *et al.*,[158] located in the hinge region between the C_H2 and C_H3 domains of Fc fragment. The main CBS's amino acids involved are His 460, **His 464**, **Asn 465**, **His 466** and **Tyr 467**. In bold are amino acids reported in the literature as anchoring points for the natural binding domain SpA, or affinity ligands as 22/8 or A2P to the Fc domain.[150,159,165] Particularly, Tyr 467 has a pivotal behaviour by anchoring the TPN-BM ligand and exposing it to a histidine rich environment (His 460, His 464, His 466), which will have a key role in the pH-dependent behaviour at elution conditions. The His 466 side chain establishes a close contact (≤5 Å distance) with the naphtol O_{AV} group of the ligand during 80% of the simulation time (Fig. 4.3 B). Moreover, His 464 and His 460 side chains also have a significant contribution for the ligand binding at a short distance between 3 and 5 Å. Therefore, the CBS site for the Fc_TPN-BM system is maintained mostly by histidine residues. An alternative binding site to the CBS located in the heavy chain K was also investigated. The main residues involved in this binding site are His 302, Thr 306, Asn 303 and Lys 287 (Fig. 4.3 A).

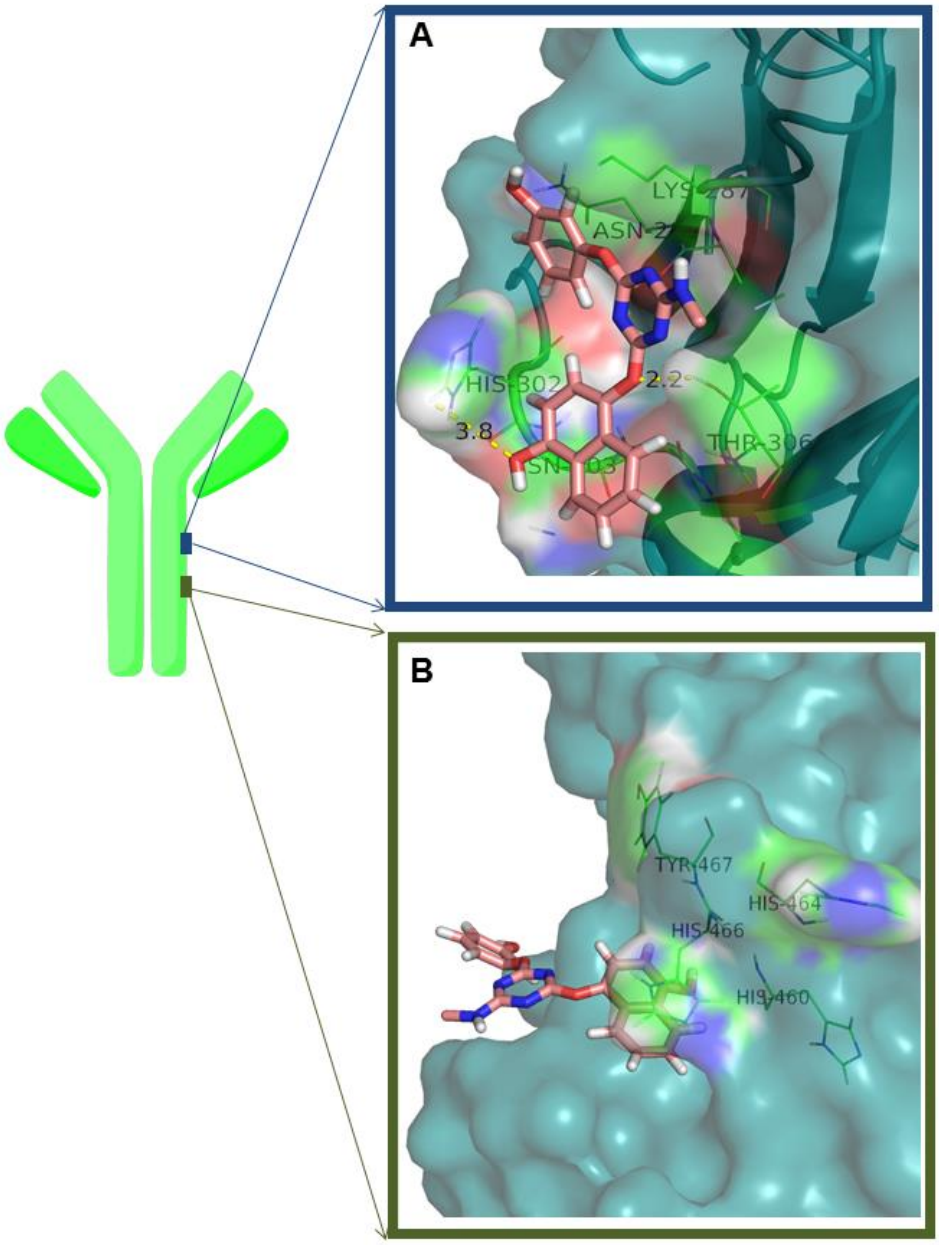

Figure 4.3 - Image showing alternative binding sites of ligand TPN-BM in the Fc fragment of IgG (PDB code 1HZH). Highlighted region in the Fc represents the residues that are within 5Å from TPN-BM, colored by hydrophobicity. (Software used: Pymol 1.3. and VMD 1.9.1).

However, His 302:H_{AZ} and Thr 306:O_{AV} at the naphtol side play the most important role to anchor the TPN-BM bound to the Fc domain during 24% and 56% of the simulation time, respectively (see Table 4.3). Smaller contributions from Asn 303 (interaction during 5% of the simulation time with O_{AZ} from the naphtol ring) and Lys 287 (interaction during 10% of the simulation time with O_{AW} from the phenol ring) also contribute to the stabilization of the ligand.

Table 4.3 - Resume of the main type of interactions and their contributions over simulation time for TPN-BM_IgG complexes.

IgG target	Binding site	MD trajectory ID	Main Interactions	Interactions type	Contribution (%)	
					pH 7	pH 3
Fab	1	103	Tyr 53 – O_{BA}; H_{AZ}; O_{AV}: O_{AW}	Hydrophobic $\pi - \pi^*$ (aromatic staking)	21	11
			Trp 50 - O_{BA}		N/O	9
	1	049	Leu 104 - H_{BA}	H-bonds	N/O	26
			Arg106 - O_{AZ}		N/O	43
	1	024	Trp 50 - O_{AW}	Hydrophobic	13	N/O
			Tyr 98 - O_{AW}	H-bond	10 (4-6Å)	10
			Asn 31 - O_{AW}	H-bond	N/O	31
			Asn 34 - O_{AV}	H-bond	N/O	23
	2	145	Trp 100 - O_{AZ}	H-bond	24	4
			Tyr 98 - H_{BA}	$\pi - \pi^*$ (aromatic staking)	24	21
Fc	1	204	His 466 - O_{AV}	H-bond	10 (4-6Å)	N/O
			Tyr 467 - O_{AW}	H-bond	6	N/O
			His 464 and His 460 around binding site		100 (6Å)	N/O
	2	255	His 302 - H_{AZ}	H-bond	24	21
			Thr 306 - O_{AV}	H-bond	56	41

N/O: Not observed

4.3.2. pH DEPENDENCE ON THE AFFINITY BETWEEN TPN-BM AND IgG

The natural ligand SpA as well as the biomimetic affinity ligands 22/8 and A2P have shown a considerable pH dependence on IgG binding, both at experimental and theoretical levels. This dependence is of crucial importance for the capture and recovery of antibodies, as the elution process is trigger by a drastic change in the pH. In order to confirm the experimental evidence that TPN-BM affinity ligand binds and elutes IgG efficiently at pH 7 and 3, respectively, MD simulations of the complexes of TPN-BM with IgG fragments were run in parallel also at pH 3 for all solutions previously considered and evaluated at pH 7 for the binding conditions.

Regarding the Fab domain, the key interactions observed at pH 7 were conserved at pH 3 however with an inferior contribution, namely for the Trp 50, Tyr 53, Tyr 98 and Trp 100 residues (see Table 4.3). It is not surprising that the main interactions are still maintained at pH

3, since these amino acids have essentially an aromatic character and an invariant protonation state over the simulated pH range between 7 and 3. Then, the adjustment of the ligand position at pH 3 only implied a slight decrease of the interactions with Tyr 53, Tyr 98 and Trp 100 side chains and the formation of four new ones. These new interactions were established between O_{AW} and O_{AV} from the backbone of TPN-BM ligand and Asn 31 and Asn 34 of IgG, respectively, as well as the interaction between the O_{AZ} atom from the naphtol ring and O_{AW} from the phenol ring and Arg 106 and Leu 104 side chains of IgG, respectively, which account for 23-43% of the total simulation time (see Table 4.3). These results reinforced the tendency of triazine-based ligands to recognize preferentially aromatic containing binding sites in the Fab domain, despite the fact that the precise location of the TPN-BM binding site does not coincide with the ones described previously for analogue ligands.[150,165] The pH dependence results are consistent with the different amino acid nature of IgG fragment domains, since the amino acid composition of Fab binding site recognized by TPN-BM, in contrast to the His rich binding site found in Fc, is not sensitive to drastic changes in pH, in accordance with previous works.[150,158,159] In a marked contrast, the pH dependence of CBS in the Fc binding domain is considerably pronounced. At pH 3, the His and Glu residues at the CBS become protonated and the formal charge of the protein system, and in particular at the Fc binding site, increase inducing the ligand to detach from the former tightly bound pocket, as observed experimentally[161] (see Fig. 4.4). MD trajectories simulated at pH 3 have shown the ligand moving away from the binding site (8Å) and losing interactions with IgG residues at the surface. The second TPN-BM binding site found at the Fc domain involved the His 302 and Thr 306 side chains which reduced the binding interaction in 3% and 15% of simulation time at pH 3, respectively. However, special attention should be paid not only to the percentages of interactions in time, but mainly to the histidine profile at both pH's (Fig. 4.5). At lower pH the ligand is still bound through the hydrophilic interaction of Thr 467, accounting for 56% of the simulation time, nevertheless the tendency for the interaction disruption is clear. At pH 3, the ligand moved away from a closer distance between 3 and 5 Å to 15 Å from the Fc domain along the simulation trajectory. These observations suggest that, the affinity of the TPN-BM ligand to the Fc domain become weaker at lower pH, which seems to be directly related to the highly His content surrounding the Fc binding site. Also Branco *et al.*[150] found that for SpA_IgG and ligand 22/8_IgG systems the complex dissociation was reached at lower pH due to the repulsive interactions developed at the binding site. Another aspect that should be taken into account concerning the pH dependence rationalization was addressed by Huang *et al.*[159] on the influence of pH on the affinity of SpA_hIgG complex formation. It was concluded that SpA always binds the surface of hIgG during the simulation but slides slowly on the surface of hIgG and moves away from the binding site at pH 3. They understood, based on the calculation of binding free energies of electrostatic and non-polar interactions, that the dissociation at pH 3 is mainly driven by the electrostatic interactions, since the majority of SpA and IgG residues at pH 3 were positively charged, becoming favourable the electrostatic repulsion, as highlighted by the present results.

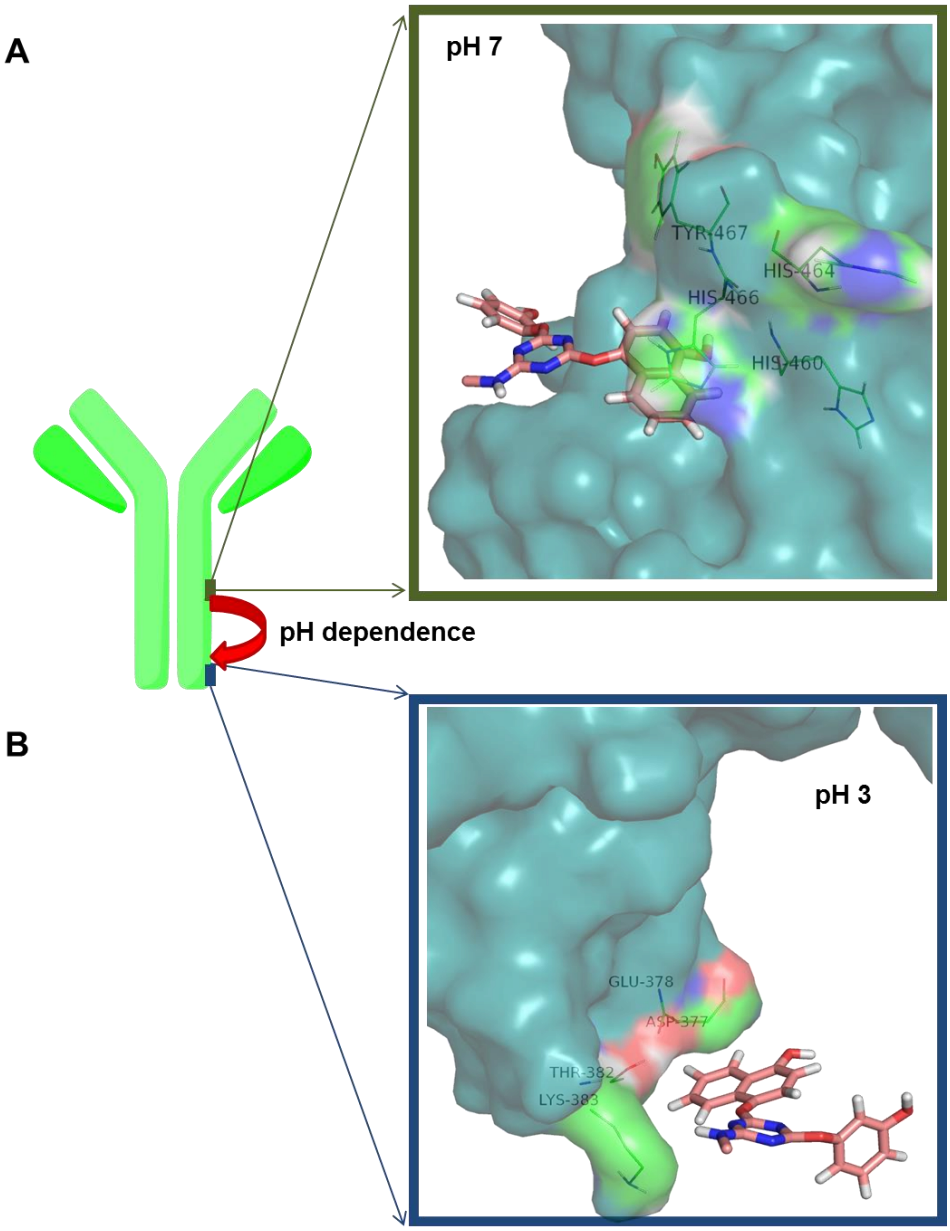

Figure 4.4 - pH dependence of ligand binding to the Fc fragment of IgG (PDB code 1HZH). Protonation state of the protein residues adjusted to pH 7 (A) where the naphtol ring of the ligand is anchored within 5 Å to the polar and hydrogen bonding interaction with the Fc domain; and pH 3 (B), where main hydrogen bond interactions were disrupted forcing the ligand to drift away from the receptor (distances above 8Å). Both regions of interactions are coloured by hydrophobicity of the correspondent residues. (Software used: Pymol 1.3 and VMD 1.9.1).

Moreover, they also pointed out the important role of His 137 of SpA. They observed that His 137 contributed for a high association to IgG at pH 7 and to a high dissociation at pH 3 due to the charge of the residue at both pH. Herein, a similar effect was observed between the imidazole rings from His and phenolic substituents of the ligand. Thus, we strongly believe that histidines present in the Fc domain are the main responsible residues for the pH dependence of TPN-BM_IgG complexes in a more general view.

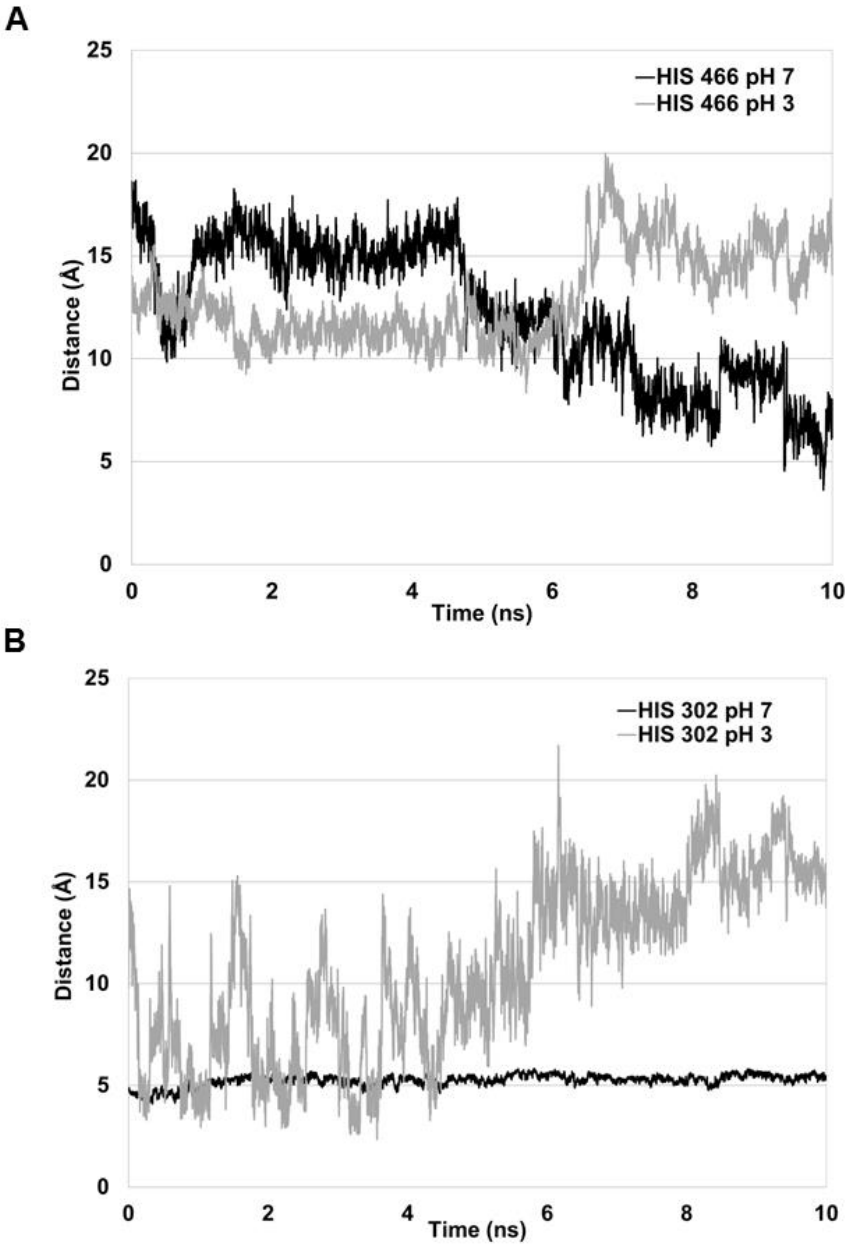

Figure 4.5 - Graphical representation of the distance between the His 466 (A) and His 302 (B) with the ligand atom type O_{AV} and O_{HAZ}, respectively at both pH (pH 7 line coloured in black and pH 3 line coloured in gray), monitored along the 10 ns of simulation time.

4.4. CONCLUDING REMARKS

Automated molecular docking coupled with MD simulations constitute a powerful set of tools to predict and evaluate the most energetically favorable binding modes of ligand TPN-BM to the Fab and Fc domains of IgG. The dynamical behavior of the best docking hits was fully characterized and compared with other SpA biomimetic analogues already described in the literature.

In particular, MD simulations revealed 3 putative binding sites on the Fab domain with an estimated affinity constant in the range of $K_a \approx 10^5$ M^{-1}. This value is comparable with previous theoretical predictions for the SpA_IgG complex ($K_a = 4.64 \times 10^7$ M^{-1}), and also for the analogue ligand 22/8_IgG complex ($K_a = 7.00 \times 10^3$ M^{-1}). Moreover, MD simulations indicate that TPN-BM interacts stronger with the Fab domain, mainly based on aromatic interactions through amino acids Trp 50, Tyr 53, Tyr 98 and Trp 100. This cavity is similar in nature to the ones reported for SpA_IgG and ligand 22/8-IgG complexes, despite the fact that these residues location does not coincide. Regarding the Fc domain, two top-ranked cluster solutions with an affinity constant of 8.60×10^4 M^{-1} were further investigated. Interesting enough, the estimated affinity constant is similar to the one measured experimentally, using CP monoliths functionalized with TPN-BM. Conversely to the Fab fragment, in the Fc domain the TPN-BM is in two histidine rich binding regions involving His 460, His 464, Asn 465 and His 466 residues. MD results suggest that the binding site found in the crystallographic structure of the systems SpA_IgG and in the simulations of the ligand 22/8-IgG complex, was also identified in the TPN-BM_IgG complex, which is localized at the hinge between C_H2 and C_H3 regions of Fc fragment involving His 464, Asn 465 and His 466 as the key players.

Moreover, the pH dependence of TPN-BM_Fc complex was tested at pH 3 and confirmed for the Fc fragment. Due to the high density of histidines at the Fc binding site, the on-off binding mechanism was validated by simulating lower pH conditions, which determined the protonation state of histidine and glutamic acid residues, and consequently induced repulsive interactions between the ligand and the protein target upon an increase in the protein surface charge. This reversible on/off binding behaviour shown by the TPN-BM_IgG complex helps to rationalize the required operating conditions during a binding/elution chromatographic purification process.

All the information presented in this chapter, although to corroborate with the obtained experimental data involving the use of a “greener chromatographic approach” (TPB-BM ligand immobilized onto CP monoliths for IgG purification) (see Chapter 3), allows understanding this affinity pair at atomic level. Additionally, all these findings can also contribute to the design of novel affinity ligands towards antibody purification as well as to evaluate their potential as a sustainable affinity chromatographic solution.

CHAPTER 5

HYBRID MONOLITHS FOR MAGNETICALLY-DRIVEN PROTEIN SEPARATIONS

SUMMARY

This work presents a hybrid approach for antibody (Ab) capture and release. Using mostly natural polymers and sustainable processes, it was possible to create macroporous monoliths with well-defined porous networks tuneable mechanical properties and easy functionalization with a biomimetic ligand specific for Ab. Magnetic nanoparticles (MNPs) were embedded on the monolith network to confer a controlled magnetic response that facilitates and accelerates Ab recovery in the elution step. The hybrid monolithic systems prepared with agarose or chitosan/poly(vinyl alcohol) (PVA) blends exhibited promising binding capacities of Abs directly from cell-culture extracts (120±10 mg Ab g^{-1} support) and controlled Ab magnetically-assisted elution yielding 95±2% recovery. Moreover, a selective capture of mAbs directly from cell culture extracts was achieved comprising 96% of purity.

Article: *Telma Barroso, Teresa Casimiro, Ana M. Ferraria, Fábio Mattioli, Ana Aguiar-Ricardo and Ana C. A. Roque, Hybrid monoliths for magnetically-driven protein separations. Submitted.*

Attended conference (oral apresentation): Telma Barroso, Ana Aguiar-Ricardo and Ana Cecília Roque, "Hybrid monoliths based on natural biopolymers for the affinity purification of biopharmaceuticals" in European Symposium on Biopolymers, 2013, Lisboa-Portugal.

5.1. INTRODUCTION

Over the last years different synthetic polymers have been used to prepare a wide range of chromatographic supports.[15] However, regulatory laws are pressing the industry to redesign products and processes toward sustainable and disposable alternatives.[23] Chitosan (CHT),[20,82] agarose (AG)[40,72] and dextran (DXT)[174] are alternative and natural polymers widely used for biomedical and biotechnological purposes,[175,176] namely in the design of macroporous structures for cell growth,[128] isolation and immobilization of proteins,[177] drug delivery and tissue engineering.[178] Natural polymers present outstanding properties; they possess high density of functional chemical groups, fouling resistance, biocompatibility and biodegradability.[71] "Smart" or "intelligent" materials[179] are also interesting due to their capacity to respond to very slight changes (pH, temperature, light and electric or magnetic field) in the surrounding environment leading to modifications in shape, surface characteristics, solubility and others.[180,181] With the rapid development of nanotechnology, iron oxide magnetic nanoparticles (MNPs) are one of the most explored smart materials in a widespread range of different fields including magnetic resonance imaging,[182,183] drug delivey,[184,185] immobilization of biomolecules and separations.[114,186] In particular, MNPs can be combined with various polymers and functionalized with ligands commonly employed in chromatographic methods, leading to nano and micro absorbents suitable for Ab purification.[1,176,187,188] The combination of hydrogels or cryogels with MNPs has also been explored for the production of different magnetic macroporous structures with interconnected pores in the micrometer range.[188,189,190] Additionally, these composite materials, in the presence of a moderate magnetic field, are able to deform which enables the flux of water or other fluids enhancing the release of biological agents like cells and proteins. Thus, this feature permits controlled actions and consequently, faster processes. However, these macroporous materials were never tested for chromatographic applications.

Inspired by these features, this work aimed (1) the design of hybrid monoliths following green chemistry guidelines, and (2) the evaluation of the hybrid monoliths as purification devices using a novel magnetically-assisted elution protocol. The hybrid concept results from the synergy between the capturing of Ab through affinity interactions and a magnetic response for improved Ab elution. Macroporous monoliths based on chitosan, agarose, dextran and PVA, with and without MNPs embedded, were prepared by combining freezing and lyophilization processes.[78] Conversely to the traditional procedures,[187,191,192] in this work the natural polymers were not chemically modified but physically entrapped by the polymeric network built from glycidyl methacrylate (GMA), acrylamide and bisacrylamide, that worked as monomers and crosslinking agents, respectively. This strategy assures the biodegradability of the monoliths, since the natural polymers remain unchanged, and offer a sustainable solution for robust materials processing. The macroporous materials were then aminated using plasma technology,[122,193] a solvent free technique, for further ligand coupling. The amination based on plasma treatment takes advantage of the high reactivity of argon(Ar)-plasma which generates free radicals sites located at monoliths surface, promoting *in situ* heterogeneous chemical reactions with gas-

phase molecules like amines (1,6-hexanediamine, in this case). The functionalities introduced allowed the coupling of TPN-BM, a synthetic affinity ligand previously developed as a Protein A mimic.[161] The presence of MNPs at the monolithic porous network will confer a magnetic response to the material which facilitates Ab recovery by controlled shrinking.

This strategy intends to develop a smart, efficient, fast and eco-friendly approach for Ab purification which can be extended to other biotechnological and biomedical applications.

5.2. EXPERIMETAL AND METHODS

5.2.1. MATERIALS

Ammonium persulfate (APS, purity≥98%), citric acid (purity≥99%), disodium hydrogen phosphate monodibasic (pa), disodium hydrogen phosphate dibasic (pa), disodium tetraborate, ethanol absolute and sodium citrate dihydrate were purchased from Merck. Isopropanol and sodium bicarbonate were purchased from Riedel-de-Haën. Agarose (electrophoresis grade) was purchased from nzytech. Acetone (purity≥99%), and ethyl acetate were supplied by Roth. Acetic acid (purity≥99%), aminocaproic acid, 3-aminophenol, 4-amino-1-naphthol hydrochloride, cyanuric chloride (purity≥98%), 1,6-hexanediamine (purity≥98%), N,N-dimethylformamide (DMF), dimethylsulfoxide (DMSO), chloridric acid (HCl), glycine, ninhydrin, iron (II) chloride tetrahydrate ($FeCl_2.4H_2O$, purity≥99%), iron (III) chloride hexahydrate ($FeCl_3.6H_2O$, purity≥99%), potassium cyanide, pyridine, sodium hydroxide (purity≥99%), sulfuric acid (H_2SO_4, purity≥95%), sodium phosphate monobasic monohydrate ($H_2NaO_4P.H_2O$, purity≥98%), di-sodium hydrogen phosphate 2-hydrate ($Na_2HPO_4.2H_2O$, purity≥98%) were purchased from Sigma Aldrich. Acrylamide (C_3H_5NO, purity≥99%), anthrone ($C_{14}H_{10}O$, purity≈97%), ammonium hydroxide (NH_4OH, 5.0N) chitosan (75~85 % deacetylated, medium molecular weight), dextran ($(C_6H_{10}O_5)n$), hydroxylamine hydrochloride ($H_3NO.HCl$, purity≥99%), poly(vinyl alcohol) (purity≈99%), *N,N*-methylenebisacrylamide (MBAm, purity≥85%), *N,N,N',N'*-tetramethylethylenediamine (TEMED, purity≈99%), bicinchoninic acid (BCA) kit, bovine serum albumin (BSA) (purity≥98%) were supplied by Sigma Aldrich. Human IgG (Gammanorm) was supplied by Octapharma (purity≥99%). 1.10-phenonthroline 1-hydrate ($C_{12}H_8N_2.H_20$, purity≈99%) was acquired from Panreac.

5.2.2. PREPARATION OF MAGNETIC NANOPARTICLES

Magnetic nanonopaticles were synthesized via alkaline precipitation of $FeCl_3$ and $FeCl_2$ using a Fe^{2+}/Fe^{3+} molar ratio of 0.5, according to Batalha *et al.*[114] In a sealed stirred reactor with agitation at approximately 1200 rpm, 250 ml of a solution of 0.7 M ammonium hydroxide in deionized water was purged with N_2 during 30 min. Then, a freshly prepared iron solution (5.4 g of $FeCl_3.6H_2O$ and 2.0 g of $FeCl_2.4H_2O$ in 25 ml of deionized water) was added dropwise. The reaction occurred for 2 h under an inert atmosphere. The pH was maintained at 10 by the addition of ammonium hydroxide. At the end, the particles were washed five times with

deionized water by magnetic separation. MNPs were characterized by dynamic light scattering (DLS) and a diameter of 384 ±19 nm was obtained with a polydispersity (PI) of 0.97± 0.11.

5.2.3. EVALUATION OF POLYMERS ADSORPTION ON MNPs

The evaluation of polymers adsorption on MNPs was performed in order to determine the ratio of MNPs/polymer necessary to prepare stable porous structures with low MNPs leaching events. The adsorption capacity of chitosan, dextran and agarose onto MNPs was studied by static partition equilibrium experiments. 10 mg of MNPs (10 mg mL^{-1}) were incubated with various solutions of polymers (0–15 mg mL^{-1}) prepared in deionized water (agarose and dextran) and in acidic deionized water (1% v/v) (chitosan). All experiments were performed in duplicates at 80 ºC, as this is the temperature employed for polymers solubilisation, at 200 rpm for 24 h. At the end, MNPs were removed from the medium by magnetic separation and the amount of adsorbed polymer was determined by the anthrone method.[194]

5.2.4. PREPARATION OF NATIVE AND MAGNETIC MONOLITHS

Native monoliths were prepared in 4 steps. (1) Chitosan (90 mg), agarose (70 mg) and dextran (70 mg) were dissolved in 3 mL of deionized water which was 1% (v/v) acidic only for chitosan-based casting solutions. In order to improve the mechanical properties of monoliths, for agarose and dextran casting solutions, 10 mg of acrylamide and 70 µL of GMA were added. In case of chitosan a new casting composed by 45 mg of chitosan and 45 mg of PVA was prepared as described by Barroso *et al.*[82] (2) The crosslinker agent, MBA, was also added (2 % (wt per wt)) to the casting solutions, which were further placed in glass tubes (1 cm of diameter and 3 cm of height) and stirred at 80 ºC to assure homogeneous solutions. (3) After a complete solubilisation of polymers and crosslinker, the initiator and catalyst, TEMED (23 µL) and APS (40 µL) respectively, were added to promote the crosslinking process (see Fig.5.1). The crosslinking process occurred at 0 ºC during 30 minutes under stirring. (4) Then, casting solutions were frozen at -80 ºC for 12 h and lyophilized (Telstar cryodos-50) until dryness (24h).

Magnetic monoliths (see Fig 5.2) were prepared following a similar procedure except that after step 2, 40 mg of MNPs were added to each casting solution and the mixture incubated at 80 ºC for 24 h in order to promote the polymer adsorption onto MNPs. Then, the casting solutions followed the same treatment as described in steps (3) and (4).

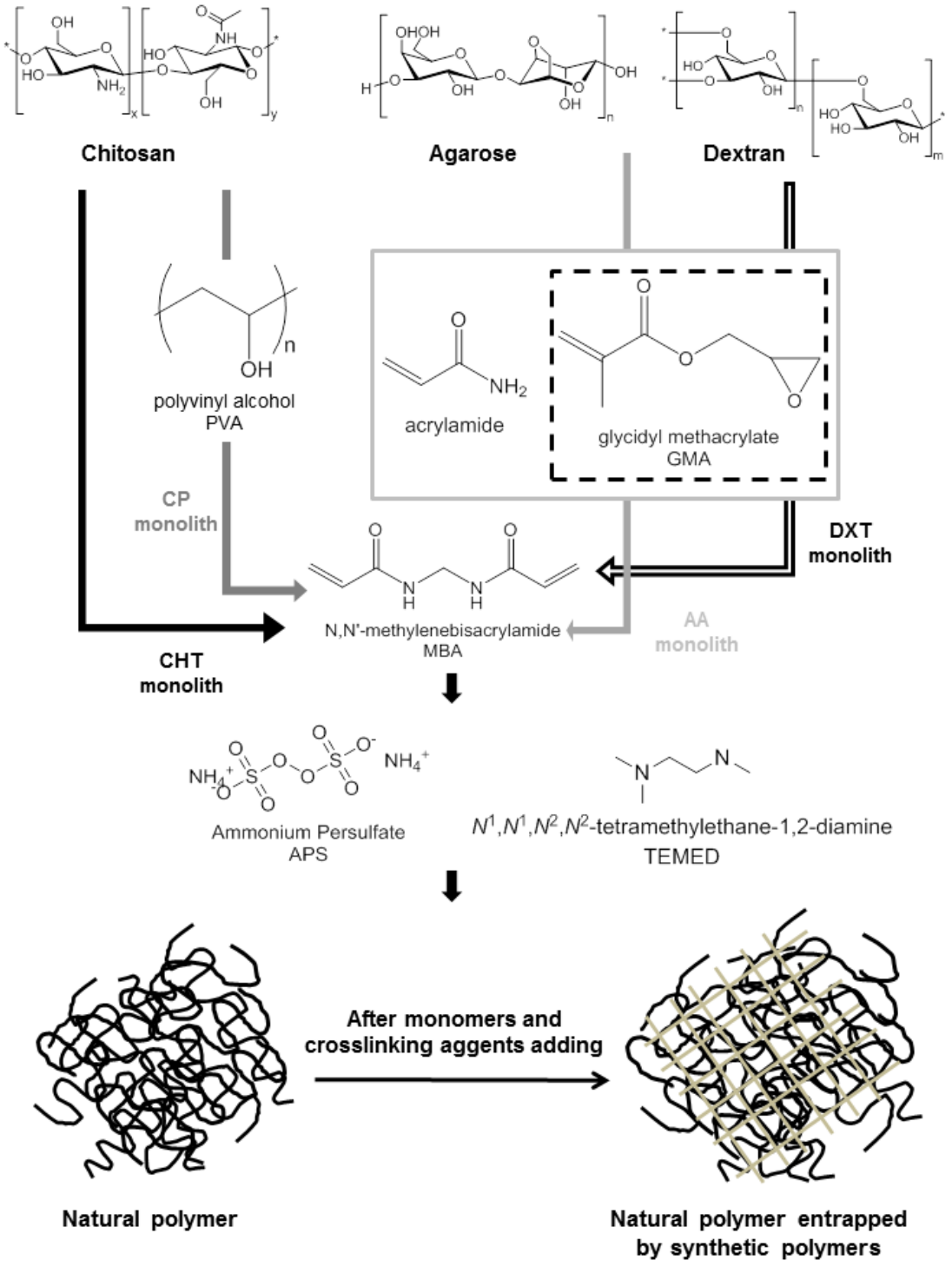

Figure 5.1 – Schematic representation of the natural-based monoliths design and composition. CHT indicates chitosan monolith, CP means chitosan/poly(vinyl alcohol) monolith, AA represents agarose/acrylamide monolith and DXT designates dextran-based monolith.

5.2.5. PREPARATION OF HYBRID MONOLITHS

Magnetic monoliths were introduced in a plasma chamber which was thoroughly purged with a continuous flow of nitrogen to reduce trace amounts of air and moisture. During the treatment, free radicals were generated under inert-gas discharge environments on selected monoliths surface. Then, 1,6-hexanediamine was fed to the reaction chamber under vacuum by evaporating the 1,6-hexanediamine contained in a flask maintained at 150 ºC. The plasma treatment occurred at a power setting of 80 W and a constant pressure of 0.3 Torr inside the chamber during 30 minutes.[195] The extent of amination was determined using the Kaiser test, as in previous works, involving the determination of amines in monoliths (Fig. 5.2 B).[82,161]

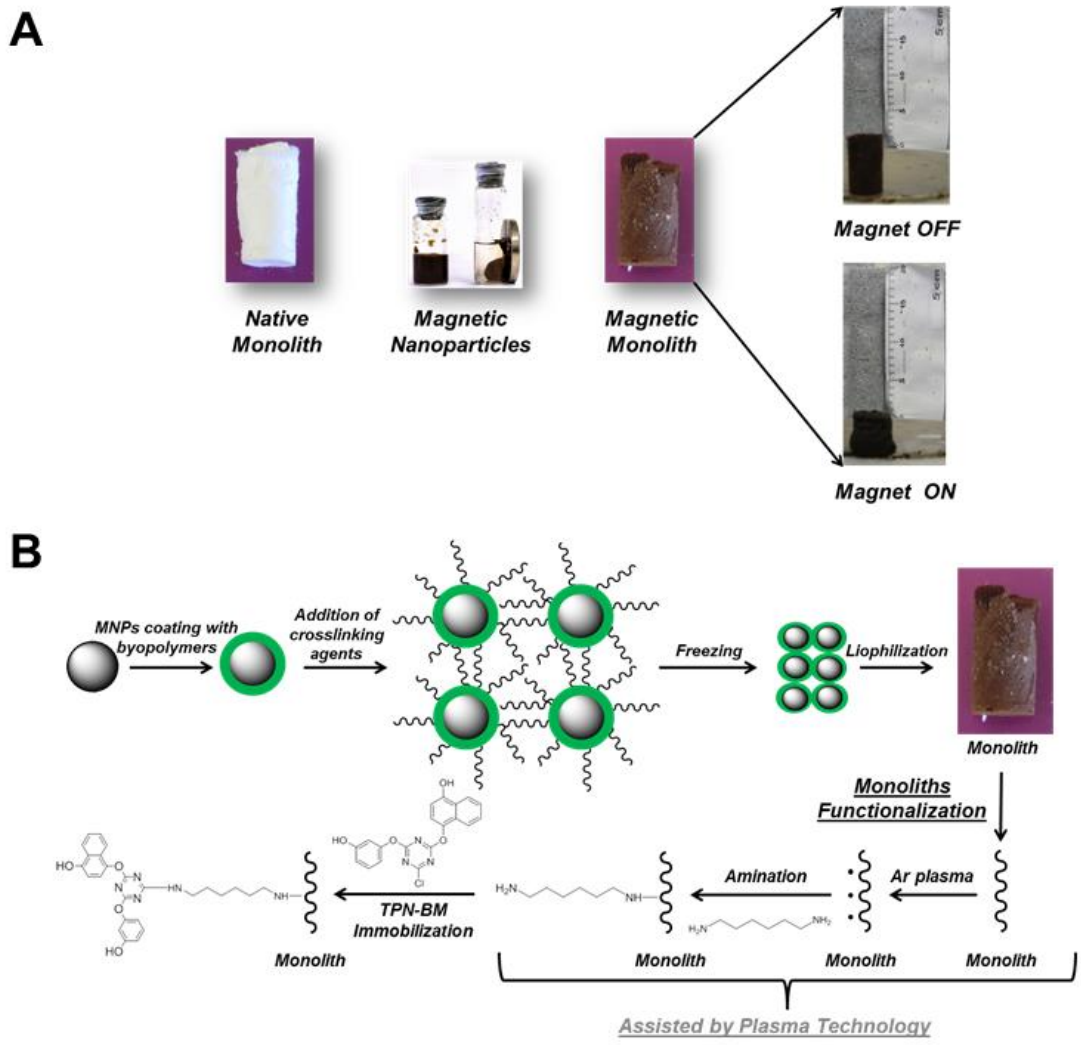

Figure 5.2 - Illustration of the materials produced in this work (A) and schematic representation of the procedures applied for the production and functionalization of the magnetic monoliths (B).

For immobilization of ligand TPN-BM, an excess of ligand (3 equiv. to the amination content, 150 mg), was added to the aminated monolith samples (approximately 60 mg) in 6 mL of DMF and incubated on a rotary shaker (140 rpm) for 72 h at 85 ºC. TPN-BM functionalized magnetic monoliths were then washed with DMF until the absorbance at 267 nm, maximum absorbance

wavelength of TPN-BM ligand, was ≤0.005. In order to assure a complete removal of physically adsorbed ligand, the functionalized monoliths were hosted in a Varian column with 3 mL of capacity and 1 cm of inner diameter, and further washes with DMF and a CIP procedure were performed. The CIP procedure involved sequential washing with NaOH 1 M, 10 mL of water, regeneration buffer (NaOH 0.1 M in 30% of isopropanol) and again with 10 mL of distilled water until the absorbance at 267 nm was ≤0.005 in each step. The functionalized monoliths were finally washed with sodium phosphate buffer (50 mM, pH 8.0), sodium citrate buffer (50 mM, pH 3.0) and glycine buffer (50 mM, pH 11) until the absorbance at 267 nm was zero. The ligand TPN-BM density was calculated by subtracting the amount of ligand collected in all washes from the initial ligand used in the immobilization step.

5.2.6. CHARACTERIZATION OF NATIVE, MAGNETIC AND HYBRID MONOLITHS

The morphological and mechanical properties of monoliths before (native) and after MNPs incorporation (magnetic), and after affinity ligand functionalization (hybrid) were investigated using SEM, MIP, water flux measurements and tensile-strain tests. SEM was performed in Hitachi S 2400 equipment with an accelerating voltage set to 15 kV. Firstly, the samples were frozen and broken in liquid nitrogen for cross-sectional analysis and, gold coated before analysis. Monoliths porosity, average pore size diameter and surface area were determined by MIP (Micromeritics, autopore IV). The water fluxes were determined at room temperature and 1 atmosphere. Due to the high porosity of the scaffold network no pressure was applied. Thus, Varian columns (with a capacity of 3 mL and an effective volume of 1.2 mL) were packed with monoliths and charged with 1 mL of distilled water. The run time was registered and at least three measurements of distilled water flux were recorded.

Uniaxial compression was used to determine the mechanical properties of the monoliths using tensile testing equipment (MINIMAT firmware v.3.1) at room temperature. Samples were prepared in a cylindrical shape (10 mm in diameter thickness). The length between clamps was set at 10 mm, the speed set to 1 mm min^{-1}, a full scale load of 20 N and maximum extension of 90 mm was used. The compression modulus was calculated from the slope of the linear portion of the stress-strain curve (see Chapters 2 and 3).[82]

Uniaxial deformation induced by magnetic field was also performed in order to evaluate the response of monoliths at different magnetic fields. Monolithic samples were submited at different permanent magnetic fields, 0.25, 0.5, 1.5 and 2.5 T, and their deformation, translated by the decrease of monolith's length, was monitored during 20 minutes. At the end, the magnetic field was removed and the reversibility of the magnetic-shape memory was assessed.[196] These tests were performed in dry and wet conditions, since the monoliths magnetic response can change according to the hydrate sate of the porous network.

X-ray photoelectron spectroscopy (XPS) analyses were performed in order to examine the elemental compositions of native, magnetic and hybrid monoliths. The studies were conducted on a XSAM800 X-ray spectrometer, operated in the fixed analyser transmission (FAT) mode, with a pass energy of 20 eV, a power of 120 W and using a non-monochromatic radiation from

Mg anode (hλ=1253.6 eV). Spectra were collected with a step of 0.1 eV, using a Sun SPARC Station 4 with Vision software (Kratos). The curve fitting for component peaks was carried out with a non-linear least-squares algorithm using a product of Gaussian and Lorentzian peak shapes. The freeware XPSPeak 4.1 was used. No flood gun was used for charge accumulation neutralization. The charge shift was corrected taking as reference the C 1s binding energy at lower energy equal to 285 eV except in the samples containing the ligand TPN-BM where the value was set to 284.7 eV due to the existence of sp2 carbons.[197] Sensitivity factors used were: C 1s – 0.25, O 1s – 0.66, N 1s – 0.44 and Fe $2p_{3/2}$ – 3.0.

The stability of hybrid materials was evaluated by immersing them (15 mg) in 500 µL of solutions with different pH values and typical solutions employed in CIP procedures using a 96 well block for 24 hours at 150 rpm. Samples of 200 µL were collected, and fresh 200 µL were added in order to maintain the total volume. The ligand leaching was quantified by absorbance at 267 nm and the release of MNP was quantified by the magnetite assay.[198]

5.2.7. DESIGN OF A PERMANENT MAGNET

In order to tailor a permanent magnet of 0.5 T with a straight-hole magnet shape to assist chromatographic experiments, FEM studies of a permanent magnet were conducted using Comsol Multiphysics Software© to identify the optimal permanent magnet characteristics (magnetic flux density strength in the z-direction, outer diameter and height) for further order. The magnet was design on purpose and supplied by First4magnets.

5.2.8. DETERMINATION OF STATIC AND DYNAMIC BINDING CAPACITIES

Partition equilibrium experiments were performed in a batch system as described by Barroso *et al*,[82,161] in order to estimate the static binding capacities. The adsorption of hIgG and BSA on the native and hybrid monoliths was investigated. Monolith samples (10 mg) were incubated with hIgG and BSA (0.0–60 mg mL^{-1}, 500 µL) prepared in phosphate buffer (50 mM, pH 8.0). All experiments were performed in duplicates at 25 ºC, at a stirring rate of 200 rpm for 24 h. After incubation, the amount of protein in the supernatants was quantified at 280 nm on a microplate reader (Tecan Infinite F200, filter, λ=280 nm). In the meanwhile, a calibration curve was prepared using hIgG and BSA in phosphate buffer solutions (50 mM, pH 8.0) (0.0–60 mg mL^{-1}). The adsorption phenomena followed the Langmuir–Freundlich model represented by:

$$q = \frac{Q_m \times (C)^n}{K_d + (C)^n}$$

Equation 5.1

where K_d is the apparent dissociation constant (M) that includes contributions from ligand binding to support, Q_m is the maximum binding capacity (mg protein g^{-1} support), C is the concentration of protein in the liquid at the equilibrium (M) and n represents the Langmuir–Freundlich coefficient.

The dynamic loading capacity of the packed columns with hybrid magnetic monoliths was determined using frontal analysis according with the equation below:

$$Q = \frac{V_e}{[Protein]_{plateau}}$$

Equation 5.2

where Q corresponds to the estimated adsorbent capacity and V_e corresponds to the elution volume. This procedure consisted in loading hIgG and BSA solutions (6 mL, 0.5 mg mL^{-1}) in sodium phosphate buffer (50 mM, pH 8.0) through the equilibrated monolithic packed columns at gravitational conditions until the protein concentration of the output and input streams were equal. At that point, packed monolithic columns were washed with phosphate buffer (50 mM, pH 8.0) to remove unbound protein and the bound protein was eluted using two different buffers, sodium citrate buffer (50 mM, pH 3.0) and glycine buffer (50 mM, pH 11.0). Samples collected (1 mL) during loading, washing and elution stages were examined by measuring absorbance at 280 nm on a 96-well format.

5.2.9. CAPTURE AND RELEASE OF IgG FROM PURE SOLUTIONS

The affinity capturing experiments were performed in a step wise adsorption–desorption process by switching eluents at room temperature and at atmospheric pressure. Columns (with diameter and length 1 and 7 cm, respectively) were packed with hybrid monoliths, and then washed and equilibrated as described in the previous section. Then, 1 mL of hIgG (3 mg mL^{-1}) was added and columns were washed with sodium phosphate buffer (50 mM, pH 8.0) until the absorbance measured at 280 nm reached ≤0.005. The IgG bound was recovered with two elution buffers, either sodium citrate buffer (50 mM, pH 3.0) or glycine buffer (50 mM, pH 11.0) with and without magnetic compression. Packed columns with functionalized magnetic monoliths were then regenerated as previously described (applying CIP), in order to be reused. These chromatographic experiments were repeated during 3 cycles and one more after auto-claving (SIP) in order to estimate the column capacity over time. The total amount of protein bound, eluted and regenerated from the hybrid monoliths was initially determined by absorbance measured at 280 nm and by the BCA method (microplate reader assay).[82]

5.2.10. PURIFICATION OF MONOCLONAL ANTIBODIES, mAbs, DIRECTLY FROM CRUDE SAMPLES

In order to evaluate the possibility to capture monoclonal antibodies directly from non-clarified crude extracts, columns packed with hybrid CP monoliths were tested with a mammalian crude extract solution (1 mL, 2 mg of total protein per millilitre). After crude extract loading, packed columns were washed with sodium phosphate buffer (5 mL, 50 mM, pH 8.0) until the absorbance measured at 280 nm reached ≤0.005, and the bound protein was further eluted with sodium citrate buffer (50 mM, pH 3.0) or glycine buffer (50 mM, pH 11) in the presence of magnetic field. All collected samples were analysed by the BCA assay to quantify the amount of

total protein bound and eluted from the monoliths. SDS-PAGE was performed on acrylamide gel (12.5%) in Tris-Glycine buffer system pH 8.3. Electrophoresis apparatus (from BIO-RAD) was connected with power supply at 120 V, 190 mA for 1 h. The gel was revealed using a silver staining kit from BIO-RAD.

5.3. RESULTS AND DISCUSSION

5.3.1. CHARACTERIZATION OF NATIVE AND MAGNETIC MONOLITHS

All monoliths, native (N-without MNPs) and magnetic (M-with MNPs), were characterized according to their morphological, mechanical, magnetic and physico-chemical properties and stability. Fig. 5.3 exhibits the SEM images of native (Fig. 5.3 A, D, G, J) and magnetic (Fig. 5.3 B, E, H, K) monoliths based on natural polymers. Regarding the porous network it is noticeable that the addition of MNPs to the 3D structure of the native monoliths did not influence significantly their architecture. The presence of MNPs well dispersed in the pore's wall of magnetic monoliths is evident. Moreover, depending on polymer composition, monolithic porous network can be adjusted and different designs can be achieved. Monoliths composed of chitosan (CHT; Fig. 5.3 A-B) crosslinked with MBA, and chitosan blended with poly(vinyl alcohol) and entrapped also by the crosslinked (MBA) network (CP; Fig. 5.3 D-E), exhibit smaller, spherical and heterogeneous pores. On the other hand, monoliths prepared from casting solutions of agarose (AG; Fig. 5.3 G-H) or dextran (DXT; Fig. 5.3 J-K), both blended with GMA cryopolymerized with acrylamide, present a lacy structure with elongated pores. These supermacroporous structures were expected since monoliths based on agarose and dextran are known to form spongy networks, independently of their processing method.[72,192,199]
All monoliths presented as semi-rigid single blocks with dimensions of the mould where they were prepared. Still, monoliths were able to fit in any support which presents the same dimensions or even with a higher diameter, since all of them were able to swell and fit to various supports wall. The average pore size diameters and the porosity values calculated by MIP for each monolith before and after MNPs addition (Table 5.1) are in agreement with the SEM images.

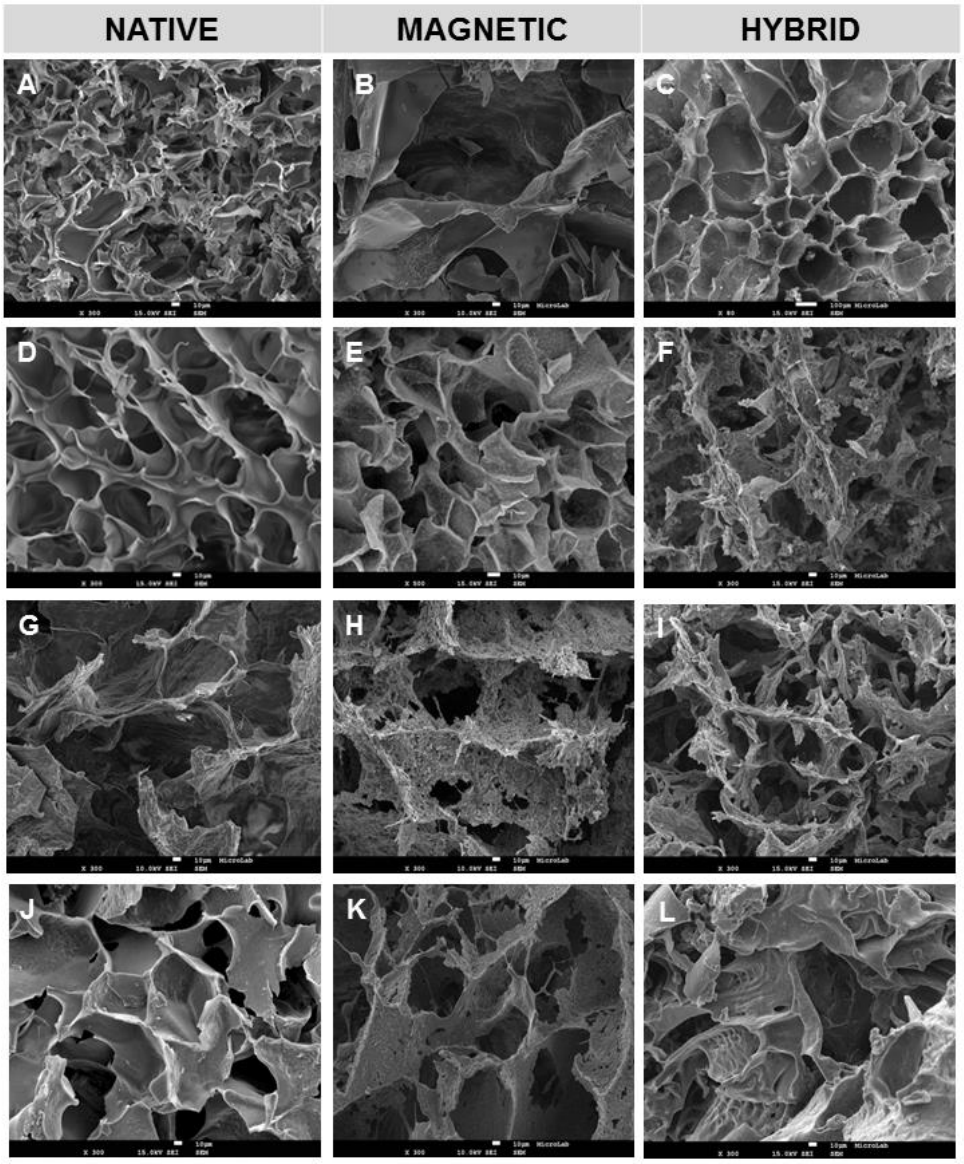

Figure 5.3 - SEM images of natural-based monoliths before (native, N) and after MNP's incorporation (magnetic, M) and hybrid monoliths (magnetic with ligand TPN-BM coupled, M_TPN-BM): (A) native chitosan monolith (CHT_N), (B) magnetic chitosan monolith (CHT_M), (C) hybrid chitosan monolith (CHT_M_TPB-BM), (D) native chitosan blended with poly(vinyl alcohol) monolith (CP_N), (E) magnetic chitosan blended with poly(vinyl alcohol) monolith (CP_M), (F) hybrid chitosan blended with poly(vinyl alcohol) monolith (CP_M_TPN-BM), (G) native agarose-based monolith (AG_N), (H) magnetic agarose-based monolith (AG_M), (I) hybrid agarose-based monolith (AG_M_TPN-BM), (J) native dextran-based monolith (DXT_N), (K) magnetic dextran-based monolith (DXT_M) and (L) hybrid dextran-based monolith (DXT_M_TPN-BM). All the micrographs have a magnification of 300 and the scale bar in white indicates 10 µm.

The magnetic monoliths exhibited some differences regarding the values of average pore size diameter comparing with the native ones. CHT and CP monoliths suffered a noticeable enlargement from 17 and 53 to 89 and 88 µm respectively, after MNPs embedding, while monoliths prepared with agarose and dextran maintained average pore size diameters between 70 and 90 µm. In addition, porosity values are similar for all monoliths (82-91%). High porosity values were expected since they are mainly related with the freeze-drying method employed in monoliths production, which normally generate high porosities.[200,201] The specific surface area

values obtained for all monoliths were within the range 0.5 and 3.0 $m^2 g^{-1}$, which it is agreement with obtained values of porosity, since the surface area varies inversely to the porosity.[202]

Materials for bioprocessing must be hydrophilic with well-organized porous networks to allow fast fluxes and easy permeations, and present mechanical stability to preserve their architecture. Table 5.1 also comprises the estimated water fluxes and compressive modulus measured, which translate the hydrophilicity and stiffness of material respectively, for all polymeric monoliths before and after MNPs addition. All monoliths presented values of water fluxes between 100 and 300 L $m^{-2} h^{-1}$. CHT and CP monoliths revealed a decrease of water flux value after the incorporation of MNPs, from 142 and 294 to 110 and 120 L $m^{-2} h^{-1}$, respectively. Conversely, AG and DXT monoliths, after MNPs addition, increased the water flux values from 102 and 100 to 212 and 176 L $m^{-2} h^{-1}$, respectively. This can be explained by morphological features and composition of each support. CHT and CP monoliths, although they exhibit an increase of pore size diameter after MNPs embedding, possess a very well organized 3D porous structure which in wet conditions, behaves homogenously with controlled swelling, namely when confined to a column. After MNPs addition, monoliths stay even better stabilized with a higher water uptake capacity. In a marked contrast, AG and DXT monoliths, which in native conditions already presented high swelling capacity, also exhibit a heterogeneous porous network that hampers a regular profile of water permeation. Furthermore, with the incorporation of MNPs, pores suffer an additional elongation due to MNPs mobility in a random way, and consequently higher water fluxes are achieved. Nevertheless, the obtained values for all supports assure efficient and convenient water fluxes.[82,203]

The compressive mechanical properties were studied by uniaxial compression measurements under dry and hydrated conditions to validate the mechanical resistance of native and magnetic monoliths. In general, higher compression modulus indicate stiffer materials.[136] Concerning the native supports, DXT monolith is stiffer at dry conditions, followed by CHT, CP and AG monoliths (Table 5.1). However, due to their larger pores, DXT in wet state becomes softer (0.6 kPa) while CHT exhibits the highest value of compressive modulus (1.9 kPa). The remaining monoliths present similar values between 0.4-0.7 kPa. The mechanical behaviour of CHT in wet conditions is mainly related with its hydrogel nature which excels in the hydrated state. The addition of MNPs to the structures kept the same trend of their mechanical behaviour concerning monolith's material, and hydration degree. Additionally, the obtained values are in the range of similar 3D porous structures.[82,200,203]

Table 5.1 - Morphological and mechanical characterization of natural-based monoliths before (native (N)) and after magnetic nanoparticles embedding (magnetic (M)). All data was obtained from duplicated and triplicated measurements.

	CHT_N		CHT_M		CP_N		CP_M		AG_N		AG_M		DXT_N		DXT_M	
Average pore size diameter (μm)[a]	17±5		89±5		53±5		88±5		73±5		71±5		96±5		75±5	
Porosity (%)[a]	91±2		90±2		88±2		86±2		93±2		92±2		82±2		98±2	
Water Flux ($L\ m^{-2}\ h^{-1}$)	142±5		110±7		294±7		120±9		102±9		212±9		100±5		176±8	
Surface Area ($m^2\ g^{-1}$)[a]	2.7±0.3		0.5±0.2		0.4±0.2		1.0±0.2		1.0±0.3		2.1±0.3		3.0±0.5		3.0±0.5	
Compressive Modulus (kPa)	Dry	Wet	Dry	Wet	Dry	Wet	Dry	Wet	Dry	Wet	Dry	Wet	Dry	Wet	Dry	Wet
	2.3±0.7	1.9±0.3	2.2±0.5	0.4±0.1	0.6±0.2	0.4±0.2	1.8±12	0.5±0.2	0.7±0.2	0.5±0.2	0.5±0.1	0.3±0.1	5.3±0.5	0.7±0.2	4.1±0.4	0.5±0.2

[a] Determined for dried monoliths by mercury porosimetry analysis.

Table 5.2 - Morphological and mechanical characterization of hybrid monoliths. All data was obtained from duplicated and triplicated measurements. [a] Determined for dried monoliths by mercury porosimetry analysis.

	CHT_M_TPN-BM		CP_M_TPN-BM		AG_M_TPN-BM		DXT_M_TPN-BM	
Average pore size diameter (μm)[a]	125±5		20±5		18±5		13±5	
Porosity (%)[a]	79±9		75±9		76±5		61±5	
Water Flux ($L\ m^{-2}\ h^{-1}$)	176±9		135±8		186±9		78±5	
Surface Area ($m^2\ g^{-1}$)[a]	1.4±0.2		1.1±0.2		2.9±0.2		3.4±0.2	
Compressive Modulus (kPa)	Dry	Wet	Dry	Wet	Dry	Wet	Dry	Wet
	0.3±0.1	0.2±0.1	191±9	55±5	0.5±0.2	0.5±0.2	0.7±0.4	0.3±0.2

In order to evaluate the magnetic response of magnetic monoliths, samples in dry and wet conditions, with 1 cm of diameter and height, were placed in contact with different permanent magnets, and the physical deformation (shrinkage) was monitored over time. Fig. 5.4 shows the magnetic deformation of each support after 20 minutes in contact with permanent magnets with different intensities (0-2.5 T in dry and wet state).

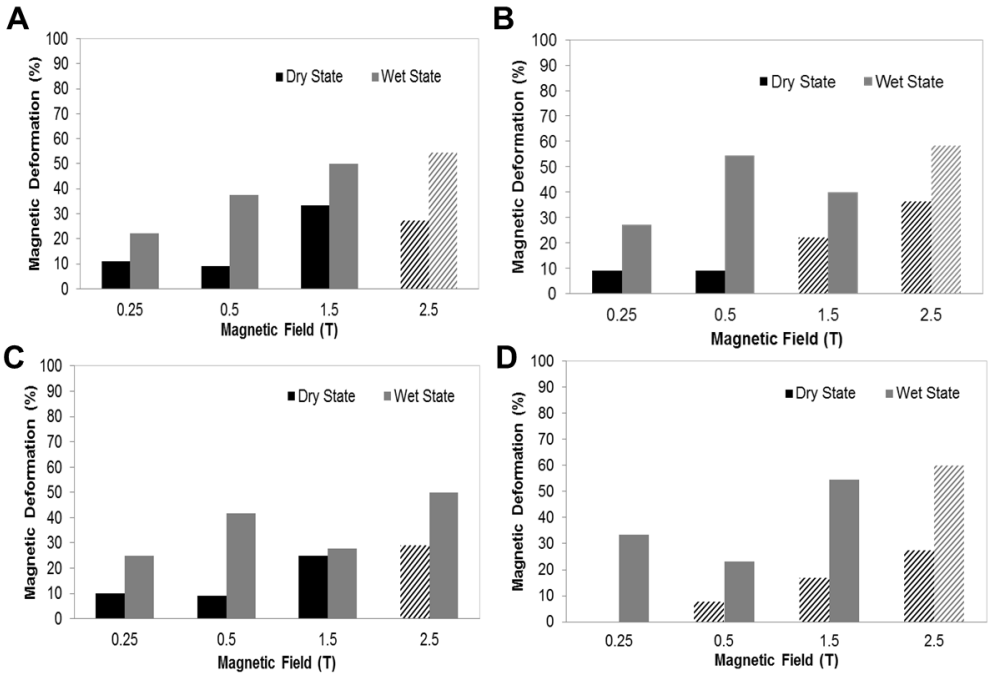

Figure 5.4 - Magnetic deformations of different magnetic natural-based monoliths: chitosan, CHT_M (A), chitosan- poly(vinyl alcohol), CP_M (B), agarose, AG_M (C) and dextran, DXT_M (D). All data was obtained from triplicated measurements with errors of ± 5.

In general, independently of the monolith`s composition all wet supports presented higher magnetic deformations. This was expectable since beside in wet conditions the monoliths are less stiff, the MNPs inside offer a higher mobility to all 3D structure allowing a pronounced shrinking. Contrarily, dry magnetic samples are more rigid, therefore the shrinking capacity is inferior or negligible. Another aspect studied was the reversibility of the magnetically induced shrinkage. At low magnetic fields (0.25 and 0.5 T) monoliths have no magnetic memory as they can return to the initial position at both dry and wet conditions (Fig. 5.4). At 1.5 T the magnetic deformation varies depending on the monolith porous architecture and hydrated state. Thus, CHT_M and AG_M in dry and wet conditions present magnetic response while CP_M and DXT_M only exhibit it in wet conditions. At 2.5 T all monoliths revealed higher magnetic deformations which led to a total collapse of 3D porous structures and consequently to the loss of a magnetic reversible response. Thus, analyses suggest that a magnetic field of 0.5 T is enough to operate with natural magnetic based monoliths in on-off magnetic cycles without damaging the porous network. All macroporous monoliths were tested over four ON-OFF cycles at 0.5 T and always maintained their superparamagnetic behaviour.

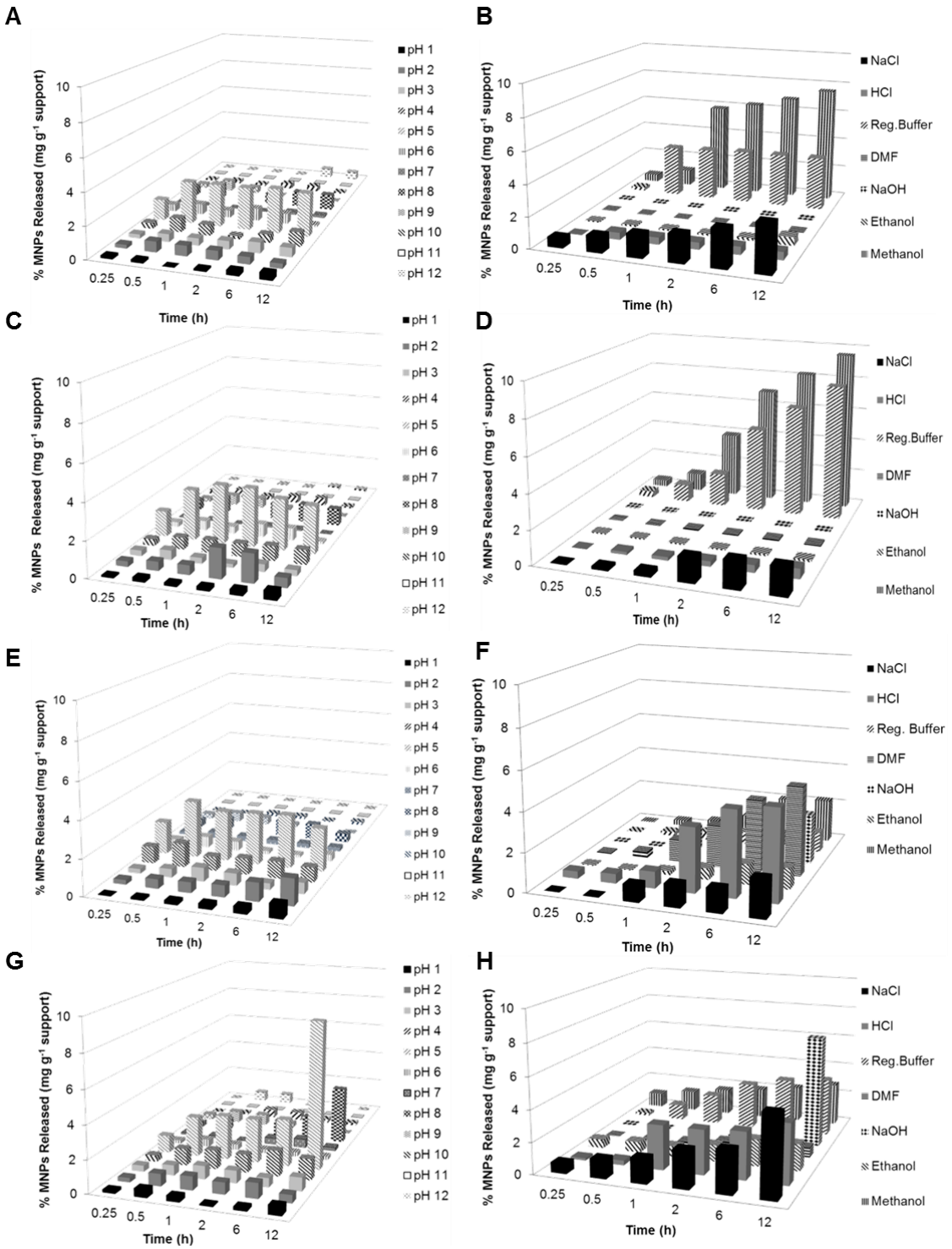

Figure 5.5 - Evaluation of magnetic nanoparticles (MNPs) leaching from chitosan, CHT_M (A, B), chitosan- poly(vinyl alcohol), CP_M (C, D), agarose, AG_M (E, F) and dextran, DXT_M (G, H) magnetic monoliths immersed over 12 h in solutions with pH values between 1 and 12 and typically used during cleaning-in-place (CIP) procedures, respectively. All data was obtained from duplicated measurements with errors of ±8.

For an efficient operation with magnetic monoliths, iron leaching is an important issue to address. The leaching of MNPs was investigated at different conditions employed in Ab purification processes mainly during the cleaning and regeneration steps. Fig. 5.5 shows the

MNPs leaching profiles from different natural magnetic based monoliths over time (12 hours). In general, MNPs leaching is negligible since the highest values achieved were around 4-6% at pH 5 after 4 h, and between 4 and 9% upon contact with alcohols, after 1h. Chitosan has a pKa around 6-6.5 and at pH 5, chitosan based-structures exhibit high swelling capacity (porous network opening) which justifies the accentuated MNPs leaching. In addition, although agarose and dextran are uncharged polysaccharides, the acrylamide presented in monoliths composition has a NH_2 group with a pKa value around 6, which, due to the same reason previously mentioned, leads to high MNPs release at pH 5. DXT_M revealed the most unstable support since, except with regeneration buffer and NaOH solution, the MNPs leaching is higher. This MNPs leaching control was crucial since it allowed choosing the best conditions to operate with each support, assuring their magnetic properties.

5.3.2. PREPARATION AND CHARACTERIZATION OF HYBRID MONOLITHS

Magnetic monoliths were functionalized with TPN-BM affinity ligand resulting in a hybrid material. The immobilization of functional molecules onto polymeric materials surfaces requires the presence of active chemical groups as primary amines.[88] Plasma technology was the selected tool to fulfil this requirement in a green and sustainable way as it allows diverse solvent free modifications on supports within short periods.[193,195,204,] Firstly free radicals were generated under inert-gas discharge environments on selected monoliths surface, followed by a second step reaction in which the 1,6-hexanediamine was dragged under vacuum condition (*in situ*) to react with the activated supports for further ligand coupling (Fig. 5.6 A). As shown in Fig. 5.6 B, large densities of amines were introduced in all magnetic supports, particularly in CHT_M (460±44 µmol of NH_2 per gram of support). The application of plasma technology for the activation and amination of monoliths saved time and solvents consumption when comparing with traditional procedures applied for the same purpose.[88,114] In this work, 30 minutes were sufficient to aminate the supports in contrast with the typical 13 hours needed in the traditional approach (1h for the epoxyactivaction and 12h for the amination).[23] It should be noted that in Chapters 2 and 3, it was possible to improve the activation step from 1h to 5 min. However, in this work it was possible to save 12h of the traditional amination procedure, and use only 30 minutes to activate and aminate the supports. Aminated monolithic platforms were subsequently functionalized with ligand TPN-BM. Different yields of ligand immobilization were reached according with the previous amination levels (Fig. 5.6 B). The highest immobilization value of TPN-BM was obtained for CHT_M and DXT_M monoliths (around 400 µmol TPN-BM g^{-1} support) followed by CP_M, and AG_M (370 and 280 µmol TPN-BM g^{-1} support, respectively). The results from ligand immobilization suggest that most of amines reacted with TPN-BM which makes the immobilization strategy, herein proposed, extremely effective. After TPN-BM immobilization all magnetic supports were again characterized.

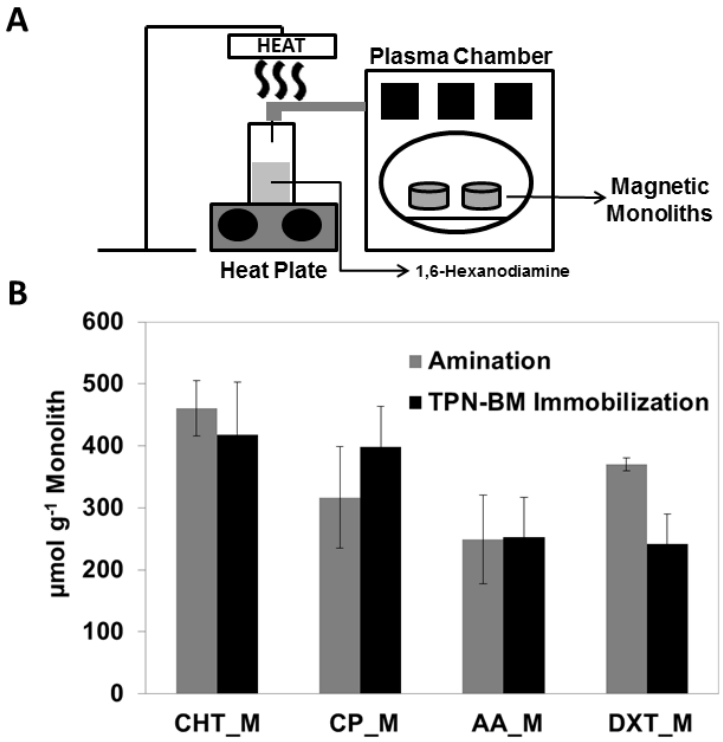

Figure 5.6 – Schematic representation of: (A) the amination procedure, assisted by plasma technology, of magnetic natural-based monoliths. (B) Graphical representation of the amination and TPN-BM immobilization yields obtained for all magnetic monoliths.

SEM images presented in Fig. 5.3 F and I show that the porous networks of hybrid CP and AG monoliths (CP_M_TPN-BM and AG_M_TPN-BM respectively) were maintained after the functionalization procedure. Contrarily, hybrid CHT and DXT monoliths (CHT_M_TPN-BM (Fig. 5.3 C) and DXT_M_TPN-BM (Fig. 5.3 L), respectively) exhibited morphological differences, namely pore enlargement and deformation coiled pores, respectively. In addition, all monoliths presented an increase in pores thickness which might be indicative of the ligand attachment. Differences regarding average pore size diameter, porosity and surface area values of supports after ligand coupling were also registered (Table 5.2). The CHT_M_TPN-BM registered an increase in average pore size diameter (from 89 to125 µm) while the remaining registered a 3-fold decrease of the pore size. After TPN-BM coupling, all monoliths revealed a higher rigidity and, in dry conditions used during MIP analysis, the pores are more collapsed turning hard the mercury intrusion porosimetry. Porosity and surface area values kept close to the ones obtained before functionalization. The water flux values decreased for all supports which can be explained by the hydrophobic nature of TPN-BM. Still, all monoliths exhibited acceptable water uptake capabilities that assure the permeation of Ab or other large biomolecules. The compressive modulus of CHT_M_TPN-BM and DXT_M_ TPN-BM decreased, which is in agreement with the enlargement and winding of the porous network upon functionalization, since larger pores and high porosities led to soft materials.[136] Conversely, CP_M_TPN-BM became stiffer in dry and wet conditions (~20-fold comparing to non-functionalized supports) which is in accordance with the pore size decrease. AG_M_TPN-BM maintained their mechanical behaviour. In addition all supports were tested for magnetic response under a

magnetic field of 0.5 T. All monoliths maintained the deformation in both states, dry and wet, as before ligand coupling, except for CP_M_TPN-BM which lost magnetic response in dry condition.

Also the surface chemical composition was analysed by XPS for hybrid monoliths CP_M_TPN-BM and AG_M_TPN-BM. For control, the corresponding amination step (CP_M_Amine and AG_M_Amine) as well as the native monoliths (CP_N and AG_N) were analysed and compared. Detailed XPS regions C 1s, N 1s, and Fe 2p are shown in Fig. 5.7 A – F. In CP_N besides the aliphatic carbons at a binding energy (BE) of 285 eV from PVA, C 1s also includes peaks centred at 286.0, 286.7 and 288.2 eV assigned mainly to chitosan carbons C-N, C-O and O-C-O, respectively.[197] Carbon singly bound to oxygen also exists in PVA and the peak at 286.0 eV can also include the contribution of C-N from the cross-linker (MBA), as attested by the peak centred at 288.8 eV attributed to N-C=O from MBA.[197] The C 1s region of agarose-based native monolith, AG_N, was fitted with four peaks centred at 285, 286.7, 288.2 and 290.2 eV. The most intense peak (at 286.7 eV) corresponds mostly to C-O in agarose, and the peak centred at 288.2 eV includes not only agarose O-C-O carbons, but also N-C=O from acrylamide and/or the MBA cross-linker, which existence is attested by the presence of nitrogen. Finally, the peak centred at higher BE can be attributed to carbon in a very electronegative neighbourhood such as a carbonate for instance. However, since carbonates are not likely to exist in this system, this shifted peak is compatible with a differential charge effect, i.e. it can correspond to carbon atoms in a phase with a loose electrical contact with the other phase, revealing an heterogeneous sample. In both native monoliths (which are composed by chitosan or agarose entrapped by PVA or acrylates respectively, (see Fig.5.1), the XPS N 1s regions include the contribution of amines and amides. Even in the presence of MNP and after functionalization with diamines followed by the ligand (TPN-BM), just one single peak centred at 399.8 eV was fitted. In fact, this peak can be the sum of different nitrogen atoms (in samples with ligand it can also include aromatic N), regardless the different chemical neighbourhoods.[197] The only exception is N 1s of AG_N that shows two narrower peaks slightly shifted to higher BE which is most probably due to a differential charge effect already suspected in C 1s region.

A large decrease of iron was observed since Fe 2p region is rarely or not detected in functionalized samples, revealing an efficient coating of the MNPs. However, in aminated samples iron was detected. Fe $2_{p3/2}$ has three peaks, centred at 709.3, 711.1 and 713.4 eV, assigned to Fe^{2+}, Fe^{3+} in oxide (Fe_2O_3) or oxyhydroxide (Fe(OH)O) and iron in a very electronegative environment superimposed to a multiplet structure typical of Fe^{2+} oxides, respectively.[205,206]

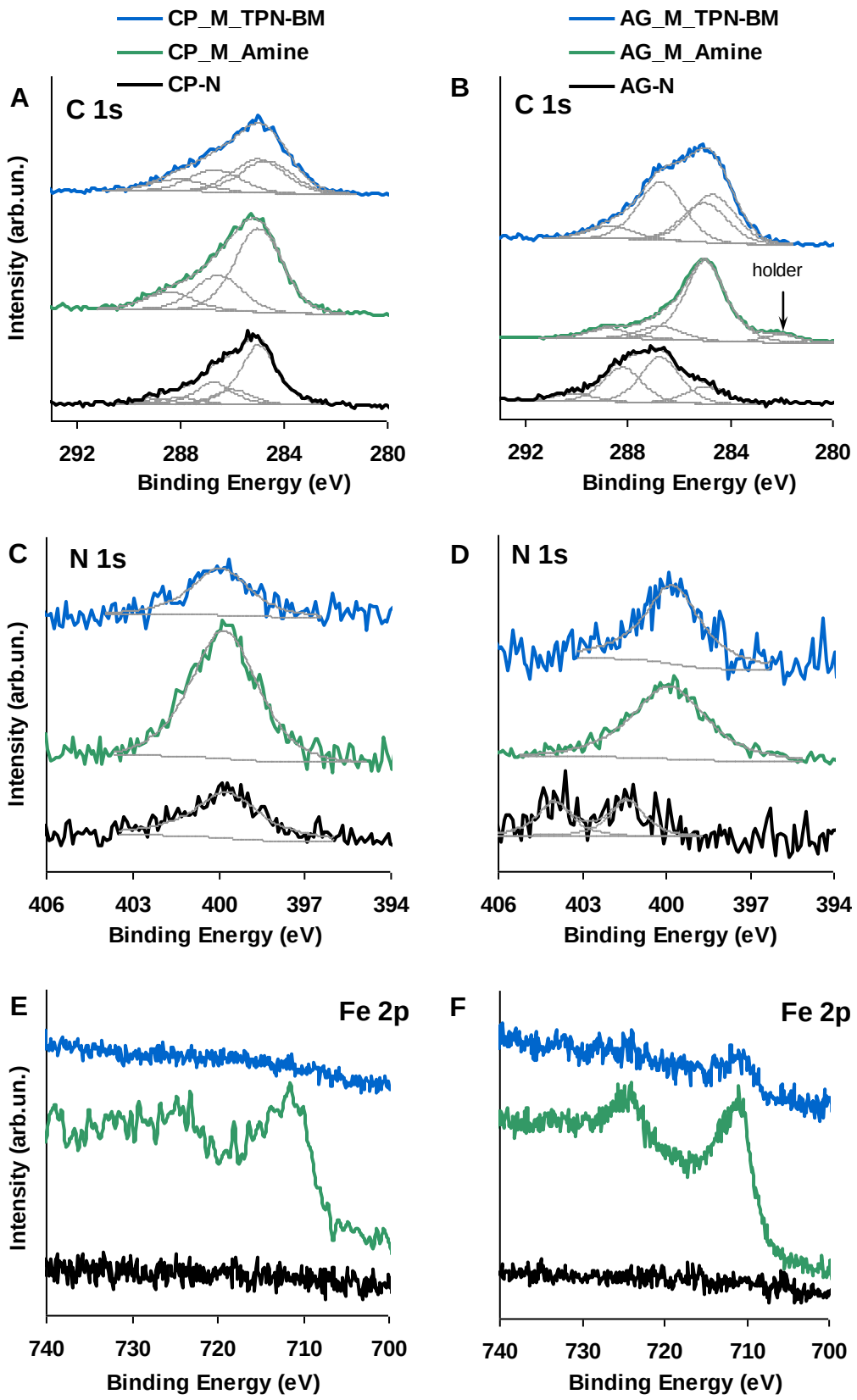

Figure 5.7 – XPS regions C 1s, N 1s, and Fe 2p of native monoliths (black), magnetic and aminated (green) and hybrid monoliths (blue).

Also the quantitative results were gathered in Table 5.3.

Table 5.3 – Binding Energies (eV) ± standard deviations and quantitative results obtained for chitosan/poly(vinyl alcohol)(CP) and agarose based-monoliths (AG) in native (N), magnetic (M), aminated (A) and hybrid (TPN-BM) conditions.

XPS peak (BE, eV)	AG_M_ TPN-BM	AG_M_ Aminated	N-AG	CP_M_ TPN-BM	CP_M_ Aminated	N-CP
C 1s (284.7±0.1)	20.6	n.o.	n.o.	21.8	n.o.	n.o.
C 1s (285.0±0.1)	16.8	48.6	10.5	23.0	38.0	36.2
C 1s (286.0±0.1)	n.o.	n.o.	n.o.	n.o.	n.o.	9.0
C 1s (286.7±0.1)	24.7	8.3	29.3	14.9	15.9	13.7
C 1s (288.2±0.2)	n.o.	n.o.	22.0	8.2	7.9	4.1
C 1s (288.8±0.1)	5.4	6.4	n.o.	n.o.	n.o.	3.0
C 1s (290.2±0.1)	n.o.	n.o.	4.9	n.o.	n.o.	n.o.
O 1s (530.4±0.1)	4.4	9.4	n.o.	n.o.	n.o.	n.o.
O 1s (531.7±0.3)	n.o.	137	6.6	8.1	26.5	5.9
O 1s (533.1±0.5)	23.7	5.5	23.1	19.3	n.o.	20.9
N 1s (399.8±0.1)	4.1	6.6	n.o.	4.8	10.5	7.3
N 1s (401.4±0.1)	n.o.	n.o.	1.9	n.o.	n.o.	n.o.
N 1s (404.0±0.1)	n.o.	n.o.	1.8	n.o.	n.o.	n.o.
Fe $2p_{3/2}$ (709.3±0.2)	0.1	0.3	n.o.	n.o.	0.5	n.o.
Fe $2p_{3/2}$ (711.1±0.3)	0.2	0.9	n.o.	n.o.	0.5	n.o.
Fe $2p_{3/2}$ (713.4±0.4)	0.1	0.4	n.o.	n.o.	0.4	n.o.
Atomic Ratios						
Fe/C	0.007	0.026	n.o.	n.o.	0.021	n.o.
N/C	0.06	0.10	0.06	0.07	0.17	0.11

n.o.: Not observable

Comparison of monoliths containing MNPs show that the MNPs were effectively embedded in the polymer matrix since upon functionalization with TPN-BM, the XPS atomic ratio Fe/C decreased (becoming almost zero when the ligand is present). Moreover, comparing CP_M_TPN-BM and AG_M_TPN-BM, it is also evident that MNPs coating with polymer/amine/TPN-BM is more efficient in the CP-based hybrid (where the Fe/C ratio in the aminated monolith is lower and decreases to values that were not quantifiable when the ligand TPN-BM was added) than in the AG-based one. Additionally, the XPS N/C atomic ratio is larger in aminated monoliths than in the native ones, showing that in fact, the monoliths were efficiently modified with 1,6-hexanodiamine through the functionalization strategy based on plasma technology. Also, the N/C ratio is larger in aminated monoliths than in the monoliths subsequently functionalized with the ligand TPN-BM. This parameter, again, confirms that the

more superficial layer is, in fact, the TPN-BM since the stoichiometric ratio N/C in di-hexamine is 1/3 whereas in the ligand (TPN-BM) is 3/11.

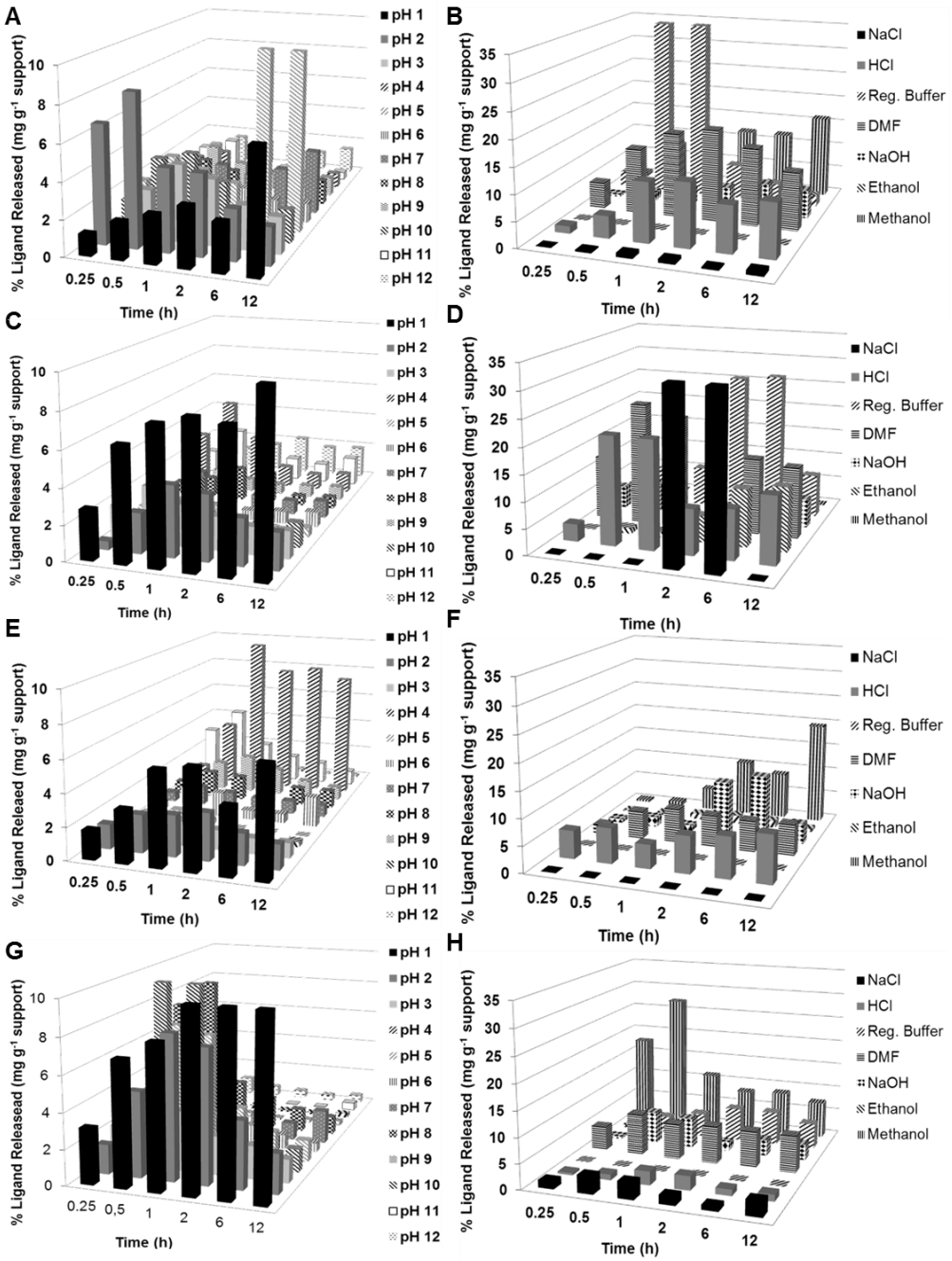

Figure 5.8 – Evaluation of TPN-BM leaching from hybrid chitosan, CHT_M_TPN-BM (A, B), chitosan-poly(vinyl alcohol), CP_M_TPN-BM (C, D), agarose, AG_M_TPN-BM (E, F) and dextran, DXT_M_TPN-BM (G, H) monoliths immersed over 12 h in solutions with pH values between 1 and 12 and typically used during cleaning-in-place (CIP) procedures, respectively. All data was obtained from duplicated measurements with errors of ±11.

The leaching of ligand TPN-BM was also evaluated for all hybrid supports, under the same conditions tested for MNPs leaching. Once again, considering the time of exposure to the harsh conditions tested (supports are never exposed more than 1 hour), the monoliths stability is assured except for DXT_M_TPN-BM (Fig. 5.8).

5.3.3. HYBRID MONOLITHS IN Ab PURIFICATION

Once completely characterized and evaluated, magnetic and hybrid monoliths were submitted to static partition equilibrium measurements with hIgG and BSA (a model contaminant protein), in order to estimate the maximum binding capacity to the target molecule (hIgG) as well as the level of non-specific adsorption (BSA). The experimental data was fitted using a Langmuir–Freundlich isotherm that is the indicated model for porous structures with heterogeneous morphology and it was also already successfully applied in similar supports.[137,153] Fig. 5.9 exhibits the adsorption profiles, while Table 5.4 shows the different affinity constants (K_a), theoretical maximum capacities (Q_{max}) and Langmuir–Freundlich coefficients (n) estimated.

Table 5.4 - Summary of the estimated parameters of the Langmuir–Freundlich isotherms for all magnetic and hybrid monoliths.

	K_a / (10^4 M^{-1})		Q_{max} (mg g^{-1} support)		n	
			hIgG			
	Control	*TPN-BM*	*Control*	*TPN-BM*	*Control*	*TPN-BM*
CHT_M	0.9	3.0	600	1400	0.9	1.3
CP_M	1.2	2.0	180	800	0.8	1.2
AG_M	1	3.0	500	800	0.8	1.3
DXT_M	0.2	4.0	500	700	0.9	1.2
			BSA			
CHT_M	0.2	0.2	550	600	0.9	0.9
CP_M	0.3	0.2	100	200	0.8	0.8
AG_M	0.2	0.2	625	665	0.8	0.9
DXT_M	0.6	0.5	450	450	0.8	0.8

Considering the studies involving hIgG, the controls always exhibit lower K_a, Q_{max} and n values comparing with the functionalized ones. This observation suggests that the addition of TPN-BM ligand to the magnetic supports increases their specificity towards hIgG. Concerning the experiments with BSA, very few differences between magnetic and hybrid monolithic samples were found, suggesting that TPN-BM ligand coupling does not affect BSA adsorption and consequently, no affinity for BSA is manifested as expected.

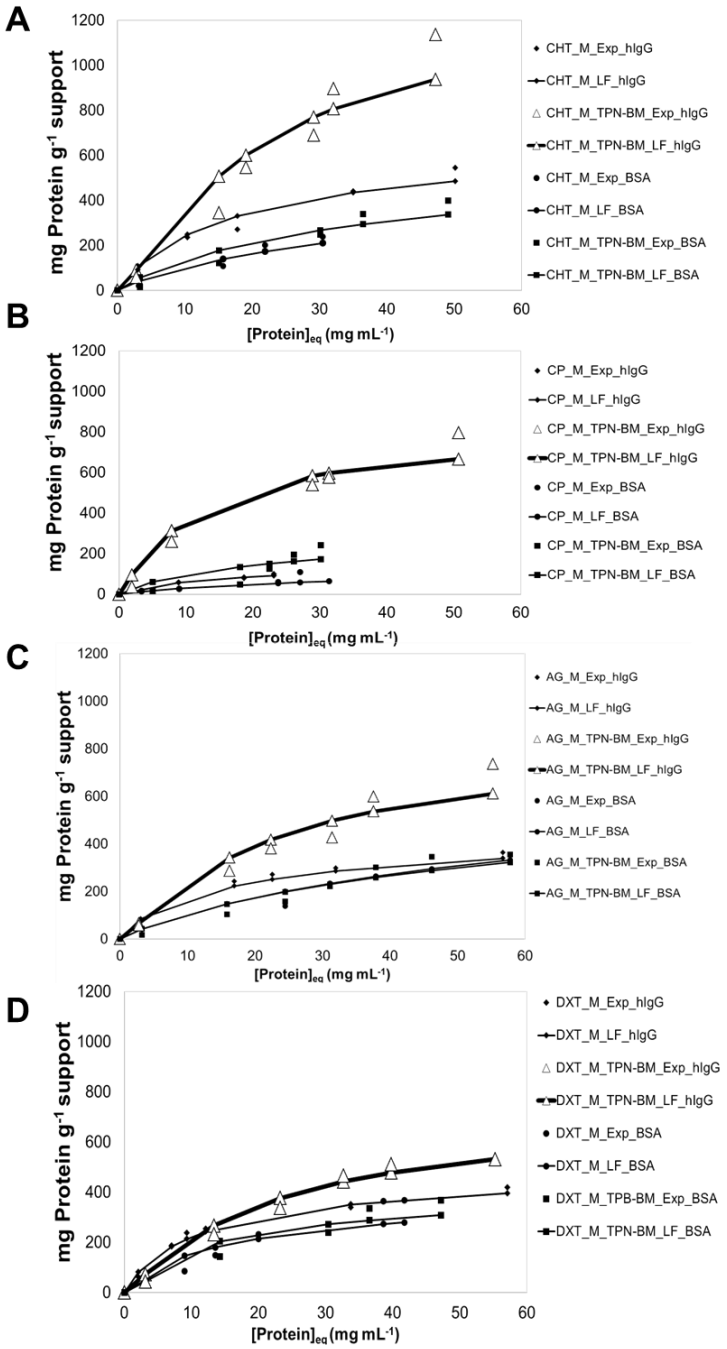

Figure 5.9 – Graphical representation of experimental adsorption isotherms (Exp) fitted by Langmuir-Freundlich (LF) model for magnetic (M) and hybrid (M-TPN-BM) monoliths: (A) CHT_M and CHT_M_TPB-BM (B) CP_M and CP_M_TPN-BM (C) AG_M and AG_M_TPN-BM (D) DXT_M and DXT_M_TPN-BM.

In order to explore dynamic binding and mass transfer properties for the hybrid monoliths, breakthrough curves of pure hIgG solutions were estimated in duplicate (Fig. 5.10). Protein recovery was estimated using pH 3 (Fig 5.10 A) and pH 11 (Fig. 5.10 B) buffers. Elution buffer with pH 3 was chosen for being efficient in IgG recovery when ligands 22/8 and TPN-BM were coupled onto CHT and CP monoliths.[82,88]

A

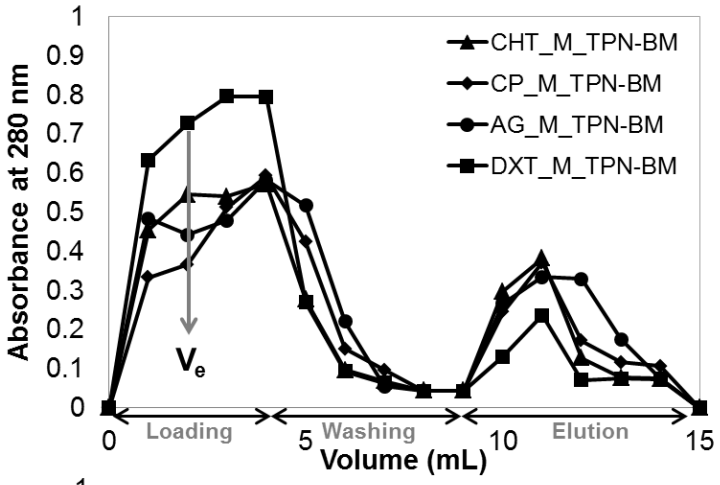

B

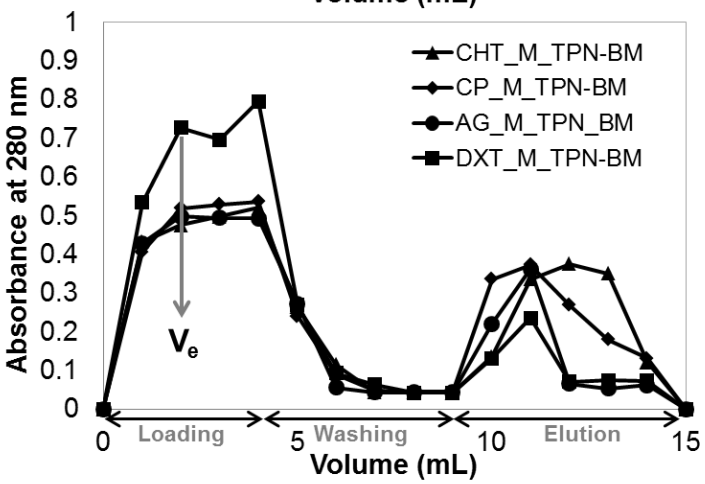

C

	Binding (mg hIgG g^{-1} support)	Elution at pH 3 % (mg hIgG g^{-1} support)	Elution at pH 11 % (mg hIgG g^{-1} support)
CHT_M_TPN-BM	100±10	73±3	42±15
CP_M_TPN-BM	99±12	77±10	65±10
AG_M_TPN-BM	103±10	63±12	45±5
DXT_M_TPN-BM	80±7	28±5	14±3

Figure 5.10 – Breakthrough profiles for human IgG upon CHT_M_TPB-BM (▲), CP_M_TPN-BM (♦), AG_M_TPN-BM (●) and DXT_M_TPN-BM (■) monoliths, performing the elution at pH 3 (A) and pH 11 (B). (C) Summarizes the binding and elution capacities estimated through breakthrough curves at different elution conditions.

On the other hand, pH 11 buffer demonstrated to be the best elution condition for MNPs functionalized with the affinity ligand 22/8.[114]

Regarding the monoliths capacity, DXT_M_TPN-BM monolith presented the poorest scenario since it was able to capture 80 mg hIgG per gram of support. Nevertheless, CHT_M_TPN-BM, CP M_TPN-BM and AG M_TPN-BM monoliths exhibited better values of hIgG retention translated by appreciable values of binding (100, 99 and 103±10 mg hIgG g^{-1} support, respectively). Considering the elution profile, DXT_M_TPN-BM monolith showed a lower hIgG

recovery (28% of total hIgG bound at pH 3 and 14% of total hIgG bound at pH 11), as opposed to CHT_M_TPN-BM, CP M_TPN-BM and AG M_TPN-BM (73, 77 and 63±7%, respectively).In addition, elution at pH 3 revealed better values compared to those obtained at pH 11.

In order to assess the effect of magnetic deformation for a better recovery yield, a tailored permanent magnet was designed. This was performed taking into consideration that: (1) the magnet needs to provide the required magnetic effect on the monolith without loss of magnetic responsive behaviour and, (2) its shape needs to help the extraction of antibody from the monolith by mechanical shrinking.

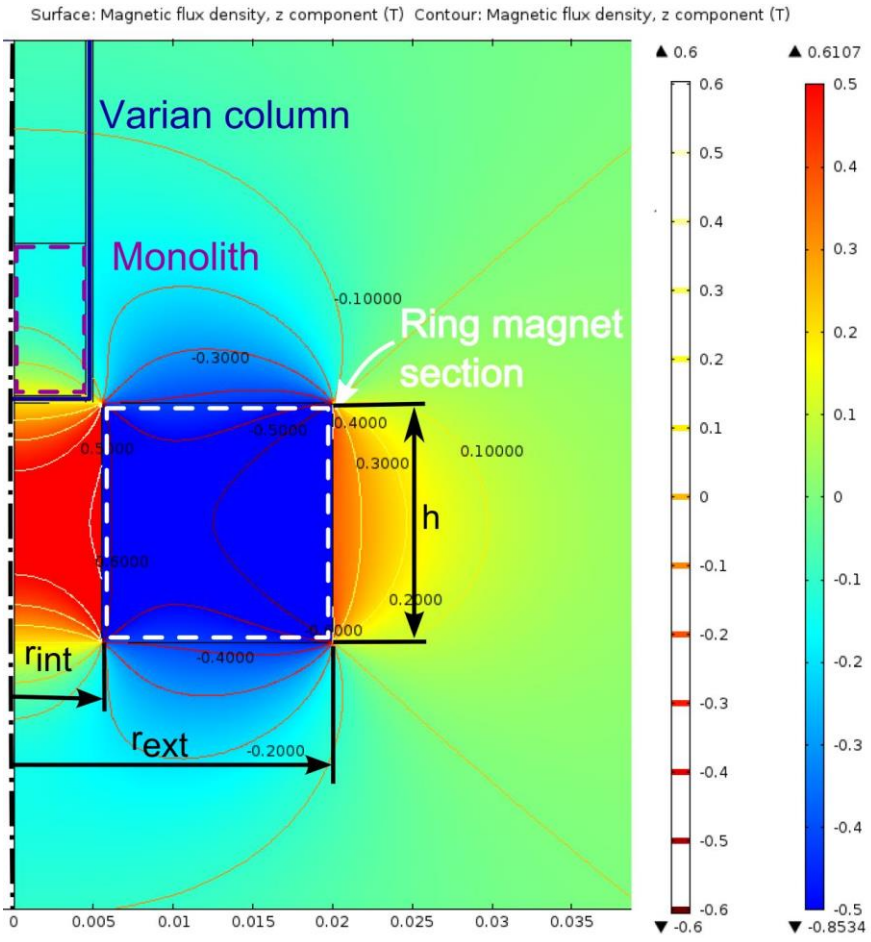

Figure 5.11 – Map of the magnetic flux density strength in the z-direction, highlighting the key components of the setup. Magnet dimensions: internal radius r_int = 5.5 mm, external radius r_ext = 20 mm, height h = 15 mm.

In order to satisfy the point (1), a FEM parametric analysis led to the magnet optimal shape (Fig 5.11) and the magnetic material adopted was neodymium 52, N52, (1.44 T of magnetic remanence). For the point (2), a geometrical constraint was fixed: the need to have a straight-hole magnet shape, with a diameter of 11 mm, i.e. the monolith case diameter. Hence, the monolith case was able to be placed inside the magnet's hole to work as a magnetic chromatographic approach. Thus, in a typical chromatographic operation, the loading of the sample is performed without magnetic field assuring that all pores of monoliths are completely available to process proteins extract without blocking. The same happens during the washing

step, where unspecific bound proteins are removed. The elution step is performed in the presence of the tailored made magnet as to induce a mechanical deformation onto the hybrid monoliths Fig. 5.12 A. The elution capacities (at pH 3.0) for all hybrid supports with and without magnetic field are shown in Fig. 5.12 B. After charging the monolithic supports with 1 mL of pure hIgG solution (2 mg mL^{-1}), it was possible to accomplish a faster recovery of 15% more hIgG under a magnetically-assisted elution. CP_M_A and AG_M_A monoliths revealed higher binding capacities and an elution capability of 90±5% when assisted by a magnetic field. Moreover, the magnetically-assisted elution takes half time (≤ 30 seconds) than a normal elution, which is also a great benefit in terms of time consumption and efficiency.

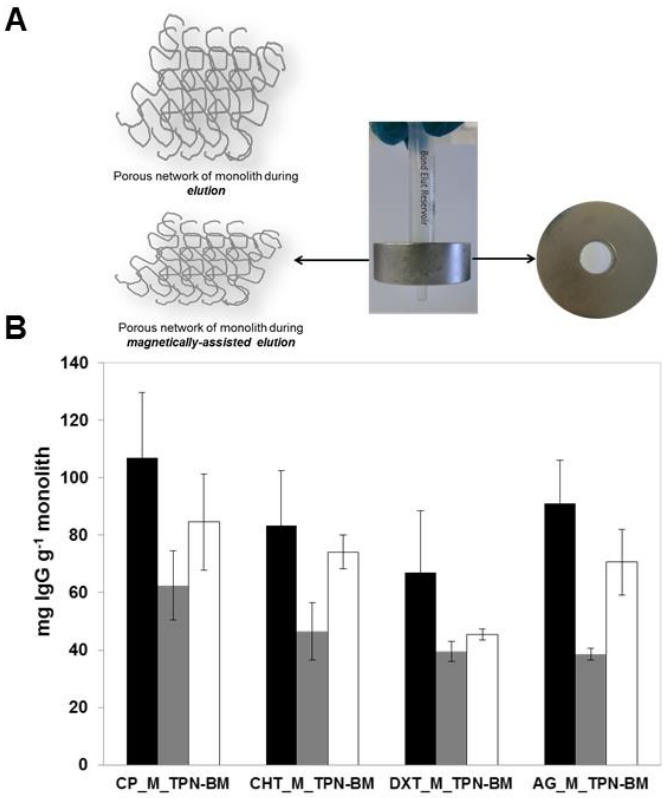

Figure 5.12 – (A) Schematic representation of the porous network availability of hybrid monoliths during typical and magnetically-assisted elution of chromatographic experiments. (B) Graphical representation of binding (black), normal elution (grey) and magnetically-assisted elution (white) of hybrid natural-based monoliths.

In order to evaluate the re-use capability of the hybrid monoliths, three consecutive chromatographic cycles and a fourth one after monolith autoclaving (After_AC) were performed, in duplicates, at an approximated flow rate of 1 mL min^{-1} (Fig. 5.13).

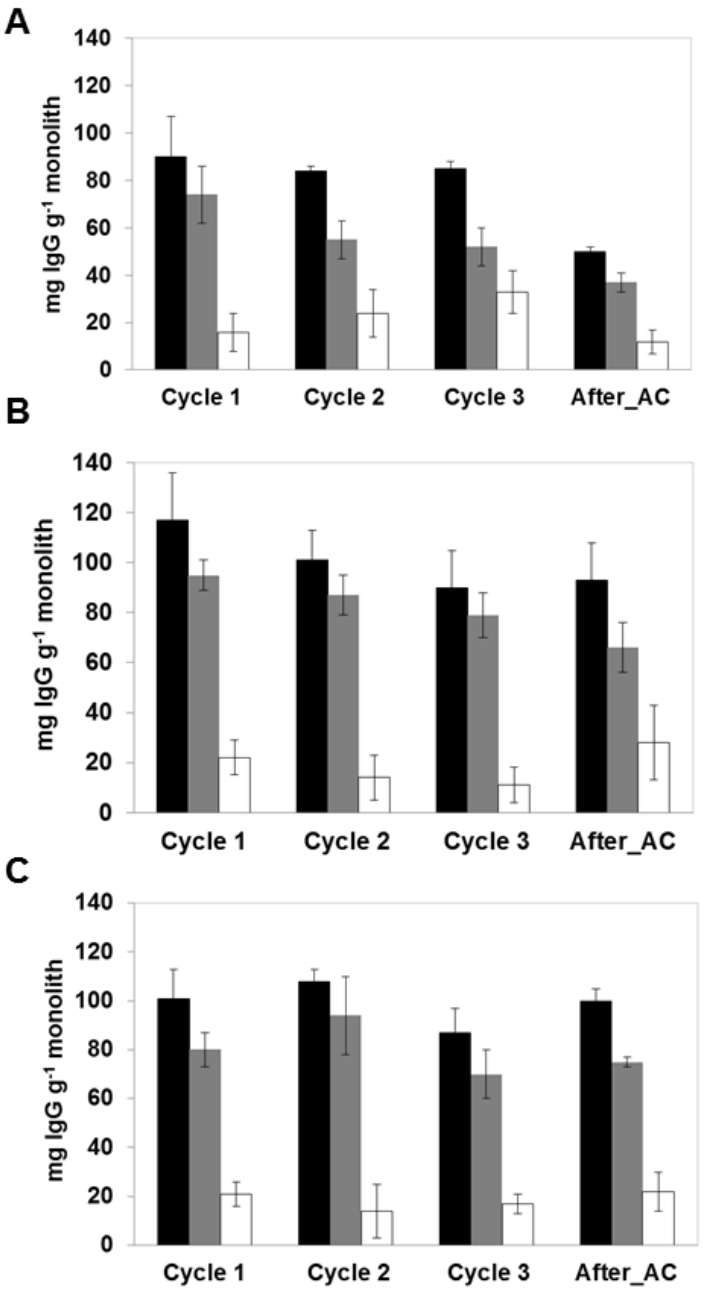

Figure 5.13 – Evaluation of chromatographic performance of (A) CHT_M_TPN-BM, (B) CP_M_TPN-BM and (C) AG_M_TPN-BM monoliths using pure IgG solutions. The chromatographic procedures, bind (black), elution (grey) and regeneration (white) steps, were performed consecutively along four cycles at a flow rate of 1 mL min^{-1}. The last cycle was performed after autoclaving (After_AC). The elution was assisted by the permanent magnet (0.5 T).

The DXT_M_TPN-BM monolith was not tested due to its fragile appearance and weak performance. Over four cycles, CHT_M_TPN-BM, CP M_TPN-BM and AG M_TPN-BM monoliths displayed a similar profile of binding, magnetically-assisted elution and regeneration, suggesting a reproducible behaviour in the capture and recovery of hIgG. CP M_TPN-BM monolith showed to be the most promising one since its binding capacity achieved 125 mg±15 mg hIgG g^{-1} support, followed by AG M_TPN-BM (115±10 mg hIgG g^{-1} support) and CHT_M_TPN-BM (90±13 mg hIgG g^{-1} support). Concerning the efficiency of hIgG recovery, CP M_TPN-BM monolith remains the best one since it is able to release 90±5% of the total hIgG

bound, and only 8±5% is removed from the support at drastic conditions (regeneration step). AG M_TPN-BM monolith also registered a promising elution profile translated by the recovery hIgG value of 88±4%. The lowest elution capacity was verified for CHT_M_TPN-BM monolith since it was only possible to recover 70±8% of hIgG bound remaining 30±2% of hIgG in the support that was only excluded in the regeneration step. Probably the enlargement of pore size that chitosan monoliths suffered until achieved a hybrid character, decreased its stiffness penalizing its chromatographic performance. Magnetic monoliths (control) were also tested but only 25 mg of IgG per gram of support approximately were retained. In the elution and regeneration steps the amount of IgG retained was then recovered.

The most challenging issue was to evaluate the selectivity of the hybrid materials for mAbs purification. As CP_M_TPN-BM and AG_M_TPN-BM monoliths revealed encouraging chromatographic profiles, they were selected to proceed with chromatographic studies involving mAbs from unclarified crude extracts. Fig. 5.14 summarizes the total amount of protein captured and eluted from both supports, at different magnetically-assisted elution conditions (pH 3 and 11) (A) as well as SDS-PAGE gels (B). Considering the binding capacity, both supports revealed similar performance (17±5 mg total protein per gram of monolith) however, in the elution capability clear differences are visible. CP_M_TPN-BM exhibits the highest elution value (98% of total protein bound) at pH 3 while AG_M_TPN-BM monolith achieved the same at pH 11. In order to assure that the total amount of protein previously quantified corresponds to mAbs, SDS gels were performed (Fig. 5.13 B and C). CP_M_TPN-BM (Fig. 5.14 B) and AG_M_TPN-BM (Fig. 5.14 C) monoliths proved high selectivity for mAbs since that, in elution fractions (lanes 7, 8, 9 and 10) only bands that correspond to mAbs fragments (50-25 kDa) are visible with a purity of approximately 97% (estimated by ImageJ analysis). All other components were excluded in washes (lanes 4, 5 and 6). These results suggest that CP_M_TPN-BM and AG_M_TPN-BM are promising supports for Ab recognition and isolation. CP_M and AG_M monoliths (control) revealed no affinity for mAbs capture.

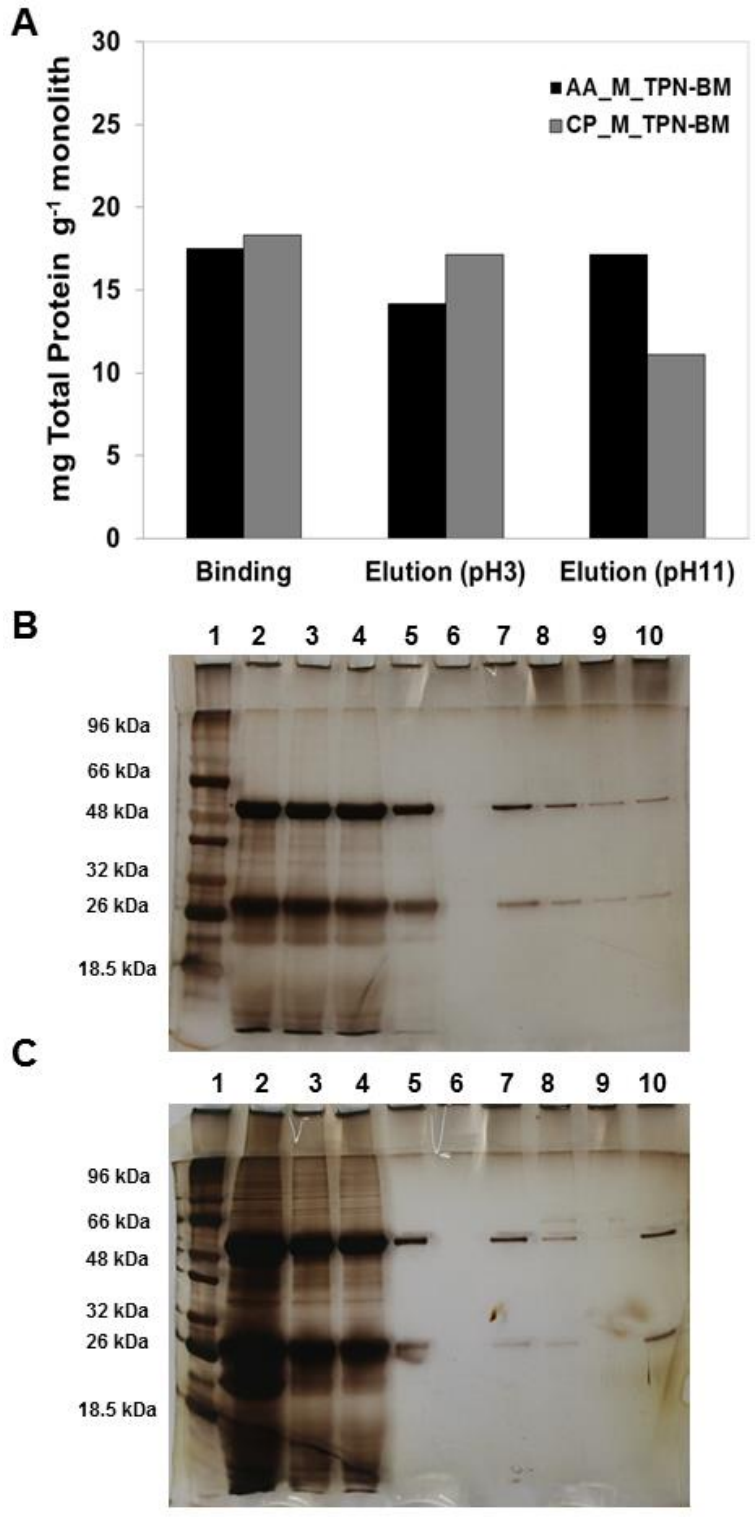

Figure 5.14 – Chromatographic performance of CP_M_TPN-BM and AG_M_TPN-BM in mAbs purification from a non-heterogeneous crude sample with an associated error of ±5.0.(A)The acrylamide gel from SDS- PAGE performed with the fractions collected during the mAbs purification using CP_M_TPN-BM and AG_M_TPN-BM (B and C) at the best conditions of elution: lane 1 corresponds to the molecular weight marker, lane 2 represents the loading, lane 3 is the flowthrough, from lane 4 to lane 6 are represented the washes (phosphate buffer (50 mM, pH 8.0)), and from lane 7 to lane 10 are represented the elution fractions with sodium citrate buffer (50 mM, pH 3.0)) (B) and (glycine buffer (50 mM, pH 11.0)) (C), respectively.

5.4. CONCLUDING REMARKS

The use of antibodies and derivative structures as effective therapeutics for cancer, autoimmune, infectious and inflammation diseases increased exponentially with an annual market worth tens of billions of US dollars. Thus, in order to give an answer to such demand, herein it is reported report the preparation of hybrid materials for Ab purification. These materials based on natural polymers were prepared in such a way that macroporous networks with great morphological and mechanical properties were created. Magnetic nanoparticles were embedded and an artificial ligand mimicking Protein A (TPN-BM) was coupled into the monoliths, turning them hybrid supports. The functionalization with TPN-BM conferred selectivity to the supports while the MNPs incorporation increased and accelerated Ab recovery. Green and solvent free strategies were employed to prepare and modify the hybrid monoliths, namely freeze-drying method and plasma technology.

The presented hybrid platforms distance from others due to three main aspects: (1) they were prepared following metrics of green chemistry and engineering principles in order to save solvents, time and energy consumption, and designed for degradation; (2) they gather in just one material two main properties, affinity and magnetic response, already employed in different purification systems, and (3) they allow an efficient and fast operation, as the magnetic response facilitates the release of the target molecule that is typically performed under drastic acidic pH. The hybrid materials also exhibited a considerable stability towards CIP and SIP which underline their robustness.

The magnetically-assisted elution process was efficient, faster and selective for Ab purification since CP_M_TPN-BM and AG_M_TPN-BM monoliths were able to bind 120 mg±10mg of hIgG per gram of monolith and to elute 91±5% for at least four consecutive cycles. Moreover, when tested with crude samples, both supports showed a good specificity for mAbs, recovering them with 97% of purity.

The hybrid structures and the magnetically-assisted elution can be easily extended to the recognition and separation of different biomolecules with high added value by changing only the immobilized ligand. In addition, the application of these systems in biosensing or biomedical devices is also envisaged.

CHAPTER 6

POROUS CHITOSAN-BASED MONOLITHS PREPARED FROM THE BEST COMBINATION OF SUSTAINABLE MATERIALS AND TECHNIQUES

SUMMARY

This work aims to redesign antibody purification processes combining the best and greener tools from the materials and techniques points of view, to achieve desirable performances. Thus, chitosan-based monoliths, with and without magnetic nanoparticles embedded, were produced following two strategies: (1) composed by gelation, water-acetone substitution followed by $scCO_2$ phase-inversion and (2) involving swelling and freeze-drying methods, after monolith conception by the first strategy, to control the pore opening and, therefore, generating new porous network starting points. Both strategies allowed the production of different monolithic platforms with high control in pores architecture, great stiffness, magnetic and physico-chemical stability and easily functionalized with the biomimetic ligand TPN-BM, specific for antibodies. The elution of antibodies from the monolithic systems was tested in the absence and in the presence of a magnetic field (0.5 T). CP monoliths prepared only by the first strategy, and the magnetic ones further submitted to pores opening attempt, CP 25:75_TPN-BM and CP 25:75_M_TPN-BM^{FD} respectively, exhibited an indicative affinity behaviour towards IgG which comprises acceptable estimated affinity parameters and encouraging binding capacities of 55 and 32 mg IgG g^{-1} support, respectively. Moreover, CP 25:75_M_TPN-BM^{FD} monolith revealed an encouraging performance for mAbs isolation being able to elute magnetically 50% of mAbs with 75% of purity however, with low selectivity.

6.1. INTRODUCTION

Over this thesis, the importance of mAbs and the significance of affinity chromatography as the major platform for mAbs purification have been widely discussed considering the ligand and supports points of view. In this chapter, the main focus is directed for the techniques that allow the monoliths production: from the most common to the alternative ones.

Monoliths have been produced from polymerization of different acrylate monomers and by chemical modifications of natural or synthetic polymers combining the sol-gel, gelation, and freeze-drying methods.[20,61,82,207,208] These strategies have enabled the fabrication of numerous monolithic platforms with distinguished architectures. However, they are very time consuming and/or involve organic solvents which are difficult to eliminate, remaining entrapped inside the polymeric network.[209] Furthermore, there are also difficulties in the achievement and preservation of high levels of porosity and of the three-dimensional structure.[22] Thus, sustainable and rigorous methods to design a very well-tuned porous network with macro and microstructural characteristics are still required in order to extend monolith applications to new targets.

Over the last decades, supercritical fluids (SCF) have been successfully applied for polymer synthesis and processing.[210] A supercritical fluid is any substance at a temperature and pressure above its critical point, that presents liquid like densities and gas like viscosities and diffusivities.[21] Carbon dioxide (CO_2) is the most typical substance used at supercritical conditions. Besides the environmental advantages of CO_2 such as its low cost, non-toxicity, non-flammability, availability in high purity from numerous sources and its relative low critical temperature (T_c=31 ºC) and critical pressure (P_c=73.8 Pa), supercritical carbon dioxide ($scCO_2$) can be used to prepare highly pure materials with high controlled morphology.[211] Moreover, since CO_2 can be easily removed from the pores without leaving any solvent residues, $scCO_2$ based processes are considered sustainable and green alternatives for the controlled design and production of polymeric porous structures.[21] Therefore, different SCF-assisted processes, specially involving CO_2, have been established such as: non-reactive gelation of SCF solutions using organogelators,[22,212,213] crystallization of SCF-swollen crosslinked polymers (CSX),[22,214] foaming[215,216] and phase inversion.[210,217,218] Basically, in each process, $scCO_2$ assumes different roles (e.g. as solvent, anti-solvent or porogenic agent) and acts in different stages of the processes (in the beginning or in the middle of porous structure process formation).[22] Particularly, the fact of being organic solvent free procedures, SCF-based processes offer significant environmental benefits: the drying steps are energy intensive, porous structure collapse is avoided, (since SCF do not give rise to a liquid-vapor interface, allowing high mass transfer, due to SCF low solvent viscosity) and polymers plasticization is permitted because it exhibits a great plasticizer ability.[22,219] The efficiency of these tools for the design of tuned porous networks is translated in the variety of particles,[220,221,222] scaffolds,[223,224,225] and membranes[210,226,227] that have been produced to be employed in tissue engineering,[209,228] drug delivery,[78] and bioseparation fields.[210,229] Moreover, process parameters such as pressure, temperature, CO_2 flow and depressurization rate can be adjusted and controlled easily, and

thus are additional process parameters that can be optimized when pursuing a specific morphological design.[226]

Inspired on this panoply of green and efficacious SCF-based methods to produce porous platforms, herein it is intended to develop monoliths prepared from blends of chitosan and PVA (CP),[82] and evaluate their performance as monolithic platforms for antibody purification. A strategy composed by gelation, water-acetone substitution followed by $scCO_2$ phase-inversion was applied, and evaluated to prepare CP monoliths (with and without magnetic nanoparticles, MNPs, embedded) with a controlled pore adjustment. A second attempt to control the pore opening, involving swelling and freeze-drying methods, was also performed after magnetic CP monoliths conception.

This strategy once established, can open the boundary of monoliths application for different targets in bioseparation, tissue engineering, cells growth and biomedical applications.

6.2. EXPERIMENTAL AND METHODS

6.2.1. MATERIALS

Disodium hydrogen phosphate monodibasic (PA), disodium hydrogen phosphate dibasic (pro analysis), disodium tetraborate, ethanol absolute and sodium citrate dihydrate were purchased from Merck. Isopropanol and sodium bicarbonate were purchased from Riedel-de-Haën. Acetone (purity≥99%), and ethyl acetate were supplied by Roth. Acetic acid (purity≥99%), aminocaproic acid, 3-aminophenol, 4-amino-1-naphthol hydrochloride, cyanuric chloride (purity≥98%), 1,6-hexanediamine (purity≥98%), N,N-dimethylformamide (DMF), dimethylsulfoxide (DMSO), chloridric acid (HCl), glycine, ninhydrin, iron (II) chloride tetrahydrate ($FeCl_2.4H_2O$, purity≥99%), iron (III) chloride hexahydrate ($FeCl_3.6H_2O$, purity≥99%), maleic acid ($C_4H_4O_4$≥99%), potassium cyanide, pyridine, sodium hydroxide (purity≥99%), sulfuric acid (H_2SO_4, purity≥95%), sodium phosphate monobasic monohydrate ($H_2NaO_4P.H_2O$, purity≥98%), di-sodium hydrogen phosphate 2-hydrate ($Na_2HPO_4.2H_2O$, purity≥98%) were purchased from Sigma Aldrich. Chitosan (75~85 % deacetylated, medium molecular weight), hydroxylamine hydrochloride ($NH_2OH.HCl$, purity≥ 99%), poly(vinyl alcohol) (purity≈99 %), bicinchoninic acid (BCA) kit, bovine serum albumin (BSA) (purity≥98%) were supplied by Sigma Aldrich. Human IgG was purchased by Octapharma (Gammanorm, purity≥99%). 1.10-phenonthroline 1-hydrate ($C_{12}H_8N_2.H_20$, purity≈99%) was acquired from Panreac. Carbon dioxide (CO_2) was supplied by Air Liquid with 99.998% purity. All reagents were used without any further purification.

6.2.2. MONOLITHS PREPARATION

Chitosan-poly(vinyl alcohol) (CP) monoliths were prepared following a strategy based on the combination of three protocols already established.[209,215,228] The methodology starts with the preparation of casting solutions by solubilizing chitosan (ranging between 14% and 25%, w/w) and poly(vinyl alcohol) (ranging between 76% and 86%, w/w) in acidic water (1% v/v) with a

composition of 14 wt%. The casting solutions were homogenized by heating up to 60 ºC with continuous stirring at 150 rpm. Then, a crosslinker, 2% of maleic acid (w/w, regarding the total mass of PVA),[230] was added and the reticulation occurred under stirring at 90º C during 90 minutes. Next, the casting solutions were poured into steel molds having an internal diameter of 2 cm and height of 1 cm, and further frozen at −20 ◦C for 24 h to obtain a hydrogel (gelation process). The hydrogels were removed from the steel containers, immersed in acetone at −20 ◦C during 48 h for water-acetone replacement, and finally dried using $scCO_2$.

$ScCO_2$ gel drying was performed according to the following procedure: firstly the steel containers were loaded again with the hydrogels (1), secondly they were introduced in the high-pressure cell (2), which was closed and introduced in a thermostatized water bath, where CO_2 was added until the desired pressure, with an exact flow, using a Gilson 305 piston pump, (3) and finally, after reaching the normal operational pressure, the supercritical solution passes through a back pressure regulator (Jasco 88081) which separates the CO_2 from the solvent (acetone) (4) (see Fig. 6.1). All these experiments were performed at 20.0±0.7 MPa with a CO_2 flow of 10.0 g min^{-1} during 3 h (estimated time was 1 hour per monolith). At the end, the system was depressurized during 10 min and dried porous monoliths were obtained (5).

The same procedure was applied using CP casting solutions with MNPs. Casting solutions of 25:75 of CHT-PVA (w/w) were prepared with 2 g of magnetic nanoparticles (MNPs), for a concentrated polymeric casting solution of 7 wt% The concentration reduction of the casting solution from 14 to 7% was performed to assure the mobility of MNPs in the monolithic constructs in order to take advantage of a magnetic monolithic response in the last stage (elution) of antibody purification.

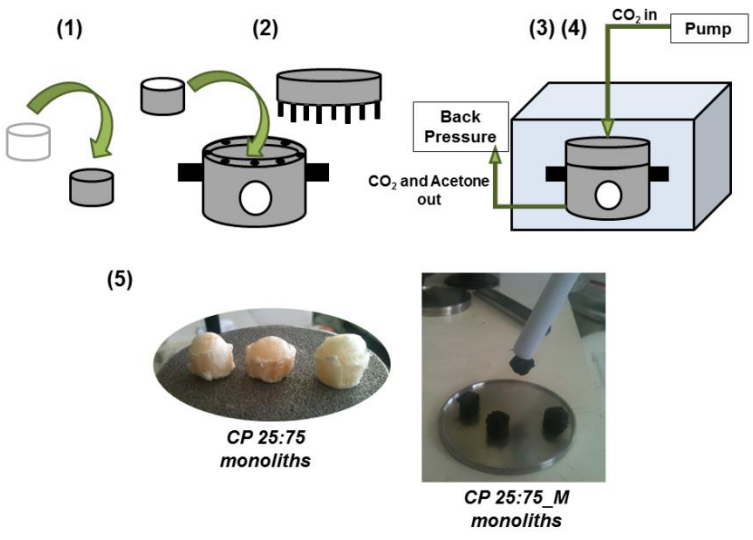

Figure 6.1 – Schematic representation of the chitosan-poly(vinyl alcohol) (CP) hydrogels drying under supercritical carbon dioxide ($scCO_2$ drying).

Another strategy was also attempted, and consisted into swelling the magnetic CP 25:75 monoliths (CP 25:75_M) until the desired water uptake degree was achieved, and then

lyophilize them (Fig. 6.2). This approach aims to control the pore opening after monolithic platforms achievement. After 2 hours of swelling in water, CP 25:75_M were frozen at -20 ºC during 5 hours and lyophilized during 12 hours. At the end, a larger porous network was obtained.

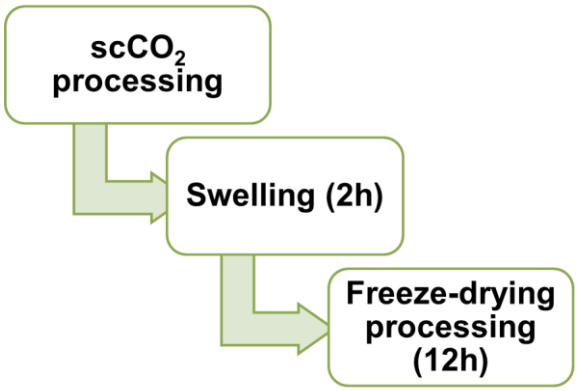

Figure 6.2 – Schematic representation of the additional procedure for the opening of porous network of chitosan-poly(vinyl alcohol) (CP) monolith: after obtaining CP monoliths by $scCO_2$ drying, monoliths swelled 2 hours in water and then were frozen at -20ºC and lyophilized.

6.2.3. PREPARATION OF AFFINITY MONOLITHS

Native CP monoliths (with and without MNPs) were introduced in a plasma chamber which was thoroughly purged with a continuous flow of nitrogen to reduce trace amounts of air and moisture. Then, the CP monoliths modification followed two steps: (1) surface activation followed by (2) *in-situ* amination. The activation occurs through the radicals generated by Argon (Ar)-plasma and the amination by dragging 1,6-hexanediamine into the plasma chamber. For the amination step, after 5 minutes of Argon (Ar)-plasma treatment, gaseous1,6-hexanediamine was fed to the reaction chamber under vacuum by vaporizing the 1,6-hexanediamine contained in a flask that was maintained at 150 ºC, as mentioned in Chapter 5. The entire plasma process occurred at a power setting of 80 W and a constant pressure of 0.3 Torr inside the chamber during 30 minutes. According to what was previously described on Chapters 2, 3 and 5, the degree of amine functionalization was determined using the Kaiser test.[82,161] For ligand TPN-BM immobilization, an excess of ligand (3 equiv. to the amination content, 180 mg), was added to the aminated CP monolith samples (approximately 150 mg) in 10 mL of DMF, and incubated on a rotary shaker (140 rpm) for 72 h at 85 ºC. TPN-BM functionalized monoliths were then washed with DMF until the absorbance at 267 nm, maximum absorbance wavelength of TPN-BM ligand, becomes less than 0.005. In order to assure a complete removal of physically adsorbed ligand, the functionalized monoliths were hosted in syringes with 3 and 10 mL of capacity and 1.5 cm of inner diameter, and submitted to washes with DMF and to a CIP. The CIP procedure involved sequential washes with NaOH 1 M (until the absorbance at 267 nm was ≤0.005), 10 mL of water, regeneration buffer (NaOH 0.1 M in 30% of isopropanol) and lastly, again with 10 mL of distilled water until the absorbance at 267 nm become lower than 0.005. The functionalized monoliths were finally washed with sodium phosphate buffer (50 mM, pH

8.0) and sodium citrate buffer (50 mM, pH 3.0), typical buffer solutions employed in affinity chromatographic experiments, until the absorbance at 267 nm become negligible. The total ligand TPN-BM density (µmol g^{-1} support) was calculated by subtracting the amount of ligand collected in all washes from the initial ligand used in the immobilization step.

6.2.4. CHARACTERIZATION OF NATIVE AND FUNCTIONALIZED MONOLITHS

The morphological and mechanical properties of native (with and without MNPs) and functionalized monoliths with TPN-BM were investigated using SEM, MIP, water flux measurements and tensile-strain tests. SEM was performed in Hitachi S 2400 equipment with an accelerating voltage set to 15 kV. Firstly, the samples were frozen and broken in liquid nitrogen for cross-sectional analysis and, gold coated before analysis. Monoliths porosity, average pore size diameter and surface area were determined by MIP (Micromeritics, autopore IV). The water fluxes were determined at room temperature and atmospheric pressure. Varian columns with a capacity of 3 mL and an effective volume of 1.2 mL or syringes with 10 mL of capacity and 1.5 cm of inner diameter were packed with native and functionalized CP monoliths (bare and magnetic ones). The run time was registered and at least three measurements of distilled water flux were recorded.

Uniaxial compression was used to determine the mechanical properties of the monoliths using tensile testing equipment (MINIMAT firmware v.3.1) at room temperature. Samples were prepared in a cylindrical shape (10-15 mm in diameter thickness). The length between clamps was set at 5-10 mm, the speed set to 1 mm min^{-1}, a full scale load of 20 N and maximum extension of 90 mm was used. The compression modulus was calculated from the slope of the linear portion of the stress-strain curve (see Chapters 2 and 3).

Uniaxial deformation induced by magnetic field was also performed for native and functionalized magnetic CP monoliths in order to evaluate their response at a magnet field of 0.5 T, the one selected as suitable for monolith shrinking without irreversible deformation (Chapter 5). This evaluation occurred during 30 minutes and at the end, the magnetic field was removed and the reversibility of the magnetic-shape memory was assessed. These tests were performed in dry and wet conditions, since the monoliths magnetic response can change according the hydrate sate of the porous network, as mentioned in Chapter 5.

To evaluate the stability of native and functionalized monoliths, samples (15 mg) were immersed in 500 µL of solutions with different pH values, including typical solutions employed in CIP procedures, using a 96 well block for 24 hours at 150 rpm. Over the experience, samples of 200 µL were collected and fresh 200 µL were added in order to maintain the total volume. The MNPs and ligand leaching were quantified by measuring the absorbance at 490 nm (following the magnetite assay)[198] and 267 nm, respectively.

6.2.5. DETERMINATION OF STATIC BINDING CAPACITIES

In order to estimate the static binding capacities, partition equilibrium experiments were performed in a batch system as described by Barroso *et al.*.[82] The adsorption of hIgG on the

native and functionalized monoliths was investigated. Particularly, monolithic samples (30 mg) were incubated with hIgG (0.0–20 mg mL^{-1}, 500 µL prepared in phosphate buffer 50 mM, pH 8.0) at 25 ºC, 200 rpm during 24 h. These experiments were performed in duplicates. After incubation, the amount of protein in the supernatants was quantified at 280 nm on a microplate reader (Tecan Infinite F200, filter, l = 280 nm). Meanwhile, a calibration curve was determined using hIgG in phosphate buffer solutions (50 mM, pH 8.0) (0.0–20 mg mL).The adsorption phenomenon followed the Langmuir–Freundlich model and it was represented by:

$$Q = \frac{Q_m \times (C)^n}{K_d + (C)^n}$$

Equation 6.1

where K_d is the apparent dissociation constant (M) that includes contributions from ligand binding to the support, Q_m is the maximum binding capacity (mg protein g^{-1} support), C is the concentration of protein in the liquid at the equilibrium (M) and n represents the Langmuir–Freundlich coefficient.

6.2.6. DETERMINATION OF DYNAMIC BINDING CAPACITIES

The dynamic loading capacity of the packed columns with native and functionalized CP monoliths was determined using frontal analysis according with the equation below:

$$Q = \frac{V_e}{[Protein]_{plateau}}$$

Equation 6.2

where Q corresponds to the estimated adsorbent capacity and V_e corresponds to the elution volume. This process consists in loading hIgG (6 mL, 0.5 mg mL^{-1}) in sodium phosphate buffer (50 mM, pH 8.0) through the equilibrated monolithic packed columns at gravitational conditions until the protein concentration of the output and input streams were equivalent. At this point, packed monolithic columns were washed with phosphate buffer (50 mM, pH 8.0) to remove unbound protein, and the bound one was eluted in the presence or absence of the permanent magnet using sodium citrate buffer (50 mM, pH 3.0). Samples collected (1 mL) during loading, washing and elution stages were examined by measuring absorbance at 280 nm on a 96-well format.

6.2.7 MONOLITHS PERFORMANCE OVER CYCLES OF PROTEIN CAPTURE AND RELEASE

The monoliths performance over cycles was conducted in an adsorption–desorption process by switching eluents at room temperature and at atmospheric pressure. Varian columns with a capacity of 3 mL and 1 cm of inner diameter and, syringes with 10 mL of capacity and 1.5 cm of inner diameter were packed with CP monoliths and then washed and equilibrated as described

in previous section. At that point, 1 mL of hIgG solution (2 mg mL^{-1}) was added and columns were washed with sodium phosphate buffer (50 mM, pH 8.0) until the absorbance measured at 280 nm reached ≤0.005. The bound protein was recovered with sodium citrate buffer (50 mM, pH 3.0) with and without magnetic field. Packed columns were then regenerated as previously described (applying CIP), in order to be reused. These chromatographic experiments were repeated during 3 cycles in order to evaluate the column capacity over time. The amount of protein was initially determined by absorbance measured at 280 nm and by the BCA method (microplate reader assay).

6.2.8. PURIFICATION OF mAbs DIRECTLY FROM CRUDE SAMPLES

In order to evaluate the possibility to directly capture antibodies from non-clarified crude extracts, packed columns with bare and magnetic CP monoliths, before and after ligand TPN-BM coupling, were tested with two different mammalian crude extract solutions: one containing monoclonal antibodies (mAbs) and another comprising the single chain (scFv) (1 mL, approximately 2 and 10 mg of total protein per millilitre, respectively). After loading with crude extract, the packed columns were washed with the sodium phosphate buffer (5 mL, 50 mM, pH 8.0) until the absorbance measured at 280 nm reached less than 0.005. At that point the bound protein was eluted and recovered with sodium citrate buffer (50 mM, pH 3.0) at the presence and absence of magnetic field. All collected samples were analysed by the BCA assay to quantify the amount of total protein bound and eluted from the monoliths. SDS-PAGE was performed on acrylamide gel (12.5%) in Tris-Glycine buffer system pH 8.3. Electrophoresis apparatus (from BIO-RAD) was connected with power supply at 120 V, 190 mA for 1 h. The gel was revealed using a silver staining kit from BIO-RAD.

6.3 RESULTS AND DISCUSSION

CP monolithic structures with a well-defined porous network were prepared following an integrated strategy involving: (1) gelation process, (2) water-acetone substitution and (3) $scCO_2$ phase-inversion/drying. A further optimization, which consisted in submitting monoliths to an additional treatment for opening porous network through swelling and freeze-drying procedures, was also investigated. Then, monoliths were functionalized with the biomimetic ligand TPN-BM, following the procedure described in Chapter 5, which introduces the activation and amination of the surface of the monolith in one step, induced by plasma treatment. A detailed morphological, mechanical, magnetic and physico-chemical characterization before and after TPN-BM coupling was performed, in order to select the best monolith candidate to proceed with the studies of antibody purification involving pure and crude samples.

6.3.1. MONOLITHS PREPARATION AND FUNCTIONALIZATION

Chitosan-PVA (CP) solutions were prepared by dissolving chitosan (ranging between 15% and 25%, w/w) in acidic water (1% v/v) with a composition of 14 wt%, following the steps described

in the section 6.2. Then, the casting solutions were frozen at -20ºC in order to form a hydrogel, that once formed, was immersed in acetone also at -20 ºC. The frozen water, upon contact with acetone, due to the melting depression effect, acquires mobility and start to be substituted by acetone (48h), which can easily be removed by drying the hydrogel under supercritical conditions (20 MPa, 40 ºC) and using a flow rate of 10 mL min^{-1} during 1 h /monolith. The depressurization time was 10 minutes.

Different methodologies were attempted to achieve dried monoliths. Gelation, water-acetone replacement and $scCO_2$ drying times, were significantly optimized. Particularly, water-acetone substitution is a crucial step since the polymers involved are only soluble in water that has a poor solubility in $scCO_2$. Thus, by a simple immersion in acetone (step 2) of the frozen hydrogels, the water crystals formed during gelation step suffer a melting depression which enables an easy water/acetone replacement.[231,232] Since acetone has a great solubility in $scCO_2$, its further removal using $scCO_2$ becomes easier (step 3). As Cardea *et al.* established,[228] for a successful monolith gelation, time and temperature are extremely important for the formation of the structure of the gel. This gelation temperature will affect the stability of the structure in further processing steps, thus, gelation at low temperatures is necessary. The chosen temperature for gelation and subsequent water-acetone substitution, -20 ºC, assures that the gel formation occurs in a stable phase allowing for the water-acetone substitution without damaging the gel structure previously achieved.[228,233] Thus, the water-acetone replacement is thermodynamically possible since it is established that in the presence of salts or organic solvents, the hydrogen bonds (HB) organization of water is severely disrupted, and new HB between super-cooled water and acetone are established.[231,232]

The second attempt to tune monoliths porous network consisted in taking advantage of monolith's swelling degree. Once established, monoliths were immersed in water to swell, and consequently, open their porous network. This "opening" was stopped by freezing the supports in hydrated state for subsequent lyophilization to attain a larger porous structure. This approach enables: (1) to estimate the monolith dimensions in hydrated state and (2) to define a new porous network starting point of the monoliths without repeating the entire process of monoliths production.

Once obtained, CP monoliths were modified by plasma treatment for further TPN-BM ligand coupling. The modification of CP monoliths consisted in their surface activation with argon (Ar)-plasma that allows the radicals formation for subsequent 1,6-hexanediamine immobilization, also assisted by plasma treatment. This greener strategy already discussed and evaluated in Chapter 5, was once more applied due to its great potential of surface modification saving organic solvents and time consuming.

Hereupon, native and functionalized CP monoliths (bare and magnetic) were characterized in terms of morphological, mechanical, magnetic and physico-chemical features.

6.3.2. CHARACTERIZATION OF CP MONOLITHS BEFORE AND AFTER TPN-BM COUPLING

SEM images presented in Fig. 6.3 exhibits bare and magnetic monoliths CP 25:75 monoliths before (Fig. 6.3 A, B and C) and after TPN-BM coupling (Fig. 6.3 D, E and F), respectively. Native bare and magnetic CP 25:75 monoliths (A and B) exhibit small spherical pores. After TPN-BM ligand coupling (D, E) the porous network of both supports is kept as well as their homogeneity. Considering the magnetic monolith processed by the additional step (swelling and freeze drying process (FD), CP 25:75_M^{FD}) (Fig. 6.3 C), it is possible to observe a significant increase of porous network, even after its functionalization (CP 25:75_M_TPN-BM^{FD}) (F), as the homogeneity of the support is maintained. This result comprising CP 25:75_M_TPN-BM^{FD} monolith suggests that the freeze-drying step added after support swelling can be an optional strategy to monitor and redefine monoliths pore size in dry conditions. SEM micrographs of CP 14:86 monoliths were not considered due to high heterogeneity, low stability and poor mechanical properties in dry and wet state exhibited by this support (Table 6.1).

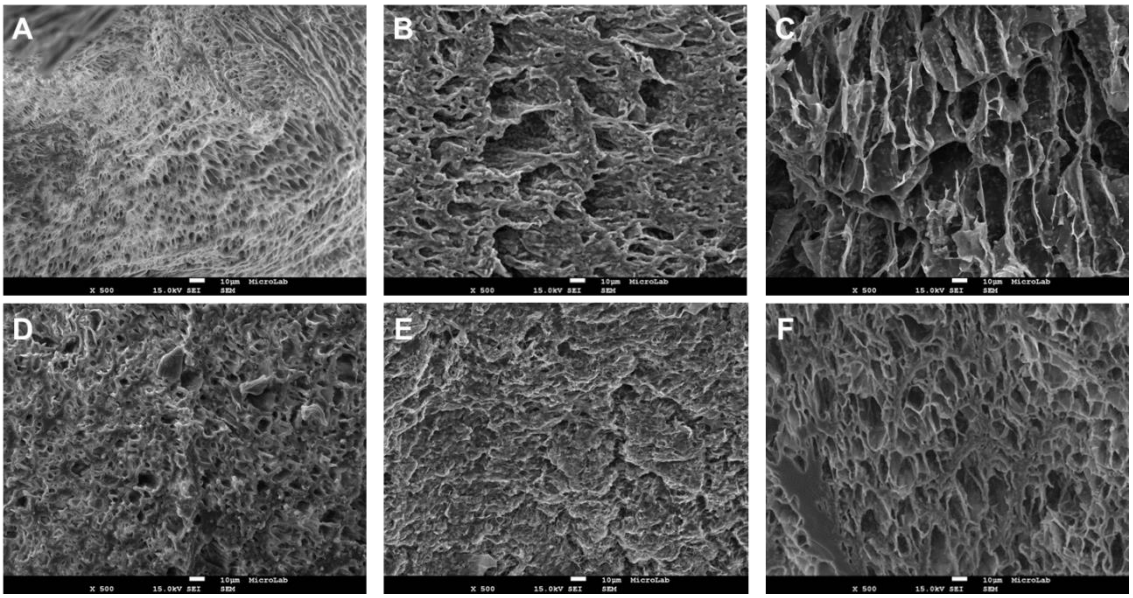

Figure 6.3 – SEM images of bare and magnetic chitosan-poly(vinyl alcohol) (CP) monoliths before and after functionalization with TPN-BM. Particularly, (A) bare CP monolith, CP 25:75, (B) magnetic CP monolith CP 25:75_M and (C) magnetic CP monolith submitted to an additional treatment for opening porous network involving swelling and freeze-drying procedures, CP 25:75_M^{FD}. The corresponding SEM images obtained after functionalization with TPN-BM are shown in D, E and F respectively: (D) CP 25:75_TPN-BM, (E) CP 25:75_M_TPN-BM and (F) CP 25:75_M_TPN-BM^{FD}. All the images have a magnification of 500 and the scale bar in white indicates 10 µm.

Morphological data obtained by SEM is in agreement with the data obtained by (MIP) (Fig. 6.4). Fig. 6.4 A compares the pore size distribution of CP monoliths herein prepared (CP 25:75 and CP 14:86) and of CP 50:50 prepared by freeze-drying method described in Chapter 2. Clearly, the pores architecture of CP monolithic supports prepared from both methods is different. CP 50:50 reveals a broad pore size diameter (one sharp peak around 10 µm and a larger one between 30-60 µm) and a higher mercury intrusion, ≈ 3.5 mL g^{-1}, which means greater porosity (70%).[82] Conversely, the mercury intrusion for CP 25:75 and CP 14:86, is around 0.5 mL g^{-1} which translates a lower porosity value around 40% (Table 6.1), and a decrease in average

pore size diameter (between 0.5-10 and 20 µm). These results addressed to the sharper style of pore size distributions, justify the improvement of monoliths porous network production, with higher control, using the methodology composed by gelation process, water-acetone substitution and $scCO_2$ phase-inversion/drying, herein presented. Fig. 6.4 B shows the pore size distribution of magnetic CP 25:75 prepared by both strategies: the one previously mentioned and another one involving freeze-drying after monoliths swelling (FD).

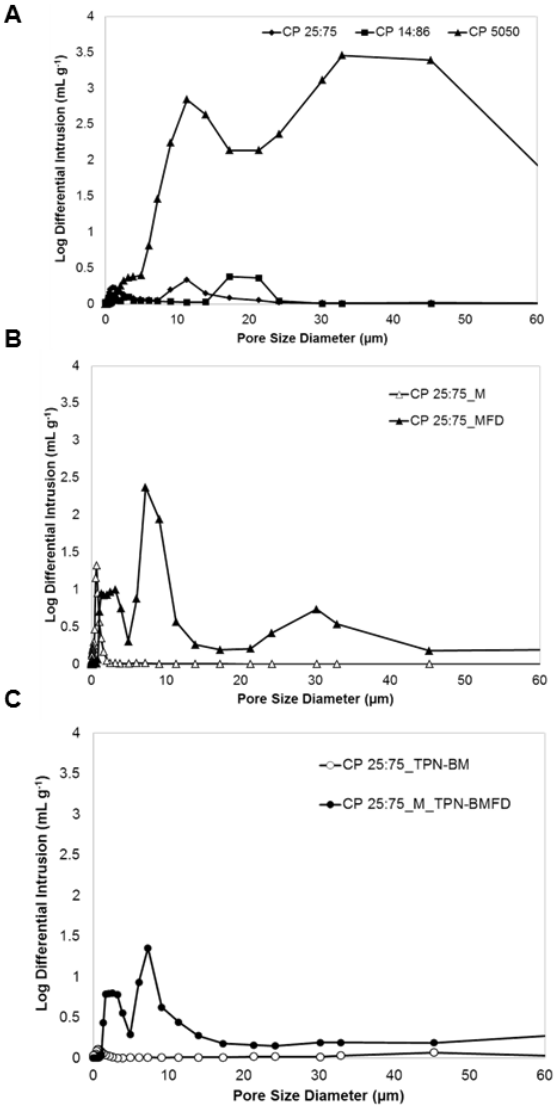

Figure 6.4 – Distributions of pore size diameter of all chitosan-poly(vinyl alcohol) (CP) monoliths. Particularly, (A) represents bare CP monoliths: (●) CP 25:75, (■) CP 14:86 and, (▲) CP 50:50; (B) represents magnetic CP monoliths: (Δ) CP 25:75_M and (▲) CP 25:75_M^{FD} and (C) represents CP monoliths functionalized with TPN-BM: (○) CP 25:75_TPN-BM and (●) CP 25:75_M_TPN-BM^{FD}. ^{FD} means that monoliths were submitted to an additional treatment for opening porous network involving swelling and freeze-drying procedures.

It is clear the enlargement of pore size diameter of CP 25:75_M^{FD} (around 10 µm in average) comparing with CP 25:75_M (around 0.6 µm). Nevertheless, the porosity is similar (Table 6.1) for magnetic CP monoliths treated by different strategies. Although the strategy that comprises swelling and freeze-drying procedures has allowed a pore size enlargement, the monolith volume also increased. Since the porosity translates the quotient between the pore volume and

the total volume (support volume plus pore volume),[228] the volumes ratio was not significantly affected, resulting a similar porosity for magnetic CP monoliths treated differently. Fig. 6.4 C illustrates the pore size distribution of bare CP monolith after TPN-BM immobilization (CP 25:75_TPN-BM), and the magnetic one submitted to pores opening method also after TPN-BM coupling (CP 25:75_M_TPN-BM^{FD}). For CP 25:75_TPN-BM, the porosity as well as the pore size diameter decreased, approximately from 43 to 28% and 5 to 0.6 µm, respectively. This was expected since the ligand coupling process normally leads to a decrease (Table 6.1) of these morphological features.[82,161] Addressed to this, the value of compression modulus in dry state increased significantly, as expected. However, the stiffness of the material in wet state is very similar before and after TPN-BM coupling, suggesting that independently of the monolith composition, no significant differences are registered upon hydration (Table 6.1). Additionally, the post-treatment combining the swelling with further freeze drying process (only applied for magnetic monoliths in order to take advantage of their magnetic behaviour), originated monoliths (CP 25:75_M^{FD} and CP 25:75_M_TPN-BM^{FD}) with pore size diameter around 9±2 µm, porosities above 50% (53-55%) and a strong mechanical behaviour (around 16.0±2 and 3.0±0.5 kPa) for CP 25:75_M^{FD} and CP 25:75_M_TPN-BM^{FD}, respectively. These values are within the range of values that are required for chromatographic supports to enable the processing of viscous and crude samples.[140]

Table 6.1 - Morphological and mechanical characterization of bare and magnetic chitosan-poly(vinyl alcohol) (CP) monoliths before and after functionalization with ligand TPN-BM. All data was obtained from triplicated measurements. ^{FD} means that monoliths were submitted to an additional treatment for opening porous network involving swelling and freeze-drying procedures.

Monolith	Average pore size diameter[a] (µm)	Porosity[a] (%)	Surface area[a] (m^2g^{-1} monolith)	Compressive modulus (kPa)	
				Dry	Wet
CP 25:75	5±2	43±5	7.4±0.2	8±2	4.0±0.2
CP 14:86	20±5	39±5	4.2±0.2	1.4±0.2	1.5±0.2
CP 25:75_TPN-BM	0.6±0.2	28±5	6.2±0.5	22±2.0	2±1
CP 25:75_M	0.6±0.2	49±5	11.3±0.5	21±2.0	3±1
CP 25:75_M_TPN-BM	0.9±0.2	28±5	6.2±0.5	2±1	2±1
CP 25:75_M^{FD}	7±2	53±5	1.7±0.2	14±2	2.8±0.5
CP 25:75_M_TPN-BM^{FD}	9±3	55±5	1.2±0.2	17±2	3.2±.0.5

[a] Determined for dried monoliths by mercury porosimetry analysis.

If the swelling time was extended, probably larger pore sizes could be generated and thus, a correlation between both parameters could open new insights for the preparation of different starting points of porous structures.

In agreement with these morphological and mechanical features are the water fluxes (Fig. 6.5).

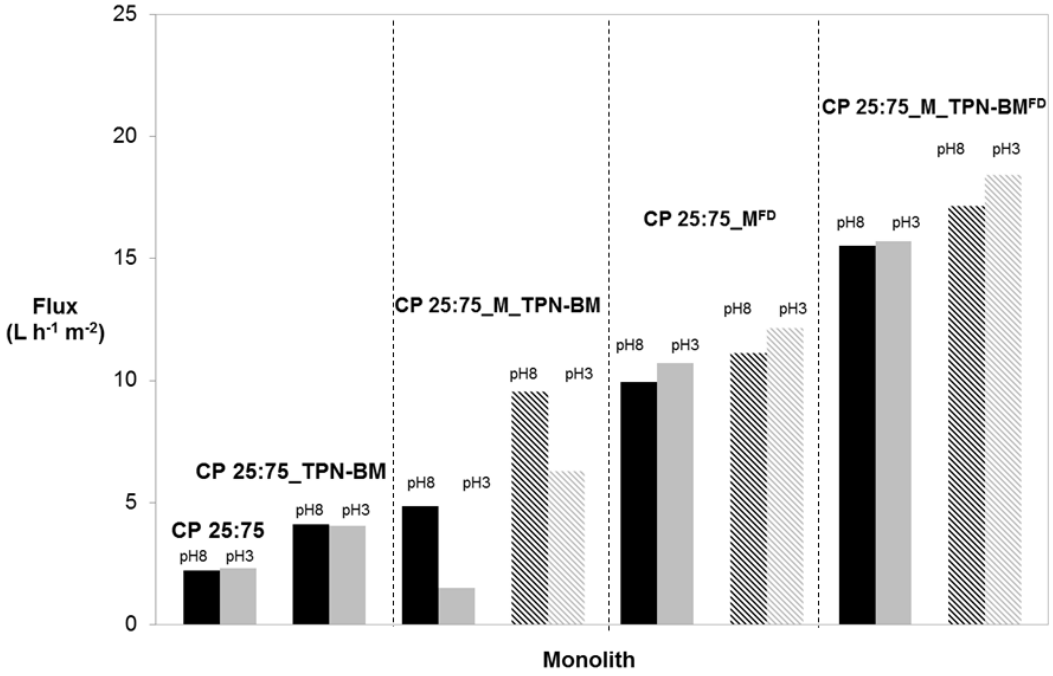

Figure 6.5 – Water fluxes of bare and magnetic chitosan-poly(vinyl alcohol) (CP) monoliths before and after functionalization with ligand TPN-BM at the absence and presence (represented by bars with strikes) of a permanent magnet of 0.5 T. ^{FD} means that monoliths were submitted to an additional treatment for opening porous network involving swelling and freeze-drying procedures.

The water fluxes for different CP 25:75 monoliths were measured at the pH conditions applied for antibody capture and release, pH 8 and 3, respectively.[11,82,161] It must be noted that the housings used for water flux measurements were different and dependent on the monolith type (bare or magnetic). The permanent magnet used to measure the magnetically-assisted water fluxes was designed to allocate a housing (column) with 1 cm of diameter (all the calculations and details are referred in Chapter 5). However, the monoliths herein produced have 1.5 cm of diameter. Thus, the magnetic monolith, CP 25:75_M, was cut to be fitted in a column with 1 cm of diameter, which was than inserted in the hole of the permanent magnet. Nevertheless, the water flux remained impossible to be measured at the gravitational conditions, due to monolith negligible swelling capacity, as there was no available apparatus that could work under pressure. Conversely, the magnetic ones, submitted to the additional treatment for opening porous network, were tested in a column with 1 cm of inner diameter, after incubation with water overnight to improve their swelling behaviour. The column was closed at the bottom to assure that the monolith was able to swell and fit to the column walls homogeneously. The water flux measurements of bare CP monoliths, before and after TPN-BM coupling, were performed in a column with 1.5 cm of diameter, since the bare supports were not evaluated under magnetically-assisted conditions. CP 25:75 and CP 25:75_TPN-BM presented similar fluxes at pH 8 and 3 (between 3 and 4 L h^{-1} m^{-2}) suggesting that, although the differences of pore size diameters and porosity values obtained for these two supports, both might have a very well interconnected porous network. Predominantly, it is expected that supports with larger pores and higher porosity lead to higher fluxes. However, if the pores are interconnected, the water

fluxes can be similar and comparable between two distinguished porous networks.[234] Regarding magnetic monoliths, although exhibiting high stiffness and a closed porous network, the flux of CP 25:75_M_TPN-BM was possible to be measured (Fig. 6.5). CP 25:75_M_TPN-BM always presented higher water flux at pH 8 than at pH 3, either in the absence or in the presence (represented in the Fig. 6.5 by bars with sticks) of the magnet. At low pH, chitosan (pKa≈6.5) is deprotonated and thus, swells more.[78] However, as the monolith is fitted into a column, the matrix swelling is limited by column dimensions, leading to a water flux reduction. Another and fundamental observation is that under a magnetic field (0.5 T), CP 25:75_M_TPN-BM shows higher flux values at pH 8 and 3 (9 and 6.5 L h^{-1} m^{-2}, respectively) rather than in the absence of the magnetic field (5 and 2.5 L h^{-1} m^{-2}, respectively). These observations clearly suggest that: (1) the monolith is able to respond to a magnetic field of 0.5 T and (2) the MNPs embedded into monolith network increase its hydrophilicity and then, the water fluxes. Lastly, the monoliths submitted to the swelling and freeze drying post-treatment, CP 25:75_M^{FD}, exhibited evidently higher water fluxes at both pH conditions studied (approximately 10 L h^{-1} m^{-2}), comparing with the ones not submitted to pores opening, with further increase when under the action of the magnetic field (approximately 13 L h^{-1} m^{-2}). Moreover, after TPN-BM coupling, CP 25:75_M_TPN-BM^{FD} achieved the higher water flux at pH 3 under the presence of the magnet (approximately 18 L h^{-1} m^{-2}), demonstrating the potential acceleration of antibody recovery in downstream processes when using these monoliths in a real application.

In order to evaluate the magnetic deformation, magnetic CP 25:75 monoliths were placed into a permanent magnet of 0.5 T, and the size decrease was monitored in dry and wet conditions (Fig. 6.6).

Non-functionalized magnetic CP monoliths (CP 25:75_M and CP 25:75_M^{FD}) in dry state exhibited a negligible magnetic deformation (≈ 2%). The stiffness of the supports does not allow a significant magnetic deformation, only an attraction to the magnet. Conversely, in wet state, these supports are able to deform approximately 12%. In addition, after magnet removal, they are able to recover 6% of their initial size, but a total return to the initial position is not detectable. Functionalized magnetic CP monoliths (CP 25:75_M_TPN-BM and CP 25:75_M_TPN-BM^{FD}) also did not deform suggestively in dry state. However, in wet state both supports reveal higher magnetic deformation (between 16 and 21%, respectively) with the capacity to return to their initial position.

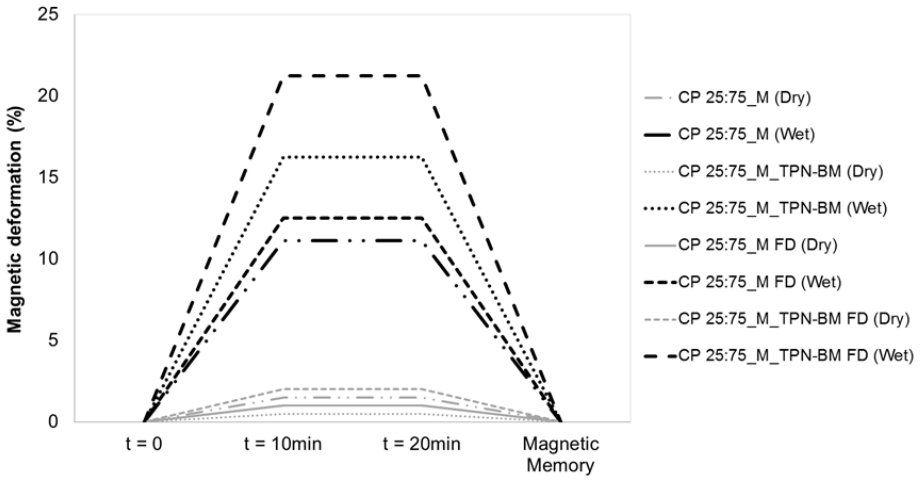

Figure 6.6 – Magnetic deformation of magnetic chitosan-poly(vinyl alcohol) (CP) monolith, CP 25:75_M, magnetic CP monolith submitted to an additional treatment for opening porous network involving swelling and freeze-drying procedures, CP 25:75_M^{FD}, and CP 25:75 and CP 25:75_M^{FD} monoliths after functionalization with TPN-BM, CP 25:75_M_TPN-BM and CP 25:75_M_TPN-BM^{FD}, respectively, in dry and wet states, at the presence of a permanent magnet of 0.5 T.

The higher magnetic deformation was achieved with the wet magnetic CP monoliths which were submitted to the swelling and freeze-drying stages (FD), functionalized with TPN-BM (CP25:75_M_TPN-BM^{FD}). This result is in agreement with the morphological properties previously discussed, since magnetic CP 25:75 monoliths treated with the "pores opening" approach presented larger pores, that facilitate the porous network mobility and, consequently, greater magnetic deformations are achieved.

Considering all morphological and mechanical properties as well the ability to respond to magnetic stimulus, CP 25:75_M_TPN-BM^{FD} monolith appears as the most promising support for the purpose of this study. Thus, in order to evaluate the stability of CP 25:75_M_TPN-BM^{FD} monolith, regarding MNPs and TPN-BM leaching issues, studies of release profiles over 12 hours were performed immersing CP monolithic samples in different solvents and in pH buffer and CIP solutions (most typically used in bioseparation) (Fig. 6.7).

MNPs leaching from CP 25:75_M_TPN-BM^{FD} was practically negligible since MNPs release after 12h only occurred using HCl (Fig. 6.7 A). Considering other solution conditions, less than 2% of MNPs were released. This result suggests that CP monoliths fabricated by the strategy herein reported can be as much or more robust and stable than the ones produced by freeze-drying method (Chapter 2, 3 and 5).[82,161] Considering the TPN-BM leaching (Fig. 6.7 B), also the stability of the monolith is evident because the maximum amount of TPN-BM released (9%) occurs after 12 h using NaOH and regeneration buffer solutions. Nevertheless, CP 25:75_M_TPN-BM^{FD} is never exposed more than half an hour to those harsh conditions herein tested.

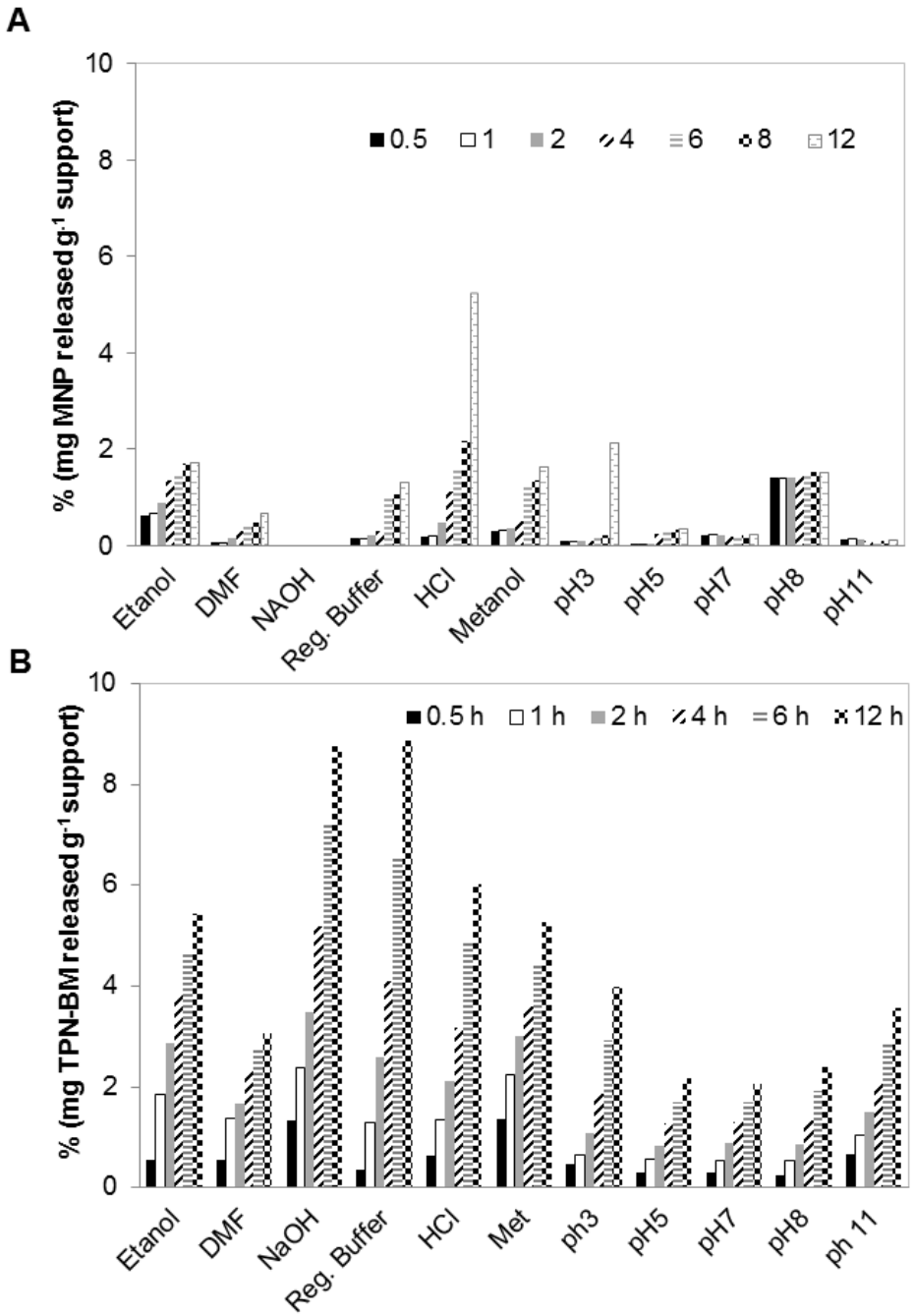

Figure 6.7 – Stability evaluation of magnetic chitosan-poly(vinyl alcohol) (CP) monolith submitted to an additional treatment for opening porous network involving swelling and freeze-drying procedures, functionalized with TPN-BM, CP 25:75_M_TPN-BM^{FD}, regarding (A) magnetic nanoparticles (MNPs) and (B) TPN-BM leaching, when immersed over 12 h in solutions typically used during cleaning-in-place (CIP) procedures, including solutions with pH values of 3, 5, 7, 8 and 11. All data was obtained from duplicated measurements with errors ± 3%.

The CP monoliths functionalization strategy was also monitored and evaluated. CP monoliths were activated and aminated under plasma treatment for further TPN-BM coupling. Particularly, the activation occurs through the radicals generated by argon (Ar)-plasma at the supports surface. Thus, the activated monoliths react with the 1,6-hexanediamine which is dragged by plasma system. TPN-BM was further immobilized promoting the reaction of the free chlorine presented in TPN-BM ligand and free NH_2 onto aminated CP monoliths, in DMF batch system.

After the functionalization procedure, amines and TPN-BM yields were estimated by Kaiser test (see Chapter 2) and by subtracting the initial and final amount of TPN-BM, respectively (Fig. 6.8).

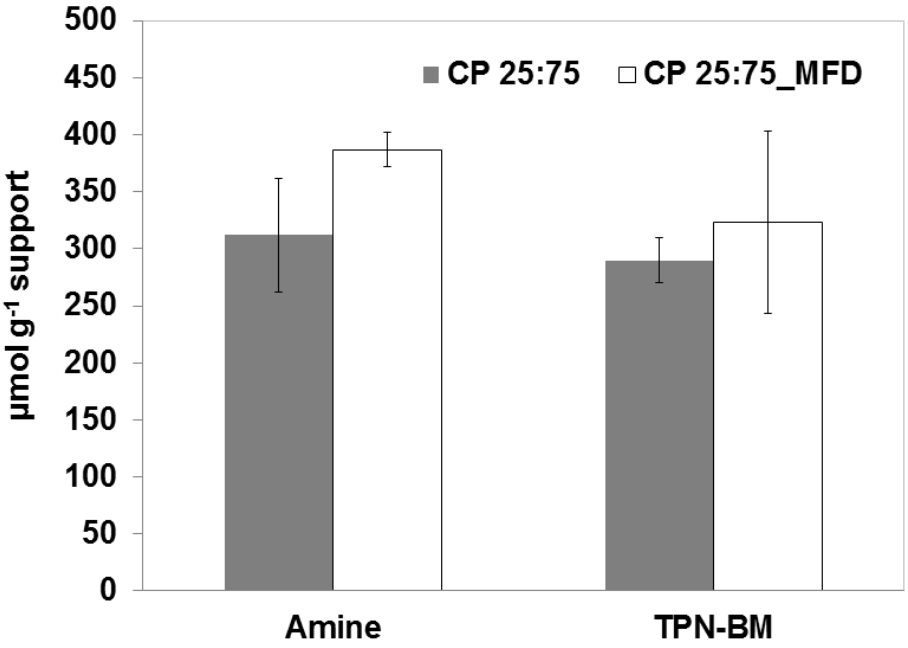

Figure 6.8 – Amines and ligand TPN-BM densities of native and magnetic chitosan-poly(vinyl alcohol) (CP) monoliths, CP 25:75 and CP 25:75_M^{FD} respectively, both produced using the functionalization strategy based on plasma technology. ^{FD} refers to monoliths that have undergone further swelling and freeze-drying procedures for additional opening of porous network.

Fig. 6.8 exhibits and compares the efficiency of CP monoliths functionalization for two supports processed by different methods and thus, exhibiting different morphological properties. CP 25:75 was not submitted to a porous network opening through swelling and freeze-drying procedures after water-acetone substitution and $scCO_2$ drying as CP 25:75_M^{FD} was. Therefore, different morphological features were obtained (as previously discussed) and consequently different amination and TPN-BM yields were achieved. CP 25:75_M^{FD} presented higher values of amination (370±10 µmol NH_2 g^{-1} support) and TPN-BM coupling (320±20 µmol TPN-BM g^{-1} support) yields, than CP 25:75 (310±40 µmol NH_2 g^{-1} support and 290±10 µmol NH_2 g^{-1} support, respectively). Both monoliths were functionalized following the same procedure. Thus, functionalization strategies based on plasma treatment may be more efficient for materials modifications if the materials exhibit large pores. Particularly, as larger pores allow a better efficiency of argon diffusion, more activated radical groups at the matrix surface are enabled, and consequently, higher density of bonded amines and successive ligand couplings can be reached.

6.3.3. EVALUATION OF TPN-BM FUNCTIONALIZED MONOLITHS FOR ANTIBODY PURIFICATION

To evaluate the adsorption capacities of CP monoliths for IgG, and consequently to estimate the affinity parameters involved, partition equilibrium studies were performed in duplicate, and the experimental data was fitted according to Langmuir-Freundlich (LF) isotherm. Langmuir-Freundlich isotherm was the chosen adsorption model because its assumptions fulfils the characteristics of CP monoliths-IgG systems: (1) CP monoliths present heterogeneous nature (2) that involve unequal binding sites and, (3) at low concentration of IgG, the experimental data is not linear which is characteristic of Freundlich model, while for higher IgG concentrations the experimental profile of CP monoliths behave as a monolayer adsorption, typical of Langmuir model.[139,141,137] Fig. 6.9 A exhibits the experimental (exp) and theoretical (LF) profiles for adsorption of IgG onto CP 25:75 and CP 25_75_M^{FD} before and after TPN-BM coupling. Fig. 6.9 B shows the different affinity constants (K_a), theoretical maximum capacity (Q_{max}) and Langmuir–Freundlich coefficients (n) that were obtained for each CP monolith, with an error of ±0.5, ±30 and ±0.1, respectively. Functionalized monoliths, CP 25:75_TPN-BM and CP 25_75_M_TPNBM^{FD}, always offered higher values of K_a, Q_{max} and n, when compared to the non-functionalized ones. This observation suggests the importance of TPN-BM coupling to improve the binding capacity of CP monoliths for IgG. Curious is the similar K_a value obtained for non-functionalized magnetic monolith, CP 25_75_M^{FD} (1.5×10^4 M^{-1}), comparing with the bare one after TPN-BM coupling, CP 25:75_TPN-BM (1.2×10^4 M^{-1}). Although CP 25:75_TPN-BM present similar K_a value than CP 25_75_M^{FD}, the Q_{max} and n values are higher, 550 mg IgG g^{-1} support and 1.8, in comparison with 255 mg IgG g^{-1} support and 1.1 of CP 25_75_M^{FD}, respectively. Furthermore, calculated K_a values exhibit the same order of magnitude (10^4), usually obtained for similar affinity devices fitted with Langmuir–Freundlich isotherm,[82,139,141] indicating a medium affinity interaction, which is considered optimal for bioseparation processes while facilitating protein recovery.[6]

The values of Q_{max} for CP 25:75_TPN-BM and CP 25_75_M_TPNBM^{FD} were 550 and 515 mg IgG g^{-1} support, respectively, which are higher than the ones observed for CP 25:75 and CP 25_75_M^{FD} (210 and 255 mg IgG g^{-1} support, respectively), and analogous to the values for similar functionalized platforms used for the same purposes.[82,136,141,161]

A

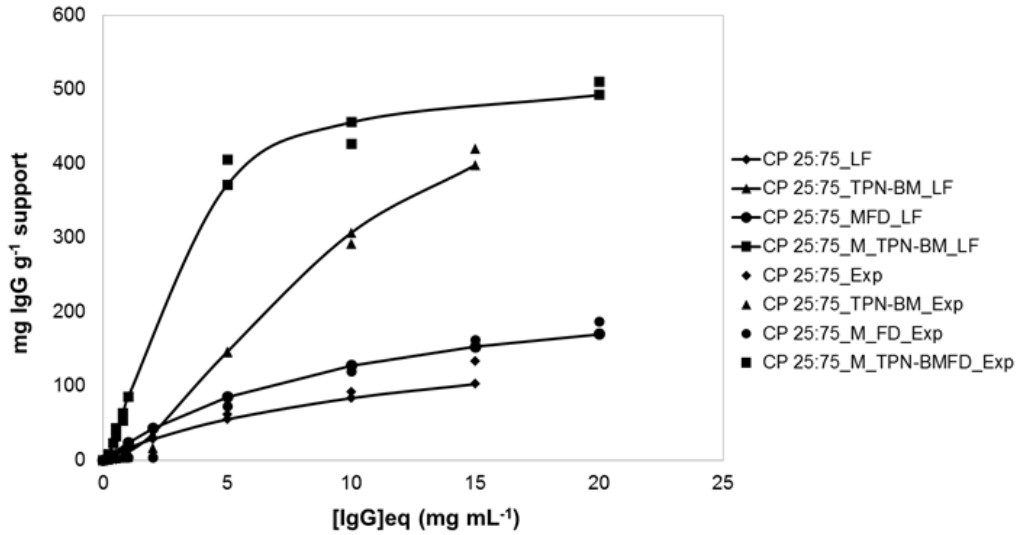

B

Monolith	$K_a \times 10^4$ (M^{-1})	Q_{max} (mg IgG g^{-1} support)	n	R^2
CP 25:75	0.29	210	0.9	0.96
CP 25:75_TPN-BM	1.2	550	1.8	0.98
CP 25:75_M^{FD}	1.5	255	1.1	0.97
CP 25:75_M_TPN-BM^{FD}	2.9	515	1.6	0.98

Figure 6.9 – (A) Langmuir–Freundlich adsorption isotherms for bare and magnetic chitosan-poly(vinyl alcohol) (CP) monoliths before, CP 25:75 and CP 25_75_M^{FD}, and after TPN-BM immobilization (CP 25:75_TPN-BM and CP 25_75_M_TPNBM^{FD} and (B) summary of the estimated affinity parameters of Langmuir–Freundlich isotherms for bare and magnetic chitosan-poly(vinyl alcohol) (CP) monoliths before and after TPN-BM immobilization. ^{FD} refers to monoliths that have undergone further swelling and freeze-drying procedures for additional opening of porous network.

The *n* is normally employed as an empirical coefficient that represents the type and the extent of cooperativity presented in the binding interaction. Therefore, *n*>1 demonstrates good binding capacity (positive cooperativity between protein and adsorbent) and a heterogeneous feature of adsorption. Conversely, *n*=1 and *n*<1 indicate purely independent non interacting sites and negative cooperativity, respectively. Thus, for CP 25:75_TPN-BM and CP 25_75_M_TPNBM^{FD} the *n* values are closer to 2, meaning a positive cooperativity in binding (attractive forces due to lateral interactions) and a heterogeneous nature of protein adsorption, while for CP 25:75 and CP 25_75_M^{FD}, *n* values are between 0 and 1 suggesting a poor or inexistent cooperativity.

Summing up, CP monoliths functionalized with TPN-BM showed higher affinity parameters than those non-functionalized, result obtained from an accurate approximation of the fitting of experimental data with LF isotherm. The sigmoidal behaviour at low IgG concentration and a

linear profile at higher IgG concentrations of experimental data explain the use of LF isotherms as an indicated model to explain the adsorption phenomena of CP monoliths-IgG systems.

In order to estimate the dynamic binding capacity of CP monoliths, breakthrough curves were performed using bare and magnetic CP monoliths before and after TPN-BM coupling: CP 25:75 (control), CP 25:75_TPN-BM, CP 25:75_M^{FD} (control) and CP 25:75_M_TPN-BM^{FD} (Fig. 6.10).

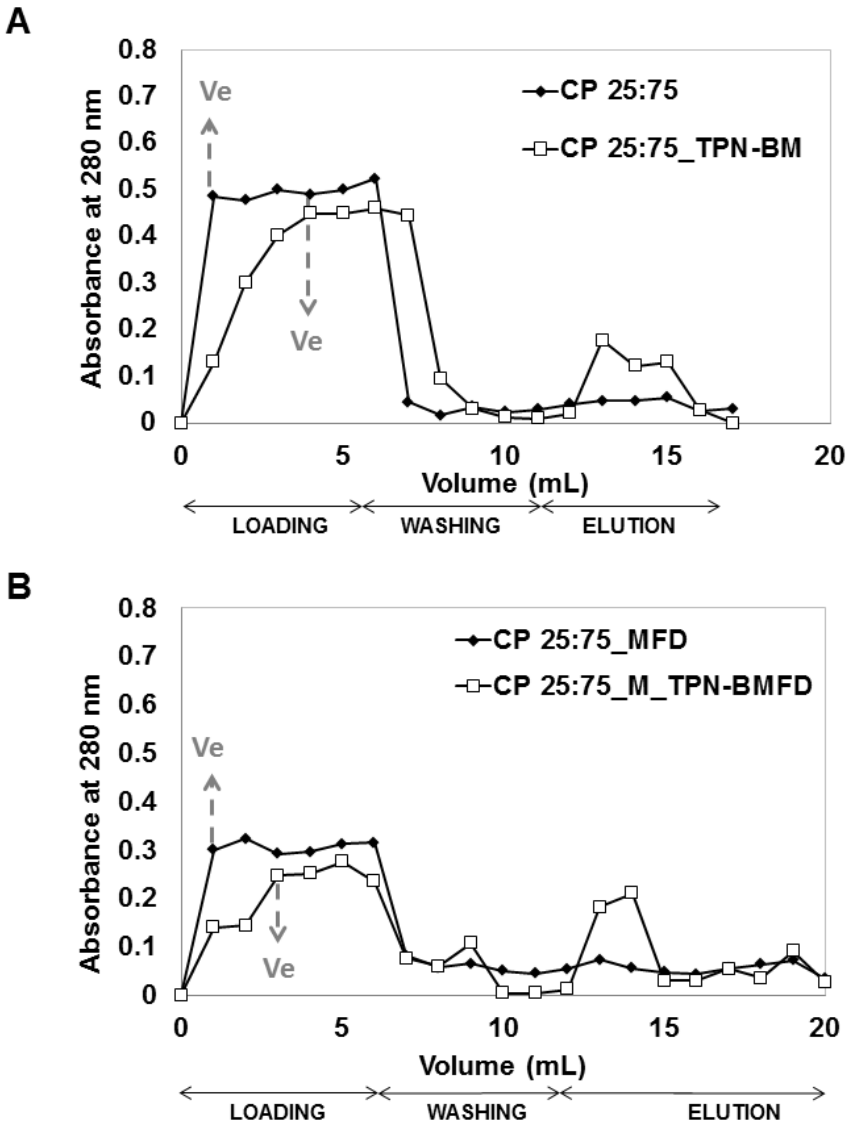

Figure 6.10 – Breakthrough profiles for human IgG upon chitosan-poly(vinyl alcohol) (CP) 25:75 monoliths: (A) bare and (B) magnetic, before and after TPN-BM coupling. Bare CP monoliths before and after TPN-BM coupling, CP 25:75 and CP 25:75_TPN-BM respectively, were tested in a column with 1.5 cm of diameter and thus, in the absence of a permanent magnet (A) while magnetic CP monoliths before and after TPN-BM coupling, CP 25:75_M^{FD} and CP 25:75_M_TPN-BM^{FD} respectively, were tested in a column with 1 cm of diameter and under magnetic elution conditions of 0.5 T (B). ^{FD} refers to monoliths that have undergone further swelling and freeze-drying procedures for additional opening of porous network.

Bare CP monoliths with or without TPN-BM coupling, were placed in a larger column (1.5 cm of diameter) since they did not need to be cast in a column with 1 cm of diameter to fit in the hole of the permanent magnet, to be tested under magnetically-assisted conditions as magnetic monoliths needed. Therefore, both tested conditions, for bare and magnetic supports, are not directly comparable since the swelling degree of each support, and consequently the porous

network availability, is different due to the restrictions of column dimensions. Thus, the profiles of CP monoliths observed in Fig. 6.10 led to different amounts of IgG bound and eluted (Table 6.2) since they must be considered independent systems.

Table 6.2 - Binding and elution dynamic capacities of chitosan-poly(vinyl alcohol) monoliths, CP 25:75 and CP 25:75_M^{FD}, before and after TPN-BM coupling, CP 25:75_TPN-BM and CP 25:75_M_TPN-BM^{FD}, respectively; the values were obtained from the breakthrough profiles for human IgG.

Monolith	hIgG Bound (m IgG g^{-1} support)	% hIgG eluted (m IgG Eluted g^{-1} support)
CP 25:75	15 ± 5	63 ± 5
CP 25:75_TPN-BM	55 ± 5	58 ± 5
CP 25:75_M^{FD}	7 ± 2	32 ± 5
CP 25:75_M_TPN-BM^{FD}	32 ± 4	65 ± 10

Non-functionalized CP monoliths always exhibit lower binding capacities (15±5 and 7±2 mg IgG per gram of monolith for CP 25:75 and CP 25:75_M^{FD}, respectively) comparing with the functionalized ones (55±5 and 32±4 mg IgG per gram of monolith for CP 25:75_TPN-BM and CP 25:75_M_TPN-BM^{FD}, respectively). Thus, the high values of IgG binding revealed by CP monoliths modified with TPN-BM prove the fundamental role of TPN-BM to recognize, and consequently, to retain the IgG. In addition, also the IgG recovery is inferior for non-functionalized monoliths comparing to those TPN-BM-functionalized. The percentages of recovery for both functionalized supports, CP 25:75_TPN-BM and CP 25:75_M_TPN-BM^{FD} is around 60%. Before the monoliths insertion in each housing, CP 25:75_M_TPN-BM^{FD} displayed a larger porous network than CP 25:75_TPN-BM which could enable high efficiency in IgG capture and release. However, to take advantage of the magnet behaviour, CP 25:75_M_TPN-BM^{FD} was fitted in smaller column (to be allocated in the hole of the magnet) that in some way restricts the monolith swelling. Consequently, the advantages of the magnetically-assisted elution of IgG were attenuated. Nevertheless, it should be underlined that the magnetically-assisted elution was faster (less than 1 minute) comparing with the typical one employed for CP 25:75_TPN-BM (two minutes), which from an operational point of view, turn the chromatographic process less time consuming.

6.3.4. REPRODUCIBILITY AND OPTIMIZATION OF TPN-BM FUNCTIONALIZED CP MONOLITHS FOR ANTIBODY PURIFICATION

The performance reproducibility of CP 25:75_TPN-BM and CP 25:75_M_TPN-BM^{FD} was evaluated over cycles using pure solution of IgG (Fig. 6.11 A and B, respectively).

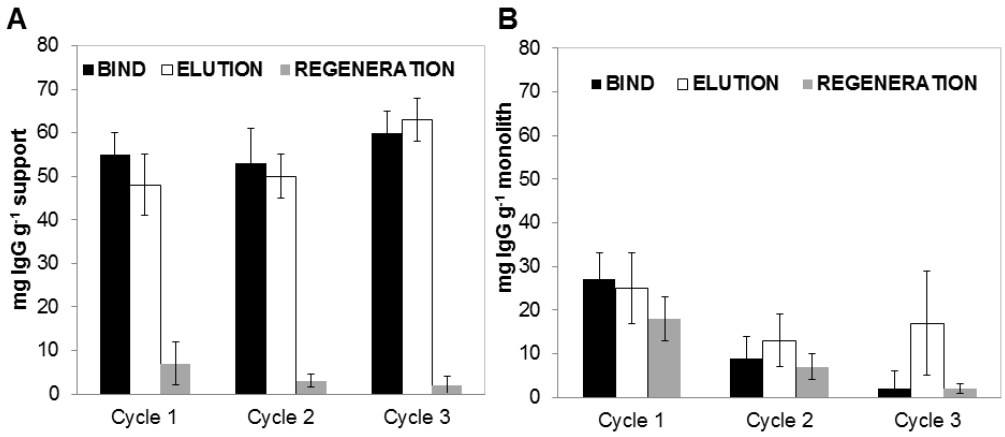

Figure 6.11 – Evaluation of chromatographic performance of TPN-BM functionalized chitosan-poly(vinyl alcohol) (CP) monoliths: (A) CP 25:75_TPN-BM and (B) CP 25:75_M_TPN-BM^{FD}. ^{FD} refers that have undergone further swelling and freeze-drying procedures for additional opening of porous network. The chromatographic procedures (bind, elution and regeneration steps) were performed consecutively along three cycles at a gravitational flow rate.

CP 25:75_TPN-BM monolithic platforms over cycles (Fig. 6.11 A) exhibit a periodic behaviour suggesting that the binding, elution and regeneration profiles are constant during each tested cycle (55, 42 and 8 mg IgG per gram of monolith, respectively). Conversely, for CP 25:75_M_TPN-BM^{FD} this periodicity is not so evident. Over cycles, some amount of IgG (20%) was physically entrapped into porous network avoiding an outstanding performance of the support during its operation time as it is observed in Fig 6.11 B. Thus, it is the CP 25:75_TPN-BM (Fig. 6.11 A) that revealed better binding and elution profiles, being in agreement with breakthrough curves previously discussed. It should be remembered that CP 25:75_TPN-BM was casted in a larger column due to no need to be tested under magnetically-assisted elution. Therefore, the support was able to swell easily facilitating the availability of TPN-BM (immobilized onto supports) to interact with IgG.

The optimization performed for magnetic CP monoliths, which involved an additional treatment for opening porous network comprising swelling and freeze-drying procedures (CP 25:75_M_TPN-BM^{FD}), was attenuated by the column dimensions that is able to be allocated in the magnet to perform magnetically-assisted elution. Due to this, the experimental data obtained for CP 25:75_M_TPN-BM^{FD} suggest that under tested operation conditions (smaller columns and gravitational flux) its reusability is not completely assured. Nevertheless, these preliminary results also indicate that with a different permanent magnet, designed to allocate a larger column, certainly better performances and greater binding and elution capacities could be achieved, instead of the maximum 25 and 15 mg of IgG g^{-1}support, respectively, as herein demonstrated. In addition, it is important to mention that all chromatographic assays were performed using a piston in the regeneration step to force the expulsion of IgG imprisoned physically to the support. Still, 5% of IgG remained in the supports between cycles, possibly due to the absence of fixed and constant operation parameters such as pressure and flow rate.

In order to give a step further concerning the possible potential of CP monolithic platforms as promising devices for antibody purification, CP 25:75, CP 25:75_TPN-BM and CP 25:75_M_TPN-BM^{FD} were tested with two different crude extracts: (1) one containing a single

chain fragment, scFv, produced in *Pichia Pastoris* (approximately 10 mg of total protein per millilitre) and (2) another containing monoclonal antibodies (mAbs) produced by CHO cells (approximately 2 mg of total protein per millilitre). Once again, CP 25:75 and CP 25:75_TPN-BM were tested in a larger column (1.5 cm of diameter since their elution profiles are not dependent on a magnetic field, Fig. 6.12 A and B). Conversely, CP 25:75_M_TPN-BM^{FD} was evaluated casted in a column with 1 cm of diameter due to the magnetically-assisted elution (Fig. 6.12 C). CP 25:75_M monoliths were not tested due to difficulties in measuring their fluxes under gravitational conditions as previously mentioned.

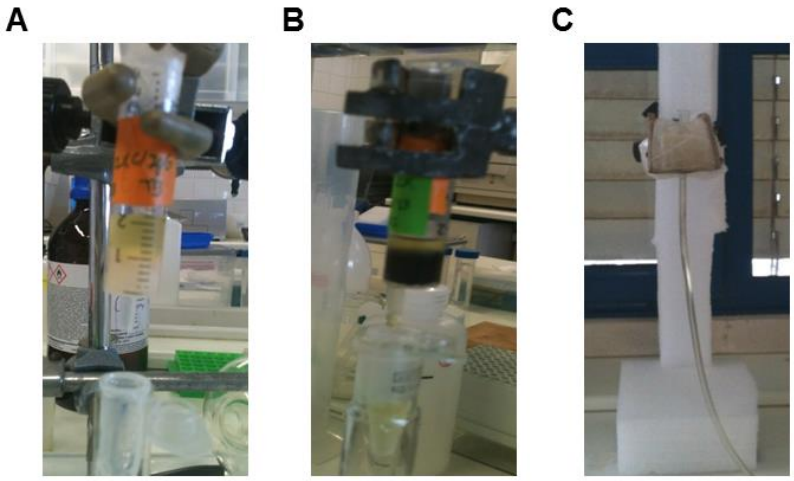

Figure 6.12 – Images of gravitational chromatographic apparatus employed for bare and magnetic chitosan-poly(vinyl alcohol) (CP) monoliths before, CP 25:75 (A), and after TPN-BM coupling, CP 25:75_TPN-BM (B) and CP 25:75_M_TPN-BM^{FD} (C). A and B are performed in the absence of a permanent magnet and C in the presence of a permanent magnet of 0.5 T. ^{FD} refers to monoliths that have undergone further swelling and freeze-drying procedures for additional opening of porous network.

SDS-page gels resulting from the chromatographic experiments with two different crude extracts using CP monoliths are presented in Fig. 6.13. Fig. 6.13 A, C and D correspond to CP 25:75, CP 25:75_TPN-BM and CP 25:75_M_TPN-BM^{FD} monoliths tested with mAbs crude extract and, accordingly, Fig. 6.13 B, D and E correspond to the same supports but using scFv crude samples. CP 25:75, which works as a control, shows in the first elution (E1 in Fig. 6.13 A) two bands corresponding to mAbs fractions. These results show unspecific retention of mAbs on the monoliths network. For scFv (Fig. 6.13 B) native CP 25:75 show no protein binding to the support and also no protein in the elution lanes. Fig. 6.13 C and D reveals the CP25:75_TPN-BM ability in mAbs and scFv purification, respectively, and for both cases, it is not observed again, mAbs or scFv fractions in elution lanes. This result can be explained by the blocking that might occur when crude extracts with larger biomolecules are being permeated, through CP 25:75_TPN-BM monolith operating under gravitational conditions.

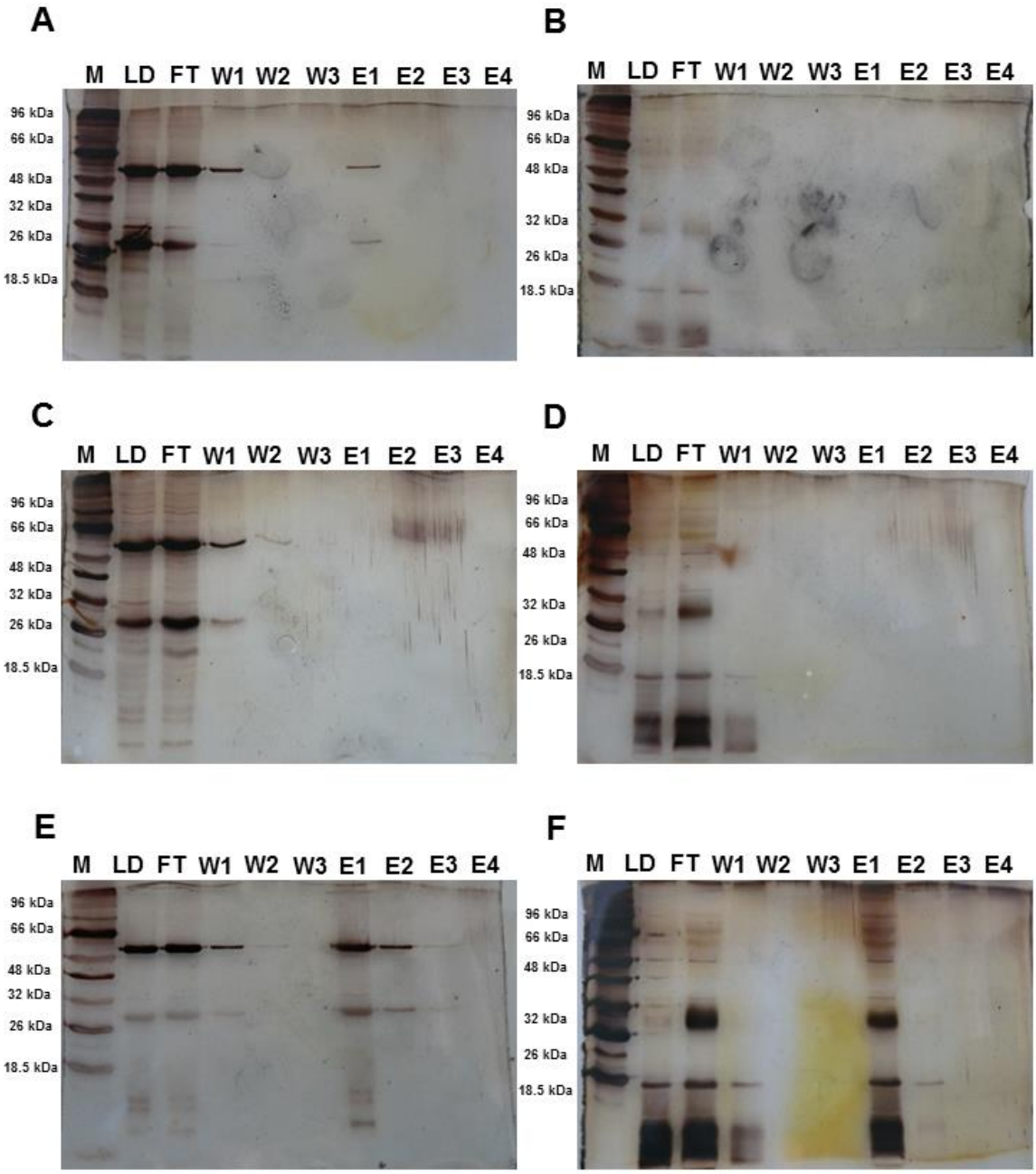

Figure 6.13 –The acrylamide gels from SDS-PAGE performed with the fractions collected during the mAbs (A, C, E) and scFv purification (B, D, F) using bare and magnetic chitosan-poly(vinyl alcohol) (CP) monoliths before and after TPN-BM coupling: (A, B) CP 25:75, (C, D) CP 25:75_TPN-BM and (E, F) CP 25:75_M_TPN-BM^{FD}; ^{FD} refers to monoliths have undergone further swelling and freeze-drying procedures for additional opening porous network; lane M corresponds to the molecular weight marker, lane LD represents the loading, lane FT is the flowthrough, lane W1, W2 and W3 corresponds to the washes (phosphate buffer (50 mM, pH 8.0)), and lane E1, E2, E3 and E4 are the elution fractions (sodium citrate buffer (50 mM, pH 3.0)).

Interesting is the CP 25:75_M_TPN-BM^{FD} elution behaviour for mAbs (E) and scFv purification (F). Conversely to CP 25:75 and CP 25:75_TPN-BM, in first, second and third elutions (Fig. 6.13 E, E1, E2, E3), mAbs fractions are evident, although with limited purity: 75% in the first one while in the others two (E1 and E2) present 97% purity. Similar profile is exhibited when the same support purifies scFv (Fig. 6.13 F, E1, E2, E3). These results clearly suggest two important points: (1) in fact, the magnetically-assisted elution is crucial to help the exclusion of

mAbs and scFv from the porous network of monolithic platform, however, (2) this support is not able to capture and elute mAbs and scFv selectively and with low non-specific adsorption background, since in the elution lanes other proteins are presented.

Fig. 6.14 represents quantitatively the capacity of CP 25:75_M_TPN-BM^{FD} in binding, elution and regeneration stages considering the total protein concentration. The elution is higher for scFv crude extract (10 mg total protein per millilitre considering 1 gram of support) comparing to mAbs crude extract in which the amount of total protein is lower (7 mg total protein per millilitre considering 1 gram of support). Since the SDS-PAGE gel correspondent of mAbs purification is slightly pure that the one related to scFv, although both present low selectivity, it is possible to infer that mAbs are more abundant in the elution fractions, collected during chromatographic procedures, than scFv. Thus, although mAbs are larger than scFv, which in a first glance could be an unfavourable point for an efficient operation of CP monoliths with a close porous networks, CP 25:75_M_TPN-BM^{FD} revealed an encouraging performance for mAbs purification (cross information from Fig. 6.13 E and F and Fig. 6.14), rather than scFv (40% of purity).

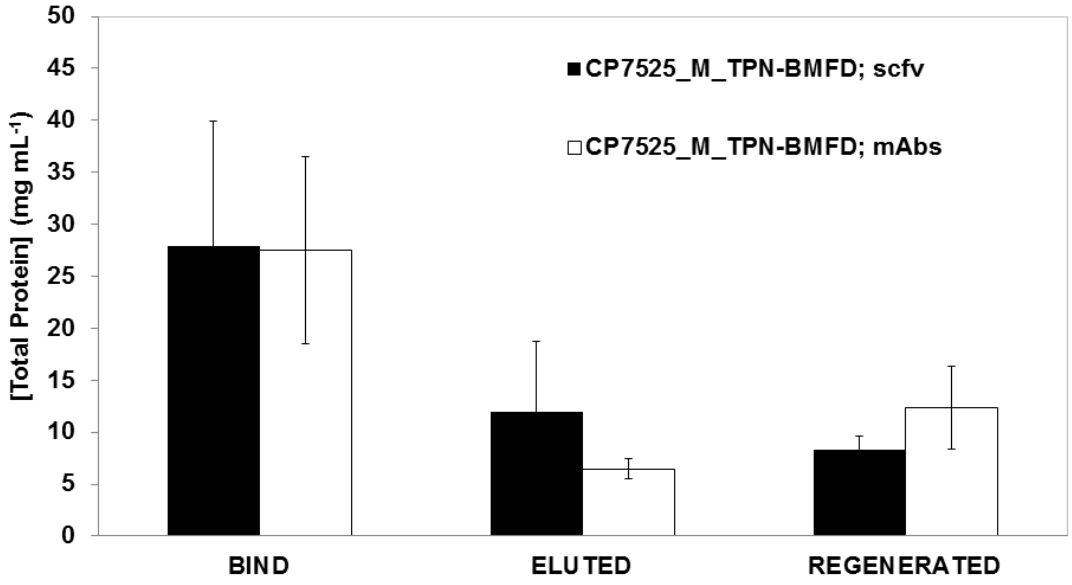

Figure 6.14 – Performance of binding, elution and regeneration of TPN-BM functionalized magnetic chitosan-poly(vinyl alcohol) (CP) monoliths submitted to an additional treatment for opening porous network involving swelling and freeze-drying procedures, CP 25:75_M_TPN-BM^{FD}, using two different crude extracts: one contain only the single chain fractions (scFv) and another one containing monoclonal antibodies (mAbs).

Probably, this suggestive preference for mAbs purification instead of scFv is not related only with the porous network, which in fact is restricted due to column dimensions, but also with the type of interactions that are established between the target molecule and TPN-BM immobilized onto monoliths. It was found and mentioned in Chapter 4 that TPN-BM revealed a pH dependence especially for Fc domain of IgG. However, in opposition to mAbs, the scFv extract only comprises part of the Fab domain which, also based on the knowledge acquired from the studies described in Chapter 4, establishes preferentially hydrophobic interactions (not pH dependent) with TPN-BM. Thus, this fact helps to explain why the elution lanes of scFv crude

extract (Fig. 6.13 F) are slightly more contaminated than the lanes correspondent to mAbs extract (including Fab and Fc domains). Probably, for CP 25:75_M_TPN-BMFD_mAbs system, the elution, despite being of low selectivity considering all porous structure constraints, might have been executed by a pH dependence.

Regarding the regeneration step, in both cases, it was not 100% efficient since these supports still retain 15-20% of total protein. Once more, the operation of CP 25:75_M_TPN-BM^{FD} under pressure will be desired in order to assure not only an effective CIP procedure, but also an effective and established operation mode. In addition, a slight increase in porous network, namely pore size diameter, could also be a promising solution.

6.4. CONCLUDING REMARKS

In the present study, microporous monoliths composed by different ratios of chitosan and poly(vinyl alcohol) (CP) with and without embedded magnetic nanoparticles (MNPs), were successfully prepared by using a combination between gelation and supercritical CO_2 ($scCO_2$) assisted processes. A second approach for CP monoliths porous network opening at dry state was performed, and consisted in creating a new porous network starting point, based on swelling and freeze-drying methods. Both strategies generated different structures with distinct morphological, mechanical, magnetic and physico-chemical properties. CP monoliths were further modified using plasma treatment (firstly argon (Ar) plasma generated the radicals and secondly, the 1,6-hexanediamine dragged by the plasma system reacted with activated CP monoliths, aminating them) for further coupling of TPN-BM, a triazine-based affinity ligand. After CP monoliths functionalization, the supports were again characterized and tested as affinity chromatographic platforms. CP 25:75 monoliths, with and without MNPs embedded, prepared by both methods, and after TPN-BM coupling (CP 25:75_TPN-BM and CP 25:75_M_TPN-BM^{FD}) exhibited a promising affinity behaviour towards IgG which com,prises acceptable estimated affinity parameters and encouraging binding capacities (55 and 32 mg IgG g^{-1} support, respectively). However, some optimizations regarding the pore size diameter of monoliths and their operation mode should be considered to improve the preliminary affinity profile herein demonstrated. Particularly, considering the pore size, other casting solution concentrations should be tested and the high pressure parameters varied. In addition, and considering the second strategy of porous network opening, the swelling time should also be enlarged in order to promote higher water uptake degrees, and consequently to generate new porous network starting points comprising larger pores. Considering the operation mode: i) for an appropriate gravitational condition, a new permanent magnet should be designed to allocate larger columns to allow magnetically-assisted operations without restrictions of monoliths swelling and expansion; ii) under pressure operations, the ideal should be to test these supports in appropriate equipment (e.g. AKTA) in order to define the optimum process parameters (pressures and flow rates). Nevertheless, the obtained results suggest a good beginning to use CP monoliths herein prepared as affinity chromatographic platforms, especially CP 25:75_M_TPN-BM^{FD} which was able to bind approximately 25 mg of total protein and to elute selectivity 50% of mAbs with 98% of purity, when tested with crude samples (mAbs crude extracts). The methods herein proposed to generate CP monoliths combined with the functionalization strategy based on plasma technology, revealed to be a robust and efficient solution. Furthermore, they can be used not only for other bioseparation purposes but also for many other applications regarding tissue engineering, drug delivery and cell growth where the preparation of well-defined 3D structures is crucial.

CHAPTER 7

EVALUATION OF GREEN CHEMISTRY IMPACT

SUMMARY

On this chapter, the greenness of two strategies performed in this thesis was evaluated: (1) the synthesis of biomimetic ligand TPN-BM and (2) the monoliths functionalization strategy based on plasma treatment. This evaluation was perfrmed following green chemistry metrics. The calculations revealed that both alternative routes revealed maximum atom economy (AE), mass productively (MP), carbon efficiency (CE) and reaction mass efficiency (RME) values while those obtained for E-factor and mass intensity (MI) were minimized.

Overall, this chapter shows the green impact of these two strategies herein developed and consequently, the most important contributions for the development of sustainable practises.

7.1. INTRODUCTION

7.1.1 GREEN CHEMISTRY AND GREEN ENGINEERING

During the last decade, chemists and engineers have made a strong effort to reverse the negative publicity associated to chemistry regarding ecological and social points of view.[235] Normally, chemical industries generate large amount of waste which was becoming increasingly expensive to industry but also to environment.[236] Thus, these associated costs started working as an important driving force for important and significant changes in science and industry to achieve economic, environmental and social benefits. As a result of this, new topics such as "green chemistry" and "green engineering" started appearing to alert people for the reactions optimization considering materials and energy usage, waste reduction from all sources, and overall cost minimization.[237] This remarkable change in the world of chemistry was accomplished by the new European chemicals legislation REACH, the Registration Evaluation and Authorization of Chemicals, which has become probably the most important chemicals legislation we have ever seen.[238] Moreover, this "green philosophy" also aims the minimization of toxicity and hazards, and the maximization of safety practices in the design of chemical reactions, products and processes, to operate under a safe chemical code. Based on this, 12 principles of green chemistry and green engineering (Table 7.1) introduced by Paul Anastas and John Warner in 1998 were established to guide chemists and engineers in laboratories or industries in how to develop greener and sustainable products or processes.[235,239]

More recently, these 12 principles of green chemistry and green engineering were summarized into the more suitable and impressive acronym, PRODUCTIVELY and IMPROVEMENTS, respectively (Fig. 7.1).[235,236]

Although some minds outside Europe still look to REACH in a threatening way due to possible restructuration and investments that it can oblige, it is not surprising that it has been applied to numerous industry sectors.[238] From aerospace, automobile, cosmetics, electronics, energy, household products, pharmaceutical, agriculture, there are hundreds of examples of successful applications of award winning, economically competitive technologies.[236] This green revolution in the chemistry world has stimulated all creative ability, which is one of the most famous features of the chemistry field; researchers and engineers have to find out new and sustainable strategies to redesign processes and products considering all the stages of their life cycle.[240] Therefore, in order to measure the "greenness" of processes some metrics were created as well as basic tools to access the life cycle of a product or process.[151,237,241]

Table 7.1 – 12 Principles of Green Chemistry.[235]

Principle	Description
1. Inherent Rather Than Circumstantial	All materials and energy inputs and outputs to be as inherently non-hazardous as possible.
2. Prevention Instead of Treatment	It is better to prevent waste than to treat or clean up waste after it is formed.
3. Design for Separation	Separation and purification operations should be designed to minimize energy consumption and materials use.
4. Maximize Efficiency	Products, processes, and systems designed to maximize mass, energy, space, and time efficiency.
5. Output-Pulled Versus Input-Pushed	Products, processes, and systems should be "output pulled" rather than "input pushed" through the use of energy and materials.
6. Conserve Complexity	Embedded entropy and complexity must be viewed as an investment when making design choices on recycle, reuse, or beneficial disposition.
7. Durability Rather Than Immortality	Targeted durability, not immortality, should be a design goal.
8. Meet Need, Minimize Excess	Design for unnecessary capacity or capability (e.g., "one size fits all") solutions should be considered a design flaw.
9. Minimize Material Diversity	Material diversity in multicomponent products should be minimized to promote disassembly and value retention.
10. Integrate Material and Energy Flows	Design of products, processes, and systems must include integration and interconnectivity with available energy and materials flows.
11. Design for Commercial "Afterlife"	Products, processes, and systems should be designed for performance in a commercial "afterlife".
12. Renewable Rather Than Depleting	Material and energy inputs should be renewable rather than depleting.

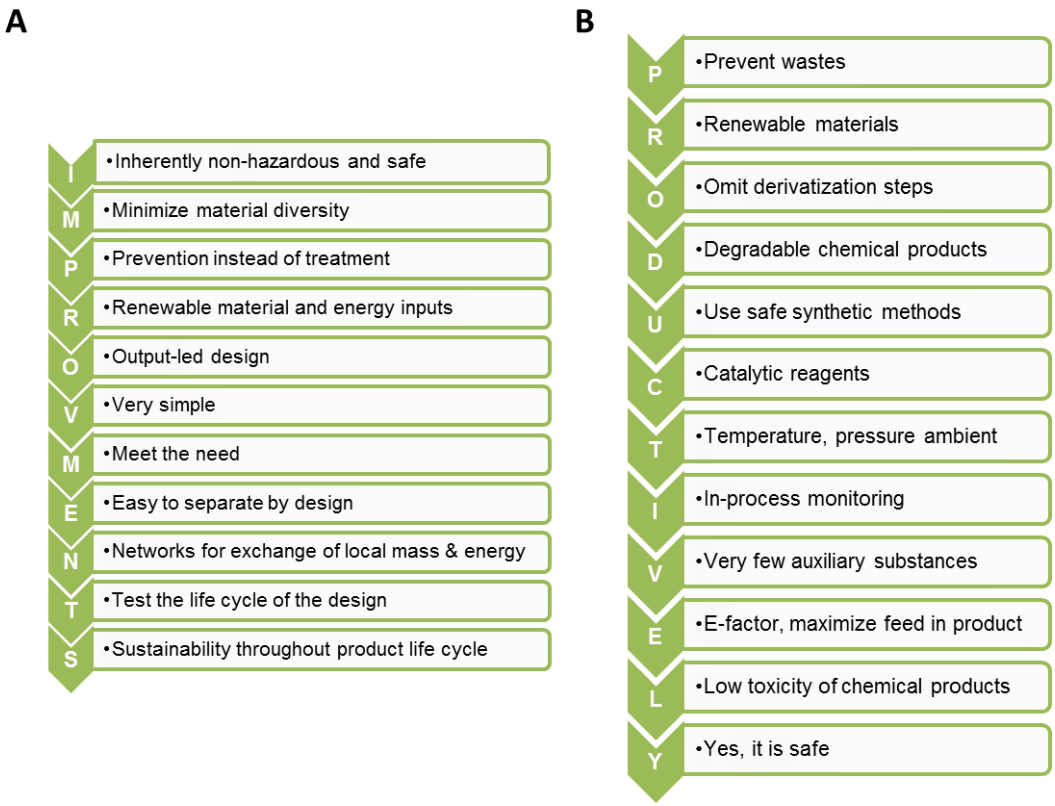

Figure 7.1 - Schematic representation of the meaning of IMPROVEMENT and PRODUCTIVELY from the green chemistry point of view.[242]

7.1.1.1. GREEN METRICS

In order to access how much a process is sustainable or not, some green metrics were established and further translated in mass indicators. The different mass indicators are: atom economy (AE), E-factor, mass intensity (MI), mass productivity (MP), carbon efficiency (CE) and reaction mass efficiency (RME). Also the energetic intensity can be calculated.[235,237,243]

Atom economy (AE) aims to calculate how much of the reactants persist in the final product (equation 7.1).

$$AE = \frac{\sum Molecular\ weight\ of\ Product\ \ (Kg)}{\sum Molecular\ weight\ of\ Reagents\ (Kg)}$$

Equation 7.1

Its calculation involves key assumptions such as: to ignore the reaction yield and molar excess of reactants and it does not take into account with the solvents and reagents. For a generic reaction A + B → C, AE can be calculated according to equation 7.2:

$$AE = \frac{Molecular\ weight\ of\ C\ (Kg)}{Molecular\ weight\ of\ A\ (Kg) + Molecular\ weight\ of\ B\ (Kg)}$$

Equation 7.2

For a generic synthetic process involving multisteps:

A + B → C (1)

C + D → E (2)

E + F → G (3)

AE is calculated according to equation 7.3:

$$AE = \frac{MW\ of\ G\ (Kg)}{MW\ of\ A\ (Kg) + MW\ of\ B\ (Kg) + MW\ of\ D\ (Kg) + MW\ of\ F\ (Kg)}$$

Equation 7.3

Since the calculation of AE disregards the intermediates, because they are formed and immediately consumed. The greener is a process, the greater is AE.

E-factor is another mass indicator which is related to the waste that is produced from the beginning to the end of a process. Since it is calculated from the quotient between the kg of waste that is produced to obtain a kg of product (equation 7.4), it is desirable that E-factor could be as low as possible because it means that few wastes are created.

$$E\ Factor = \frac{Total\ Waste\ (kg)}{Kg\ Product}$$

Equation 7.4

For this evaluation it is extremely important to define precisely what is considered as "waste" and divided it in different categories since depending on its nature (e.g: organic, inorganic, solid). For each type of waste, different treatments can be applied and consequently the overall greenness of the process must be re-evaluated. The value of E-factor is limited and it does not take into account the nature and the environmental impact of the generated waste. In order to achieve a more accurate prediction, the E-factor can be multiplied by an environmentally hazardous quotient, Q. Thus, Q depends on the species involved in the reactions and, based on this, a computer program has been developed (EATOS: environmental assessment tool for organic synthesis). The deliverables of this program can be used to compare and improve chemical reactions.[237]

Mass intensity is another indicator given by the quotient between the total mass that is produced in a process and the mass of the product, taking into account the yield and stoichiometry (equation 7.5).

$$MI = \frac{Total\ mass\ used\ in\ a\ process\ or\ process\ step\ (kg)}{Mass\ of\ product\ (Kg)}$$

Equation 7.5

Regarding the total mass, this metric includes everything that is employed in a process or process step such as: reactants, reagents, catalysts, solvents, acids, bases, extractions, crystallisations, among others. The water is not considered due to its no significant environmental impact.

It can also be possible to correlate MI with E-factor through the following equation (equation 7.6):

$$E\ Factor\ = MI - 1$$

Equation 7.6

In addition, by expressing MI as a percentage, it appears in a similar form to an effective mass yield and atom economy designated by mass productivity (equation 7.7).

$$MP\ = \frac{1}{MI} \times 100$$

Equation 7.7

Carbon efficiency (CE) allows determining the amount of carbon present in the reactants that are incorporated into the final product and, it is expressed in percentage (equation 7.8). This calculation considers the yield and stoichiometry of reactants and products.

$$CE\ = \frac{Amount\ of\ carbon\ in\ product\ (mol)}{Total\ amount\ of\ carbon\ present\ in\ reactants\ (mol)} \times 100$$

Equation 7.8

The last green metric is designated by reaction mass efficiency (RME) and it is defined as the percentage of the mass of reactants that remain in the final product. Basically, it is very similar to the yield, and considers the stoichiometry of reactants (equation 7.9)

$$RME\ = \frac{Mass\ of\ product}{Total\ mass\ of\ reagents} \times 100$$

Equation 7.9

For an accurate evaluation, all metrics should be taken into account to achieve a global overview of a process.

7.1.2. LIFE CYCLE ASSESSMENT (LCA)

Life cycle assessment (LCA) is a technique to assess the environmental aspects and potential impacts associated with a product, process, or service, by: (1) performing a list of relevant energy and material inputs and environmental releases, (2) evaluating the potential environmental impacts regarding inputs and releases, and (3) understanding the results to help in a more informed and precise decision.[21,244] Thus, a LCA of a product or process includes four stages: (1) raw material acquisition, (2) manufacturing, (3) use/reuse/maintenance, and (4) recycle/waste management. In these 4 stages, important aspects must be considered for an accurate analysis (Fig. 7.2).

LCA is the only pillar that has been standardized to date (ISO 2006a, b). UNEP (2009) has published guidelines for social LCAs and is currently developing methodological sheets for impact subcategories.[238]

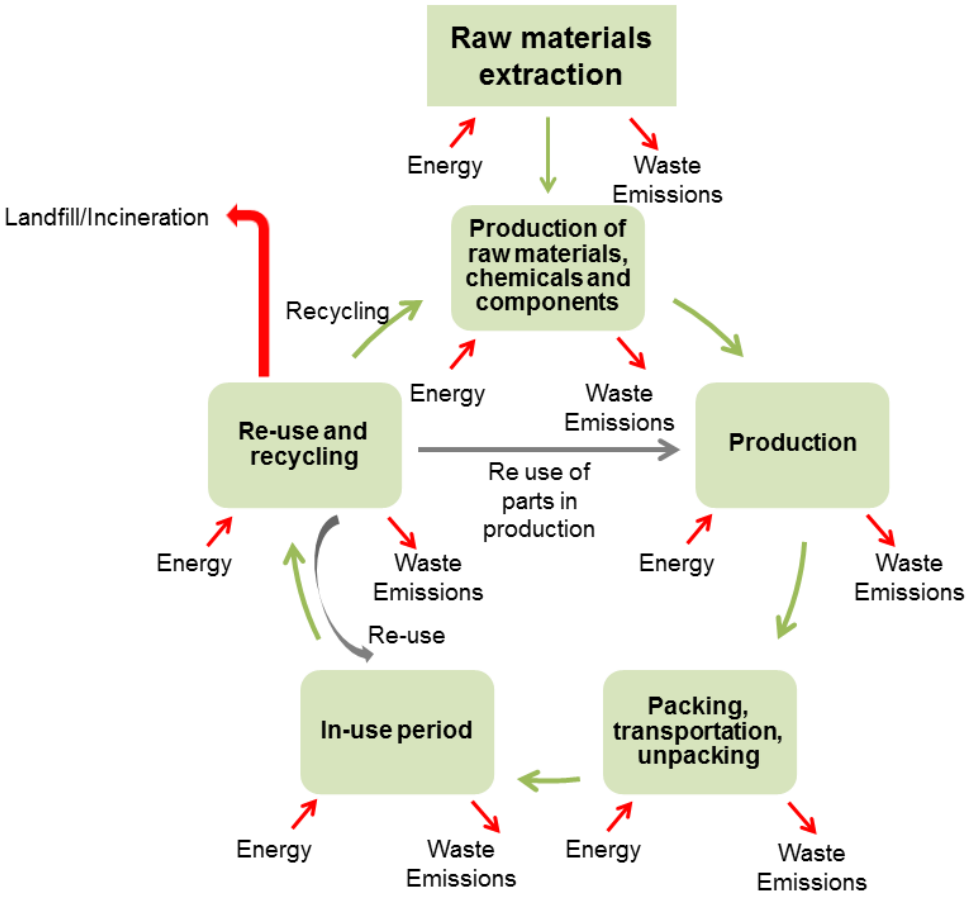

Figure 7.2 - Schematic representation of a typical diagram of LCA.[244]

During the last two decades a special attention has been given to this technique and different LCA studies regarding pharmaceuticals,[5,245] polymers,[246,247] food,[248] biodiesel,[249,250] textiles,[251] and pesticides[252] have been developed. Concerning pharmaceutical manufacturing companies, which are the scenario that includes the problematic of this thesis, there is an increasing pressure to ensure that information, and data about their processes are accurate and reproducible. However, the current environmental regulations (e.g. for eco-products) are not yet specifically oriented to be applied to pharmaceutical products (including biopharmaceutical ones involving mAbs) and processes. Moreover, no standard methods are available to guide companies in the integration and evaluation of sustainability. Thus, the evaluation of industrial processes is normally based on metrics or indicators, depending on the company environmental and sustainability goals.[5,245,253]

Regarding pharmaceutical and biopharmaceutical products or processes, very few LCA studies can be found in the literature. This might be due to three main reasons: (1) difficulties in measuring the inputs and outputs data, (2) lack of information and methodologies to evaluate the environmental impacts of some chemical compounds used, and (3) the need for protecting

the intellectual property.[5] The limited studies available for biotechnological processes recommend that the most effective way for increasing the process environmental performance is by optimizing material and energy efficiency.[5,245,254]

Generally, pharmaceutical processes are divided in two main processing stages. The first one is related to the active pharmaceutical ingredients (API) production and the second to the final drug formulation that includes the API (see Fig. 7.3).[5]

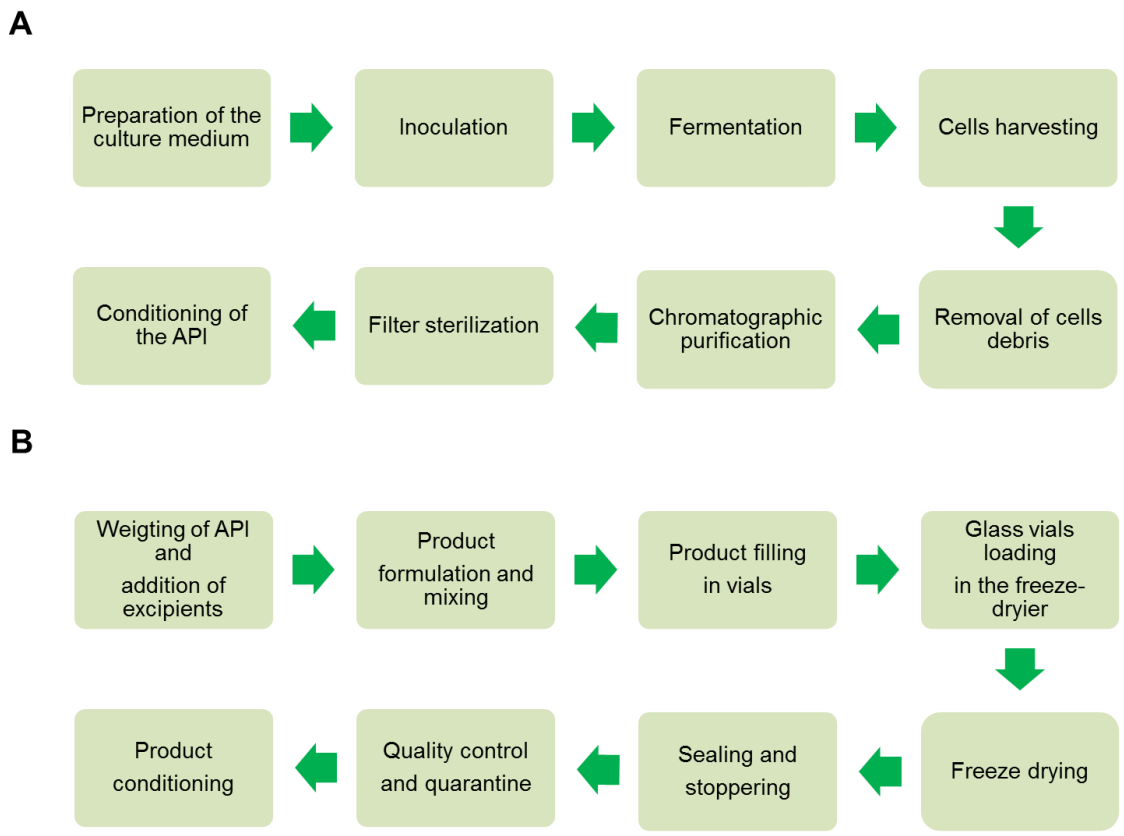

Figure 7.3 - Schematic representation of the two main processing stages of pharmaceutical processes: primary processing (A) and second processing (B).[5]

The most challenging step considering all process is the downstream stage which comprises cell harvesting, protein concentration, and final purification. This step, although already established and optimized, involves the use of a large amount of solvents, materials, energy and time consuming. Thus, after an exhaustive study about all pharmaceutical process a model of LCA was designed based on 8 indicators which are described in Table 7.2.[5]

Table 7.2 – LCA tool to perform sustainability evaluations of pharmaceutical processes based on indicators.[5]

Indicator	Unit	Description
Energy intensity	MJ/vial*	Total energy consumed in the production of one vial.
Process material intensity	kg/vial	Total amount of non-renewable resources needed to obtain a unit mass of product.
Process water intensity	L/via	Total amount of water required to obtain a unit mass of product.
Potential chemical risk	-	Potential risk to human health associated with manipulation, storage, and use of hazardous chemical compounds.
Carbon footprint	kg CO2-eq/ vial	Potential contribution of different greenhouse gas emissions (e.g. CO_2, CH_4, N_2O) to global warming.
Freshwater aquatic toxicity	kg 1,4-dichlorobenzene - eq/vial	Measures the impact of substances emitted to the aquatic environment during manufacture activities.
Net cash flow generated	€/vial	A measure of the company's financial health.
Direct employment	persons/ vial	Number of persons involved in the pharmaceutical product manufacture per unit of product.

This recent LCA tool specifically designed for pharmaceutical processes, in particular the biotechnological based ones, is still under development, but its results are already being used in the design and implementation of a biopharmaceutical API production process with the perspective that in a near future could be extended to enlarge the system boundary.[5]

Since this thesis aims to develop sustainable functional polymeric platforms to employ in downstream stages of biopharmaceutical processes, this study pretends to evaluate the greenness of two strategies developed in this thesis: (1) the synthesis of biomimetic ligand TPN-BM and (2) the monoliths functionalization strategy based on plasma treatment.

The remaining steps reported in this thesis were not evaluated according to green metrics or LCA due to the high complexity of each one as well as the absence of data in the literature to support and to compare the results.

7.2. CASE STUDY 1: EVALUTION OF TPN-BM LIGAND SYNTHESIS

In this case study, it is intended to determine how much is sustainable the TPN-BM synthesis reported in Chapter 3.[161] The TPN-BM synthesis came up with the need of solubility improvement of ligand 22/8 also known as artificial Protein A.[11] Once established this objective, the synthesis was projected and conducted following some principles of green chemistry as previously described. However, in order to evaluate in a more quantitative way the "greenness" of the synthetic procedure, green metrics were applied.

Fig. 7.4 exhibits a schematic representation of the chemical synthetic route followed for the preparation of ligand 22/8 (A) and the alternative one, ligand TPN-BM (B).

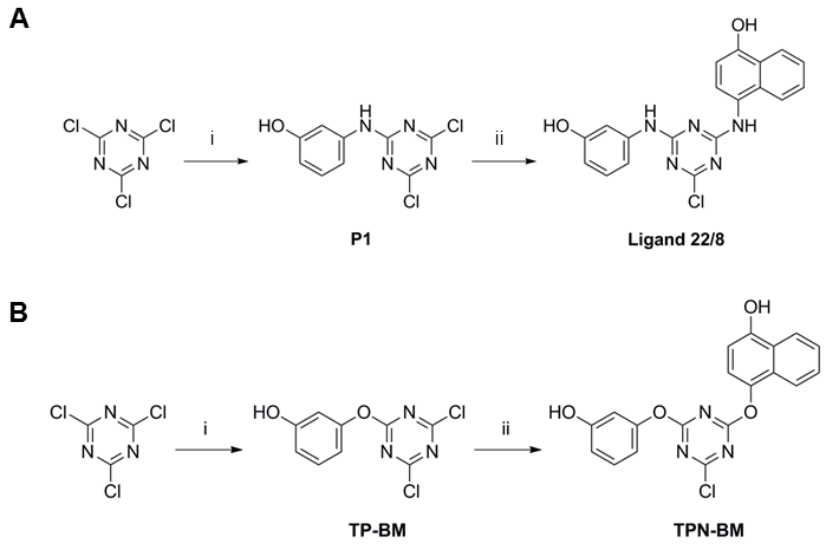

Figure 7.4 - Schematic representation of chemical synthetic route followed for the preparation of (A) ligand 22/8: (i) 3-aminophenol, $NaHCO_3$, acetone, water, 0 ºC, 2h; (ii) 4-amino-1-naphthol hydrochloride, $NaHCO_3$, acetone, water, 45 ºC, 5h, and (B) ligand TPN-BM: (i) resorcinol, DIPEA, dry THF, 0 ºC, 2h; (ii) 1,4-dihydroxynaphthalen, DIPEA, dry THF, 0 ºC, 2h. DIPEA= diisopropylethylamine.

The two synthetic routes are similar however, the reactants and the solvents involved as well as the synthesis conditions are different (the details of reactions are mentioned in Chapters 2 and 3). Mass indicators such as AE, E-factor, MI, MP, CE and RME were applied to both synthesis and the results are presented in Table 7.3.

Table 7.3 – Mass indicators for ligands 22/8 and TPN-BM.

Ligand	AE (%)	E-factor	MI	MP (%)	CE (%)	RME (%)
22/8[82,88]	77	40	30	2.4	60	46
TPN-BM[161]	84	2.9	3.3	26	76	74

Accordingly to all values resulted from mass indicators, it is clearly visible that better values were obtained for ligand TPN-BM synthesis. Particularly, AE, MP, CE and RME are mass indicators which should be maximized, since they translate in general the idea that all reactants employed in a process are converted into the final product. Thus, the waste represented by E-factor and the MI that gives an overview of all reaction intervenients (reactants, solvents, catalysts, etc) must be minimized.[235] Considering this reasoning, ligand TPN-BM represents not only (Chapter 3) an efficient experimental solution[161] but also a sustainable alternative considering their improved mass indicator values compared to those of ligand 22/8.[82,88]

Summing up, in TPN-BM synthesis, it was possible to improve AE and CE in 10%, E-factor, MI and RME in approximately 30% and MP in 20%. In addition, it is important to highlight the obtained values are in the range values of other chemistries.[237]

In order to compare and to rank both synthesis, a qualitative estimation resulted from the quantitative evaluation above presented together with the details described in Chapter 3 (table 7.4), can be performed (Table 7.5).

Table 7.4 – Comparison of ligand 22/8 and ligand TPN-BM synthesis.[161]

Process Parameters	Ligand 22/8	TPN-BM	Green Chemistry Principles
Solvents involved	6	4	Safer solvents
Temperatures (ºC)	0-45	0	Energy efficiency
Purification Steps	6	4	Design for separation
Time consumption (h)	7	4	Time saving
Mass Productivity (%)	2.4	26	Atom economy

Table 7.5 is divided in 4 categories in which: (1) the environment involves all mass indicators and life cycle-emissions, (2) the safety comprises care consideration about process, materials and exposure controls, (3) the efficiency covers the yield, conversion, purity, number of unit operations, processing time and operability and (4) the energy includes energy requirements considering cooling, heating and electricity. The colours also represent different scenarios: green denotes alternatives with significant advantages, red means alternatives with significant disadvantages and yellow suggests alternatives that do not exhibit significant advantages or disadvantages.

Table 7.5 – Qualitative evaluation of ligand 22/8 and ligand TPN-BM synthesis. The colours represent different scenarios: green denotes alternatives with significant advantages, red means alternatives with significant disadvantages and yellow suggests alternatives that do not exhibit significant advantages or disadvantages.

Ligand	Environment	Safety	Efficiency	Energy
22/8[82,88]				
TPN-BM[161]				

Thus, observing Table 7.5 it is obvious that TPN-BM synthesis offers great advantages to ligand 22/8 synthesis considering all main topics involved in the evaluation of the process.

20 years ago, ligand 22/8 was produced as a template to mimic Protein A. Based on the biomimetic approach, this attempt was already in that time an application of green chemistry early before the concept was coined.[21] However, the time is always changing and challenging scientists to improve and to optimize processes, and ligand TPN-BM is an example of this effort as well as being a more efficient biomimetic solution with improved solubility than ligand 22/8, was synthesised following a more sustainable procedure.

7.3 CASE STUDY 2: EVALUATION OF PLASMA TREATMENT AS A METHOD FOR SURFACES MODIFICATION

To create a functional support, the first step that is normally taken involves the introduction of amines onto materials surface for subsequent functionalization.

Herein it is intended to evaluate two methods of monoliths functionalization (monoliths of chitosan and polyvinyl alcohol, CP): (1) traditional one: performing epoxy-activation followed by the amination procedure[82] (reported in the Chapters 2 and 3) and (2) an alternative one (reported in Chapter 5): using plasma treatment for one step activation and amination (Fig. 7.5).

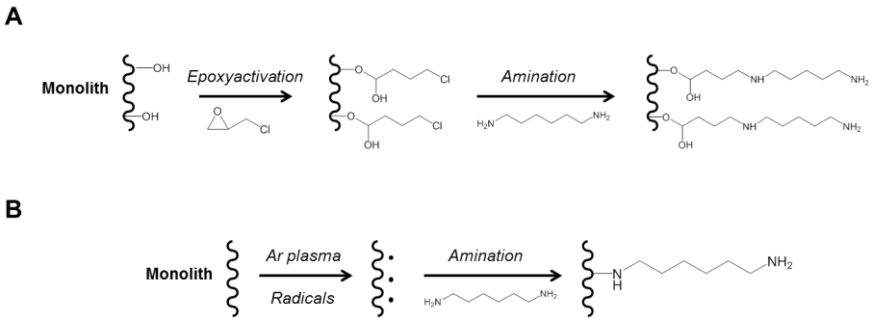

Figure 7.5 - Schematic representation of two methods of materials functionalization: (1) traditional one: performing epoxy-activation followed by the amination procedure and (2) the alternative one: using plasma treatment for one single step of activation and amination.

Both functionalization strategies, the traditional and the one involving plasma treatment, are composed by two steps where the first one regards the introduction of two different reactive chemical species, epoxy rings and radicals, respectively. The amination step is common in both functionalization routes but it is performed at different conditions, since the alternative one occurs under the plasma chamber. This new approach involves different reagents, time and energy consumptions, therefore mass indicators were applied and the different metrics were compared (Table 7.6).

Table 7.6 – Mass indicators for both strategies of monoliths functionalization: traditional and induced by plasma treatment.

Strategy	AE (%)	E-factor	MI	MP (%)	CE (%)	RME (%)
Traditional[82]	56	296	297	0.3	0.1	0.7
Plasma	99	0.1	1.1	95	77	77

It is known that immobilization strategies on solid supports require time, excess of reagents and that the steric hindrance prevails. Therefore it is urgent to overcome these drawbacks creating new strategies of immobilization which should be kept in mind not only their efficiency but also their sustainability. Hereupon, and considering the mass indicator values for both functionalization strategies, it is clear that the one based on plasma treatment revealed to be more efficient than the traditional route of surfaces modification. Although plasma technique is fast, it allowed to maximize all mass indicators at least in 2-fold, contributing for the greenness of the functionalization process. The amount of Argon used to radical's formation was not accounted because its use belongs to a transient step to enable the amination step. Nevertheless, it is possible to assume that all radicals formed, reacted efficiently due to higher estimated values of green metrics in amination step.

In an overview, considering environment, safety, efficiency and energy impacts of both functionalization routes, a qualitative analysis was also performed. In Table 7.7, the colours represent different scenarios; green - significant advantages, red - alternatives with significant disadvantages and yellow - alternatives that do not exhibit significant advantages or disadvantages.

Table 7.7 – Qualitative evaluation of both strategies of monoliths functionalization: traditional and induced by plasma treatment. The colours represent different scenarios: green denotes alternative with significant advantages, red means alternatives with significant disadvantages and yellow suggests alternatives that do not exhibit significant advantages or disadvantages.

Strategy	Environment	Safety	Efficiency	Energy
Traditional[82]				
Plasma				

The methodology with plasma treatment as a tool for the surface modification represents an efficient and sustainable alternative. Particularly, in less time (30 minutes) it is possible to achieve higher amines density (330 µmol NH_2 g^{-1} support) minimizing the environmental impact, while the traditional route involving more organic species required 13 hours to achieve an amine density of 226 µmol NH_2 g^{-1} support. Moreover, to obtain 226 µmol NH_2 g^{-1} support through the traditional strategy, the amount of reactants involved is much higher becoming this functionalization route uninteresting from the green chemistry and economic point of views. Plasma treatment being a solvent free technique justify in this way why it has been increasingly studied and been a focus of high attention in the field of surfaces modification.

7.4 CONCLUDING REMARKS

The future of green chemistry is as broad as the future of chemistry as a whole, and it is therefore difficult to predict. Just as chemistry has always been a journey rather than a conclusion, green chemistry is also based on the statement that continual improvement, discovery, and innovation is the path towards a more sustainable world. Therefore, it is very important to make researchers and manufactures aware of this, because although the growing of green chemistry acceptance, there is still a friction that avoids its total agreement.

It is understandable that it is impossible to reduce all the waste involved in an entire process, to obtain only yields of 100% or even to reduce totally the organic solvents of a process step. However, it is incomprehensible that scientists and industrial engineers have no consciousness and care about the environment when designing and implementing new processes at laboratory, pilot or industrial scales. Therefore, it is urgent to invert this, and try to act always, in a sustainable way to reduce the use of toxic compounds and feed-stocks, by-products, solvents, waste and energy consumptions. Thus, this work led to the development of greener synthetic route comprising the design: (1) of new strategies for the synthesis of biomimetic ligands and (2) the new routes for the functionalization of polymeric platforms used to purify antibodies. The results obtained from mass indicators demonstrate that the alternative strategies followed in this thesis fulfil the requirements of green chemistry. Particularly, the alternative synthesis of the biomimetic ligand as well as the functionalization strategy based on plasma treatment enabled the significant reduction of waste and solvents used and, at the same time, the increase of reaction yields, atom economy, mass productivity and carbon efficiency. Therefore, this study clearly shows that the main goals of a process can be maintained even improving its sustainability.

CHAPTER 8: CONCLUDING REMARKS AND FUTURE PERSPECTIVES

8.1 CONCLUDING REMARKS

Up to now, polymeric monoliths are known as the more recent and fashionable generation of chromatographic supports. However, more than trendy, they are effective 3D porous supports due to their very-well organized and interconnected porous network which enables the faster permeation of both viscous fluids and large biomolecules. These main features have been attracting high attention in the chromatography world, especially for antibody and virus purification. Monoliths have been prepared mainly using synthetic monomers processed *via* radical, cationic and anionic polymerizations. Although highly robust, most of these polymeric monoliths need extensive cleaning protocols to prepare them for contact with biological samples. Additionally, the functionalization strategies employed for ligand attachment involve numerous steps and toxic chemicals.

In order to minimize costs and the environmental impact, monoliths produced mainly from natural polymeric resources (chitosan, agarose and dextran) blended with low contents of synthetic polymers (PVA or acrylate species) were investigated as potential chromatographic platforms to intensify antibody purification processes. The main benefit of this approach comprises the fact that biopolymers were not chemically modified but, physically entrapped in the chemical network already established between the synthetic polymers. The idea was to improve the mechanical stability of the natural monoliths without compromising their potential of biodegradability and disposability.

The freeze drying processes as well as supercritical fluid technology are techniques that have been widely used to generate porous structures in which the pore control is crucial, e.g., tissue engineering and drug delivery. Aware of the same requirement, these methodologies were successfully applied for natural-based monoliths preparation, and generated distinguished 3D structures for bioseparation purposes. Thus, the combination of these two strategies offered the creation of a panoply of porous supports with different pore size ranges and mechanical properties, in cleanable and rigorous modes, comparing with intensive chemical steps normally established.

For the sake of monolithic platforms optimization regarding antibody purification purposes, efficiency and time processing, natural monoliths were embedded with magnetic nanoparticles (MNPs) to confer them a magnetic responsive behaviour. Two great advantages attached to the magnetically-assisted elution were found: (1) the amount of protein was higher (15% more)

operating under magnetic conditions and (2) the time for antibody elution was reduced to half, which greatly decreases protein damage under the drastic pH conditions employed in the recovery step. This strongly reinforces the important role of MNPs entrapped in the monoliths network to operate faster under antibody purification processes.

Plasma technology, known as an organic solvent free technique, also demonstrated to be an alternative and powerful strategy to compete with the traditional organic functionalization routes. The main contributions of this methodology comprised: (1) the reduction of functionalization procedure in 12 hours and (2) the use of organic species to half, and (3) an increase of the amines and ligands densities in 2-fold (confirmed by XPS, a highly sensitive technique), in comparison to the "old-style" (epoxyactivaction and amination). In fact, there are not many techniques with the same demonstrated efficiency. Thus, more than design for sustainability, that was always kept in mind during this project, the successful modification strategy of monoliths was evident, and opens new insights, not only for antibody purification purposes, but for enzymes immobilization or small protein couplings.

The redesign of antibody chromatographic processes was also extended to the affinity ligands. The new artificial Protein A, ligand TPN-BM, came up as a greener and practical solution to upgrade the selectivity of monoliths for antibody purification. Its synthesis, based on green chemistry principles, highly contributed for the reduction of organic solvents, time and energy consumptions. Furthermore, the reaction yields, mass productively and carbon efficiency, were higher when compared with known chemical routes applied for biomimetic ligand synthesis. Thus, TPN-BM, more than a biomimetic approach, that by itself is already a sustainable solution, it is doubtless a workable and reproducible Protein A substitute. This strong affinity behaviour for antibody recognition was confirmed by *in silico* studies through automated molecular docking and MD simulations. These studies allowed to validate experimental affinity constants, and to explain the ON/OFF mechanism observed for this affinity pair at binding (pH 7) and elution (pH 3) conditions (see Table 8.1). Moreover, the computational findings were similar to the ones discovered for the natural affinity ligand most used in affinity antibody purification methods. Thus, all these statements highlight the great evolution achieved in affinity ligand design, and the potential of TPN-BM monolithic platforms as strong competitors to established Protein A-agarose beads.

Remarkably, all the findings of this thesis enabled to make a real progress, since a step further in the green chemistry and in the affinity chromatography was achieved.

Table 8.1 – Comparison of binding and elution capacities of natural-based monoliths produced in this thesis as well as the purity of mAbs purified from crude samples.

Monolith	Protein bound (mg IgG g^{-1} support)	Protein eluted (mg IgG g^{-1} support)	Purity of purified mAbs (%)
CP_22/8	150±15	138±5	98
CG_22/8	26±8	16±5	n.t
CP_TPN-BM	160±10	140±10	98
CG_TPN-BM	60±5	24±5	n.t
CHT_M_TPN-BM	100±10	80±10	n.t
CP_M_TPN-BM	120±10	105±10	98
AA_M_TPN-BM	103±10	83±10	97
DXT_M_TPN-BM	80±7	23±5	n.t
CP 25:75_TPN-BM	55±5	35±5	n.t
CP 25:75_M_TPN-BM^{FD}	32±5	19±5	75

n.t.: not tested

8.2. FUTURE PERSPECTIVES

In nature, monolith is known as a single large block of stone employed in architecture/sculpture, which needs of continuum improvements, to be admired and remembered as a marker of history. In science, as in Nature, this block requires to be carved towards a better performance in different applications.

This thesis fulfilled some gaps in the field of monoliths applied in antibody purification, particularly in view of monoliths composition, preparation and functionalization with biomimetic ligands prepared by green chemistry approaches. Still, there is scope for improvement regarding mechanical stability and pore homogeneity. $ScCO_2$ technology is a promising tool to achieve higher control of pores according to their use for analytical or industrial requests. This tuning will affect and consequently improve, the efficiency of antibodies binding, since homogeneous networks with a controlled pore size will generate better platforms for ligand attachment, and antibody capture. Also, these monoliths should be tested not only under gravitational conditions but under pressure using specific equipment, as AKTA. Moreover, the

scale up of these supports is still limited and therefore this is an area that must be addressed to monoliths optimization in order to definitely push monolith applicability to industry.

Nevertheless, the possible acceptance by the industry of the strategies herein presented is probably far away. Nowadays, the industry is formatted preferentially to design products for a life time, and not always assuring its biodegradability or disposability. Only with a change of mind-set will it be possible to spread the potential of these affinity monoliths, moving from the research bench to sustainable large-scale chromatographic processes and other engineering applications.

However, the true is, as Paul Anastas reinforces in all his papers,[21,151,235,239] the green chemistry and practices are more than a stylish philosophy; it is a state of spirit for which chemists and engineers must be aware when they develop or optimize products or processes.

REFERENCES

1. Marichal-Gallardo, P. A. & Alvarez, M. M. State-of-the-art in downstream processing of monoclonal antibodies: process trends in design and validation. *Biotechnol.Progr.* **28,** 899–916 (2012).

2. Elvin, J. G., Couston, R. G. & van der Walle, C. F. Therapeutic antibodies: market considerations, disease targets and bioprocessing. *Int. J. Pharm.* **440,** 83–98 (2013).

3. Kelley, B., Blank, G. & Lee, A. *Downstream processing of monoclonal antibodies: current practices ans future opportunities*. *Process Scale Purification of Antibodies* 1–24 (Jonh Wiley & Sons, Inc, 2009).

4. Low, D., O'Leary, R. & Pujar, N. S. Future of antibody purification. *J. Chromatogr. B* **848,** 48–63 (2007).

5. Mata, T., Martins, A. & Neto, B. LCA tool for sustainability evaluations in the pharmaceutical industry. *Chem. Eng. Trans.* **26,** 261–266 (2012).

6. Winzor, D. Quantitative affinity chromatography. *J. Biochem. Bioph. Meth.* **49,** 99–121 (2001).

7. Gagnon, P. Technology trends in antibody purification. *J. Chromatogr. A* **1221,** 57–70 (2012).

8. Rowe, L., Khoury, G. El & Lowe, C. R. *Affinity chromatography : historical and prospective overview*. *Biopharm. Prod. Technol.* 225–282 (Wiley-VCG Verlag GmbH & Co. KGaA, 2012).

9. Roque, A. C. A., Silva, C. S. O. & Taipa, M. A. Affinity-based methodologies and ligands for antibody purification: advances and perspectives. *J. Chromatogr. A* **1160,** 44–55 (2007).

10. Teng, S. F., Sproule, K., Hussain, A & Lowe, C. R. A strategy for the generation of biomimetic ligands for affinity chromatography. Combinatorial synthesis and biological evaluation of an IgG binding ligand. *J. Mol. Recognit.* **12,** 67–75 (1999).

11. Teng, S. F., Sproule, K., Husain, A. & Lowe, C. R. Affinity chromatography on immobilized "' biomimetic '" ligands Synthesis , immobilization and chromatographic assessment of an immunoglobulin G-binding ligand. *J. Chromatogr. B* **740,** 1–15 (2000).

12. Qian, J. *et al.* A synthetic Protein G adsorbent based on the multi-component Ugi reaction for the purification of mammalian immunoglobulins. *J. Chromatogr. B* **898,** 15–23 (2012).

13. Josić, D. & Buchacher, A. Application of monoliths as supports for affinity chromatography and fast enzymatic conversion. *J. Biochem. Bioph. Meth.* **49,** 153–174 (2001).

14. Tetala, K. K. R. & Van Beek, T. a. Bioaffinity chromatography on monolithic supports. *J. Sep. Sci.* **33,** 422–438 (2010).

15. Calleri, E., Ambrosini, S., Temporini, C. & Massolini, G. New monolithic chromatographic supports for macromolecules immobilization: challenges and opportunities. *J. Pharm. Biomed. Anal.* **69,** 64–76 (2012).

16. Jungbauer, A. & Hahn, R. Polymethacrylate monoliths for preparative and industrial separation of biomolecular assemblies. *J. Chromatogr. A* **1184,** 62–79 (2008).

17. Siouffi, A. Silica gel-based monoliths prepared by the sol–gel method: facts and figures. *J. Chromatogr. A* **1000,** 801–818 (2003).

18. Hortigüela, M. J., Aranaz, I., Gutiérrez, M. C., Ferrer, M. L. & del Monte, F. Chitosan gelation induced by the in situ formation of gold nanoparticles and its processing into macroporous scaffolds. *Biomacromolecules* **12,** 179–186 (2011).

19. Lozinsky, V. I. *et al.* Polymeric cryogels as promising materials of biotechnological interest. *Trends Biotechnol.* **21,** 445–451 (2003).

20. Sun, S. *et al.* Preparation of agarose/chitosan composite supermacroporous monolithic cryogels for affinity purification of glycoproteins. *J. Sep. Sci.* **35,** 1–8 (2012).

21. Anastas, P. T. & Warner, J. C. *Green Chemistry Theory and Pratice*. 1–131 (OXFORD UNIVERSITY PRESS, 1998).

22. Cooper, A. I. Porous Materials and Supercritical Fluids. *Adv. Mater.* **15,** 1049–1059 (2003).

23. Ayyar, B. V., Arora, S., Murphy, C. & O'Kennedy, R. Affinity chromatography as a tool for antibody purification. *Methods* **56,** 116–129 (2012).

24. Liu, Y., Lu, Y. & Liu, Z. Restricted access boronate affinity porous monolith as a protein A mimetic for the specific capture of immunoglobulin G. *Chem. Sci.* **3,** 1467–1471 (2012).

25. Gottschalk, U. Bioseparation in antibody manufacturing: the good, the bad and the ugly. *Biotechnol.Progr.* **24,** 496–503 (2008).

26. Arrua, R. D. & Alvarez Igarzabal, C. I. Macroporous monolithic supports for affinity chromatography. *J. Sep. Sci.* **34,** 1974–1987 (2011).

27. Svec, F. & Huber, C. Monolithic materials: promises, challenges, achievements. *Anal. Chem.* **1,** 2101–2107 (2006).

28. Majors, R. Stationary-phase technology in separation science. *LCGC* **18,** 1214–1227 (2000).

29. Jungbauer, A. & Hahn, R. Monoliths for fast bioseparation and bioconversion and their applications in biotechnology. *J. Sep. Sci.* **27,** 767–778 (2004).

30. Arrua, R. D., Causon, T. J. & Hilder, E. F. Recent developments and future possibilities for polymer monoliths in separation science. *Analyst* **137,** 5179–5189 (2012).

31. Gunasena, D. N. & Rassi, Z. El. Organic monoliths for hydrophilic interaction electrochromatography/chromatography and immunoaffinity chromatography. *Electrophoresis* **33,** 251–261 (2012).

32. Kato, M., Sakai-Kato, K. & Toyo'oka, T. Silica sol-gel monolithic materials and their use in a variety of applications. *J. Sep. Sci.* **28,** 1893–1908 (2005).

33. Muldar, M. *Basic Principles of Membrane Technology*. *Zeitschrift für Physikalische Chemie* 1–557 (Kluer Academic Publishers, 1997).

34. Reilly, J. & Ultee, M. *Antibody, purification: monoclonal (MAB) and polyclonal*. *Encyclopedia of Industrial Biotechnology* 1–9 (Jonh Wiley & Sons, Inc, 2009).

35. Przybycien, T. M., Pujar, N. S. & Steele, L. M. Alternative bioseparation operations: life beyond packed-bed chromatography. *Curr. Opin. Biotech.* **15,** 469–478 (2004).

36. Hjerté, S., Liao, J.-L. & Zhang, R. High-performance liquid chromatography on continuous polymer beads. *J. Chromatogr.* **473,** 273–275 (1989).

37. Tennikova, T., Svec, F. & Belenkii, B. High-performance membrane chromatography. A novel method of protein separation. *J. Liq. Chromatogr.* **13,** 63–70 (1990).

38. Rods, C. & Media, C. S. Continuous rods of macroporous polymer as high-performance liquid. *Anal. Chem.* **64,** 820–822 (1992).

39. Qi, T. *et al.* Synthesis and borate uptake of two novel chelating resins. *Ind. Eng. Chem. Res.* **41,** 133–138 (2002).

40. Mallik, R. & Hage, D. S. Affinity monolith chromatography. *J. Sep. Sci.* **29,** 1686–1704 (2006).

41. Viklund, C., Svec, F., Fréchet, J. & Irgum, K. Monolithic,"molded", porous materials with high flow characteristics for separations, catalysis, or solid-phase chemistry: control of porous properties during polymerization. *Chem. Mater.* **8,** 744–750 (1996).

42. Vlakh, E. & Tennikova, T. Preparation of methacrylate monoliths. *J. Sep. Sci.* **30,** 2801–2813 (2007).

43. Li, Y. & Lee, M. Biocompatible polymeric monoliths for protein and peptide separations. *J. Sep. Sci.* **32,** 3369–3378 (2009).

44. Sushma, K., Vijayalakshmi, M. A., Krishnan, V. & Satheeshkumar, P. K. Cloning, expression, purification and characterization of a single chain variable fragment specific to tumor necrosis factor alpha in Escherichia coli. *J. Biotechnol.* **156,** 238–244 (2010).

45. Feng, S., Yang, N., Pennathur, S., Goodison, S. & Lubman, D. M. Enrichment of glycoproteins using nanoscale chelating concanavalin A monolithic capillary chromatography. *Anal. Chem.* **81,** 3776–3783 (2009).

46. Hahn, R., Podgomik, A., Merhar, M., Schallaun, E. & Jungbauer, A. Affinity monoliths generated by in situ polymerization of the ligand. *Anal. Chem.* **73,** 5126–5132 (2001).

47. Luo, Q., Zou, H., Zhang, Q., Xiao, X. & Ni, J. High-performance affinity chromatography with immobilization of protein A and L-histidine on molded monolith. *Biotechnol. Bioeng.* **80,** 481–489 (2002).

48. Wei, X., Qi, L., Yang, G. & Wang, F. Preparation and characterization of monolithic column by grafting pH-responsive polymer. *Talanta* **79,** 739–475 (2009).

49. Dhivya, A. P., Kumar, B. P., Prasanna, R. R., Jayaprakash, N. S. & Vijayalakshmi, M. a. Purification of monoclonal antibodies from cell-culture supernatant by use of anion-exchange convective interaction media (CIM) monolithic columns. *Chromatographia* **72,** 1183–1188 (2010).

50. Pecher, H. S., Zimathies, A. & Weller, M. G. Oligoepoxide-based monoliths: synthesis and application as affinity capillary column for enrichment of immunoglobulin G. *Macromol. Chem. Phys.* **213,** 2398–2403 (2012).

51. Jmeian, Y. & El Rassi, Z. Tandem affinity monolithic microcolumns with immobilized protein A, protein G', and antibodies for depletion of high abundance proteins from serum samples: integrated microcolumn-based fluidic system for simultaneous depletion and tryptic digestion. *J. Proteom. Res.* **6,** 947–954 (2007).

52. Gupalova, T. V, Lojkina, O. V, Pàlàgnuk, V. G., Totolian, a a & Tennikov, T. B. Quantitative investigation of the affinity properties of different recombinant forms of protein G by means of high-performance monolithic chromatography. *J. Chromatogr. A* **949,** 185–193 (2002).

53. Uzun, L., Say, R. & Denizli, A. Porous poly(hydroxyethyl methacrylate) based monolith as a new adsorbent for affinity chromatography. *React. Funct. Polym.* **64,** 93–102 (2005).

54. Uzun, L., Say, R., Unal, S. & Denizli, A. Hepatitis B surface antibody purification with hepatitis B surface antibody imprinted poly(hydroxyethyl methacrylate-N-methacryloyl-L-tyrosine methyl ester) particles. *J. Chromatogr. B* **877,** 181–188 (2009).

55. Rajak, P., Vijayalakshmi, M. a & Jayaprakash, N. S. Purification of monoclonal antibodies, IgG1, from cell culture supernatant by use of metal chelate convective interaction media monolithic columns. *Biomed. Chromatogr.* **26,** 1488–1493 (2012).

56. Neff, S. & Jungbauer, A. Monolith peptide affinity chromatography for quantification of immunoglobulin M. *J. Chromatogr. A* **1218,** 2374–2380 (2011).

57. Gagnon, P., Hensel, F., Lee, S. & Zaidi, S. Chromatographic behavior of IgM:DNA complexes. *J. Chromatogr. A* **1218,** 2405–2412 (2011).

58. Kamalanathan, A. S., Goulvestre, C., Weill, B. & Vijayalakshmi, M. A. Proteolysis activity of IgM antibodies from rheumatoid arthritis patients' sera: evidence of atypical catalytic site. *J. Mol. Recognit.* **23,** 577–582 (2010).

59. Breen, L. *et al.* High-throughput fractionation of human plasma for fast enrichment of low- and high-abundance proteins. *Blood Transfusion* **10,** 89–100 (2012).

60. Gautam, S. & Loh, K.-C. Immunoglobulin-M purification-challenges and perspectives. *Biotechnol. Adv.* **29,** 840–849 (2011).

61. Platonova, G. A. & Tennikova, T. B. Affinity processes realized on high-flow-through methacrylate-based macroporous monoliths. *J. Chromatogr. A* **1065,** 19–28 (2005).

62. Kumar, A., Plieva, F. M., Galaev, I. Y. & Mattiasson, B. Affinity fractionation of lymphocytes using a monolithic cryogel. *J. Immunol. Methods* **283,** 185–194 (2003).

63. He, X., Yao, K., Shen, S. & Yun, J. Freezing characteristics of acrylamide-based aqueous solution used for the preparation of supermacroporous cryogels via cryo-copolymerization. *Chem. Eng. Sci.* **62,** 1334–1342 (2007).

64. Dainiak, M. B., Kumar, A., Galaev, I. Y. & Mattiasson, B. Detachment of affinity-captured bioparticles by elastic deformation of a macroporous hydrogel. *Proceedings of the National Academy of Sciences of the United States of America* **103,** 849–854 (2006).

65. Dainiak, M. B., Galaev, I. Y. & Mattiasson, B. Affinity cryogel monoliths for screening for optimal separation conditions and chromatographic separation of cells. *J. Chromatogr. A* **1123,** 145–150 (2006).

66. Lozinsky, V. I., Plieva, F. M., Galaev, I. Y. & Mattiasson, B. The potential of polymeric cryogels in bioseparation. *Bioseparation* **10,** 163–188 (2001).

67. Babac, C., Yavuz, H., Galaev, I. Y., Pişkin, E. & Denizli, A. Binding of antibodies to concanavalin A-modified monolithic cryogel. *React. Funct. Polym.* **66,** 1263–1271 (2006).

68. Alkan, H., Bereli, N., Baysal, Z. & Denizli, A. Selective removal of the autoantibodies from rheumatoid arthritis patient plasma using protein A carrying affinity cryogels. *Biochem. Eng. J.* **51,** 153–159 (2010).

69. Alkan, H., Bereli, N., Baysal, Z. & Denizli, A. Antibody purification with protein A attached supermacroporous poly(hydroxyethyl methacrylate) cryogel. *Biochem. Eng. J.* **45,** 201–208 (2009).

70. Bereli, N., Ertürk, G. & Denizli, A. Histidine containing macroporous affinity cryogels for immunoglobulin G purification. *Sep. Sci. Technol.* **47,** 1813–1820 (2012).

71. Lansing, E. Biodegradable polymers: opportunities and challenges. *J. Macromol. Sci. Polym. Rev.* **3,** 481–505 (2007).

72. Gustavsson, P. E. & Larsson, P. O. Continuous superporous agarose beads in radial flow columns. *J. Chromatogr. A* **925,** 69–78 (2001).

73. Bhat, S. & Kumar, A. Cell proliferation on three-dimensional chitosan-agarose-gelatin cryogel scaffolds for tissue engineering applications. *J. Biosci. Bioeng.* **114,** 663–670 (2012).

74. Shanmugam, S. *et al.* Natural polymers and their applications. *Nat. Prod. Rad.* **4,** 478–481 (2005).

75. Xu, F. *et al.* Porous CS monoliths and their adsorption ability for heavy metal ions. *J. Hazard. Mater.* **188,** 148–55 (2011).

76. Cheng, Y., Luo, X., Payne, G. F. G. & Rubloff, G. G. W. Biofabrication: programmable assembly of polysaccharide hydrogels in microfluidics as biocompatible scaffolds. *J. Mater. Chem.* **22,** 7659–7666 (2012).

77. Temtem, M. *et al.* Supercritical CO_2 generating chitosan devices with controlled morphology. Potential application for drug delivery and mesenchymal stem cell culture. *J. Supercrit. Fluid* **48,** 269–277 (2009).

78. Temtem, M., Barroso, T., Casimiro, T., Mano, J. F. & Aguiar-Ricardo, A. Dual stimuli responsive poly(N-isopropylacrylamide) coated chitosan scaffolds for controlled release prepared from a non residue technology. *J. Supercrit. Fluid* **66,** 398–404 (2012).

79. Hedström, M., Plieva, F., Galaev, I. Y. & Mattiasson, B. Monolithic macroporous albumin/chitosan cryogel structure: a new matrix for enzyme immobilization. *Anal. Bioanal. Chem.* **390,** 907–912 (2008).

80. Lü, Z., Zhang, P. & Jia, L. Preparation of chitosan functionalized monolithic silica column for hydrophilic interaction liquid chromatography. *J. Chromatogr. A* **1217,** 4958–4964 (2010).

81. Sun, S. *et al.* Monolithic cryogels made of agarose-chitosan composite and loaded with agarose beads for puification of immunoglobulin G. *Int. J. Biol. Macromol.* **50,** 1002–1007 (2012).

82. Barroso, T., Roque, A. C. A. & Aguiar-Ricardo, A. Bioinspired and sustainable chitosan-based monoliths for antibody capture and release. *RSC Advances* **2,** 11285–11294 (2012).

83. Zhu, S. *et al.* Dissolution of cellulose with ionic liquids and its application: a mini-review. *Green Chem.* **8,** 325–327 (2006).

84. Boeden, H. F. *et al.* Bead cellulose derivatives as supports for immobilization and chromatographic purification of proteins. *J. Chromatogr.* **552,** 389–414 (1991).

85. Manganaro, J. L. & Goldberg, B. S. Protein purification with novel porous sheets containing derivatized cellulose. *Biotechnol.Progr.* **9,** 285–290 (1993).

86. Necina, R. *et al.* Peptide affinity chromatography of human clotting factor VIII. Screening of the vWF-binding domain. *J. Chromatogr. B* **715,** 191–201 (1998).

87. Kosan, B., Michels, C. & Meister, F. Dissolution and forming of cellulose with ionic liquids. *Cellulose* **15,** 59–66 (2008).

88. Barroso, T., Temtem, M., Hussain, A., Aguiar-Ricardo, A. & Roque, A. C. A. Preparation and characterization of a cellulose affinity membrane for human immunoglobulin G (IgG) purification. *J. Memb. Sci.* **348,** 224–230 (2010).

89. Prasanna, R. R. & Vijayalakshmi, M. A. Characterization of metal chelate methacrylate monolithic disk for purification of polyclonal and monoclonal immunoglobulin G. *J. Chromatogr. A* **1217,** 3660–3667 (2010).

90. Brne, P. *et al.* Fast and efficient separation of immunoglobulin M from immunoglobulin G using short monolithic columns. *J. Chromatogr. A* **1144,** 120–125 (2007).

91. Dainiak, M. B., Kumar, A., Plieva, F. M., Galaev, I. Y. & Mattiasson, B. Integrated isolation of antibody fragments from microbial cell culture fluids using supermacroporous cryogels. *J. Chromatogr. A* **1045,** 93–98 (2004).

92. Ahlqvist, J. *et al.* Affinity binding of inclusion bodies on supermacroporous monolithic cryogels using labeling with specific antibodies. *J. Biotechnol.* **122,** 216–225 (2006).

93. Bereli, N., Şener, G., Altıntaş, E. B., Yavuz, H. & Denizli, A. Poly(glycidyl methacrylate) beads embedded cryogels for pseudo-specific affinity depletion of albumin and immunoglobulin G. *Mat. Sci. Eng. C* **30,** 323–329 (2010).

94. Billen, J. & Desmet, G. Understanding and design of existing and future chromatographic support formats. *J. Chromatogr. A* **1168,** 73–99 (2007).

95. Miyabe, K. & Guiochon, G. Characterization of monolithic columns for HPLC. *J. Sep. Sci.* **27,** 853–873 (2004).

96. Urban, J., Eeltink, S., Jandera, P. & Schoenmakers, P. J. Characterization of polymer-based monolithic capillary columns by inverse size-exclusion chromatography and mercury-intrusion porosimetry. *J. Chromatogr. A* **1182,** 161–168 (2008).

97. Al-bokari, M. & Guiochon, G. Determination of the porosities of monolithic columns by inverse size-exclusion chromatography. *J. Chromatogr. A* **975,** 275–284 (2002).

98. Petter, C. H., Heigl, N., Bonn, G. K. & Huck, C. W. Fast, noninvasive and simultaneous near-infrared spectroscopic characterisation of physicochemical stationary phases' properties: from silica particles towards monoliths. *J. Sep. Sci.* **31,** 2541–2550 (2008).

99. Gillespie, E., Macka, M., Connolly, D. & Paull, B. Evaluation of capillary ion exchange stationary phase coating distribution and stability using radial capillary column contactless conductivity detection. *The Analyst* **131,** 886–888 (2006).

100. Teisseyre, T. & Urban, J. Remotely detected NMR for the characterization of flow and fast chromatographic separations using organic polymer monoliths. *Anal. Chem.* **83,** 6004–6010 (2011).

101. Phases, M. *et al.* A more informative approach for characterization of polymer monolithic phases: small angle neutron scattering/ultrasmall angle neutron scaterring. *Anal. Chem.* **83,** 9201–9205 (2011).

102. Kinniburgh, D. G. General purpose adsorption isotherms. *Environ. Sci. Technol.* **20,** 895–904 (1986).

103. Yamamoto, S. & Kita, A. Rational design calculation method for stepwise elution chromatography of proteins. *Food Bioprod. Proc.* **84,** 72–77 (2006).

104. Bertolini, J., Gomme, P. & Thomas, P. Large-scale protein chromatography. *Met. Mol. Biol.* **251,** 211–224 (2004).

105. Plieva, F. M., Seta, E. De, Galaev, I. Y. & Mattiasson, B. Macroporous elastic polyacrylamide monolith columns: processing under compression and scale-up. *Sep. Purif. Technol.* **65,** 110–116 (2009).

106. Vidic, J. *et al.* Chemical and chromatographic stability of methacrylate-based monolithic columns. *J. Chromatogr. A* **1144,** 63–71 (2007).

107. Podgornik, A. *et al.* Large-scale methacrylate monolithic columns: design and properties. *J. Biochem. Bioph. Meth.* **60,** 179–189 (2004).

108. Yoo, M. J. & Hage, D. S. Evaluation of silica monoliths in affinity microcolumns for high-throughput analysis of drug-protein interactions. *J. Sep. Sci.* **32,** 2776–2785 (2009).

109. Schiel, J. E., Mallik, R., Soman, S., Joseph, K. S. & Hage, D. S. Applications of silica supports in affinity chromatography. *J. Sep. Sci.* **29,** 719–737 (2006).

110. Fuentes, M., Mateo, C., Fernández-Lafuente, R. & Guisán, J. M. Detection of polyclonal antibody against any area of the protein-antigen using immobilized protein-antigens: the critical role of the immobilization protocol. *Biomacromolecules* **7,** 540–544 (2006).

111. Goto, Y., Matsuno, R., Konno, T., Takai, M. & Ishihara, K. Polymer nanoparticles covered with phosphorylcholine groups and immobilized with antibody for high-affinity separation of proteins. *Biomacromolecules* **9,** 828–833 (2008).

112. Mondal, K. & Gupta, M. N. The affinity concept in bioseparation: evolving paradigms and expanding range of applications. *Biomol. Eng.* **23,** 59–76 (2006).

113. Labrou, N. E. Design and selection of ligands for affinity chromatography. *J. Chromatogr. B* **790,** 67–78 (2003).

114. Batalha, I. L., Hussain, A. & Roque, A. C. A. Gum Arabic coated magnetic nanoparticles with affinity ligands specific for antibodies. *J. Mol. Recognit.* **23,** 462–471 (2010).

115. Bayramoglu, G., Senel, A. U. & Arica, M. Y. Effect of spacer-arm and Cu(II) ions on performance of l-histidine immobilized on poly(GMA/MMA) beads as an affinity ligand for separation and purification of IgG. *Sep. Purif. Technol.* **50,** 229–239 (2006).

116. Williams, J. L. Monolith structures, materials, properties and uses. *Catal. Today* **69,** 3–9 (2001).

117. Peskoller, C., Niessner, R. & Seidel, M. Development of an epoxy-based monolith used for the affinity capturing of Escherichia coli bacteria. *J. Chromatogr. A* **1216,** 3794–3801 (2009).

118. Plieva, F. M., Kirsebom, H. & Mattiasson, B. Preparation of macroporous cryostructurated gel monoliths, their characterization and main applications. *J. Sep. Sci.* **34,** 2164–2172 (2011).

119. Tripathi, A. & Kumar, A. Multi-featured macroporous agarose-alginate cryogel: synthesis and characterization for bioengineering applications. *Macromol. Biosci.* **11,** 22–35 (2011).

120. Nge, T. T., Nogi, M., Yano, H. & Sugiyama, J. Microstructure and mechanical properties of bacterial cellulose/chitosan porous scaffold. *Cellulose* **17,** 349–363 (2010).

121. Deville, S. Freeze-casting of porous biomaterials: structure, properties and opportunities. *Materials* **3,** 1913–1927 (2010).

122. Desmet, T. *et al.* Nonthermal plasma technology as a versatile strategy for polymeric biomaterials surface modification : a review. *Biomacromolecules* **10,** 2351–2378 (2009).

123. Cho, J., Denes, F. S. & Timmons, R. B. Plasma processing approach to molecular surface tailoring of nanoparticles: improved photocatalytic activity of TiO2. *Chem. Mater.* **18,** 2989–2996 (2006).

124. Schulze, M., Yanguas-Gil, A., Von Keudell, A. & Awakowicz, P. A robust method to measure metastable and resonant state densities from emission spectra in argon and argon-diluted low pressure plasmas. *J. Phys. D: Appl. Phys.* **41,** 065206 (2008).

125. O'Brien, F. Influence of freezing rate on pore structure in freeze-dried collagen-GAG scaffolds. *Biomaterials* **25,** 1077–1086 (2004).

126. Barry, J. J. A., Silva, M. M. C. G., Shakesheff, K. M., Howdle, S. M. & Alexander, M. R. Using plasma deposits to promote cell population of the porous interior of three-dimensional Poly(D,L-Lactic Acid) tissue-engineering scaffolds. *Adv. Funct. Mater.* **15,** 1134–1140 (2005).

127. Barroso, T. *et al.* Influence of poly(N -isopropylacrylamide) and poly(N , N ′-diethyl acrylamide) coatings on polysulfone/polyacrylonitrile-based membranes for protein separation. *Polym. Adv. Technol.* **23,** 1381–1393 (2012).

128. Choi, S.-W., Xie, J. & Xia, Y. Chitosan-based inverse opals: three-dimensional scaffolds with uniform pore structures for cell culture. *Adv. Mater.* **21,** 2997–3001 (2009).

129. Wei, Y. C., Hudson, S. M., Mayer, J. M. & Kaplan, D. L. The crosslinking of chitosan fibers. *J. Polym. Sci. A* **30,** 2187–2193 (1992).

130. Casettari, L. *et al.* PEGylated chitosan derivatives: synthesis, characterizations and pharmaceutical applications. *Prog. Polim. Sci.* **37,** 659–685 (2012).

131. Jain, E., Karande, A. a & Kumar, A. Supermacroporous polymer-based cryogel bioreactor for monoclonal antibody production in continuous culture using hybridoma cells. *Biotechnol.Progr.* **27,** 170–180 (2010).

132. Arvidsson, P., Plieva, F. M., Lozinsky, V. I., Galaev, I. Y. & Mattiasson, B. Direct chromatographic capture of enzyme from crude homogenate using immobilized metal affinity chromatography on a continuous supermacroporous adsorbent. *J. Chromatogr. A* **986,** 275–290 (2003).

133. Kathuria, N., Tripathi, A., Kar, K. K. & Kumar, A. Synthesis and characterization of elastic and macroporous chitosan-gelatin cryogels for tissue engineering. *Acta. Biomater.* **5,** 406–418 (2009).

134. Wang, A., Ao, Q., Cao, W. & Yu, M. Porous chitosan tubular scaffolds with knitted outer wall and controllable inner structure for nerve tissue engineering. *J. Biomed. Mater. Res.* **79A,** 36–46 (2006).

135. Bronshtein, A., Aharonson, N., Turniansky, A. & Altstein, M. Sol−Gel-Based Immunoaffinity Chromatography: Application to Nitroaromatic Compounds. *Chem. Mater.* **12,** 2050–2058 (2000).

136. Dai, C.-F., Weng, C.-J., Li, P.-R. & Yeh, J.-M. Influences of template concentration and epoxy functionality on porous epoxy systems: Characteristics of thermal stability, optical, dielectric, and mechanical properties. *Polym. Degrad. Stabil.* **95,** 600–609 (2010).

137. Wongchuphan, R. *et al.* Application of dye-ligands affinity adsorbent in capturing of rabbit immunoglobulin G. *Biochem. Eng. J.* **45,** 232–238 (2009).

138. Berruex, L. G., Freitag, R. & Tennikova, T. B. Comparison of antibody binding to immobilized group specific affinity ligands in high performance monolith affinity chromatography. *J. Pharm. Biomed. Anal.* **24,** 95–104 (2000).

139. Li, H., Nie, L. & Yao, S. Adsorption isotherms and sites distribution of caffeic acid? Imprinted polymer monolith from frontal analysis. *Chromatographia* **60,** 425–431 (2004).

140. Sproß, J. & Sinz, A. Monolithic media for applications in affinity chromatography. *J. Sep. Sci.* **34,** 1958–1973 (2011).

141. Aquino, L. C. L., Miranda, E. A., Duarte, I. S., Rosa, P. T. V. & Bueno, S. M. A. Adsorption of human immunoglobulin G onto ethacrylate and histidine-linked methacrylate. *Braz. J. Chem. Eng.* **20,** 251–262 (2003).

142. Carreira, R. J. *et al.* New findings for in-gel digestion accelerated by high-intensity focused ultrasound for protein identification by matrix-assisted laser desorption ionization time-of-flight mass spectrometry. *J. Chromatogr. A* **1153,** 291–299 (2007).

143. Neuhoff, V., Arold, N., Taube, D. & Ehrhardt, W. Improved staining of proteins in polyacrylamide gels including isoelectric focusing gels with clear background at nanogram sensitivity using Coomassie Brilliant blue G-250 and R-250. *Electrophoresis* **9,** 255–262 (1988).

144. Sproule, K. *et al.* New strategy for the design of ligands for the purification of pharmaceutical proteins by affinity chromatography. *J. Chromatogr. B* **740,** 17–33 (2000).

145. Shukla, A. A., Hubbard, B., Tressel, T., Guhan, S. & Low, D. Downstream processing of monoclonal antibodies--application of platform approaches. *J. Chromatogr. B* **848,** 28–39 (2007).

146. Roque, A. C. A., Taipa, M. A. & Lowe, C. R. Synthesis and screening of a rationally designed combinatorial library of affinity ligands mimicking protein L from Peptostreptococcus magnus. *J. Mol. Recognit.* **18,** 213–224 (2005).

147. Roque, A. C. A., Taipa, M. Â. & Lowe, C. R. An artificial protein L for the purification of immunoglobulins and Fab fragments by affinity chromatography. *J. Chromatogr. A* **1064,** 157–167 (2005).

148. Bilgicer, B. & Kiziltepe, T. Engineering multifunctional nanoparticles to selectively target multiple myeloma cells and overcome cell adhesion mediated drug resistance. *J. Bios. Bioelectr.* **2,** 6210 (2012).

149. Tscheliessnig, A. & Jungbauer, A. High-performance monolith affinity chromatography for fast quantitation of immunoglobulin G. *J. Chromatogr. A* **1216,** 2676–2682 (2009).

150. Branco, R. J. F., Dias, A. M. G. C. & Roque, A. C. A. Understanding the molecular recognition between antibody fragments and protein A biomimetic ligand. *J. Chromatogr. A* **1244,** 106–115 (2012).

151. Mulvihill, M. J., Beach, E. S., Zimmerman, J. B. & Anastas, P. T. Green chemistry and green engineering: a framework for sustainable technology development. *Annu. Rev. Env. Res.* **36,** 271–293 (2011).

152. Wang, M.-X. & Yang, H.-B. A general and high yielding fragment coupling synthesis of heteroatom-bridged calixarenes and the unprecedented examples of calixarene cavity fine-tuned by bridging heteroatoms. *JACS* **126,** 15412–22 (2004).

153. Umpleby, R. J., Baxter, S. C., Chen, Y., Shah, R. N. & Shimizu, K. D. Characterization of molecularly imprinted polymers with the Langmuir-Freundlich isotherm. *Anal. Chem.* **73,** 4584–4591 (2001).

154. Karush, F. *The affinity of antibody: range, variability, and the role of multivalence*. *Immunoglobulins* **5,** 85–116 (Plenum Publishing Corporation, 1978).

155. Hübner, K., Sahle, S. & Kummer, U. Applications and trends in systems biology in biochemistry. *FEBS* **278,** 2767–2857 (2011).

156. Viegas, A. *et al.* Molecular determinants of ligand specificity in family 11 carbohydrate binding modules: an NMR, X-ray crystallography and computational chemistry approach. *FEBS* **275,** 2524–2535 (2008).

157. Filizola, M. & Weinstein, H. The study of G-protein coupled receptor oligomerization with computational modeling and bioinformatics. *FEBS* **272,** 2926–2938 (2005).

158. Huang, B., Liu, F.-F., Dong, X.-Y. & Sun, Y. Molecular mechanism of the affinity interactions between protein A and human immunoglobulin G1 revealed by molecular simulations. *J. Phys. Chem. B* **115,** 4168–4176 (2011).

159. Huang, B., Liu, F.-F., Dong, X.-Y. & Sun, Y. Molecular mechanism of the effects of salt and pH on the affinity between protein A and human immunoglobulin G1 revealed by molecular simulations. *J. Phys. Chem. B* **116,** 424–433 (2012).

160. Salvalaglio, M., Zamolo, L. & Busini, V. Molecular modeling of Protein A affinity chromatography. *J. Chromatogr. A* **1216,** 8678–8686 (2009).

161. Barroso, T. *et al.* A green approach toward antibody purification: a sustainable biomimetic ligand for direct immobilization on (bio)polymeric supports. *J. Mol. Recognit.* (2013). doi:10.1002/jmr.2309

162. Saphire, E. O. *et al.* Crystal structure of a neutralizing human IGG against HIV-1: a template for vaccine design. *Science* **293,** 1155–1159 (2001).

163. Morris, G. & Goodsell, D. Automated docking using a Lamarckian genetic algorithm and an empirical binding free energy function. *J. Comput. Chem.* **19,** 1639–1662 (1998).

164. Mehler, E. L. & Solmajer, T. Electrostatic effects in proteins: comparison of dielectric and charge models. *Protein Eng.* **4,** 903–910 (1991).

165. Zamolo, L., Busini, V. & Moiani, D. Molecular dynamic investigation of the interaction of supported affinity ligands with monoclonal antibodies. *Biotechnol.Progr.* **24,** 527–539 (2008).

166. Hess, B. & Kutzner, C. GROMACS 4: Algorithms for highly efficient, load-balanced, and scalable molecular simulation. *J. Chem. Theor. Comput.* **4,** 435–447 (2008).

167. Schüttelkopf, A. W. & Van Aalten, D. M. F. PRODRG: a tool for high-throughput crystallography of protein-ligand complexes. *Acta Crystallogr. D* **60,** 1355–1363 (2004).

168. Oostenbrink, C., Villa, A., Mark, A. E. & van Gunsteren, W. F. A biomolecular force field based on the free enthalpy of hydration and solvation: the GROMOS force-field parameter sets 53A5 and 53A6. *J. Comput. Chem.* **25,** 1656–1676 (2004).

169. Berendsen, H. J. C., Postma, J. P. M., van Gunsteren, W. F., DiNola, A. & Haak, J. R. Molecular dynamics with coupling to an external bath. *J. Chem. Phys.* **81,** 3684–3690 (1984).

170. Bussi, G., Donadio, D. & Parrinello, M. Canonical sampling through velocity rescaling. *J. Chem. Phys.* **126,** 014101–014107 (2007).

171. Hess, B., Bekker, H., Berendsen, H. J. C. & Fraaije, J. G. E. M. LINCS: A linear constraint solver for molecular simulations. *J. Comput. Chem.* **18,** 1463–1472 (1997).

172. DeLano, W. L. DeLano Scientific LLC, San Carlos, CA, USA. (2002).

173. Humphrey, W., Dalke, A. & Schulten, K. VMD: visual molecular dynamics. *J. Mol. Graph.* **14,** 33–38 (1996).

174. Lévesque, S. G., Lim, R. M. & Shoichet, M. S. Macroporous interconnected dextran scaffolds of controlled porosity for tissue-engineering applications. *Biomaterials* **26,** 7436–7446 (2005).

175. Dang, J. M. & Leong, K. W. Natural polymers for gene delivery and tissue engineering. *Adv. Drug Deliver Rev.* **58,** 487–499 (2006).

176. Dias, A. M. G. C., Hussain, A., Marcos, A. S. & Roque, A. C. A. A biotechnological perspective on the application of iron oxide magnetic colloids modified with polysaccharides. *Biotechnol. Adv.* **29,** 142–155 (2011).

177. Boddohi, S. & Kipper, M. J. Engineering nanoassemblies of polysaccharides. *Adv. Mater.* **22,** 2998–3016 (2010).

178. Bhattarai, N. *et al.* Natural-synthetic polyblend nanofibers for biomedical applications. *Adv. Mater.* **21,** 2792–2797 (2009).

179. Kumar, A., Srivastava, A., Galaev, I. Y. & Mattiasson, B. Smart polymers: physical forms and bioengineering applications. *Prog. Polim. Sci.* **32,** 1205–1237 (2007).

180. Ratna, D. & Karger-Kocsis, J. Recent advances in shape memory polymers and composites: a review. *J. Mater. Sci.* **43,** 254–269 (2007).

181. Zhao, X. *et al.* Active scaffolds for on-demand drug and cell delivery. *Proceedings of the National Academy of Sciences of the United States of America* **108,** 67–72 (2011).

182. Le Sage, D. *et al.* Optical magnetic imaging of living cells. *Nature* **496,** 486–489 (2013).

183. Goodwill, P. W. *et al.* X-space MPI: magnetic nanoparticles for safe medical imaging. *Adv. Mater.* **24,** 3870–3877 (2012).

184. Hao, R. *et al.* Synthesis, functionalization, and biomedical applications of multifunctional magnetic nanoparticles. *Adv. Mater.* **22,** 2729–2742 (2010).

185. Chertok, B. *et al.* Iron oxide nanoparticles as a drug delivery vehicle for MRI monitored magnetic targeting of brain tumors. *Biomaterials* **29,** 487–496 (2008).

186. Koh, I. *et al.* Magnetic iron oxide nanoparticles for biorecognition: evaluation of surface coverage and activity. *J. Phys. Chem. B* **110,** 1553–1558 (2006).

187. Griffin, T., Mosbach, K. & Mosbach, R. Magnetic biospecific affinity adsorbents for immunoglobulin and enzyme isolation. *Appl. Biochem. Biotech.* **6,** 283–292 (1981).

188. Nagireddy, N. R. *et al.* Preparation and characterization of magnetic nanoparticles embedded in hydrogels for protein purification and metal extraction. *J. Polym. Res.* **18,** 2285–2294 (2011).

189. Liang, Y.-Y., Zhang, L.-M., Jiang, W. & Li, W. Embedding magnetic nanoparticles into polysaccharide-based hydrogels for magnetically assisted bioseparation. *Chemphyschem* **8,** 2367–2372 (2007).

190. Kumar, A. & Srivastava, A. Cell separation using cryogel-based affinity chromatography. *Nature protocols* **5,** 1737–1747 (2010).

191. Furlan, M., Brand, B. & Lattuada, M. Magnetic gelation: a new method for the preparation of polymeric anisotropic porous materials. *Soft Matter* **6,** 5636–5644 (2010).

192. Plieva, F., Oknianska, A., Degerman, E., Galaev, I. Y. & Mattiasson, B. Novel supermacroporous dextran gels. *J. Biomat. Sci.* **17,** 1075–1092 (2006).

193. Morent, R. & Geyter, N. De. Plasma surface modification of biodegradable polymers: a review. *Plasma Process. Polym.* **8,** 171–190 (2011).

194. Leyva, A. *et al.* Rapid and sensitive anthrone-sulfuric acid assay in microplate format to quantify carbohydrate in biopharmaceutical products: method development and validation. *Biologicals* **36,** 134–141 (2008).

195. Kolluri, O. & Johanson, R. Plasma deposited film networks. *US Patent 5,723,219* 1–13 (1998).

196. Müllner, P., Chernenko, V. A. & Kostorz, G. A microscopic approach to the magnetic-field-induced deformation of martensite (magnetoplasticity). *J. Magn. Magn. Mater* **267,** 325–334 (2003).

197. Beamson, G. & Briggs, D. High resolution XPS of organic polymers: the Scienta ESCA300 database. (1992). at <http://www.getcited.org/pub/102983780>

198. Sabaté, R., Barnadas-Rodríguez, R., Callejas-Fernández, J., Hidalgo-Alvarez, R. & Estelrich, J. Preparation and characterization of extruded magnetoliposomes. *Int. J. Pharm.* **347,** 156–162 (2008).

199. Wang, M., Xu, J., Zhou, X. & Tan, T. Modification with DEAE-dextran, an alternative way to prepare anion-exchange monolithic column with lower pressure drop. *Biochem. Eng. J.* **34,** 76–81 (2007).

200. Correia, V. G. *et al.* Anti-biofouling 3D porous systems : the blend effect of oxazoline-based oligomers on chitosan scaffolds. *Biofouling* **29,** 273–282 (2013).

201. Nandi, S., Kundu, B. & Basu, D. Protein growth factors loeaded highly porous chitosan scaffold: a comparasion of bone healing properties. *Mat. Sci. Eng. C* **33,** 1–9 (2013).

202. Cooper, A. I. & Holmes, A. B. Synthesis of Molded Monolithic Porous Polymers Using Supercritical Carbon Dioxide as the Porogenic Solvent. *Adv. Mater.* **11,** 1270–1274 (1999).

203. Wang, J. & Hon, M. Sugar-mediated chitosan/poly(ethylene glycol)- B-dicalcium pyrophosphate composite: mechanical and microstructural properties. *J. Biomed. Mater. Res.* **64A,** 262–272 (2002).

204. Gan, S., Yang, P. & Yang, W. Photoactivation of alkyl C-H and silanization: a simple and general route to prepare high-density primary amines on inert polymer surfaces for protein immobilization. *Biomacromolecules* **10,** 1238–1243 (2009).

205. Lin, T.-C., Seshadri, G. & Kelber, J. A. A consistent method for quantitative XPS peak analysis of thin oxide films on clean polycrystalline iron surfaces. *Appl. Surf. Sci.* **119,** 83–92 (1997).

206. Naumkin, A. V., Kraut-Vass, A., Gaarenstroom, S. W. & Powell, C. J. NIST X-ray Photoelectron Spectroscopy Database. (2012).

207. Nair, N. B., Elferink, J. W., Keizer, K. & Verweij, H. Sol – gel synthesis and characterization of microporous silica membranes I: SAXS study on the growth of polymeric structures. *J. Colloid Interf. Sci.* **570,** 565–570 (1996).

208. Barroso, T., Hussain, A., Roque, A. C. A. & Aguiar-Ricardo, A. Functional monolithic platforms: chromatographic tools for antibody purification. *Biotechnol. J.* **8,** 671–681 (2013).

209. Ozdemir, E., Sendemir-urkmez, A. & Yesil-celiktas, O. Supercritical CO_2 processing of a chitosan-based scaffold: Can implantation of osteoblastic cells be enhanced? *J. Supercrit. Fluid* **75,** 120–127 (2013).

210. Barroso, T., Temtem, M., Casimiro, T. & Aguiar-ricardo, A. Development of pH-responsive poly (methylmethacrylate-co-methacrylic acid) membranes using $scCO_2$ technology. Application to protein permeation. *J. Supercrit. Fluid* **51,** 57–66 (2009).

211. Cooper, A. I. Recent Developments in Materials Synthesis and Processing Using Supercritical CO_2. *Adv. Mater.* **13,** 1111–1114 (2001).

212. Shi, C. The Gelation of CO_2: A Sustainable Route to the Creation of Microcellular Materials. *Science* **286,** 1540–1543 (1999).

213. Huang, Z., Shi, C., Enick, R. & Beckman, E. Generation of microcellular materials via self-assembly in carbon dioxide. *Chem. Mater.* **40,** 4273–4280 (2002).

214. Lam, U. T., Mammucari, R., Suzuki, K. & Foster, N. R. Processing of Iron Oxide Nanoparticles by Supercritical Fluids. *Ind. Eng. Chem. Res.* **47,** 599–614 (2008).

215. Gualandi, C. *et al.* Scaffold for tissue engineering fabricated by non-isothermal supercritical carbon dioxide foaming of a highly crystalline polyester. *Acta. Biomater.* **6,** 130–136 (2010).

216. Sauceau, M., Fages, J., Common, A., Nikitine, C. & Rodier, E. New challenges in polymer foaming: a review of extrusion processes assisted by supercritical carbon dioxide. *Prog. Polim. Sci.* **36,** 749–766 (2011).

217. Temtem, M. *et al.* Development and characterization of a thermoresponsive polysulfone membrane using an environmental friendly technology. *Green Chem.* **11,** 638–645 (2009).

218. Barroso, T., Casimiro, T. & Aguiar-ricardo, A. Antifouling performance of poly(acrylonitrile)-based membranes: From green synthesis to application. *J. Supercrit. Fluid* **56,** 312–321 (2010).

219. Tai, H. *et al.* Control of pore size and structure of tissue engineering scaffolds produced by supercritical fluid processing. *Eur. Cells Mater.* **14,** 64–77 (2007).

220. Kamrupi, I. R., Pokhrel, B., Kalita, A., Boruah, M. & Dolui, S. K. Synthesis of Macroporous Polymer Particles by Suspension Polymerization Using Supercritical Carbon Dioxide as a Pressure- Adjustable Porogen. *Adv. Polym. Technol.* **00,** 1–9 (2011).

221. Jennings, J. *et al.* One-pot synthesis of block copolymers in supercritical carbon dioxide: a simple versatile route to nanostructured microparticles. *JACS* **134,** 4772–4781 (2012).

222. Goren, K., Okan, O. B., Chen, L., Schadler, L. S. & Ozisik, R. Supercritical carbon dioxide assisted dispersion and distribution of silica nanoparticles in polymers. *J. Supercrit. Fluid* **67,** 108–113 (2012).

223. Kumari, R. & Dutta, P. K. Physicochemical and biological activity study of genipin-crosslinked chitosan scaffolds prepared by using supercritical carbon dioxide for tissue engineering applications. *Int. J. Biol. Macromol.* **46,** 261–266 (2010).

224. Pisanti, P., Yeatts, A. B., Cardea, S., Fisher, J. P. & Reverchon, E. Tubular perfusion system culture of human mesenchymal stem cells on poly-L-lactic acid scaffolds produced using a supercritical carbon dioxide-assisted process. *J. Biomed. Mater. Res. A* **100,** 2563–2572 (2012).

225. Floren, M., Spilimbergo, S., Motta, A. & Migliaresi, C. Porous poly(D,L-lactic acid) foams with tunable structure and mechanical anisotropy prepared by supercritical carbon dioxide. *Journal of biomedical materials research. Part B, Applied biomaterials* **99,** 338–349 (2011).

226. Temtem, M., Casimiro, T. & Aguiar-Ricardo, A. Solvent power and depressurization rate effects in the formation of polysulfone membranes with CO_2-assisted phase inversion method. *J. Memb. Sci.* **283,** 244–252 (2006).

227. Temtem, M., Casimiro, T., Mano, J. F. & Aguiar-Ricardo, A. Preparation of membranes with polysulfone/polycaprolactone blends using a high pressure cell specially designed for a CO_2-assisted phase inversion. *J. Supercrit. Fluid* **43,** 542–548 (2008).

228. Cardea, S., Pisanti, P. & Reverchon, E. Generation of chitosan nanoporous structures for tissue engineering applications using a supercritical fluid assisted process. *J. Supercrit. Fluid* **54,** 290–295 (2010).

229. Ratanajiajaroen, P. & Ohshima, M. Preparation of highly porous β-chitin structure through nonsolvent–solvent exchange-induced phase separation and supercritical CO_2 drying. *J. Supercrit. Fluid* **68,** 31–38 (2012).

230. Gohil, J. M., Bhattacharya, a. & Ray, P. Studies On The Crosslinking Of Poly (Vinyl Alcohol). *J. Polym. Res.* **13,** 161–169 (2005).

231. Malsam, J. & Aksan, A. Hydrogen bonding and compartmentalization of water in supercooled and frozen aqueous acetone solutions. *J. Phys. Chem. B* **114,** 4238–4245 (2010).

232. Ozmen, M. M. & Okay, O. Superfast responsive ionic hydrogels with controllable pore size. *Polymer* **46,** 8119–8127 (2005).

233. Karakeçili, A. & Arikan, A. Preparation of Chitosan-Nanohydroxyapatite Composite Scaffolds by a Supercritical CO_2 Assisted Process. *Polym. Comp.* **33,** 1215–1223 (2012).

234. Physics, E. & Feld, I. N. A numerical experiment on pore size, pore connectivity, water retention, permeability, and solute transport using network models. *Eur. J. Soil Sci.* **51,** 99–105 (2000).

235. Anastas, P. & Eghbali, N. Green chemistry: principles and practice. *Chem. Soc. Rev.* **39,** 301–312 (2010).

236. Clark, J. Green chemistry: today (and tomorrow). *Green Chem.* **8,** 17–21 (2006).

237. Constable, D., Curzons, A. & Cunningham, V. Metrics to “green”chemistry —which are the best? *Green Chem.* **4,** 521–527 (2002).

238. Curran, M. Life cycle assessment: principles and practice. 1–88 (2006).

239. Zimmerman, J. B. & Anastas, P. T. Through the 12 principles green engineering. *Environ. Sci. Technol.* 94–101 (2003).

240. Dunn, P. J. The importance of green chemistry in process research and development. *Chem. Soc. Rev.* **41,** 1452–1461 (2012).

241. Sheldon, R. a. Fundamentals of green chemistry: efficiency in reaction design. *Chem. Soc. Rev.* **41,** 1437–1451 (2012).

242. Asfaw, N. *et al.* The 13 principles of green chemistry and engineering for a greener Africa. *Green Chem.* **13,** 1059–1060 (2011).

243. Andraos, J. & Sayed, M. On the use of“ green” metrics in the undergraduate organic chemistry lecture and lab to assess the mass efficiency of organic reactions. *J. Chem. Educ.* **84,** 1004–1010 (2007).

244. Ortiz, O., Castells, F. & Sonnemann, G. Sustainability in the construction industry: a review of recent developments based on LCA. *Const. Buil. Mater.* **23,** 28–39 (2009).

245. Martins, M., Mata, T., Martins, A. & Neto, B. LCA tool adaptation to pharmaceutical processes. 1–39 (2010).

246. Pietrini, M., Roes, L., Patel, M. K. & Chiellini, E. Comparative life cycle studies on poly(3-hydroxybutyrate)-based composites as potential replacement for conventional petrochemical plastics. *Biomacromolecules* **8,** 2210–2218 (2007).

247. Vink, E. T. H., Rábago, K. R., Glassner, D. A. & Gruber, P. R. Applications of life cycle assessment to NatureWorks™ polylactide (PLA) production. *Polym. Degrad. Stabil.* **80,** 403–419 (2003).

248. Eide, M. Life cycle assessment (LCA) of industrial milk production. *Int. J. LCA* **7,** 115–126 (2002).

249. Kiwjaroun, C., Tubtimdee, C. & Piumsomboon, P. LCA studies comparing biodiesel synthesized by conventional and supercritical methanol methods. *J. Clean. Prod.* **17,** 143–153 (2009).

250. Von Blottnitz, H. & Curran, M. A. A review of assessments conducted on bio-ethanol as a transportation fuel from a net energy, greenhouse gas, and environmental life cycle perspective. *J. Clean. Prod.* **15,** 607–619 (2007).

251. Nieminen, E., Linke, M., Tobler, M. & Beke, B. Vander. EU COST Action 628: life cycle assessment (LCA) of textile products, eco-efficiency and definition of best available technology (BAT) of textile processing. *J. Clean. Prod.* **15,** 1259–1270 (2007).

252. Brentrup, F., Küsters, J., Lammel, J., Barraclough, P. & Kuhlmann, H. Environmental impact assessment of agricultural production systems using the life cycle assessment (LCA) methodology II. The application to N fertilizer use in winter wheat production systems. *Eur. J. Agron.* **20,** 265–279 (2004).

253. Constable, D. J. C. *et al.* Key green chemistry research areas - a perspective from pharmaceutical manufacturers. *Green Chem.* **9,** 411–420 (2007).

254. Raymond, M. J., Slater, C. S. & Savelski, M. J. LCA approach to the analysis of solvent waste issues in the pharmaceutical industry. *Green Chem.* **12,** 1826–1834 (2010).